ROLE OF NUCLEAR LAMINS IN CHROMOSOME POSITIONING AND GENOME STABILITY

A THESIS

SUBMITTED IN PARTIAL FULFILLMENT OF THE REQUIREMENTS

OF THE DEGREE OF

DOCTOR OF PHILOSOPHY

BY

DEVIKA RAVINDRA RANADE

20103086

INDIAN INSTITUTE OF SCIENCE EDUCATION AND RESEARCH PUNE

2017

DECLARATION

I declare that this written submission represents my ideas in my own words and where others' ideas have been included; I have adequately cited and referenced the original sources. I also declare that I have adhered to all principles of academic honesty and integrity and have not misrepresented or fabricated or falsified any idea/data/fact/source in my submission. I understand that violation of the above will be cause for disciplinary action by the Institute and can also evoke penal action from the sources which have thus not been properly cited or from whom proper permission has not been taken when needed.

DRR

Devika Ravindra Ranade

Roll No. 20103086

Date: 6.12.2016

CERTIFICATE

Certified that the work incorporated in the thesis entitled '**Role of nuclear lamins in chromosome positioning and genome stability**' submitted by **Devika Ravindra Ranade** was carried out by the candidate, under my supervision. The work presented here or any part of it has not been included in any other thesis submitted previously for the award of any degree or diploma from any other University or institution.

Kundan Sengupta

Dr. Kundan Sengupta

Assistant Professor

IISER Pune

Date: 6.12.2016

Acknowledgements

I would like to acknowledge my Ph.D supervisor Dr. Kundan Sengupta for providing me a well guided opportunity to work in his lab and pursue my interests in the field of chromosome biology. I am thankful to him for his constant encouragement, support, enthusiasm, troubleshooting and advice on various aspects of this work.

I acknowledge members of my Research Advisory committee – Dr. Girish Ratnaparkhi, Dr. Sanjeev Galande, Dr. Jomon Joseph for their timely inputs and periodic critical comments on my work which helped me better plan the trajectory of my work. I am thankful to Genotypic, Bangalore for the gene expression microarray hybridization experiment and Bionivid, Bangalore for microarray data analysis. I acknowledge Dr. Binay Panda and his lab members for help with the experiments for copy number variation (CNV) calling.

I thank my funding agencies Council of Scientific and Industrial Research (CSIR) and IISER-Pune for funding during my Ph.D tenure and Wellcome-DBT India Alliance for funding the research in the lab. I am thankful to the facilities and authorities at IISER Pune for excellent management and upkeep of the equipment and facilities at IISER, Pune. I also acknowledge all the faculty members and students at the Biology department at IISER, Pune for help with reagents and technical assistance in experiments.

The execution of my project in the lab would have been very difficult in the absence of helpful lab members. I am thankful to all past and present lab members of the Chromosome Biology Lab for maintaining a very positive and healthy lab atmosphere, for coming up with excellent ideas and critical comments and timely help in the lab. I acknowledge members of the lab in its early days – Mihir, Joyce, Brajesh, Aishwarya, Sumit, Shivsmriti - all of us set up the initial lab equipments and protocols. I would like to thank members of the present lab and fellow Ph.D students – Ayantika, Roopali, Ajay, Maithilee, Apoorva, Sishil, Neelima, Shalaka for being great companions to work with in the lab. I am especially thankful to Roopali for constructive and thought provoking discussions on the role of Lamin A-Emerin in chromosome positioning. I am thankful to other friends and batchmates in the Department – Trupti, Ankitha, Manasi, Sushmitha for their help, support and academic as well as non academic discussions.

This thesis would have been difficult to achieve without support and encouragement from family and friends. Acknowledgements are due to my extremely supportive husband Hrishikesh who was a constant source of optimism and encouragement throughout the tenure of my Ph.D. My parents, grandparents, my in-laws, my brother and his family, my sister-in-law and her family have been equally encouraging and understanding towards my work and I acknowledge their support towards my project. Lastly, I thank my close friends and cousins for being by my side throughout the course of this project.

Contents

Essential Abbreviations

µM	micromolar
µl	microliter
µg	microgram
BAC	Bacterial artificial chromosome
CSK	Cytoskeleton Buffer
CT	Chromosome Territory
DNA	Deoxyribonucleic acid
FISH	Fluorescence *in situ* hybridization
Kb	Kilobase
Kd	Knockdown
LAD	Lamina associated domain
LAP	Lamina associated Polypeptide
LEM-D	LAP2A- Emerin - MAN1 domain
LINC	Linker of Nucleoskeleton and Cytoskeleton
Mbp	Megabase pair
PBS	Phosphate buffered saline
PFA	Paraformaldehyde
RD	Radial Distance
RNA	Ribonucleic acid
SSC	Saline sodium citrate
TF	Transcription factor

ABSTRACT

Chromosome territories are non-randomly organized in the interphase nucleus with gene rich chromosomes predominantly localized towards the nuclear interior and gene poor chromosomes towards the nuclear periphery. Such an arrangement is conserved across evolution and largely conserved across cell types. In addition, gene loci that are orders of magnitude smaller than chromosome territories are also non-randomly organized in the nucleus, with transcriptionally active genes being 'looped out' of their chromosome territories. The molecular basis of a non random arrangement in the nucleus is not completely understood. Nuclear Lamins are type V intermediate filament proteins that form a meshwork beneath the inner nuclear membrane. In addition, both A and B type Lamins also show nucleoplasmic pools in the nuclear interior. In this study, we have investigated the role of Lamin A/C and Lamin B2 in the organization of chromosome territories and genome stability. This study was performed in diploid colorectal cancer cells – DLD1 and showed non overlapping functions for nuclear Lamins A/C and B2 in regulating genome stability and organization. Lamin A/C and Lamin B2 knockdown revealed specific sets of chromosomes that were transcriptionally deregulated. Depletion of Lamins A/C and B2 induced aneuploidy in otherwise diploid DLD1 cells, as revealed by an increase in the number of chromosome territories in the interphase nucleus. Aneuploid chromosome territories showed a mislocalization in the interphase nucleus in a sub-population of Lamin B2 but not Lamin A/C depleted cells, suggesting a specific role for Lamin B2 in the regulation of spatial positions of aneuploid chromosome territories. Lamin B2 depletion also showed a wide spectrum of nuclear and chromosomal instabilities ranging from micronuclei, nuclear blebbing, chromosomal losses and gains that further implicate Lamin B2 in enhancing cancer associated genomic instabilities. In contrast, Lamin A/C regulates the spatial positions of gene rich chromosome territories in association with its interacting partner Emerin. Lamin A/C functions with Emerin in positioning gene rich chromosome territories towards the nuclear interior potentially through a regulation of the organization of components of the cytoskeleton - actin and nuclear myosin I. Taken together, we have uncovered two unique roles for Lamin B2 and Lamin A/C in the maintenance of genome organization and stability - Lamin B2 functions as a sensor of chromosome numbers both in mitosis and interphase while Lamin A/C primarily functions to regulate the positions of gene rich chromosome territories in association with its interactor Emerin.

SYNOPSIS

Introduction

Chromosomes occupy a finite three dimensional space in the interphase nucleus, referred to as 'Chromosome territory (CT)'. Early evidence for chromosome territories originated from Theodor Boveri's visualization of the nucleus from blastomeres of roundworms (Theodor Boveri, 1909). The organization of CTs in the interphase nucleus is non-random, and is consistent with gene density. Gene rich chromosome territories are localized towards the nuclear interior and gene poor chromosomes are proximal to the nuclear periphery (Cremer et al., 2001; Croft et al., 1999). For example, human chromosome 18 (gene density ~8.2 genes/Mbp) occupies a predominantly peripheral position in the interphase nucleus, while human chromosome 19 (~37.0 genes/Mbp) is localized towards the nuclear interior (Cremer et al., 2001; Croft et al., 1999). Such an arrangement is conserved through evolution and is largely conserved across cell types, suggesting a functional significance for such a non-random organization (Mayer et al., 2005; Tanabe et al., 2002). Advances in synthesis of fluorochromes and imaging technologies substantiated the non-random spatial organization of chromosome territories in the interphase nucleus. Further, technological advances in next generation sequencing based approaches enabled the mapping of chromatin contacts based on proximity of chromatin in chromosome conformation capture assays, which also recapitulated a gene density based arrangement of chromosomes in the interphase nucleus (Kalhor et al., 2011; Lieberman-Aiden et al., 2009; van Berkum et al., 2010). The structural organization of the nucleus reflects its functional organization, since gene rich chromosomes towards the nuclear interior are relatively more transcriptionally active as compared to gene poor chromosomes (Goetze et al., 2007). At a significantly lower DNA content (~10^5 fold lower as compared to whole chromosome territories), gene loci also are non random in their organization, since certain actively transcribing gene loci "loop-out" of their respective chromosome territories, or may associate with nuclear landmarks such as the nuclear lamins that largely repress gene activity (Chambeyron et al., 2005; Peric-Hupkes et al., 2010; Shachar et al., 2015; Volpi et al., 2000).

The molecular basis of the non-random organization of the genome, whether at the level of chromosome territories or gene loci remains poorly understood. Nuclear lamins along with their interacting partners regulate the structural and functional organization of gene loci in the interphase nucleus. Nuclear lamins form a filamentous sheath beneath the inner nuclear

membrane (Aebi et al., 1986; Gerace et al., 1978; Goldman et al., 1986). The nuclear lamina in higher eukaryotes is composed of two major types of lamins – A type (Lamin A and Lamin C produced as splice variants from the same gene) and B type (Lamin B1 and Lamin B2 coded by two different genes) (Biamonti et al., 1992; Höger et al., 1990; Lin and Worman, 1993; Lin and Worman, 1995; Machiels et al., 1996; Maeno et al., 1995). B type lamins are expressed in all cell types while Lamin A/C is expressed primarily in differentiated cells (Constantinescu et al., 2006; Röber et al., 1989). Lamins are organized as filaments at the nuclear periphery, and as a faster diffusing nucleoplasmic pool (Hozák et al., 1995; Moir et al., 2000; Muralikrishna et al., 2004). Lamins A, C, B1 and B2 form separate but interacting micro-domains in the nuclear lamina (Shimi et al., 2015). Lamin interactors at the nuclear periphery include Lamin B Receptor (LBR), Emerin and Lamina associated polypeptide2β (LAP2β), while Lamin interactors at the nuclear interior include LAP2α and BANF1 (Simon and Wilson, 2013). The specific contribution of lamin interactors to the maintenance of chromosome organization is unclear. Lamins and its interactors at the nuclear periphery associate with chromatin at 'Lamina associated domains' (LADs) characterized by the presence of Lamina associated sequences (LASs), low density of coding genes, high density of repeats and presence of the inactive histone mark H3K9me2/3 (Guelen et al., 2008; Harr et al., 2015; Towbin et al., 2012). LADs are enriched on gene poor chromosomes but are not solely confined to the nuclear periphery (Guelen et al., 2008; Kind et al., 2013).

The role of both A and B type lamins have been examined in chromosome positioning in both human and murine cell types (Malhas et al., 2007; Meaburn et al., 2007; Mewborn et al., 2010; Shimi et al., 2008). Fibroblasts derived from Lamin B1 knockout mice showed a mislocalization of chromosome 18 territories away from the nuclear periphery, while cells expressing a Lamin A mutant (E161K) revealed a mislocalization of human chromosome 13 towards the nuclear interior (Malhas et al., 2007; Mewborn et al., 2010). Mutations in Lamin proteins, primarily Lamin A collectively result in a group of diseases referred to as 'laminopathies' that include muscular and skeletal dystrophies, lipodystrophies and early aging syndromes (Worman et al., 2010). These diseases are characterized by a loss of chromatin organization and nuclear shapes coupled with gene expression changes, reiterating the fundamental role of Lamins in the regulation of nuclear structure and function. In addition to the maintenance of nuclear structure, lamins are also involved in transcription, DNA replication and repair, mitosis, senescence and

differentiation (Constantinescu et al., 2006; Shimi et al., 2011; Spann et al., 2002; Tang et al., 2008; Tsai et al., 2006).

Several questions that remain unanswered are (i) what is the relative contribution of A versus B type lamins in chromosome organization in the interphase nucleus? (ii) How do lamins regulate chromosome stability in cancer cells? (iii) Do lamins regulate the organization and function of the genome at two diverse scales of genomic content i.e chromosome territories and gene loci? (iv) What are the specific contributions of lamin associated protein-protein interactomes in regulating chromosome positioning? Considering these largely unanswered questions in the area of nuclear structure and function, this thesis is organized into the following sub-aims that attempt to address the role of lamins in chromosome organization, function and genome stability:

We examined the role of Lamins in:

I. Transcriptional regulation
II. Regulating the spatial organization of transcriptionally deregulated chromosomes
III. Maintenance of genomic stability
IV. The role of lamin dependent interactors in maintenance of chromosome positions

I. To investigate the role of nuclear lamins in transcriptional regulation in diploid colorectal cancer cells

To examine the consequences of Lamin depletion on the transcriptome, we performed lamin knockdowns (Kd) in diploid colorectal cancer cells (DLD1). These cells were selected considering their karyotypic stability across multiple passages, which distinguish them from aneuploid cell lines, replete with numerous chromosomal aberrations and instabilities. We performed gene silencing using siRNA mediated depletion of Lamin A/C and Lamin B2 in DLD1 cells and examined its impact on genome wide expression profiles using microarrays. This data revealed that ~1% of the genome (~300 genes) were transcriptionally deregulated independently upon either Lamin A/C or Lamin B2 depletion. Interestingly, these gene sets were non-overlapping, with only a small subset of ~22 genes that were commonly deregulated between Lamin A/C and B2 depletion. We also ascertained that the transcript levels of candidate genes were restored to their endogenous levels in cells that were allowed to recover from lamin depletion.

We found that the genes deregulated upon Lamin A/C or Lamin B2 depletion typically mapped to specific human chromosomes. Interestingly, transcriptional deregulation of chromosomes in Lamin B2 knockdown showed a greater correlation with the gene density of chromosomes (r^2=0.4629) as compared to Lamin A/C Kd (r^2=0.1823). Furthermore, the functional clustering of transcriptionally deregulated genes revealed non overlapping GO categories upon Lamin A/C and Lamin B2 depletion such as cell cycle, nuclear and chromosome organization, metabolism and organogenesis in Lamin A/C depletion, while Lamin B2 depletion enriched for GO categories of membrane associated functions, neurological processes and immunological processes. This further revealed that Lamin A/C or B2 depletion targets unique genes and therefore elicits specific transcriptional changes.

II. To examine the spatial organization of transcriptionally deregulated chromosomes in the interphase nucleus upon Lamin depletion

We sought to examine the nuclear organization of transcriptionally deregulated chromosomes in Lamin depleted cells by 3D-Fluorescence *in situ* hybridization (3D-FISH). Chromosomes 1,16 and 11 and 17 were examined upon Lamin A/C and Lamin B2 depletion respectively. In addition, chromosomes 18 and 19 were examined in both Lamin A/C and Lamin B2 depletion in DLD1 cells. Interestingly, both Lamin A/C and Lamin B2 Kd showed extra copies of chromosomes in ~25% cells. Chromosomes 18 and 19 were aneuploid in Lamin A/C depleted cells, while Lamin B2 depletion, induced aneuploidy for chromosomes 11,17,18 and 19 respectively. Aneuploidy is a common feature of several cancer cells of epithelial origin, which positively correlates with transcription (Grade et al., 2007). Our studies revealed that the resulting chromosomal aneuploidies upon Lamin A/C or Lamin B2 depletion showed both transcriptional up and downregulation. We therefore examined the spatial positioning of these aneuploid chromosome territories. Surprisingly, notwithstanding lamin depletions, chromosome territory localizations were largely conserved for diploid chromosomes in a gene density dependent manner in the interphase nucleus. However, 3D-FISH analyses of the Lamin depleted cells predominantly revealed a mislocalization of the aneuploid chromosome territories as compared to diploid chromosome territories upon Lamin B2 but not Lamin A/C depletion. This suggests that while both Lamin A/C and Lamin B2 serve to regulate ploidy of DLD1 cells, the

spatial positions of aneuploid chromosome territories are maintained specifically by Lamin B2. At a much lower scale of genomic content i.e gene loci in contrast to relatively larger chromosome territories, a candidate gene – *ZNF570* (Chr. 19q13.12) which was upregulated upon Lamin B2 depletion, was repositioned away from the nuclear lamina in diploid as well aneuploid cells. Furthermore, such a mislocalization was accompanied by an increase in *ZNF570* transcript suggesting a role for Lamin B2 in the structural and functional maintenance of genes in diploid and aneuploid cells.

Since aneuploidy is a common feature of several epithelial cancer cells, we next asked whether cancer cells with inherent chromosomal aneuploidies show conserved chromosome positions. Aneuploid cancer cell lines showed a partial loss of conserved gene density dependent positioning patterns of chromosome territories, since gene rich and gene poor chromosome territories in the interphase nuclei of aneuploid cells were closer to one another as compared to that diploid cell lines. Furthermore, modulating the levels of Lamin B2 in SW480 cells - an aneuploid cell line derived from colorectal cancer, impacts the spatial positions of aneuploid chromosome territories.

Thus, Lamin B2 is involved in the generation of aneuploidy during mitosis, and in the maintenance of aneuploid CTs at their cognate locations in the interphase nucleus. Examining Lamin B2 associations in late mitosis and interphase led us to examine Lamin B receptor (LBR) – that binds to heterochromatic subdomains during segregation of chromosomes in mitosis and maintains heterochromatin binding during interphase. We surmise Lamin B2-LBR as an important axis in the regulation of genome organization.

III. Role of lamins in the maintenance of genome stability

Here we examined the role of lamins in regulating genome and chromosomal stability. Interestingly, depletion of Lamin B2 but not Lamin B1 or Lamin A/C revealed enhanced nuclear blebbing and micronuclei formation. Furthermore, we detected chromosomal aberrations including chromosomal breaks, losses, gains and non recurrent translocations in Lamin B2 (but not Lamin A/C) depleted cells by Spectral Karyotyping (SKY) analyses.

Since Lamin depletion revealed chromosomal aberrations, we examined the extent of copy number variations (CNVs) in Lamin depleted cells. Array CGH showed non overlapping CNVs upon Lamin depletion. Common CNVs were full deletion, single copy deletion, single copy insertion, full copy insertion and Loss of heterozygosity (LOH). The predominant subtype of CNV detected upon Lamin A/C and Lamin B1 Kd were single copy insertions, while those upon Lamin B2 Kd were single copy deletions. To further address the role of lamins in inducing CNVs, we examined copy numbers of candidate genes that were robustly expressed in colon cancer cells upon Lamin A/C depletion. 2D-FISH was performed to examine the copy numbers of *DNMT1* (Chr.19p13.2) in Lamin depleted cells. Upon Lamin A/C but not Lamin B1 or Lamin B2 Kd, we detected an increase in the copy number of *DNMT1* (> 2 copies) in DLD1 cells. Interestingly, another candidate gene *WDR8* (Chr.1p36.32) did not show an increase in copy numbers upon either Lamin A/C or B type Lamin depletion. DLD1 cells inherently show Microsatellite instability (MSI) which results in an amplification of short repeat stretches in the genome. Moreover, in SW480 cells, which are MSI-, *DNMT1* does not show amplification upon Lamin A/C depletion. We surmise a potential correlation between Lamin A/C and factors associated with the MSI pathway in the induction of gene amplifications.

IV. To investigate the role of interacting partners of nuclear lamins in the maintenance of chromosome positions

Since we detected a conserved chromosome positioning in diploid DLD1 cells upon the depletion of either Lamin A/C or Lamin B2, we next tested the role of Lamin interactors at the nuclear envelope in maintaining chromosome positions. Gene expression profiling using qRT-PCR arrays revealed transcriptional feedback responses from various lamin interactors such as the LINC complex (*SUN1*, *EMD*), nucleolar proteins (*FBL*), nucleoporins (*NUP62*,*NUP93*) and transcription factors (*BCLAF1*, *FOS*, *HOXA7*) upon Lamin A/C or Lamin B2 depletion. A significant upregulation was detected for the Lamin A/C interactor - Emerin and likewise Lamin A/C transcript was upregulated upon depletion of Emerin. The combined depletion of Lamin A/C and Emerin showed a repositioning of primarily the gene rich chromosome 19 territories toward the nuclear periphery (from its otherwise conserved position in the nuclear interior). Gene

poor chromosome 18 was unaffected in terms of its preferential peripheral nuclear position in either single or combined knockdown of Lamin A/C and Emerin. Concomitantly, Fluorescence Recovery After Photobleaching (FRAP) assays performed on H2A-mCherry as a reporter of chromatin mobility revealed greater mobility in the nuclear interior as compared to the nuclear periphery upon Lamin A/C and Emerin depletion. Lamin A/C and Emerin associate in a complex with the motor protein nuclear myosin I (NM1) and actin. We examined the organization of NM1 and actin upon single and combined knockdowns of Lamin A/C and Emerin. Lamin A/C depletion mislocalized NM1 into cytoplasmic aggregates with accompanied by an increase in the numbers of intranuclear foci of NM1- in an Emerin dependent manner. In addition, Emerin co-depleted with Lamin A/C showed an increased reorganization of actin in the cytoplasm in the form of stress fibres. Depolymerization of actin in Lamin A/C and Emerin co-depleted cells rescued the enhanced mobility of H2A-mCherry in the nuclear interior to levels comparable with control cells. We speculate that actin reorganization in Lamin A/C and Emerin co-depleted cells may contribute to increased chromatin mobility in the nuclear interior. The precise regulatory mechanism of actin and myosin organization in Lamin A/C and Emerin co-depleted cells and its impact on the spatial positions of chromosome territories however remains to be investigated.

Summary

Taken together, this thesis proposes unique and non-overlapping roles of Lamin A/C and Lamin B2 in the maintenance of nuclear structure-function relationships. Our studies have unravelled a unique and novel role for Lamin B2 in functioning as a ‘sensor’ of chromosome numbers during the cell cycle. We surmise that Lamin B2 regulates chromosome numbers via common interactors such as LBR during mitosis and interphase. In contrast, Lamin A/C largely regulates positions of gene rich chromosome territories at the nuclear interior in association with its interacting partners - Emerin, actin and nuclear myosin. Furthermore, Lamin A/C maintains genomic stability and copy numbers in the genome, while Lamin B2 is also involved in maintaining overall chromosome integrity. A comprehensive characterization of these regulatory associations will have far reaching consequences in understanding the role of Lamins in the organization of the genome in colorectal cancers.

Results from this work were published as a part of the manuscript:

Ranade, D., Koul, S., Thompson, J., Prasad, K. B. and Sengupta, K. (2016). Chromosomal aneuploidies induced upon Lamin B2 depletion are mislocalized in the interphase nucleus. *Chromosoma*.

References

Aebi, U., Cohn, J., Buhle, L. and Gerace, L. (1986). The nuclear lamina is a meshwork of intermediate-type filaments. *Nature* **323**, 560–564.

Biamonti, G., Giacca, M., Perini, G., Contreas, G., Zentilin, L., Weighardt, F., Guerra, M., Della Valle, G., Saccone, S. and Riva, S. (1992). The gene for a novel human lamin maps at a highly transcribed locus of chromosome 19 which replicates at the onset of S-phase. *Mol Cell Biol* **12**, 3499–3506.

Chambeyron, S., Da Silva, N. R., Lawson, K. A. and Bickmore, W. A. (2005). Nuclear re-organisation of the Hoxb complex during mouse embryonic development. *Development* **132**, 2215–2223.

Constantinescu, D., Gray, H. L., Sammak, P. J., Schatten, G. P. and Csoka, A. B. (2006). Lamin A/C expression is a marker of mouse and human embryonic stem cell differentiation. *Stem Cells* **24**, 177–185.

Cremer, M., von Hase, J., Volm, T., Brero, A., Kreth, G., Walter, J., Fischer, C., Solovei, I., Cremer, C. and Cremer, T. (2001). Non-random radial higher-order chromatin arrangements in nuclei of diploid human cells. *Chromosome Res* **9**, 541–567.

Croft, J. A., Bridger, J. M., Boyle, S., Perry, P., Teague, P. and Bickmore, W. A. (1999). Differences in the localization and morphology of chromosomes in the human nucleus. *J Cell Biol* **145**, 1119–1131.

Gerace, L., Blum, A. and Blobel, G. (1978). Immunocytochemical localization of the major polypeptides of the nuclear pore complex-lamina fraction. Interphase and mitotic distribution. *J Cell Biol* **79**, 546–566.

Goetze, S., Mateos-Langerak, J., Gierman, H. J., de Leeuw, W., Giromus, O., Indemans, M. H. G., Koster, J., Ondrej, V., Versteeg, R. and van Driel, R. (2007). The three-dimensional structure of human interphase chromosomes is related to the transcriptome map. *Mol Cell Biol* **27**, 4475–4487.

Goldman, A. E., Maul, G., Steinert, P. M., Yang, H. Y. and Goldman, R. D. (1986). Keratin-like proteins that coisolate with intermediate filaments of BHK-21 cells are nuclear lamins. *Proc Natl Acad Sci U S A* **83**, 3839–3843.

Grade, M., Hörmann, P., Becker, S., Hummon, A. B., Wangsa, D., Varma, S., Simon, R., Liersch, T., Becker, H., Difilippantonio, M. J., et al. (2007). Gene expression profiling reveals a massive, aneuploidy-dependent transcriptional deregulation and distinct differences between lymph node-negative and lymph node-positive colon carcinomas. *Cancer Res* **67**, 41–56.

Guelen, L., Pagie, L., Brasset, E., Meuleman, W., Faza, M. B., Talhout, W., Eussen, B. H., de Klein, A., Wessels, L., de Laat, W., et al. (2008). Domain organization of human chromosomes revealed by mapping of nuclear lamina interactions. *Nature* **453**, 948–951.

Harr, J. C., Luperchio, T. R., Wong, X., Cohen, E., Wheelan, S. J. and Reddy, K. L. (2015). Directed targeting of chromatin to the nuclear lamina is mediated by chromatin state and A-type lamins. *J Cell Biol* **208**, 33–52.

Höger, T. H., Zatloukal, K., Waizenegger, I. and Krohne, G. (1990). Characterization of a second highly conserved B-type lamin present in cells previously thought to contain only a single B-type lamin. *Chromosoma* **100**, 67–69.

Hozák, P., Sasseville, A. M., Raymond, Y. and Cook, P. R. (1995). Lamin proteins form an internal nucleoskeleton as well as a peripheral lamina in human cells. *J Cell Sci* **108 (Pt 2)**, 635–644.

Kalhor, R., Tjong, H., Jayathilaka, N., Alber, F. and Chen, L. (2011). Genome architectures revealed by tethered chromosome conformation capture and population-based modeling. *Nat Biotechnol* **30**, 90–98.

Kind, J., Pagie, L., Ortabozkoyun, H., Boyle, S., de Vries, S. S., Janssen, H., Amendola, M., Nolen, L. D., Bickmore, W. A. and van Steensel, B. (2013). Single-cell dynamics of genome-nuclear lamina interactions. *Cell* **153**, 178–192.

Lieberman-Aiden, E., van Berkum, N. L., Williams, L., Imakaev, M., Ragoczy, T., Telling, A., Amit, I., Lajoie, B. R., Sabo, P. J., Dorschner, M. O., et al. (2009). Comprehensive mapping of long-range interactions reveals folding principles of the human genome. *Science* **326**, 289–293.

Lin, F. and Worman, H. J. (1993). Structural organization of the human gene encoding nuclear lamin A and nuclear lamin C. *J Biol Chem* **268**, 16321–16326.

Lin, F. and Worman, H. J. (1995). Structural organization of the human gene (LMNB1) encoding nuclear lamin B1. *Genomics* **27**, 230–236.

Machiels, B. M., Zorenc, A. H., Endert, J. M., Kuijpers, H. J., van Eys, G. J., Ramaekers, F. C. and Broers, J. L. (1996). An alternative splicing product of the lamin A/C gene lacks exon 10. *J Biol Chem* **271**, 9249–9253.

Maeno, H., Sugimoto, K. and Nakajima, N. (1995). Genomic structure of the mouse gene (Lmnb1) encoding nuclear lamin B1. *Genomics* **30**, 342–346.

Malhas, A., Lee, C. F., Sanders, R., Saunders, N. J. and Vaux, D. J. (2007). Defects in lamin B1 expression or processing affect interphase chromosome position and gene expression. *J Cell Biol* **176**, 593–603.

Mayer, R., Brero, A., von Hase, J., Schroeder, T., Cremer, T. and Dietzel, S. (2005). Common themes and cell type specific variations of higher order chromatin arrangements in the mouse. *BMC Cell Biol* **6**, 44.

Meaburn, K. J., Cabuy, E., Bonne, G., Levy, N., Morris, G. E., Novelli, G., Kill, I. R. and Bridger, J. M. (2007). Primary laminopathy fibroblasts display altered genome organization and apoptosis. *Aging Cell* **6**, 139–153.

Mewborn, S. K., Puckelwartz, M. J., Abuisneineh, F., Fahrenbach, J. P., Zhang, Y., MacLeod, H., Dellefave, L., Pytel, P., Selig, S., Labno, C. M., et al. (2010). Altered chromosomal positioning, compaction, and gene expression with a lamin A/C gene mutation. *PLoS ONE* **5**, e14342.

Moir, R. D., Yoon, M., Khuon, S. and Goldman, R. D. (2000). Nuclear lamins A and B1: different pathways of assembly during nuclear envelope formation in living cells. *J Cell Biol* **151**, 1155–1168.

Muralikrishna, B., Thanumalayan, S., Jagatheesan, G., Rangaraj, N., Karande, A. A. and Parnaik, V. K. (2004). Immunolocalization of detergent-susceptible nucleoplasmic lamin A/C foci by a novel monoclonal antibody. *J Cell Biochem* **91**, 730–739.

Peric-Hupkes, D., Meuleman, W., Pagie, L., Bruggeman, S. W. M., Solovei, I., Brugman, W., Gräf, S., Flicek, P., Kerkhoven, R. M., van Lohuizen, M., et al. (2010). Molecular maps of the reorganization of genome-nuclear lamina interactions during differentiation. *Mol Cell* **38**, 603–613.

Röber, R. A., Weber, K. and Osborn, M. (1989). Differential timing of nuclear lamin A/C expression in the various organs of the mouse embryo and the young animal: a developmental study. *Development* **105**, 365–378.

Shachar, S., Pegoraro, G. and Misteli, T. (2015). HIPMap: A High-Throughput Imaging Method for Mapping Spatial Gene Positions. *Cold Spring Harb Symp Quant Biol* **80**, 73–81.

Shimi, T., Pfleghaar, K., Kojima, S., Pack, C.-G., Solovei, I., Goldman, A. E., Adam, S. A., Shumaker, D. K., Kinjo, M., Cremer, T., et al. (2008). The A- and B-type nuclear lamin networks: microdomains involved in chromatin organization and transcription. *Genes Dev* **22**, 3409–3421.

Shimi, T., Butin-Israeli, V., Adam, S. A., Hamanaka, R. B., Goldman, A. E., Lucas, C. A., Shumaker, D. K., Kosak, S. T., Chandel, N. S. and Goldman, R. D. (2011). The role of nuclear lamin B1 in cell proliferation and senescence. *Genes Dev* **25**, 2579–2593.

Shimi, T., Kittisopikul, M., Tran, J., Goldman, A. E., Adam, S. A., Zheng, Y., Jaqaman, K. and Goldman, R. D. (2015). Structural organization of nuclear lamins A, C, B1, and B2 revealed by superresolution microscopy. *Mol Biol Cell* **26**, 4075–4086.

Simon, D. N. and Wilson, K. L. (2013). Partners and post-translational modifications of nuclear lamins. *Chromosoma* **122**, 13–31.

Spann, T. P., Goldman, A. E., Wang, C., Huang, S. and Goldman, R. D. (2002). Alteration of nuclear lamin organization inhibits RNA polymerase II-dependent transcription. *J Cell Biol* **156**, 603–608.

Tanabe, H., Müller, S., Neusser, M., von Hase, J., Calcagno, E., Cremer, M., Solovei, I., Cremer, C. and Cremer, T. (2002). Evolutionary conservation of chromosome territory arrangements in cell nuclei from higher primates. *Proc Natl Acad Sci U S A* **99**, 4424–4429.

Tang, C. W., Maya-Mendoza, A., Martin, C., Zeng, K., Chen, S., Feret, D., Wilson, S. A. and Jackson, D. A. (2008). The integrity of a lamin-B1-dependent nucleoskeleton is a fundamental determinant of RNA synthesis in human cells. *J Cell Sci* **121**, 1014–1024.

Theodor Boveri, 1909 *Theodor Boveri, 1909*.

Towbin, B. D., González-Aguilera, C., Sack, R., Gaidatzis, D., Kalck, V., Meister, P., Askjaer, P. and Gasser, S. M. (2012). Step-wise methylation of histone H3K9 positions heterochromatin at the nuclear periphery. *Cell* **150**, 934–947.

Tsai, M.-Y., Wang, S., Heidinger, J. M., Shumaker, D. K., Adam, S. A., Goldman, R. D. and Zheng, Y. (2006). A mitotic lamin B matrix induced by RanGTP required for spindle assembly. *Science* **311**, 1887–1893.

Van Berkum, N. L., Lieberman-Aiden, E., Williams, L., Imakaev, M., Gnirke, A., Mirny, L. A., Dekker, J. and Lander, E. S. (2010). Hi-C: a method to study the three-dimensional architecture of genomes. *J Vis Exp*.

Volpi, E. V., Chevret, E., Jones, T., Vatcheva, R., Williamson, J., Beck, S., Campbell, R. D., Goldsworthy, M., Powis, S. H., Ragoussis, J., et al. (2000). Large-scale chromatin organization of the major histocompatibility complex and other regions of human chromosome 6 and its response to interferon in interphase nuclei. *J Cell Sci* **113 (Pt 9)**, 1565–1576.

Worman, H. J., Ostlund, C. and Wang, Y. (2010). Diseases of the nuclear envelope. *Cold Spring Harb Perspect Biol* **2**, a000760.

Chapter 1:

Introduction and review of literature

1.1 Chromosome positioning

1.1.1 Introduction

Chromosomes in the interphase nucleus are confined to a specific three dimensional space in the nucleus occupied by chromatin from the chromosome. Such a space is referred to as a 'chromosome territory (CT)' (Theodor Boveri, 1909). The human interphase nucleus harbors 46 different CTs corresponding to 46 chromosomes. Carl Rabl first documented the territorial confinement of chromosomes while the term CT was originally coined by Theodre Boveri (Theodor Boveri, 1909).Theodre Boveri noted the presence of intensely stained chromatin in cells of roundworm referred to as 'Chromosome territory' (Theodor Boveri, 1909). Zorn et al were the first to demonstrate the presence of CTs through a series of UV based laser irradiation incident on a specific nuclear region (Cremer et al., 1982; Zorn et al., 1976; Zorn et al., 1979). Irradiation was performed on interphase nuclei of Chinese hamster ovary (CHO) cells, and chromatin breaks were seen to map to a small number of chromosomes (Cremer et al., 1982; Zorn et al., 1976). This suggested the organization of chromosomes in a unique sub-volume in the nucleus, which were later established as chromosome territories, in contrast to the randomly intermingling spaghetti model of chromatin fibres.

Subsequent advances in *in situ* hybridization to visualize chromatin and fluorescent microscopy, enabled the visualization of chromosomes in the interphase nucleus (Cremer et al., 2008; Manuelidis, 1985; Schardin et al., 1985). This provided the first microscopic evidence for CTs, since in situ labeling of a chromosome shows a single confined region occupied by a particular chromosome. Advances in the fields of fluorescence and confocal microscopy led to further analyses of the organization of chromosome territories and gene loci within these CTs and revealed a non-random organization of CTs in the nucleus (Cremer et al., 2001; Croft et al., 1999). More recently, super resolution imaging is being employed to examine the organization of chromatin in greater details (Beliveau et al., 2015; Smeets et al., 2014).

More recent techniques to study chromatin structure and organization use proximity dependent ligation methods to determine the proximity between chromatin elements. These methods are referred to as chromosome conformation capture (CCC) assays,and involve 3C, 4C, 5C and the most recent Hi-C methods and they measure interaction frequency of two regions of chromatin

based on their ligation frequencies (van Berkum et al., 2010). Hi-C maps generated for interphase nuclei genomes reveal that chromosomes show greater interactions in *cis* as compared to that in *trans* (Kalhor et al., 2011). This also suggests a territorial confinement of chromosomes in the interphase nucleus (Kalhor et al., 2011). Thus, the presence of CTs has been demonstrated using conventional fluorescent microscopy methods as well as the more recent chromatin proximity ligation based biochemical methods.

1.1.2 Factors that influence chromosome positioning

The advancement in the field of confocal microscopy led to several important discoveries about the organization of CTs. Several factors were shown to impact the positions of chromosomes in the nucleus:

i. Gene density: The most widely studied factor that influences chromosome positioning is the gene density of chromosomes. Gene density refers to the number of coding genes per Mbp of chromosomes. Gene rich chromosomes are predominantly localized toward the nuclear interior, and gene poor chromosomes towards the nuclear periphery, for example human chromosome 18 with low gene density (8.2 genes/Mbp) has a preferential localization proximal to the nuclear periphery, while human chromosome 19 of a comparable size and higher gene density (37.0 genes/Mbp) is localized towards the nuclear centre (Cremer et al., 2001; Croft et al., 1999) (Fig.1.1A-B). A plot of gene density versus chromosome positions reveals a negative correlation.

ii. Chromosome size: Chromosome size is an important factor that influences chromosome positions especially in nuclei that show a flattened morphology (Bolzer et al., 2005). Chromosomes of a smaller size tend to be closer to one another in the nuclear interior, while larger sized chromosomes occupy the peripheral regions inside the interphase nucleus (Bolzer et al., 2005).

iii. Replication timing: Early replicating regions of the genome are localized in the nuclear interior while late replicating regions toward the nuclear periphery. Thus, chromosomes with more number of early replication foci are localized more towards

the nuclear interior (Jackson and Pombo, 1998; Zink et al., 1999). Subsequently, it was also discovered that late replicating foci associate with the molecules at the periphery of the nucleus (Guelen et al., 2008).

Chromosome positioning at any stage in the nucleus is dependent on a critical balance between these factors listed above.

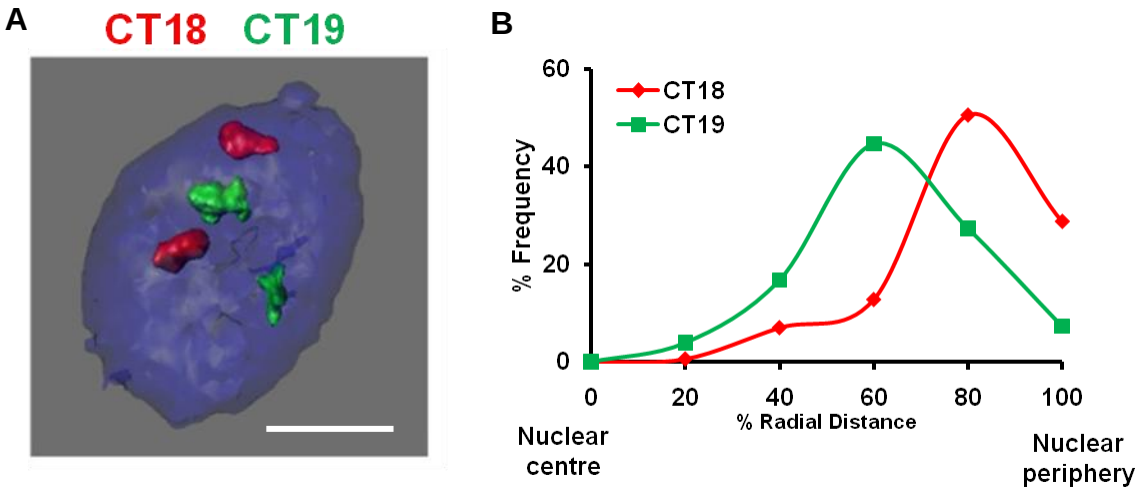

Figure 1.1 Correlation of gene density and chromosome positions in the interphase nucleus

A. 3D reconstruction of a human colorectal cancer cell line (DLD1) nucleus depicting gene rich CT19 (green) towards the nuclear interior and gene poor CT18 (red) towards the nuclear periphery. Scale bar ~5µm B. Graph depicting the positions of CT18 and CT19 in DLD1 cells. CT19 is preferentially positioned towards the nuclear centre and CT18 towards the nuclear periphery.

1.1.3 Conservation of gene density based chromosome positioning

Chromosomes are non randomly positioned in the interphase nucleus, with gene rich CTs towards the nuclear interior and gene poor towards the nuclear periphery (Cremer et al., 2001; Croft et al., 1999). Human chromosome 18 for example, has a low gene density (~8.2 genes/Mbp) and is localized proximal to the nuclear periphery while human chromosome 19 has a high gene density (~37.0 genes/Mbp) and is positioned towards the nuclear interior (Cremer et

al., 2001). Confocal microscopy based observations of conserved chromosome positioning are corroborated by computational contour maps generated from Hi-C data which also recapitulate a gene density based chromosome positioning (Lieberman-Aiden et al., 2009). Such an arrangement is conserved across evolution from lower primates to humans (Tanabe et al., 2002). In addition, several other cold blooded vertebrates such as reptiles and birds also show a gene density dependent chromosome organization, with radially distributed chromatin having gene rich chromatin domains at the nuclear interior and gene poor domains in the nuclear periphery (Federico et al., 2006; Neusser et al., 2007).

1.1.4 Functional significance of chromosome positioning

The functional consequences of a gene density based chromosome positioning pattern have not been completely understood. One important function of such an arrangement is to bring about compartmentalization of domains of chromatin in the nucleus (Gilbert et al., 2005; Goetze et al., 2007). This segregation of chromosomes serves to place gene poor chromosomes, which have a lesser requirement for transcription, in close association with the nuclear periphery, which maintains a generally transcriptionally repressive state in the nucleus. On the other hand, gene rich chromosomes in the nuclear interior are associated with a potentially greater permissiveness for transcription (Gilbert et al., 2005). A comparison of the transcriptional outputs across chromosomes also shows greater transcription from gene rich chromosomes in the nuclear interior as compared to gene poor at the nuclear periphery (Caron et al., 2001). Thus, a gene density based chromosome positioning order is tightly coupled to an organization of function (transcription) in the nucleus.

Changes in chromosome positioning have been reported for few cellular processes such as differentiation, immune responses, senescence, repair of DNA damage (Foster et al., 2005; Galiová et al., 2004; Mehta et al., 2007; Mehta et al., 2013; Szczerbal et al., 2009). This reiterates a fundamental functional importance to chromosome positioning which is important for functioning of the specific cellular state.

1.1.5 Molecular regulation of chromosome positions

The organization in the interphase nucleus leads us to investigate the underlying molecular mechanisms that regulate nuclear organization. This question led several labs to examine the molecules that form the structural framework of the nucleus and associate directly or indirectly with chromatin. In this regard, the nuclear lamins are important candidates that maintain the framework of the nucleus. Nuclear lamins are type V intermediate filaments that maintain nuclear structure and function (Dechat et al., 2008). Nuclear lamins and their interactors (Emerin, Lamin B receptor), actin are implicated in chromatin organization and chromosome positioning (Boyle et al., 2001; Meaburn et al., 2005; Meaburn et al., 2007; Mewborn et al., 2010; Ondrej et al., 2008; Solovei et al., 2013). In the work presented in this thesis, we have investigated the role of nuclear lamins in the context of chromosome positioning and function.

1.2 Molecular mechanisms of nuclear structure-function relationships - Nuclear Lamins

Nuclear lamins are a family of type V intermediate filaments that line the inner nuclear membrane by forming a polymerized filamentous sheath beneath the INM (Aebi et al., 1986; Gerace et al., 1978; Goldman et al., 1986). Nuclear lamins interact with a host of INM and nucleoplasmic molecules and form a nucleoskeleton. Lamins were originally co-purified from nuclear extracts and were found to have structural similarity with intermediate filaments of the cell (Fisher et al., 1986; McKeon et al., 1986). Subsequently, this family of proteins with similar range molecular weights (~60-75 kDa) was resolved into two main classes of lamins - A and B type in higher eukaryotes (Gerace and Blobel, 1980).

1.2.1 Types of lamins

Nuclear lamins are primarily localized in ~10nm beneath the inner nuclear membrane. Lamin expression is not detected in prokaryotes. Yeast cells have inner nuclear membrane lamin and their interactor analogues (Georgatos et al., 1989). Drosophila has two main types (A and B type of lamins) while most other insects have at least one type (Melcer et al., 2007). A single A type Lamin and two major Lamins are present in most vertebrates, with Xenopus being an exception

that shows an additional B type Lamin (Lehner et al., 1987; Stick, 1994). B type lamin is the most evolutionarily conserved lamin, with A type lamins appeared in evolution later (Stick, 1992). A type lamins are encoded by a single gene *LMNA* that generates alternative splicing products Lamin A, Lamin C and Lamin A del10 (Lin and Worman, 1993; Machiels et al., 1996). B type lamins are coded by 2 different *LMNB1* (product Lamin B1) and *LMNB2* (product Lamin B2) (Biamonti et al., 1992; Höger et al., 1990; Lin and Worman, 1995; Maeno et al., 1995). Lamin C2 (produced from gene *LMNA* and Lamin B3 (produced from gene *LMNB2*) are expressed in germ cells (Alsheimer and Benavente, 1996; Furukawa and Hotta, 1993; Furukawa et al., 1994) .

1.2.2 Sequence similarities between different lamins

A comparison of protein sequences of Lamins across different organisms reveals greater sequence similarity between different model organisms for the N-terminal rod domain (~18% similarity) which is the domain primarily involved in polymerization of lamin monomers into higher order polymers. The C-terminal regions shows maximum variability across lamins and is the region of binding for most lamin interactors (Dechat et al., 2008; Schirmer and Foisner, 2007; Simon and Wilson, 2013).

Alignments of Lamin A, Lamin C, Lamin B1 and Lamin B2 reveal ~58-60% identity in protein sequences across all lamins (Appendix I).

1.2.3 Domain organization of lamins

All members of the lamin family share a common domain organization characterized by a N-terminal head domain, central rod region and C-terminal tail (Dechat et al., 2008; Dittmer and Misteli, 2011) (Fig. 1.2). The central rod is composed of four alpha helical segments (coils) called 1A, 1B, 2A and 2B.

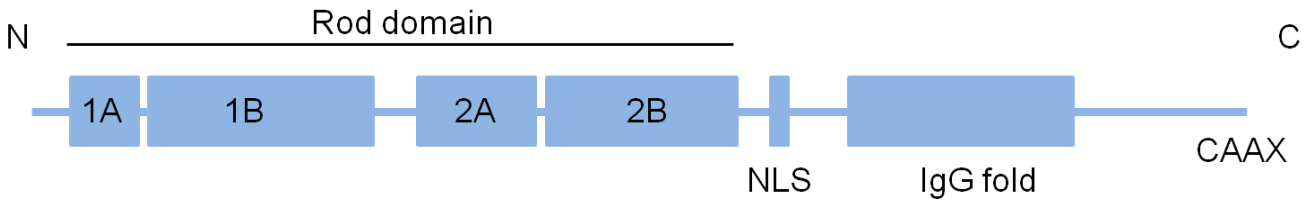

Figure 1.2 Domain map for lamins (for representation purpose only, not to scale)

N terminal – Head – Coil 1A – Linker1- Coil 1B – Linker12 – Coil2A -Linker2 - Coil 2B - Tail – C terminal. (Burke and Stewart, 2013; Dittmer and Misteli, 2011) (Fig. 1.2)

The Tail domain of lamins contains an IgG like fold structure which is an important site of protein – protein interactions (Dhe-Paganon et al., 2002; Krimm et al., 2002). The Nuclear Localization Signal (NLS) is present in between the rod domain and the IgG fold region (Loewinger and McKeon, 1988). The specific domains of Lamin A, Lamin B1 and Lamin B2 are tabulated as follows

Table 1. Sub-domain organization of Lamins (Source of protein sequences: Uniprot)

Domain	Lamin A	Lamin B1	Lamin B2
Head	1-33	2-34	1-48
Rod	34-383	35-386	49-400
Tail	384-664	387-586	401-620

1.2.4 Expression of Lamins

The timing of expression is an important differentiating factor between A and B type lamins. B type lamins are expressed in almost all vertebrate cells while A type lamins are expressed primarily in all differentiated cells (Constantinescu et al., 2006; Röber et al., 1989). Two isoforms of Lamins – Lamin C2 and Lamin B3 are germ cell specific (Alsheimer and Benavente, 1996; Furukawa and Hotta, 1993; Furukawa et al., 1994). Stem cells and undifferentiated cells

were initially thought to show nil Lamin A expression; however more recent evidences revealed low expression of A type lamins in mouse stem cells (Eckersley-Maslin et al., 2013).

Lamin expression is variable across tissue types (Broers et al., 1997; Korfali et al., 2012). The ratio of A: B type lamins is often tissue specific. This ratio correlated well with the mechanical properties of the cell type/nucleus (Swift et al., 2013). Softer tissues such as brain showed a lower expression of Lamin A, while stiffer tissues such as bone show greater expression of Lamin A (Swift et al., 2013). On the other hand, softer tissues such as brain show a greater B type lamin expression (Swift et al., 2013).

An elegant method for quantitating the exact amount of each lamin isoform present in a cell population was developed by Guo et al in 2014. This paper measured the expression levels of lamins in a cell type and showed that the assembly of higher order structures of lamins is dependent on relative expression levels of each of Lamin A, Lamin C, Lamin B1 and Lamin B2. Amongst these, Lamin B1 scaffold was found to assemble first, followed by Lamin B2 and then Lamin A/C (Guo et al., 2014).

1.2.5 Localization of lamins

A and B type lamins are localized primarily beneath the inner nuclear membrane in the form of a highly organized 10nm polymerized structure that forms a filamentous sheath (Aebi et al., 1986) (Fig. 1.3A-B). Lamin meshworks have been visualized in Xenopus cells as also human cells using electron microscopy as well as more recently super resolution microscopy methods. These suggest separate but interacting meshworks formed by each of Lamins A,C,B1 and B2 (Goldberg et al., 2008; Shimi et al., 2008; Shimi et al., 2015). B type lamins are directly anchored to the inner nuclear membrane by farnesyl anchors while A type lamins associate with B type lamins and are anchored to the lamina. In addition to a peripheral pool, a nucleoplasmic pool is also found for both A and B type lamins (Bridger et al., 1993; Broers et al., 1999; Hozák et al., 1995; Moir et al., 2000b; Muralikrishna et al., 2004). This pool for Lamin A is more mobile and freely diffusing as compared to peripheral Lamin A polymer (Moir et al., 2000b). On the other hand, intranuclear B type lamin pools represent more stable structures as compared to A type lamins, as revealed through Fluorescence correlation spectroscopy (FCS) experiments (Shimi et al.,

2008). This reflects a different organizational state for Lamin A/C as against Lamin B1 and Lamin B2. Nucleoplasmic Lamin A and Lamin C are susceptible to salt/detergent extractions while B type lamins are not (Kolb et al., 2011). The oligomerization status of lamins in the nuclear interior is not completely understood. Interference with the oligomerization of Lamin A resulted in reduced incorporation of Lamin A into the peripheral lamina (Zwerger et al., 2015). More recently, an interphase phosphorylation (S22, S392) has been detected for Lamin A which results into its localization into the nuclear interior (Kochin et al., 2014). Interphase phosphorylation for B type lamins has not been explored in details.

Although lamins show a similar localization at the nuclear lamina, Shimi et al first demonstrated that Lamin A and B1/B2 form different yet interacting microdomains at the nuclear periphery (Shimi et al., 2008). Lamin A assembly (localization) is altered in the absence of functional Lamin B1, while Lamin A $^{-/-}$ MEFs show abnormal distribution of Lamin B1 at the nuclear periphery (Sullivan et al., 1999; Vergnes et al., 2004). On the other hand, Lamin A/C distribution was found to be uniform in mice keratinocytes depleted of Lamin B1 and Lamin B2 (Yang et al., 2011). A particular threshold level of each of the Lamins was found to enable its efficient assembly in the nucleus. More recently, advances in super resolution methods in imaging have revealed a difference in the organization of Lamin A, Lamin B1 and Lamin B2 (Shimi et al., 2015). The mesh sizes and assembly kinetics of Lamins A, C, B1 and B2 are different and interdependent (Guo et al., 2014; Shimi et al., 2015). Efficient localization of Lamins A/C and Lamin B2 were shown to be dependent on the correct localization of Lamin B1 in HeLa cells (Guo et al., 2014). Lamin B1 forms mixed heterodimers with mutant Lamin A (progerin) and results in an altered lamina composition as compared to wild type Lamin A wherein Lamin A and Lamin B1 form distinct homopolymers, thereby reiterating an interdependence between lamins for their correct localization (Delbarre et al., 2006). Conversely, Lamin B1 depletion in HeLa cells was shown to form nuclear blebs enriched for Lamin A/C and not Lamin B2, alter the mesh size and assembly of Lamin A as well as Lamin B2 again suggesting a feedback between different lamins with regard to their organization (Shimi et al., 2008).

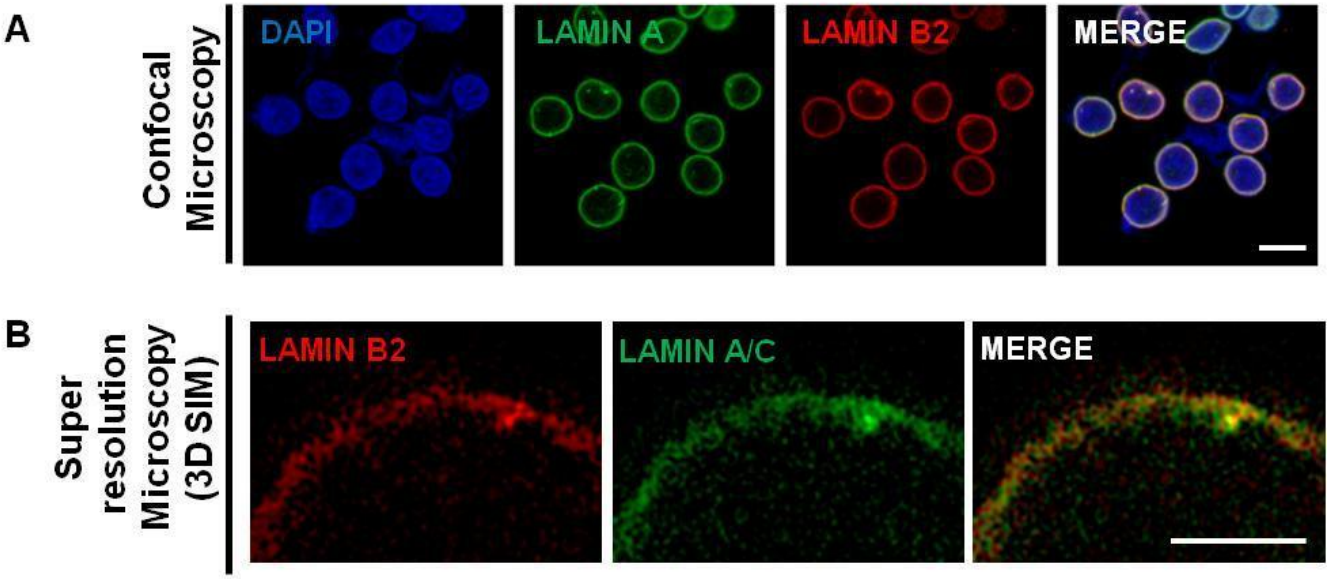

Figure 1.3 Localization of Lamins A and B2 in DLD1 cells

A. Immunofluorescence assay for Lamin A (green) and Lamin B2 (red) in DLD1 cells, imaged with confocal microscope. Scale bar ~10µm. B. High resolution imaging of the nuclear lamina using 3 dimensional structured illumination microscopy (3D-SIM), Scale bar ~5µm

1.2.6 Post translational modifications of lamins

A and B type lamins undergo extensive posttranslational modifications which are important for their efficient localization, polymerization-depolymerization, interactions and function.

Four predominant PTMs are important for lamin localization. The C terminal -CAAX motif is the major site of post translational modifications (Fig. 1.2). The main steps in the modifications are summarized below (Beck et al., 1990; Chelsky et al., 1989; Farnsworth et al., 1989; Holtz et al., 1989; Lutz et al., 1992; Sinensky et al., 1994)

1. Farnesylation – CAAX motif. This is the first step performed by farnesyl transferase in the processing of the immature lamin proteins. This involves addition of a farnesyl anchor to the C of the C terminal CAAX motif.
2. First proteolysis by Rce1/ Zmpste24 - Farnesyl transfer is followed by cleavage of the terminal amino acids as the first proteolysis step.

3. Carboxymethylation - Post proteolysis, the isoprenyl cysteine is methylated by and enzyme ICMT
4. Second proteolysis – This step is seen only during processing of prelamin A, wherein the last 15 amino acids of prelamin A protein is clipped off by Zmpste24.

Steps 1-3 occur in the cytoplasm.

The processed protein is translocated to the nucleus and the enzyme for second proteolysis is localized at the nuclear membrane (Barrowman et al., 2008).

Other posttranslational modifications on lamin protein are listed in Table 2.

PTMs on lamins serve to regulate several aspects of Lamin function. The assembly-disassembly kinetics of lamins is regulated through phosphorylation (Foisner and Gerace, 1993). Modifications such as glycosylation, acetylation are speculated to regulate interactions of lamins with other interacting proteins and chromatin (Simon and Wilson, 2013). Lamins A/C, B1 and B2 show conserved as well as unique phosphorylation sites (Table 2). The conserved sites are localized primarily at the head and tail domains, and are important for mitotic assembly and disassembly of lamins. On the other hand, unique sites are speculated to be involved in specific interactions of Lamins A/C, B1 and B2.

Table 2. Selective post translational modifications of lamins (reviewed by (Simon and Wilson, 2013))

PTM	Residues	Functional significance
Phosphorylation	Mitotic: Lamin A – Ser22, 392,404,406 Lamin B1 – Ser23 Lamin B2 – Ser 37, Thr34 Interphase: Lamin A – Ser 525, Ser- 22, 392 Lamin B2 - Ser407, Ser421 Lamin B1 – Ser Lamin A Tyr-81, Lamin B1 Tyr-359 and Tyr-377, Lamin B2 Tyr-374 and Tyr-515	Mitotic phosphorylation on head and tail regions results in disassembly of lamin polymers. Unknown Unknown
SUMOylation	Lamin A/C: SUMO1 – Lys 420, Lys486 SUMO2 – Lys201	Lamin A filament assembly and localization
Ubiquitinylation	Lamin A: Lys-97, Lys-108, Lys-270, Lys-311, Lys-378, Lys-417, Lys-450), four Lamin B1: Lys-123,157,271,483, and two Lamin B2: Lys-81,520.	Polyubiquitinylation regulates lamin turnover. Significance of mono ubiquitinylation is unknown.
Acetylation	Lamin A: Lys-97,108,114,270,311,378,417,	Unknown. Speculated to impact chromatin tethering

	450 Lamin B1: Lys-33,123,157,181,271,483 Lamin B2: Lys-47,81,393,520	activity of lamins.
Oxidation	Lamin A - Cys-522, Cys-588 and Cys-591	Mutants for these cysteine residues show premature senescence
O-GlcNAcylation (β-O-linked N-acetylglucosamine addition)	Lamin A - Ser-612 and Thr-643 (human cells)	Unknown

1.2.7 Assembly of higher order lamins

Lamins A/C, B1 and B2 show a conserved polymerization cascade to form the ~10 nm thick nuclear lamina. Each lamin monomer associates with another monomer at the coiled-coil regions of the rod domain. Such dimers of lamins associate in a head-to-tail manner to give rise to the lamin filament arrays (Heitlinger et al., 1991; Heitlinger et al., 1992). Lamin filament arrays assemble in an antiparallel manner to form the Lamin proto-filament (Gieffers and Krohne, 1991). Several protofilaments associate together to form the lamina. This assembly pattern post synthesis of lamins is conserved for all lamins (Stuurman et al., 1998).

The polymerized lamina undergoes reversible disassembly at mitosis through phosphorylation of lamins (Heald and McKeon, 1990; Peter et al., 1990). The kinetics of reassembly post mitosis vary between A and B type lamins A type lamins polymerize slower than B type lamins, and are often found as circulating pools in early G1 (Moir et al., 2000b). The structure of the lamin criss cross network formed inside cells is also different for Lamin A and Lamin B2, with Lamin A forming a thicker and a more ordered lattice as compared to Lamin B2 (Goldberg et al., 2008). Each lamin polymer can assemble independent of other lamins, when a

critical amount of Lamin expression is present (Guo et al., 2014). Lamins predominantly show a homo dimerization pattern, and higher order assembled polymers interact with each other (Delbarre et al., 2006; Schirmer and Gerace, 2004; Schirmer et al., 2001). In progeroid cells, the misfolded progerin molecule was found to heterodimerize with B type lamins (Delbarre et al., 2006). The cumulative strength and stability of the lamina is determined by efficiently formed lamin filaments contributed by each of Lamin A, C, B1 and B2 and may thus explain the variability in lamina strength across tissue types (Schirmer and Gerace, 2004).

1.2.8 Multiple connections of Lamins

1.2.8.1 Interactions with proteins

A and B type lamins contribute to nuclear structure by associating with numerous proteins and forming stable protein complexes (Gruenbaum and Medalia, 2015) (Fig. 1.4). Distinct unique sets of proteins are bound by A and B type lamins at the nuclear periphery and the nuclear interior in interphase. Moreover, both A and B type lamins show reversible phosphorylation dependent disassembly during mitosis (Foisner and Gerace, 1993). Thus, A and B type lamins show a variety of states in different phases of the cell, and each state shows associations with a variety of proteins. A and B type lamins have a structural similarity in terms of their domain organization of head – rod – tail domains (Dechat et al., 2008; Dittmer and Misteli, 2011). Regions across the rod domain of lamins are important for polymerization (homo and hetero) between and across lamins (Schirmer et al., 2001; Zwerger et al., 2015). Thus, Lamins A, C, B1 and B2 interact with each other via the rod domain. At the junction of the rod domain and C terminal tail lies the IgG domain. Flanking the IgG domain is the region showing maximum amino acid variability across Lamins. This region harbors binding sites for a host of proteins associated with lamins, and for interactors specific to A and B type Lamins (Simon and Wilson, 2013).

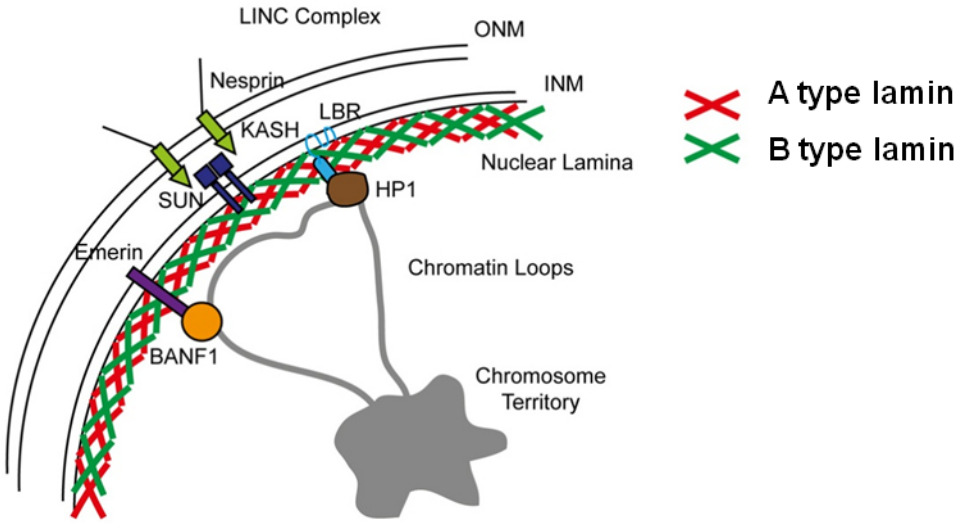

Figure 1.4 Schematic depicting selected Lamin associations at the nuclear periphery (for representation purpose only, not to scale)

1.2.8.2 Interactions with chromatin

Lamins bind to chromatin at distinct domains referred to as 'lamina associated domains' (LADs) which are ~0.1-10Mb stretches of chromatin characterized by H3K9me2/3 marks, low density of coding genes, high density or repeats and late replicating regions (Guelen et al., 2008; Harr et al., 2015; Towbin et al., 2012; Zullo et al., 2012).

Broadly, protein interactors of lamins can be classified as stable structural proteins at the nuclear membrane, transcription factors, DNA replication machinery, DNA repair proteins. Selective interactors of A and B type lamins are listed in Tables 3.1-3.2 (Fig. 1.5). In this work, we have confined ourselves to the interactors of Lamins involved in maintenance of nuclear and chromosome structure. The structural stability imparted by Lamins to the nucleus, are executed partly by Lamin interactors such as LINC Complex (Linker of nucleoskeleton and cytoskeleton) (Booth et al., 2015; Brosig et al., 2010). Interaction of Lamins at the lamina with 'Lamina associated domains' (LADs) of chromatin are also assisted by interactors of Lamins including

Emerin, Lamin B receptor, Lamina associated polypeptide (LAP2B) which also bind to LADs and impart functional redundancy between nuclear proteins (Amendola and van Steensel, 2015; Guelen et al., 2008).

Table 3.1. Selected interactors of A type lamins at the nuclear periphery and nucleoplasm (Gruenbaum and Medalia, 2015, Simon and Wilson, 2013, Dechat et al., 2008)

No.	Interactor	Site of interaction
1	Lamina associated polypeptide 2 (LAP2A)	Nucleoplasm
2	Retinoblastoma protein	Nucleoplasm
3	Nuclear matrix proteins	Nucleoplasm
4	BANF1	Nucleoplasm
5	Actin	Nuclear periphery and Nucleoplasm
6	Lamin B1/B2	Nuclear periphery
7	Emerin	Nuclear periphery
8	MAN1	Nuclear periphery
9	Nucleoporins	Nuclear periphery
10	Transcription factors - c-Fos, Jun, SREBP1	Nuclear periphery and Nucleoplasm
11	LINC Complex	Nuclear periphery

Table 3.2. Selected interactors of B type lamins at the nuclear periphery and nucleoplasm

(Gruenbaum and Medalia, 2015, Simon and Wilson, 2013, Dechat et al., 2008)

No.	Interactor	Site of interaction
1	Heterochromatin binding protein 1 (HP1)	Nuclear periphery
2	Lamin B Receptor (LBR)	Nuclear periphery
3	Lamina associated polypeptide 2 beta (LAP2B)	Nuclear periphery
4	Transcription factor Oct1	Nuclear periphery
5	PCNA	Nucleoplasm
6	Nucleophosmin	Nucleoplasm
7	Actin	Nuclear periphery and Nucleoplasm

1.2.9 Functions performed by Lamins

1.2.9.1 Contribution to nuclear organization through formation of LADs

LADs collectively refer to chromatin bound by the nuclear periphery factors - Lamins, LBR, LAP2β, Emerin. LADs were found to be conserved in 70% of all cell types (Meuleman et al., 2013). Facultative LADs are uniquely bound by each of Lamins A/C, B1, and B2 (Meuleman et al., 2013). B type lamins LADs are primarily heterochromatic, while chromatin bound by A type lamins include both euchromatin and heterochromatin (Gesson et al., 2016; Lund et al., 2015). The density of LADs was highest on heterochromatin rich chromosome 18 and lowest on gene rich chromosome 19 (Guelen et al., 2008). The length of LADs ranges from ~0.1-10Mb (average 0.5 Mb) and LAD boundaries are sharp and demarcated by binding sites for insulator protein CTCF, suggesting the involvement of Lamins with insulator proteins in mediating organization of the genome (Guelen et al., 2008). Formation of LADs is one scale of contribution by lamins to genome organization. LADs are enriched for LSS (lamina specific sequences) which show enrichment for the GAGA motif (Zullo et al., 2012). This motif enables the binding of a transcriptional repressor c-Krox which in turn binds to LAP2beta and mediates recruitment to nuclear periphery (Zullo et al., 2012). This is mediated by recognition of histone mark H3K9me2 by the enzyme G9a. Thus, presence of the GAGA motif directs the association of a genomic contig to the nuclear periphery.

LADs are primarily localized at the nuclear periphery (Guelen et al., 2008). However, more recently a live imaging system developed for visualizing LADs using the m6A-Tracer revealed that LADs are not solely confined to the nuclear periphery, and are stochastic (Kind et al., 2013). In fact, daughter cells and mother cell often do not share the exact same profile of LADs (Kind et al., 2013). LAD profiles of cells undergo changes during differentiation, with genes pertinent for the particular development being upregulated and released from LADs (Peric-Hupkes et al., 2010).

Genes within LADs are typically found to be transcriptionally repressed (Guelen et al., 2008). Thus, lamin binding confers a state of transcriptional repression to genes. However, genes do retain their transcriptional competence even when they are targeted to LADs. In other words,

proximity to the lamina confers a repressive environment to genes, however, genes can still transcribe within a LAD.

1.2.9.2 Regulation of chromosome positioning

Both A and B type lamins are implicated in the positioning of chromosomes in the interphase nucleus (Malhas et al., 2007; Meaburn et al., 2007; Mewborn et al., 2010; Tang et al., 2008). Specifically, a loss of functional Lamin B1 was associated with a repositioning of mouse chromosome 18 towards the nuclear interior (Malhas et al., 2007). Lamin A/C mutation E161K is also associated with a more internal repositioning of human chromosome 13 (Mewborn et al., 2010). Both these cases are associated with a deregulation of gene expression from clusters on the repositioned chromosomes. HeLa cells depleted of Lamin B1 are also associated with repositioning of gene rich chromosome 19 territories towards the nuclear periphery (Shimi et al., 2008; Tang et al., 2008). Laminopathy cells are also associated with a loss of chromosome positioning for a variety of chromosomes (Meaburn et al., 2007).

1.2.9.3 Regulation of transcription

Lamins A/B1 and B2 bind to chromatin at LADs and maintain a repressive state of chromatin at the nuclear periphery. Targeting of Lamins to promoters modulates the transcription state of the target gene and confers a repressive state to the gene (Finlan et al., 2008; Schlimgen et al., 2008). Artificial targeting of reporter LacO gene loci to the lamina also represses the gene. Certain exceptions have been noted for this repressive active, suggesting that genes targeted to the lamina do retain their transcriptional competence despite residing in a generally transcriptionally repressive environment (Kumaran and Spector, 2008). However, the vast majority of genes bound by lamins at the nuclear lamina show a transcriptional repression as shown for T cell receptor genes (Schlimgen et al., 2008). Developmental progression models have suggested that LADs undergo shuffling during differentiation into specific tissue types as shown for neuronal differentiation models (Peric-Hupkes et al., 2010). Genes required for differentiation into

neuronal lineage were depressed through loss of anchorage from the lamina, thereby reiterating the transcriptional regulatory role for lamins (Peric-Hupkes et al., 2010).

In addition to a regulation of transcription through direct chromatin binding, Lamins also regulate RNA Polymerase II transcription (Tang et al., 2008). A scaffold like activity has been suggested for lamins wherein lamins act as a docking site for RNA Polymerase and associated transcription factors (Spann et al., 2002). A depletion of lamins results in a delayed recruitment of general transcription factors, suggesting a role for lamins in the maintenance of general transcription. Alongwith general TFs, Lamin A also binds to and sequesters TFs such as c-Fos, AP-1, SREBP1 (Ivorra et al., 2006; Lloyd et al., 2002). These TFs are bound by Lamin A and sequestered at the nuclear periphery (Heessen and Fornerod, 2007). Upon specific signaling cues, these TFs are released from the lamin anchor and their target genes are activated.

1.2.9.4 Role of nuclear lamins in DNA replication

Purification of DNA replication foci also reveals the presence of lamins (Kennedy et al., 2000). Lamin A stabilizes DNA replication forks by imparting a structural stability to the replication fork. Biochemically, Lamin A and B1 interacts with DNA Polymerases and PCNA (Shumaker et al., 2008; Vaara et al., 2012). Loss of Lamin A results in a collapse of these foci and often slows replication as seen in Lamin A deficient MEFs and progeria mutations (Cobb et al., 2016; Singh et al., 2013). Incorporation of errors during replication is also greater in cells with lowered Lamin A expression. The importance of Lamin A in replication is also illustrated through cells with mutant Lamin A (progerin) which show replication errors and proliferation arrest. B type lamins also contribute to a scaffold like activity at replication foci. The tail domain of B type lamins possesses binding sites for PCNA (Shumaker et al., 2008).

1.2.9.5. Repair pathways of DNA damage

Lamin A is an important molecule for recruitment of DNA repair proteins 53BP1 at sites of double strand breaks. Lamin A mutant (G608G - progeria mutation) MEFs show a delayed efficiency of repair, through a delayed recruitment of 53BP1 and Rad51 to gamma H2AxX foci

(Liu et al., 2008; Redwood et al., 2011). Moreover, Lamin A deficient MEFs as also cells with Lamin A mutation G608G show decreased telomere length and altered telomere dynamics, suggesting a role for Lamin A in the NHEJ pathway which otherwise serves to repair telomere ends during S phase (Gonzalez-Suarez et al., 2009; Huang et al., 2008; Liu et al., 2005). The positional stability of DNA repair foci is also maintained by a Lamin A nucleoskeleton (Mahen et al., 2013). Nucleotide Excision Repair (NER) proteins such as DDB1, CSB and PCNA are downregulated in Lamin B1 depleted cells (Butin-Israeli et al., 2013). Lamin B1 is involved in homologous recombination based DNA repair pathways as also binds to the promoter of and regulates the expression of key DNA repair proteins including BRCA1 and Rad51 (Butin-Israeli et al., 2015; Liu et al., 2015). Taken together, Lamins are involved in various pathways of DNA repair, either as a scaffold that serves to recognize and recruit factors in DNA repair or in epigenetically regulating the transcription of genes involved in DNA repair.

1.2.9.6 Lamins in cell cycle and senescence

A and B type lamins show a functional divergence during cell cycle transitions. Although both A and B type lamins show a mitotic phosphorylation which results in their disassembly and monomerization, A type lamins are solubilized in the cytoplasm while monomers of B type lamins are retained in membranes of the ER during mitosis (Heald and McKeon, 1990). The sites of mitotic phosphorylation are listed in Table 2. Cyclin dependent kinases (Cdk) bring about mitotic phosphorylation (Peter et al., 1990). During mitosis, Lamin A forms a regulatory complex with LAP2A-BAF, which functions to regulate chromosome segregation (Qi et al., 2015). B type lamins also localize to the mitotic spindle, as also form a matrix around the spindle (Goodman et al., 2010; Kuga et al., 2014; Tsai et al., 2006). This localization of B type lamins also has regulatory functions with regard to chromosome segregation. During envelope reassembly, B type lamins assemble first on chromosomes followed by A type lamins which are found in a circulating pool in the nucleus till early G1 (Moir et al., 2000b).

After reassembly into polymers, lamins are found in a stable network at the nuclear lamina and also in the nucleoplasm throughout interphase. Lamin A forms a regulatory complex with Rb and Lap2alpha in the interphase (Ozaki et al., 1994) . This complex serves to regulate cellular

transitions from the G1 phase to S phase. Release of Rb from this complex results in signaling to the transition from G1 to S phase (Pekovic et al., 2007).

B type lamins are associated with senescence. Senescent cells are associated with a downregulation of Lamin B1 (Freund et al., 2012; Shimi et al., 2011). Chromatin domains that are reorganized during senescence overlap largely with Lamina associated domains (LADs) of Lamin B1, suggesting an involvement of lamins during senescence (Shah et al., 2013).

1.2.9.7 Mechanosignaling

The role of lamins as mechanosignaling factors is through their role at the interface of the cytoskeleton and the nucleus. Lamin A associates with the cytoskeleton via the LINC complex (SUN-KASH domain proteins) which binds to Lamin A on the nuclear side and to the actin cytoskeleton on the cytoplasmic side (Haque et al., 2006; Ostlund et al., 2009; Zhen et al., 2002). The LINC complex serves to perceive mechanical signals from the cytoskeleton and relay them to the nucleus (Brosig et al., 2010). SUN1 is mislocalized in cells with mutant Lamin A (G608G), thereby suggesting an important role for Lamin A in maintaining the integrity of the LINC complex (Chen et al., 2012). Concomitantly, cells with Lamin A deficiency or mutation (early aging syndrome - progeria) show altered mechanical properties, and low resistance to deformations (Dahl et al., 2006; Lammerding et al., 2004; Lammerding et al., 2006). Nuclear deformations also increase upon loss of a functional Lamin A, while nuclei show greater rotational motion upon Lamin B1 depletion (Ji et al., 2007; Taimen et al., 2009). The expression of Lamin A scales with mechanical properties of the cells (Swift et al., 2013). Softer tissues (such as brain) have a lowered Lamin A expression as compared to stiffer tissues (such as bone) (Swift et al., 2013). The ratio of A:B type lamin is variable across cell types and is often a determinant of mechanical properties of the cells. In addition, Lamin A shows phosphorylation in response to changes in extracellular matrix stiffness (Buxboim et al., 2014). The expression of B type lamins is a determinant of elastic properties of nuclei, while that of A type lamins determines deformability of nuclei (Dahl et al., 2006; Ferrera et al., 2014; Pajerowski et al., 2007).

1.3 Lamins in disease

Two kinds of diseases are associated with lamins – laminopathies and cancers. Laminopathies is a group of diseases resulting from mutations in Lamin proteins; primarily Lamin A (Schreiber and Kennedy, 2013). Cancers on the other hand are associated primarily with altered expression levels of lamins, although literature on cancer specific lamin mutations is emerging (Bell and Lammerding, 2016). Data from patients of these diseases has yielded insights into the functional aspects of Lamins with regard to nuclear structure and function.

1.3.1 Laminopathies

Mutations in lamins are associated with a group of diseases collectively called 'laminopathies' (Burke and Stewart, 2002). Laminopathies include muscular and skeletal dystrophies, cardiomyopathies, leukodystrophy, lipodystrophy and early aging syndromes (Burke and Stewart, 2002).These diseases result out of point mutations in nuclear envelope proteins viz; Lamins and Emerin. Over 100 different mutations have been mapped to Lamin A, which result in laminopathies. Mutations associated with dystrophies map to the rod domain of Lamin A while those associated with aging primarily map to the tail domain and the connecting IgG fold between rod domain and C terminal tail. Molecularly, mutations in the rod domain of Lamin A impact its polymerization kinetics while that near the C terminal result in aberrant posttranslational modifications.

The phenotypic spectrum of laminopathies is often tissue specific, suggesting a role for tissue specific interactions of Lamin A, which get disrupted in laminopathies. Extensive characterization of these mutant lamins and their phenotypes has revealed nuclear shape changes, loss of heterochromatin organization and chromosome repositioning, gene expression changes, loss of interactions, defects in DNA damage repair and altered mechanical properties of tissues (Bercht Pfleghaar et al., 2015; Dahl et al., 2006; Liu et al., 2008; McCord et al., 2013).

Loss of telomere integrity, defective repair responses to DNA damage and premature senescence are among the primary genomic instability phenotypes reported for progeroid cells (Benson et al., 2010; Gonzalez-Suarez et al., 2009; Gonzalo and Kreienkamp, 2015). Progeroid cells show delayed repair of DNA DSB (double strand breaks) as seen through persistent gamma H2AX signals and delayed recruitment of Rad51 (HR pathway) and 53BP1(NHEJ pathway) (Redwood

et al., 2011). Delay in activation of these pathways and persistent signaling result in checkpoint activation and cell cycle arrests. Telomere attrition and altered telomere dynamics is also an important parameter contributing to genomic instability in laminopathy cells (Decker et al., 2009; De Vos et al., 2010). This is also attributed to a defective NHEJ pathway which otherwise is responsible for capping and protecting of telomere ends during DNA replication.

Laminopathy cells show altered nuclear shapes, blebbing and defective lamin assembly (Taimen et al., 2009). Progerin interferes with the homo and hetero-dimerization of lamins, resulting in a weakening of the lamina at the nuclear periphery (Delbarre et al., 2006). Primary laminopathy fibroblasts show altered chromosome positioning (Meaburn et al., 2007). In addition, epigenetic changes in progeroid cells include a loss of peripheral H3K27me3 and H3K9me3 marks (McCord et al., 2013). Progeroid cells show lowered HP1alpha and EZH2 levels and thus show an overall loss of heterochromatin organization (McCord et al., 2013). The interaction between Lamin A and LAP2α is reduced with the mutant Lamin A (progerin) (Chojnowski et al., 2015). In addition, mechanical properties of nuclei are altered in progeroid cells (Booth et al., 2015; Zhong et al., 2010).

1.3.2 Cancers

Changes in expression levels of lamins have also been associated with several cancers in a tissue specific manner. Expression of Lamin A is lower in aggressive breast cancer and ovarian cancers (Capo-chichi et al., 2011a; Matsumoto et al., 2015). In prostate cancers however, differential data has been presented on the levels of Lamin A. An overexpression of Lamin A is associated with a more aggressive phenotype in one report, while another study suggested a correlation between downregulation of Lamin A/C and B2 (Kong et al., 2012; Saarinen et al., 2015). Similarly, there are conflicting reports on the levels of Lamin A with respect to colon cancers. While an overexpression of Lamin A is associated with a greater migratory potential and a more aggressive phenotype, several other studies involving patient datasets suggest a correlation between lower expression of Lamin A correlated with increased relapses and more invasiveness for colon cancer cells (Belt et al., 2011; Foster et al., 2011; Moss et al., 1999; Willis et al., 2008; Wu et al., 2009). Lamin B1 was found to a biomarker for liver cancer cells (Sun et al., 2010).

With regard to Lamin B2, a greater expression of Lamin B2 is associated with greater chromosomal stability as compared to colon cancers with chromosomal instability (Kuga et al., 2014). Lamins A/C as well as Lamin B2 are associated with maintenance of chromosomal ploidy in different kinds of cancers viz; Lamin A/C is associated with chromosomal stability in ovarian cancers and Lamin B2 in colon cancers (Capo-chichi et al., 2011a; Kuga et al., 2014). Furthermore, cancer cells also show properties of altered nuclear shapes, increased genomic instability and enhanced cellular migration, all of which are associated with Lamins. However, there is limited data on the precise contribution of lamins to chromosome organization and genomic stability in cancer cells.

1.4 Open questions

Despite extensive work on the role of nuclear lamins with regard to organization of the nucleus, several questions are still unanswered. An important question among these is whether different lamins A/C, B1 and B2 contribute differentially or similarly to maintenance of chromosome positioning? Do lamins possess cell type specificity in this regard? Does the relative stoichiometry of lamins influence the regulation of lamins towards chromosome positioning? The role of Lamin B2 in the maintenance of chromosome positioning has not been examined in detail. In addition, there has been no study that does a comparative examination of the role of A and B type lamins with regard to nuclear organization in the same cell system.

A variety of studies have documented an impact of Lamin A/C or Lamin B1 depletion on the positioning of chromosomes. However, the exact nature of the contribution of lamins towards the positioning of different chromosomes is unclear. It is not known whether Lamins, owing to their overarching role in the maintenance of nuclear structure, regulate the positions of chromosomes at the nuclear periphery (gene poor) and those at the nuclear interior (gene rich) similarly or differentially. Does the regulatory influence of lamins on chromosomes extend beneath the nuclear periphery into the nuclear interior? Do lamins possess similar or differential regulatory roles towards whole chromosomes (megabase pairs of DNA) as against gene loci (kilobase pairs of DNA) with regard to spatial positioning in the nucleus? Moreover, it is also unknown whether

a lamin dependent regulation on the positioning of chromosomes or gene loci is also a determinant of its functional (transcriptional) state.

Both A and B type associate with numerous structural proteins of the nucleus including LBR, Emerin, LINC complex, LEMD proteins, nuclear matrix proteins among others. The contribution of these lamin associated proteins in the maintenance of chromosome positioning has also not been characterized in detail. It is unclear whether specific lamin associated protein complexes such as those formed by LINC Complex, LEMD proteins impinge on the positioning of chromosomes? Do differential protein complexes formed by Lamin A/C as against Lamin B1 or Lamin B2 have differential contribution towards chromosome positioning?

Taking these broad unknown areas of the field into consideration, we aimed to characterize and compare the relative contribution of Lamins A/C, B1 and B2 towards different aspects of chromosome positioning and function (transcription) and stability. The following sub-aims were designed towards this central aim in the project:

To examine the role of Lamins in:

I. Transcriptional regulation
II. Regulating the spatial organization of transcriptionally deregulated chromosomes
III. Maintenance of genomic stability
IV. To investigate the role of lamin dependent interactors in maintenance of chromosome positions

Chapter 2: Materials and Methods

2.1 Methods commonly used throughout the study

2.1.1 Cell Culture – Maintenance of cell lines

All cell types were maintained in the respective medium at 37ºC with 5% CO_2. Cells were split at ~70-80% during maintenance and used at passages 3-15 for seeding for experiments. For non cancerous cells, the cells were slow growing and were split at ~50-60% confluence.

Table 4. Cell lines used in this study

No.	Name	Origin	Source	Disease state	Cell culture media used
1	DLD1	Colorectal adenocarcinoma	Dr. Thomas Ried Lab, NIH, USA	Cancer Cell line	RPMI + 10% FBS
2	SW480	Colon carcinoma	Dr. Thomas Ried Lab, NIH, USA	Cancer Cell line	DMEM + 10% FBS
3	HCT116	Colorectal carcinoma	Dr. Mayurika Lahiri Lab, IISER Pune, India	Cancer Cell line	DMEM + 10% FBS
4	A549	Lung adenocarcinoma	Dr. Amit Dutt Lab, ACTREC, India	Cancer Cell line	DMEM + 10% FBS
5	HT1080	Fibrosarcoma	ATCC	Cancer Cell line	DMEM + 10% FBS
6	CRL 1790	Colon epithelium	ATCC	Normal	MEM + 10% FBS
7	CRL 1541	Colon fibroblast	ATCC	Normal	MEM + 10% FBS

2.1.2 Karyotypic validation of cell lines

The ploidy of cell lines was validated through DAPI karyotyping (Appendix II). The details are summarized in Table 5. For normal colon cells, CRL1790, CRL 1541, karyotyping could not be performed efficiently due to a low mitotic index. However, 3D FISH performed on these cells revealed presence of two copies of chromosome 19 (Fig. 4.10).

Table 5. Karyotypic validation of all cell lines used in this study

No.	Cell line	Modal chromosome number documented in literature	Modal chromosome number determined by DAPI karyotyping
1	DLD1	44-46	45-46
2	SW480	52-58	57
3	HCT116	44-46	44
4	A549	66	66
5	HT1080	46	45-46

Data acknowledgements for karyotyping:

HCT116: Maithilee Khot

A549: Maithilee Khot

HT1080: Sishil Sushanth

2.1.3 siRNA and shRNA mediated knockdowns

The sequences of the siRNA oligonucleotides targeting Lamins are as follows: si*LMNA/C*: 5'-CAGUCUGCUGAGAGGAACA-3', si*LMNB2*: 5'- GAGCAGGAGAUGACGGAGA-3', si*LMNB2.2*: 5'-GCAAGUUUGUGCAGCUCAA-3', si*LMNA/C* scrambled: 5'-GAUGAGGCGGUUAGAUGUA-3', si*LMNB2.1* scrambled: 5'-GGAAGCGUAGACGGAAGAG-3', si*LMNB1*: 5'- AGACAAAGAGAGAGAGAUG-3', si*EMD1*: 5'- UCUGACUUGAAUUCGACUA-3' and si*EMD2*: 5'-UCCCAGAUGCUGACGCUUU-3', si*LACZ*: 5'- CGUACGCGGAAUACUUCGA-3'. DLD1 cells were transfected with 100 nM siRNA oligonucleotide using Lipofectamine RNAiMax (Invitrogen 13778-075) or DharmaFECT in media with reduced serum (OptiMEM, Invitrogen Cat. No. 31985-070). Control siRNAs used were On-target Plus non-targeting siRNA controls (Dharmacon- D-001810-01-20, D-001810-02-20) or siLac*Z*: 5'-CGUACGCGGAAUACUUCGA-3', positive control is an siRNA against the gene *PLK1* (si*PLK1*) - polo like kinase – 5'-UGACCUACAUCGACGAGAA-3'. The uptake of transfection mix was for 6 hours, followed by replenishment of complete growth medium. The total duration of the knockdown was for 48 hours at 37°C.

shRNA transfections were performed using Lipofectamine LTX and PLUS reagent. shRNAs were procured from Sigma as a part of pLKO1 vectors which code for shRNA. The sequences for shRNAs were as follows shLMNB2: CCGGCGGCAGTTCTTTGTTAAAGATCTCGAGATCTTTAACAAAGAACTGCCGTTTTT G and

shLMNA:CCGGCCCACCAAAGTTCACCCTGAACTCGAGTTCAGGGTGAACTTTGGTGG GTTTTTG. DLD1 cells were transfected with 6-8 ug of the plasmids using medium with reduced serum (OptiMEM). The uptake of transfection mix was for 6 hours, followed by replacement of complete growth medium. At 48 hours post transfection, cells were subjected to selection by Puromycin (2ug/mL for DLD1 cells). Colonies that were puromycin resistant emerged at 7-8 days post selection. These colonies were picked up using cloning discs and cultured in separate dishes. Colonies were screened for knockdown and positive colonies used for further assays.

For a combined knockdown of Lamin A/C with Emerin, the siRNA protocol followed was as follows:

siRNA transfection mix was prepared using Lipofectamine RNAimax in reduced serum medium - Opti MEM (Invitrogen Cat No. 31985-070). For the transfections, 0.2 X 10^6 cells were plated with the siRNA transfection mix for EMD (EMD1 and EMD2 oligos at 50nM conc each) on day 1. The detailed steps for combined depletion of Lamin A/C with Emerin are summarized as

Day 1: EMD knockdown (Kd) set up with EMD1 and EMD2 oligos at 50nM conc each

Day 2: EMD Kd pulse set up with EMD1 and EMD2 oligos at 50nM conc each for single EMD Kd. For single LMNA Kd, 100nM of LMNA siRNA used. For combined depletion between EMD and LMNA, EMD oligos (50nM each) and LMNA oligo (100nM each) were used.

The uptake of these mixes was allowed for 48 hours, followed by medium change. Cells were harvested for assays 24 hours after medium change.

2.1.4 Western blotting

Cell lysates were prepared using Radio Immuno-Precipitation Assay (RIPA) Buffer and quantified using BCA (Bicinchoninic Acid) Kit (Pierce, Cat. No.23225). Equal amounts of the protein were boiled in 4X Laemmli Buffer and resolved on a 10% acrylamide-bisacrylamide gel. The protein was transferred to an activated PVDF membrane at a constant voltage of 90V for 90 minutes. The membrane was blocked in 5% non-fat dried milk prepared in 1X Tris Buffered Saline-Tween20 (1X TBST) for 1 hour at RT. Primary antibodies used have been tabulated. Antibody dilutions were prepared in 0.5% non-fat dried milk in 1X TBST and incubated overnight at 4°C or for 3 hours at RT. Secondary antibodies used were sheep anti-mouse IgG-HRP (GE cat no NA9310V, 1:5000) and donkey anti rabbit IgG HRP (GE NA9340V, 1:10000) for 1 hour at RT. Blots were developed using chemiluminescent substrate -GE ECL Prime (89168-782), Thermo ECL Western Blot Substrate (32132) and images were acquired at incremental exposures of 10 seconds under a chemiluminescence system (LAS4000, GE).

Table 6. Primary antibodies used for western blotting

No.	Antibody	Dilution used
1	Rabbit anti-Lamin A (ab26300)	1:1000
2	Rabbit anti-Lamin A/C (Epitomics 2966-S)	1:5000
3	Mouse anti-Lamin A/C (Jol2 ab40567)	1:200
4	Rabbit anti-Emerin (Millipore 06-1052)	1:3000
5	Rabbit anti-Emerin (ab40688)	1:1500
6	Rabbit anti-MYO1C (ab51261)	1:1000
7	Mouse anti-Lamin B2 (ab8983)	1:400
8	Mouse anti-Actin (ab3280)	1:400
9	Rabbit anti-Lamin B1 (ab16048)	1:1000
10	Rabbit anti-GAPDH (G9545)	1:5000
11	Rabbit anti-ERK 1/2 (Cell Signaling- 9102)	1:1000
12	Rabbit anti-pERK 1/2 (Cell Signaling-9101)	1:1000

2.1.5 Immunofluorescence Assay (IFA)

Cells grown on coverslips (18X18 or 22X22 mm^2) were briefly washed using 1X Phosphate Buffered Saline (PBS, pH 7.4) (5 minutes, twice at RT) followed by cold cytoskeletal (CSK) Buffer (0.1 M NaCl, 0.3 M Sucrose, 3 mM $MgCl_2$, 10 mM PIPES (pH 7.4), 0.5%Triton-X-100) treatment on ice for 5 minutes. Cells were fixed in 4% Paraformaldehyde (PFA) (prepared in 1XPBS, pH 7.4) followed by permeabilization in 0.5% Triton-X-100 (prepared in 1X PBS) for 10 minutes. Blocking was performed for 30 min using 1% Bovine Serum Albumin (BSA) in 1X PBS at RT. Primary antibodies used are summarized in Table 7. Antibody dilutions were prepared in 0.5% BSA in 1X PBS, and incubated for 90 minutes at RT. Secondary antibodies

used were goat anti-rabbit IgG-Alexa 488 (Invitrogen (A-11034) 1:1000) and goat anti-mouse IgG-Alexa 568 (Invitrogen (A-11004) 1:1000) for 1 hour at RT. Cells were counter stained with DAPI (4',6-diamidino-2-phenylindole) for 2 minutes at RT, washed in 1X PBS, mounted in Slowfade Gold Antifade (Invitrogen S36937) and stored in 4°C until they were imaged. Quantification of fluorescence intensities of the acquired imaged was performed using Image J with line-scans manually drawn across nuclei.

Table 7. Primary antibodies used for IFA

No.	Antibody	Dilution used
1	Rabbit anti-Lamin A (ab26300)	1:1000
2	Rabbit anti-Lamin A/C (Epitomics 2966-S)	1:300
3	Mouse anti-Lamin A/C (Jol2 ab40567)	1:50
4	Rabbit anti-Emerin (Millipore 06-1052)	1:500
5	Rabbit anti-Emerin (ab40688)	1:500
6	Rabbit anti-MYO1C (ab51261)	1:75
7	Mouse anti-Lamin B2 (ab8983)	1:600
8	Rabbit anti-Lamin B1 (ab16048)	1:500
9	Rabbit anti-H3K27me3 (07-449)	1:500

2.1.6 RNA extraction and qRT-PCR

RNA extraction was performed using PureLink RNA Mini Kit (12183018A) or using TRIzol Reagent (Invitrogen). cDNA was synthesized using Inprompt II Reverse Transcriptase system (Promega A3800). Quantitative real time PCR was performed using SyBr Green (SAF Labs). Sequences of all primers used are listed in Appendix IV. *ACTIN*, *GAPDH* served as internal controls.

2.1.7 Plasmid and Bacterial Artificial Chromosome (BAC) DNA extraction

Table 8. List of plasmids used in the study

No.	Name of plasmid	Source
1.	pEGFP-Lamin A	Dr. Kaushik Sengupta, SINP, Kolkatta, India
2	Lamin B2-GFP	Dr. Tomonaga T, National Institute of Biomedical Innovation, Osaka, Japan
3	Lamin B2-mCherry	Dr. Tomonaga T, National Institute of Biomedical Innovation, Osaka, Japan
4	pLKO shLamin A 1-5	Sigma (TRCN0000061833-TRCN0000061837)
5	pLKO shLamin B2 1-5	Sigma (TRCN0000072418-TRCN0000072422)
6	H2A- mCherry	Dr. Michael Davidson (Addgene plasmid # 55054)

For plasmid DNA extraction, ~250 ml bacterial cultures were grown overnight at 37ºC at 200 rpm shaking. Extraction of DNA was performed using PureLink Maxiprep DNA Extraction Kit (Invitrogen), eluted in TE and used for transfecting mammalian cells.

Table 9. List of BAC DNA clones used in this study

No.	Name	Genes covered
1	RP11- 298C17	ANGPTL6, DNMT1, PPAN, ICAM4, S1PR2, P2RY11, SNORD105B, EIF3G, MRPL4, ICAM1, ICAM5
2	RP11- 347E20	DNMT1, S1PR2, MRPL4, ICAM1, ICAM4
3	RP11-1134K12	ZNF569 (part), ZNF570, ZNF793, ZNF571, ZNF540 (part)
4	RP11-893K17	MEGF6, WDR8, PRDM16, ARHGEF16, MIR551A, TPRG1L

For BAC DNA extraction, 400 ml bacterial cultures were grown overnight at 37ºC at 200 rpm. BAC DNA purification was performed using PureLink Hi Pure BAC DNA Extraction Kit (Invitrogen K2100-07). DNA was eluted from the column using TE, subjected to fluorescent labeling using nick translation kit (Roche) and then used for *in situ* hybridization.

2.1.8 Statistical analysis

Graphs were plotted using Graphpad Prism 5.0, Sigmaplot 11.0 and Microsoft Excel. For statistical comparisons of mean values and proportions, unpaired Student's t-test and Z test of proportions were used. For all data sets, Kolmogorov–Smirnov (K-S test) and Shapiro Wilk normality tests were performed to examine distribution profiles. Comparisons of median % R.D of chromosome territories were performed using Mann Whitney Wilcoxon sum rank test, while comparisons of distributions into different nuclear subshells were performed using Fischer's exact test and chi-square test. Statistical significance of more than two categories of distributions (recovery experiments) was performed using Kruskal Wallis non parametric ANOVA. $p<0.05$ were considered to be statistically significant.

2.2 Specific methods for Chapter 3: Impact of lamin depletion on the transcriptome

2.2.1 Gene expression profiling using microarrays

(Microarray hybridization was performed by Genotypic, Bangalore, India

Microarray data analysis was performed by Bionivid, Bangalore, India)

RNA was extracted from three independent biological replicates each from control, Lamin A/C Kd and Lamin B2 Kd DLD1 cells and its quality was ascertained using bioanalyzer (Agilent). Cy3 labeled complementary RNA was prepared using T7 promoter based linear amplification (Agilent quickamp labeling kit, Cat No. 5190-0442). Qiagen RNeasy minikit (Cat no. 74104) was used for RNA purification. Hybridization was performed using a human 8 X 60K array (Agilent single color 27114) and labeled using Agilent's *in situ* hybridization kit (Cat no. 5188-5242). Array scanning was performed and data acquired was normalized (50^{th} percentile shift normalization). Analyses of gene expression levels were based on comparison of hybridizations between knockdown and control (untreated DLD1 cells) as reference. Gene expression levels (cut-off: absolute fold change ≥ 2.0, $p<0.05$) were used for further analyses. The microarray data can be accessed using GEO Accession number GSE73269. Volcano plots for the data are represented in Appendix III. The % deregulation per chromosome was calculated as (no. of deregulated genes on a chromosome/total no. of coding genes on that chromosomes) X 100. Number of coding genes and size of chromosomes were obtained from MapViewer (NCBI). Chr. 16 (~1.3%) and Chr. 19 (~1.32%) showed the highest deregulation upon Lamin A/C and Lamin B2 Kd respectively. Chromosomes showing > 0.7% deregulation were considered significant since this represents > 50% of the total extent of transcriptional deregulation.

2.2.2 Comparison of LAD profiles with deregulated genes

The genomic regions belonging to LADs were obtained from Supplementary data deposited by (Guelen et al., 2008). We procured the genes with their promoters (1Kb downstream of the TSS) within these LADS from UCSC Genome Browser (Assembly human hg19). Comparisons were

performed between this gene list and the list of transcriptionally deregulated genes upon Lamin A/C or Lamin B2 depletion obtained from the microarray data and used for subsequent analysis.

2.2.3 Gene Set Enrichment Analysis (GSEA) Analysis for motif enrichment and transcription factors in promoters of deregulated genes

The genes that were transcriptionally deregulated in Lamin A/C and Lamin B2 depletion were subjected to analysis to examine motifs enriched in their promoter sequences and transcription factors that bind to these motifs, if known. For this purpose, we used the Gene Set Enrichment Analysis (GSEA) - Molecular Signature Database (MSigDB) (Mootha et al., 2003; Subramanian et al., 2005). Gene lists from Lamin A/C and Lamin B2 Kd – up and downregulated sets were input into this database; and compared to gene sets with annotated motifs and miRNAs from the database. The top 20 gene set categories were obtained at a FDR (q) value of 0.05.

Animal transcription factor database (Animal TFDB) was used to examine transcription factors from the microarray gene set (Zhang et al., 2012).

2.2.4 DAVID bioinformatics analysis for functional cluster enrichment

The deregulated gene targets upon Lamin A/C Kd and Lamin B2 Kd were sorted based on absolute fold change. All genes that showed a ≥ 2.0 fold absolute fold change were subjected to a functional category analysis using online software DAVID (http://david.abcc.ncifcrf.gov/). The output from the analysis consisted of GO categories from the Biological Process, Molecular Function and Cellular Components sections. A graph was plotted for the $-\log_{10}$(p-value) of enrichment for all GO categories obtained (Huang et al., 2009a; Huang et al., 2009b).

2.3 Specific methods for Chapter 4: Spatial organization of transcriptionally deregulated chromosome territories upon Lamin depletion

2.3.1 3D FISH – CT and gene loci

3D-Fluorescence *in situ* hybridization (FISH) – Chromosome Territories

Fixation and permeabilization

Cells were grown to a confluency of ~30-40% on glass coverslips (18X18 or 22X22 mm^2) placed in single wells of a 6-well plate and were subjected to siRNA knockdown. Cells were washed 3 times in 1X PBS for 5 minutes each at RT. The cells were incubated on ice for 5 minutes in pre-chilled CSK buffer and immediately fixed in 4% Paraformaldehyde (PFA - prepared in 1XPBS (pH 7.4)) for 7 minutes at RT. The cells were washed in 0.1 M Tris-HCl (pH 7.4) followed by two washes with 1X PBS for 5 minutes each at RT. The cells were re-permeabilized in 0.5% Triton-X-100 (prepared in 1X PBS) for 10 minutes and incubated in 20% glycerol (prepared in 1X PBS) for 60 minutes followed by four freeze-thaw cycles in liquid nitrogen. The cells were washed three times in 1X PBS for 5 minutes each and incubated in 0.1 N HCl for 10 minutes followed by three washes in 1X PBS for 5 minutes each. The cells were stored in 50% formamide (FA)/2X SSC (Saline Sodium Citrate) (pH 7.4) overnight at 4°C or until used for hybridization.

Hybridization

Chromosome painting probes were obtained from Applied Spectral Imaging (ASI), Israel or MetaSystems, USA. Probes were equilibrated at 37°C for 5 minutes followed by denaturation at 80°C for 5 min, and quick chilled on ice for 2 minutes followed by a pre-annealing at 37°C for 30 minutes. This denatured probe (3-4 µl) was spotted onto fixed cells, sealed with nail polish and subjected to co-denaturation at 80°C for 5 minutes. Hybridization was for 48 hours in a humidified box at 37°C.

Detection

Post hybridization, coverslips were washed in 50% FA/2XSSC (pH 7.4), thrice for 5 minutes each at 45°C, followed by three washes for 5 minutes each in 0.1XSSC at 60°C with gentle

agitation. Coverslips were briefly rinsed in 0.1% Tween20/4X SSC, and counterstained with 4',6-Diamidino-2-Phenylindole (DAPI) for 2 minutes, washed in 2X SSC and mounted in Slowfade Gold Antifade (Invitrogen S36937) and stored at 4°C until they were imaged.

Imaging (Common for FISH and IFA)

Image acquisition was performed on a Zeiss LSM 710 or 780 confocal microscope (Carl Zeiss, Thornwood, NJ, USA) with a 63X Plan-Apochromat 1.4 NA oil immersion objective using scan zoom of 2-2.5. Acquisition of Z-stacked images (voxel size of 0.105 µm X 0.105 µm X 0.34 µm) was at 512X512 pixels per frame using 8-bit pixel depth for each channel. The line averaging was set to 4 and images were collected sequentially in a three-channel mode.

2.3.2 Radial distance measurements of CTs

3D distance measurements of chromosome territories were performed using Image-Pro Plus (v 7.1), MediaCybernetics, USA. Briefly, LSM files containing optical sections (z = 0.34 µm) of the hybridized nuclei were subjected to 3D surface rendering. 3D reconstructions of each nucleus were performed on individually cropped nuclei. The acquired images were thresholded and surface rendered for each of the red, green, blue channels. The geometric center of the DAPI stained nucleus (blue channel) and the chromosome territories (red and green channels) were determined using plugins from the software, and the distance between the geometric center of the nucleus (A) and that of the territory (B) was measured (X). The vector from the geometric center of nucleus (A) to the geometric center of the chromosome territory (B) was extended to a third collinear point at the nuclear periphery (C). The distance between the geometric center (A) of the nucleus, and (C) was calculated (Y). The relative distance of a chromosome territory from the center of the nucleus was calculated as a percentage of the total distance from the center of the nucleus to the nuclear periphery, %Radial Distance (R.D) = (X/Y) * 100 (Tanabe et al. 2002).

2.3.3 3D-Immuno fluorescence *in situ* hybridization (3D-iFISH) for visualizing Lamin and gene Loci

Preparation of BAC DNA probes

BAC DNA was extracted from clones purchased from CHORI BACPAC Resources (using Hi-Pure Plasmid DNA Extraction Kit (Invitrogen K210017). BAC clones used were RP11-1134K12 for *ZNF570* gene. This DNA was nick translated using fluorescently labeled dUTP (Abbott) and Nick Translation Mix (Roche 11 745 808 910). Labeling reaction was at 15°C for 90 minutes, followed by termination of reaction using 0.5M EDTA (pH 8.0) at 65°C for 10 minutes. The DNA was precipitated using ethanol and 3M Sodium Acetate and resuspended using deionized formamide and Master Mix containing dextran sulphate and 2X Saline Sodium Citrate (SSC) Buffer.

Fixation and permeabilization of cells

Cells were grown on coverslips and subjected to desired treatment were washed twice (5 min each) with 1X PBS (pH 7.4) followed by permeabilization on ice using ice cold CSK Buffer containing 0.5% Triton X-100 for 5 min. Fixation of cells was then carried out using 4% Paraformaldehyde (PFA) solution prepared in 1X PBS for 5-7 min at RT. The fixation protocol followed was the same as that for 3D-FISH as that in sections above.

Immunostaining followed by hybridization

Cells on coverslips were washed with 1× PBS (5 min each) and blocked for 30 min using 1%bovine serum albumin(BSA) in 1×PBS at RT. This was followed by primary antibody probing (Mouse anti-Lamin B2 (Abcam (ab8983), 1:600) and Rabbit anti-Lamin A (Abcam (ab26300), 1:500 prepared in 0.5 % BSA in 1×PBS) and incubated for 90 min at RT; and secondary antibody staining (goat anti-mouse IgG–Alexa 633 (Invitrogen (A-21052) 1:1000) and goat anti-rabbit IgG–Alexa 488 (Invitrogen (A-11034) 1:1000) for 1 h at RT. Post fixation and post permeabilization were performed with 4 % PFA (5 min RT) and 0.5 % Triton X-100in1× PBS (5min RT), respectively. Cells were then washed with 1× PBS (5 min each) and 50 % FA/2× SSC (pH 7.4) (5 min – 2 washes). The BAC DNA probe for *ZNF570* was inucbated at 37 °C for 5 min followed by denaturation at 80 °C for 5 min and quick chilled on ice for 2 min. Probe was pre-annealed at 37 °C for 30–40 min, spotted onto the fixed cells that were subjected

to immunostaining for Lamin A and Lamin B2 and subjected to co-denaturation at 80 °C for 5 min. Hybridization was for 48 h in a humidified box at 37 °C.

Post hybridization washes

For washes, coverslips were washed in 50 % FA/2×SSC (pH 7.4), thrice for 5 min each at 45 °C, followed by three washes for 5 min each in 0.1× SSC at 60 °C with gentle agitation. Counterstaining with DAPI was performed for 2 min at RT, followed by mounting using Antifade and stored in 4 °C until they were imaged. The images were acquired on Zeiss LSM710 or 780 confocal microscope similarly as for CT hybridizations, using a zoom=2.0.

2.3.4 Measurements for spatial organization of gene loci - Distance measurement from the nuclear periphery

Distances of gene loci from the nuclear periphery were measured (in µm) in 3D using Lamin A signal at the nuclear periphery to demarcate the edge of the nucleus. Briefly, surface rendering was performed for the gene locus (red channel), Lamin A (green channel), Lamin B2 (Far red channel) and the nucleus (DAPI signal – blue channel) using Huygens Professional. For Lamin B2 Kd cells, the nuclei which showed a depletion of Lamin B2 (Far red channel) were used for analysis. Briefly, surface rendering for Lamin A was used as an anchor for measurements. Centre of mass (CM) was determined for the gene locus signal of interest and the closest distance between the CM and surface of anchor (Lamin A signal) was measured.

2.3.5 Preparation of Metaphase Spreads

For preparation of metaphase spreads, cells(control, Lamin Kd) were grown to an approximate confluence of 50-70% and blocked in metaphase using Colcemid (0.1µg/mL) for 90 min. Hypotonic treatment (0.075M KCl) was performed for 15-30 min at 37 ºC, followed by fixation in 5-6 drops of fixative (methanol:acetic acid 3:1). The cell pellets thus obtained were washed three washes in fresh fixative. Cells were dropped onto glass slides and metaphases were stained with DAPI, imaged and counted.

2.3.6 2Dimesional Fluorescence *in situ* Hybridization (2D-FISH)

Probe denaturation

For probe denaturation for 2D FISH, the same protocol as that for 3D FISH was followed, with the preannealing time reduced to 15-20 min at 37°C.

Slide denaturation

Separate denaturation was followed for the slides (metaphase spreads) for 2D FISH. 50 µl of 50% deionized formamide/ 2X SSC was spotted on the slide with the metaphase spread and it was denatured at 80°C for 1 min. This was followed by an ethanol series of 70% (chilled), 90% (RT) and 100% Ethanol (RT) for 2 min each. The slide was allowed to air dry.

Hybridization

The denatured probe was spotted onto the slide and allowed to hybridize for 48 hours at 37°C.

Post hybridization washes

Post hybridization washes for 2D FISH were performed similarly as that for 3D FISH.

2.3.7 RNA Fluorescence *in situ* hybridization (RNA FISH)

Probe preparation

The probe for RNA FISH for *ZNF570* was prepared by nick translation of the BAC clone (Section of Preparation of BAC DNA probes – 3D FISH for gene loci above). Upon precipitation, the DNA was resuspended in 8 µl of deionized formamide and stored at -20 ºC till further use. For hybridization, the probe was were equilibrated at 37°C for 5 minutes followed by denaturation at 80°C for 5 min, mixed with equal volume of 2X Hybridization Mix containing vanadyl ribonucleoside complex and incubated on ice for 30 min.

Fixation and Hybridization

Cells were washed twice in 1 XPBS (5 min each), followed by treatment with CSK buffer on ice for 5 min and fixation using 4% Paraformaldehyde (7 min RT). Cells were washed with 70% ethanol twice and stored at -20 ºC till further use. Prior to hybridization, cells were subjected to an ethanol series (70%-90%-100% ethanol) (2 min each, RT) and air dried. The probe was added

to cells, and incubated at 37 ºC overnight, followed by washes with 50% FA/2X SSC and 2X SSC at 42 ºC (3 washes each of 5 min each). Cells were mounted using DAPI-Antifade. All reagents for RNA FISH were made using DEPC treated water (Chaumeil et al., 2008) .

2.3.8 FACS analysis by Propidium Iodide staining

Cells (Control, Lamin Kd) were fixed in 70% ethanol (in 1X PBS), subjected to RNase treatment + Propidium Iodide staining (1 hour) on ice. Cell suspensions were subsequently run on FACS Calibur (BD Biosciences). Analysis of FACS data was performed using FlowJo.

2.3.9 Site directed mutagenesis for generation of siRNA resistant Lamin B2

Primers used for the silent mutations in Lamin B2 and Lamin A are listed in Appendix II. PCR reaction for SDM was set up using Accuprime Pfx Supermix (Invitrogen) using 100 ng of template plasmid DNA and 200nM of primer concentration. The annealing temperature was set to 65 ºC and extension time per cycle was 7 min. The PCR product after 35 cycles was subjected to Dpn I digestion and then used to transform competent bacteria *E.coli* DH5alpha. Emerging colonies were screened and subjected to Sanger sequencing to examine the incorporation of the mutation.

2.3.10 Immunofluorescence Assay performed for cells in suspension

Cells (control, Lamin Kd) were trypsinized and made into a single cell suspension. This pellet was washed with 1XPBS and fixed with 4% PFA at RT for 20 min with occasional tapping. Two washes of 1X PBS were subsequently given (900 rpm 5min RT). Permeabilization was carried out using 0.5% Triton X-100 in 1XPBS for 10 min at RT on a gentle rocker. Pellet was washed once with 1X PBS and then blocked in 1% BSA in 1X PBS for 30 min at RT on a gentle rocker. Cells were washed with 1X PBS twice and followed by addition of primary antibody and incubation for 90 min at RT. The tube was tapped gently every 15 min to prevent the cells from clumping together and settling down. Two washes were now performed with 1X PBST (PBS with 0.1% Triton X-100) followed by addition of secondary antibody for 60 min at RT. The tube

was tapped gently every 15 min to prevent the cells from clumping together and settling down. The pellet was washed twice with 1X PBST, mixed with DAPI-antifade mix and mounted.

2.3.11 Nuclear matrix preparations

Protocol adapted from (Jagatheesan et al., 1999). Cells grown on coverslips overnight at a confluence of ~50-70% were washed trice with ice cold CSK buffer containing PMSF and 1X PIC. Cells were subsequently incubated in CSK buffer containing 0.5% v/v Triton X-100 for 7 min on ice and then rinsed thrice with ice cold RSB Buffer (42.5 mM Tris-HCl, pH 8.3, 8.5 mM NaCl, 2.6 mM MgCl2, 0.05 mM PMSF and 10 µg/ml aprotinin). This was followed by incubation in RSB Buffer with 1% Tween 20 and 0.5% sodium deoxycholate for 10 min on ice. Then, two washes were performed with ice cold digestion buffer (10 mM Pipes, pH 8.3, 50 mM NaCl, 300 mM sucrose, 3 mM MgCl2, 1 mM EGTA, 0.05 mM PMSF and 1X PIC). This was followed by DNase I in digestion buffer (100 units/ml) for 30 minutes at 30°C. This reaction was stopped by adding 1 M (NH4)2SO4 was added slowly to the cells in digestion buffer to a final concentration of 0.25 M. This was incubated for 5 minutes on ice and subsequently followed by two washes in ice-cold digestion buffer. 2M NaCl treatment was performed for further extracting the nuclei. The nuclei were now fixed using 4% paraformaldehyde for 15 min at RT and processed for immunostaining with the regular protocol.

2.4 Specific methods for Chapter 5: Role of Lamins in genomic stability

2.4.1 Genomic DNA Extraction

For CNV analysis, DLD1 cells were subjected to independent knockdowns of Lamin A/C, Lamin B1 and Lamin B2 using siRNA transfections for 48 hours. The genomic DNA extraction was performed using PureLink® Genomic DNA Mini Kit (Invitrogen) and then subjected to hybridization for determination of copy number variations in DLD1 cells.

2.4.2 Determination of Copy Number Variation (CNV) using genome wide array

(Performed in collaboration with Dr. Binay Panda, GANIT labs, Bangalore)

We used Illumina OMNI2.5 whole genome SNP arrays to call copy number variations in control cells and cells with Lamin A/C, Lamin B1 and Lamin B2 knockdowns. Briefly, 200ng of high quality genomic DNA was taken as the starting material. The genomic DNA was denatured at room temperature for 10mins using 0.1N NaOH, neutralized and kept for whole genome amplification (WGA) under isothermal conditions, at 37^0C for 20hrs. Post the WGA step, the DNA was enzymatically fragmented at 37^0C for 1hr. The fragmented DNA was precipitated with isopropanol at 4^0C and resuspended in hybridization buffer provided by the manufacturer. The targets were then denatured at 95^0C for 20 mins, cooled at room temperature for 30mins. Subsequently, 35ul of each denatured target was loaded onto the Illumina HumanOmni 2.5-8 beadchip for hybridization at 48^0C for 20hr in a hybridization chamber. During this step, the target DNA anneals to the specific 50-mer probes attached to the beadchip. The un-hybridized probes were washed away and the chip was prepared for staining. Single base extension was performed following the manufacturer's specifications. Finally, the chip was scanned using a HiScan system following manufacturer's recommendations. We used all the SNPs assayed on the arrays to make copy number variation calls. CNVs were identified using the the algorithm cnvPartition 3.1.6 using a plugin within genomestudio with default parameters except for a minimum coverage of at least 10 probes per CNV with a confidence score threshold of at least 100. Individual CNVs in different chromosomes and the output file from cnvPartition was parsed for CNVs that are specific to each sample and that are common between any two or more samples**.** Further CNVs are annotated using ENSEMBLE v73.

2.4.3 Copy Number Variation analysis

The output of the CNV data obtained through array hybridization of genomic DNA post Lamin knockdowns was examined to determine the CNVs that are unique to Lamin A/C, Lamin B1 and Lamin B2 depletion. CNV profiles were determined for the control DLD1 cells (background), and CNVs unique to each of the Lamin Kds were then determined by subtracting those that were found in all control as well as Lamin knockdowns.

2.4.4 Calculation of repeat density

The genomic regions corresponding to the CNV – single copy insertions were examined for their repeat density using Repeat Masker (http://www.repeatmasker.org/). The total % of all repeats (LINE, SINE, microstaellites, Alu) in this region was procured and the fraction of repeats over the total base pair length of these regions was plotted to represent the repeat density. Simple (short) repeat data was extracted from the total repeats and plotted separately.

2.4.5 Spectral Karyotyping (SKY)

Spectral Karyotyping was performed on metaphase spreads generated from Control and Lamin depleted DLD1 cells.

Probe denaturation

SKY probes were obtained from Applied Spectral Imaging (ASI). 7.1 µl probe was used per hybridization. For denaturation, the probe was equilibrated at 37°C for 5 min, followed by denaturation at 80°C for 7 min and pre annealing at 37°C for 60 min.

Slide denaturation

Separate denaturation was followed for SKY. 50 µl of 50% deionized formamide/ 2X SSC was spotted on the slide with the metaphase spread and it was denatured at 74°C for 1 min. This was followed by an ethanol series of 70% (chilled), 90% (RT) and 100% Ethanol (RT) for 2 min each. The slide was allowed to air dry.

Hybridization

The denatured probe was spotted onto the slide and allowed to hybridize for 48 hours at 37°C.

Post hybridization detection

For detection of SKY signals, slides were washed in 50% FA/2XSSC (pH 7.4), thrice for 5 minutes each at 45°C, followed by three washes for 5 minutes each in 2XSSC at 45°C with gentle agitation. This was followed by blocking using Blocking Reagent (BSA) supplied with SKY detection kit (ASI) for 30 min at 37°C. Primary antibody – Cy5 was added at a dilution of 1:100 in 4X SSC and incubated for 1 hr at 37°C followed by three washes with 0.1% Tween20/4X SSC at 45°C. Secondary antibody – Cy 5.5 added at a dilution of 1:100 in 4X SSC and incubated for 1 hr at 37°C followed by three washes with 0.1% Tween20/4X SSC at 45°C. Coverslips were briefly rinsed in, and counterstained with 4',6-Diamidino-2-Phenylindole (DAPI) for 2 minutes, washed in 2X SSC and mounted in Slowfade Gold Antifade (Invitrogen S36937) and stored at 4°C until they were imaged.

Imaging

Imaging for Spectral Karyotyping was performed on a Carl Zeiss fluorescence microscope equipped with a SKY signal detection Spectral cube (HiSKY) from Applied Spectral Imaging (ASI).

2.5 Specific Methods for Chapter 6. Role of lamin dependent interactors in maintenance of chromosome positions

2.5.1 Gene expression profiling using qRT-PCR (TaqMan Array)

A customized array containing TaqMan probes for 43 selected genes encoding nuclear structure proteins was procured from Life Technologies. Expression profiling was performed by RNA extraction from two independent biological replicates of control (untreated), Lamin A Kd and Lamin B2 Kd DLD1 cells. RNA quality was checked using Bioanalyzer (Agilent), and cDNA synthesis carried out using cDNA synthesis Kit (ABI), followed by a cDNA quantitation using an 18S rRNA TaqMan probe (ABI). The microfluidic TaqMan Array card was loaded with cDNA and TaqMan Master Mix (ABI) and run on a ViiA 7 real time PCR system (ABI).

2.5.2 Fluorescence recovery after photobleaching (FRAP) and analysis

35 mm petridishes were used for live imaging. The bottom of the dish was covered with a glass coverslip (22 X 22mm^2) and cells were grown on it after coating with collagen (100 μg/ml). Cells were transfected with H2A-mCherry 24 hours prior to photobleaching experiment. mCherry-H2A-10 was a gift from Michael Davidson (Addgene plasmid # 55054). During FRAP experiments, cells were maintained in CO_2 independent Leibovitz L-15 medium (Gibco, 21083-027). Images were acquired using a 63X oil immersion objective on Zeiss LSM 710 confocal microscope, NA 1.4, at 3X digital zoom. Two Regions of Interest (ROI) 20 px X 20 px (1 pixel = 0.0879 μm) were used for bleaching- one ROI was in the nuclear interior and other was at the nuclear periphery. For photobleaching, we used the 561 nm laser line. 80% laser power was used for photobleaching (100 iterations for bleaching) after 10 scans of pre bleach, and image acquisition was performed every 1 sec. Images were analyzed using Zen 2011 FRAP Analysis module and Normalized Fluorescence Intensity (NFI) was calculated as follows:

ROI1: fluorescence intensity of the ROI in the nuclear interior/ nuclear periphery as per consideration, ROI2: fluorescence intensity of a 20 px X 20 px region of the nucleus that was not subjected to photobleaching, and ROI3: fluorescence intensity of a 20 px X 20 px background region selected outside the nucleus. ROI1 (t) denotes the post-bleach fluorescence intensity at time t. ROI2 (t) and ROI3 (t) denote the same for unbleached ROI and background, respectively.

ROI1 (t=0) denotes the average pre-bleach fluorescence intensity. ROI2 (t=0) and ROI3 (t=0) denote the same for unbleached ROI and background, respectively. The NFI was plotted as a function of time to generate double normalized FRAP curves.

$$NFI = \frac{ROI1(t) - ROI3(t)}{ROI2(t) - ROI3(t)} X \frac{ROI2(t=0) - ROI3(t=0)}{ROI1(t=0) - ROI3(t=0)}$$

Mobile fractions of H2A-mCherry were calculated as follows:

$$\%Mobile\ fraction = \frac{Ffinal - Fbleach}{Fprebleach - Fbleach} \times 100$$

Where, F_{final} is the NFI at maximum recovery (saturation), F_{bleach} is the NFI at the instant of bleaching and Fpre-bleach is the NFI before bleaching (Live Cell Imaging: A Laboratory Manual, Second Edition) .

2.5.3 Drug treatments – Latrunculin A

Drug treatments were performed on DLD1 cells at an approximate confluence of ~60-70% after depletion of Lamin A/C and/or Emerin. Latrunculin A was used at a concentration of 50nM. An equivalent amount of DMSO was added to the control wells as vector controls. Both these drug treatments were for a total duration of 90 min at 37ºC.

2.5.4 Co-immunoprecipitation

Co-immunoprecipitation was performed using Co-IP Lysis Buffer (50mM Tris pH8.0, 150mM NaCl, 0.5% NP-40, 1X Protease Inhibitor Cocktail (Roche, added just before use)). Briefly, cells were lysed in Co-IP Lysis Buffer, incubated on ice for 30 min and centrifuged at 14000 rpm for 15 min at 4°C. The supernatant was estimated for its protein concentration using BCA Kit. For the Co-IP, 120ug of lysate (each from Control and siLamin A/C cells) was subjected to preclearing using Protein G/A-Dynabeads for 45 min at 4°C. Primary antibody (mouse anti-Emerin sc25284, rabbit anti-MYO1C ab51261) (1 µg) and normal mouse/rabbit IgG (1 µg) were added to lysates and allowed to bind overnight at 4°C. Antigen-antibody complexes were captured for 3-4 hours using 20 ul of Protein G/A-Dynabeads that had previously been blocked with 0.5mg/ml BSA in 1X PBS for 30 min at 4°C. All incubations were carried out using end-to-

end rotor at 4°C. The beads were then washed six times with Co-IP Lysis buffer, boiled in 4X Laemmli, run on polyacrylamide gels and subjected to western blotting.

2.5.5 Preparation of nuclear and cytoplasmic extracts

Nuclear and cytoplasmic extracts were prepared according to REAP Protocol (Nabbi and Riabowol, 2015)

2.5.6 Generation of Lamin A – reduced affinity for Emerin mutant R453W

Primers used for the mutation R453W are listed in Appendix II.

PCR reaction for SDM was set up using Accuprime Pfx Supermix (Invitrogen) using 100 ng of template plasmid DNA and 200nM of primer concentration. The extension time per cycle was 7 min. The PCR product after 35 cycles was subjected to Dpn I digestion and then used to transform competent bacteria *E.coli* DH5alpha. Emerging colonies were screened and subjected to Sanger sequencing to examine the incorporation of the mutation.

Chapter 3: Impact of lamin depletion on the transcriptome

Data acknowledgements:

Figure 3.3A-B: Shivsmriti Koul

Results from this chapter are published as a part of the following manuscript:

Ranade, D., Koul, S., Thompson, J., Prasad, K. B. and Sengupta, K. (2016). Chromosomal aneuploidies induced upon Lamin B2 depletion are mislocalized in the interphase nucleus. *Chromosoma*.

3.1 Introduction

The nuclear lamina in higher eukaryotes is composed of A and B type lamins localized beneath the inner nuclear membrane (Goldman et al., 1986). Lamins bind to specific chromatin subdomains (~0.1-10 Mb) referred to as 'Lamina associated domains (LADs)' (Guelen et al., 2008). LADs are characterized by high density of repetitive elements, late replicating genes, inactive histone marks H3K9me2/3 (Guelen et al., 2008; Harr et al., 2015; Towbin et al., 2012; Zullo et al., 2012). Both A and B type lamins bind to LADs on chromatin at the nuclear periphery and the interior. In general, genomic regions anchored to the nuclear lamina are in a transcriptionally repressive state (Guelen et al., 2008).

A and B type Lamins contribute to transcription regulation as follows:

1. Direct binding to chromatin

Lamins bind to 'Lamina associated domains' (LADs) in chromatin at the nuclear periphery (Guelen et al., 2008). Both A and B type lamins possess domains for direct chromatin binding, as also bind to chromatin via interacting partners such as LBR, LAP, BANF1 among others (Glass et al., 1993; Montes de Oca et al., 2009; Stierlé et al., 2003; Taniura et al., 1995; Ye and Worman, 1994). The term 'LAD' collectively refers to chromatin that is bound by molecules at the nuclear periphery, mainly Lamin A/C, Lamin B1, Lamin B2, and the transmembrane anchoring molecules such as Emerin, Lamin B Receptor (LBR) and Lamina associated polypeptide 2 beta (LAP2β) at the nuclear periphery (Guelen et al., 2008). Constitutive LADs (~71% of total LADs) are bound by both A and B type lamins across cell types, while facultative LADs are bound by in a cell type specific manner (Meuleman et al., 2013). Lamins contribute significantly to the maintenance of LADs, facilitated by its interaction with Emerin, LAP2β and LBR (Amendola and van Steensel, 2015; Zullo et al., 2012). Functionally, LADs represent regions of transcriptional repression. LAD profiles are conserved across cell types and also across human and mouse species and represent structural organization in the nucleus (Meuleman et al., 2013). Artificial tethering of genes (LacO with GFP-LacI repressor) to LADs is associated with transcriptional repression (Finlan et al., 2008; Reddy et al., 2008). However, certain artificial reporter genes retain their transcriptional competence even when targeted to the nuclear lamina (Kumaran and Spector, 2008). Thus, although lamins impart a repressive environment to

most genomic regions that they bind to, they maintain flexibility to allow transcriptional permissiveness of genes if required. 'Lamina associating sequences (LAS) are sub-domains within LADS (enriched for "GAGA motif") and are determinants of chromatin binding to the lamina (Zullo et al., 2012). Binding of genomic regions to the nuclear periphery is mediated through transcriptionally repressive factors such as c-Krox which in turn binds to HDAC3 and LAP2β to mediate attachment to the lamina (Zullo et al., 2012). Although the term 'LAD' was initially used to refer to repressed chromatin at the nuclear periphery, live imaging studies using m6A-Tracers showed that LADs are not solely confined to the nuclear periphery (Kind et al., 2013). Association of chromatin with Lamins has been identified by (i) direct ChIP and (ii) indirect Dam ID (Guelen et al., 2008; Lund et al., 2015). Lund et al compared the outputs from these two methods and found ~90% overlap in the genomic regions captured as lamina associated domains. Lamins were also associated with chromatin at the nuclear interior. Microscopy (immunostaining) assays as well as biochemical (extractions) assays have demonstrated a greater diffusing nucleoplasmic pool for Lamin A/C over B type lamins (Kolb et al., 2011). While B type lamins bind primarily to heterochromatin at the nuclear periphery, A type lamins bind to both euchromatin (mainly in the nuclear interior) and also heterochromatin (primarily nuclear periphery) (Gesson et al., 2016; Lund et al., 2015). This is suggestive of a differential regulation between A and B type lamins, and Lamin B1 and Lamin B2 may primarily regulate heterochromatic domains, while Lamin A/C associates and regulates both euchromatin and heterochromatin.

Fine mapping of binding sites within and proximal to LADs was performed for Lamin A/C by Lund et al (2013). ChIP seq captured binding of Lamin A/C promoter and sub-promoter regions within peripheral as well as intra nuclear chromatin (Lund et al., 2013). A loss of binding to Lamin A/C primarily alters the accessibility to LAD regions thus influencing their transcriptional potential. A loss of Lamin A/C binding from direct promoter regions of a gene confers a reduced transcriptional access to these genes. On the other hand, a loss of Lamin A/C binding from the sub promoter region of a gene may confer either a reduced or increased transcriptional access dependent on the local chromatin modifications present on the promoter of the gene (Lund et al., 2013). LAP2alpha, an interactor of Lamin A/C is speculated as a mediator of these effects of Lamin A/C and its effects on chromatin function primarily in the nuclear interior (Gesson et al., 2016).

Adipogenesis, differentiation genes are controlled by Lamin A/C binding (Lund et al., 2013). Furthermore, promoters of several muscle lineage specific genes such as MyoD, muscle creatinine genes are bound by Lamin A/C which modulates their transcription status (Athar and Parnaik, 2015). LAD profiles undergo reorganization in the course of adipogenesis, neuronal differentiation, muscle differentiation (Peric-Hupkes et al., 2010). Thus, LAD profiles represent an interesting evolutionarily conserved mechanism to enable selective and tunable modulation of expression during differentiation.

2. Lamins regulate RNA Polymerase dependent transcription

An additional layer of transcriptional regulation by Lamins occurs through a regulation on RNA polymerases and its involvement in transcription. Depleting the cells of functional A or B type lamins shows a reduction in RNA Polymerase II dependent transcription (Spann et al., 2002; Tang et al., 2008). Lamins maintain a scaffold like structure which supports the assembly and functioning of transcription factors and RNA Polymerases during transcription (Spann et al., 2002). This is mediated through interactions with proteins such as TATA binding protein (TBP) (Spann et al., 2002). Modulation of functional lamins by mutations / loss of function destabilize RNA Pol II transcription foci and impact overall levels of active RNA Pol II suggesting a dependence of active transcription on functional lamins (Spann et al., 2002; Tang et al., 2008).

This binding of lamins may be different from the binding of lamins to LADs at the nuclear periphery. Binding to chromatin at LADs represents a stable structural scaffold that is formed by lamins, maintained through interphase and re-formed post mitosis. As against that, protein complexes involving lamins and RNA Polymerases may represent transient structures that assemble during active transcription.

3. Binding of lamins to transcription factors

A and B type lamins bind to transcription factors (TF) directly and sequester them at the periphery (Heessen and Fornerod, 2007). A variety of general transcription factors are assembled on a lamin scaffold during transcription. Alternatively, a lamin nucleoskeletal scaffold also

serves as a docking site for general transcription factors and RNA Polymerase II during transcription (Spann et al., 2002). Alongwith these, lamins at the periphery bind to and sequester TFs such as Rb, c-Fos, AP1, SREBP1, OCT1, MOK2 (Dreuillet et al., 2002; González et al., 2008; Ivorra et al., 2006; Lloyd et al., 2002; Malhas et al., 2009; Ozaki et al., 1994). Specifically Lamin A/C binds to and regulates the activity of Rb, GATA3, c-Fos and SREBP1 while Lamin B1 primarily binds to Oct1 (Dreuillet et al., 2002; González et al., 2008; Ivorra et al., 2006; Lloyd et al., 2002; Malhas et al., 2009; Ozaki et al., 1994). Binding of lamins to these TFs correlates with their sequestration and downregulation of target genes. These transcription factors are specific and regulate the expression of unique sets of genes. Some of these transcription factors regulate specific functions e.g. SREBP1 is involved in adipogenesis, OCT1 is involved in stress responses, Rb is involved in cell proliferation (Dorner et al., 2006; Kim and Spiegelman, 1996; Malhas et al., 2009). Loss of lamin from the periphery often results in release of these transcription factors and a corresponding upregulation of their target genes (Heessen and Fornerod, 2007).

Additional mechanisms of Lamins of regulating transcription

Lamin A/C also possesses additional epigenetic regulatory functions such as regulation of PcG protein architecture which helps in maintaining a transcriptionally repressive state of genes bound by it. Lamin A/C interacts with proteins Ezh2, Bmi1 in maintaining a repressive state at target genes, which were found to overlap between components of PcG group and Lamin A/C. Specifically, Lamin A/C interacts with Ezh2 and Bmi1 in the nuclear matrix (Cesarini et al., 2015). Additionally, Lamin A/C and Lamin B1 affect the organization and stability of splicing speckles, Lamin A/C interacts with splicing factor SC35 and regulates its organization (Kumaran et al., 2002). Loss of Lamin A/C or Lamin B1 results in a deregulation of the splicing pathway in cells, resulting in the generation of aberrantly spliced transcripts (Camps et al., 2014; Kumaran et al., 2002).

Co-regulation of transcription and spatial organization of genes by lamins

Genes at LADs are under regulation by lamins in terms of their functional (transcriptional) regulation as well as structural (spatial organization) regulation. Gene loci bound by lamins are physically proximal to the nuclear periphery; and disengagement from the lamina confers a change in transcriptional status of a gene as well as its three dimensional localization in the nucleus. This has been reported for endogenous genes such as Tcrb, involved in T cell development as also for muscle function specific *LMO7* and *MBNL2* gene clusters (Mewborn et al., 2010; Schlimgen et al., 2008). A disengagement from the lamina as revealed through 3D FISH, is also accompanied by a change in the transcription status of these genes. A screen for molecular factors associated with gene positioning also reiterates the role of the lamina as a regulator of gene positioning, as also gene expression regulation (Shachar et al., 2015). When LAD profiles undergo reorganization during differentiation of stem cells to neuronal or adipogenic lineage, cell type specific genes originally within LADs are disengaged from the lamina, repositioned toward the nuclear interior and upregulated in terms of transcription (Lund et al., 2013; Peric-Hupkes et al., 2010). A study on mouse chromosomes in cells depleted of functional Lamin B1 reveals repositioning of chromosome 18 which also harbours gene clusters with deregulated gene expression (Malhas et al., 2007). Thus, lamins are a unique class of molecules that contribute to the structural and functional aspects of gene loci. However, it is unknown whether lamin regulation is confined to the subset of genes in direct association at LADs, or does it extend beyond LADs? It is unclear whether the scale of regulation of nuclear structure-function by lamins operates at the level of whole chromosomes or is confined to gene loci that are essentially orders of magnitude smaller than whole chromosome territories. We were curious to examine the structure function coregulation by Lamins at the level of genes and whole chromosomes in a stable diploid model of colorectal cancer. We probed into the gene expression changes elicited in diploid colorectal cancer cells – DLD1 upon single depletion of Lamin A/C and Lamin B2 to identify regions that were under transcriptional regulation by lamins, either directly or indirectly. Further we intend to test whether the functional regulation by lamins also correlates with a structural regulation and if the two can be uncoupled.

In this study, we have characterized the gene expression changes upon depletion of Lamin A/C and Lamin B2 (singly) in DLD1 cells using a genome wide gene expression array.

The aim of this experiment was to identify chromosomal domains that were affected in terms of their transcriptional status upon single knockdowns of Lamin A/C and Lamin B2. We identified unique regions of transcriptional deregulation upon knockdowns of Lamin A/C and Lamin B2. A comparative study was performed of the deregulated genes and chromosomes between Lamin A/C and for Lamin B2 depletion. The gene sets found to be deregulated upon Lamin A/C and Lamin B2 depletion were analyzed for their promoter motif enrichments and GO categories to derive functional deregulation upon Lamin depletion. We further characterized regions of transcriptional deregulation upon Lamin depletion for their spatial organization. This includes transcriptionally deregulated chromosomes and gene loci upon Lamin depletion.

3.2 Results

3.2.1 SiRNA mediated Lamin depletion in DLD1 cells

We sought to examine the impact of Lamin depletion on the transcriptome in diploid colorectal cancer cells (DLD1), which are karyotypically stable across passages, distinguishing the same from other cell lines with several chromosomal aberrations. Towards this end, we first established the conditions for Lamin depletion in DLD1 cells by performing siRNA-mediated knockdowns (Fig. 3.1). Lamin Knockdown (Kd) showed cell death of ~30-40% i.e viability of ~60-70% in DLD1 cells (Fig. 3.1A). qRT-PCR ascertained that the knockdown of Lamin A/C and Lamin B2 was >70-80% (Fig. 3.1B). Immunoblots revealed that the depletions of Lamins A/C, B1 and B2 were exclusive. In addition, Lamin A/C Kd did not appreciably affect the levels of B-type Lamins (Fig. 3.1C-D). Likewise, depletion of Lamin B1 or B2 did not significantly affect Lamin A/C levels (Fig. 3.1C-D).The exclusivity of the knockdowns enabled us to interpret the consequences of a single Lamin depletion. This is noteworthy since expression levels and stoichiometry of Lamins are important determinants of Lamin localization and function in a cell type dependent manner (Guo et al., 2014; Shimi et al., 2015; Swift et al., 2013). Since the extent of siRNA mediated Lamin B1 depletion (~50-60%) was not comparable to the extent of Lamin A/C and B2 depletion (>70-80%) in our hands, we focused on examining the effects of Lamin A/C and Lamin B2 knockdowns in DLD1 cells (Fig. 3.1C-D). Immunostaining showed ~85-90% depletion of Lamin A and B2 at the single cell level (Fig. 3.1E-H). Counterstaining with Lamin B1 in Lamin A/C depleted cells and Lamin A/C upon Lamin B2 Kd, revealed distorted nuclear shapes, nuclear invaginations, blebbing and nuclear furrows (Fig. 3.1I-J) consistent with Lamin A/C and B1 depletion across cell types, HeLa cells and in cells derived from laminopathies (Dechat et al., 2008; Taimen et al., 2009).

3.2.2 Lamin A/C and B2 depletion deregulates transcription

Independently, Lamin A/C and B2 Kd were performed in DLD1 cells, followed by whole genome expression profiling using gene expression arrays in three independent biological replicates. The flowchart for this experiment is illustrated in Fig. 3.2A. The data analyses revealed ~300 genes that were significantly deregulated (inclusive of up and down regulation) in either Lamin A/C or Lamin B2 depleted cells (Fig. 3.2B). Annotated genes with fold

Figure 3.1

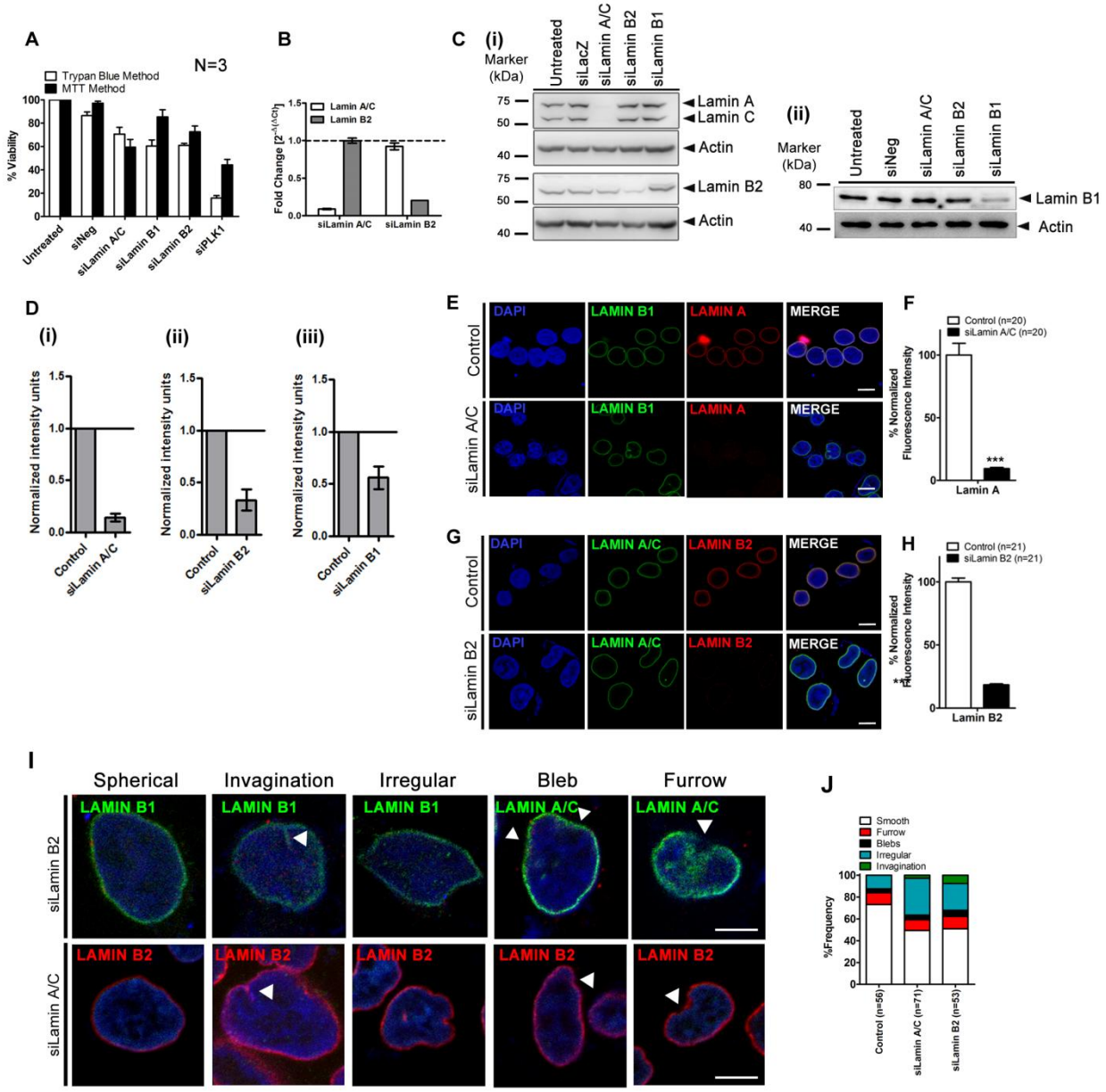

Figure3.1. siRNA mediated depletion of Lamins in DLD1 cells

A. Viability assay performed for DLD1 cells upon Lamin depletion using Trypan Blue staining and MTT uptake assays. Negative control= siNeg – universal siRNA negative control, positive control = siPLK1 (Polo like kinase 1). Data shown is a compilation from three independent biological replicates. B. qRT-PCR depicting knockdown of Lamin A/C and Lamin B2 (normalized to expression levels of *ACTIN* over non targeting control siLacZ) in DLD1 cells. Data shown is a representative result from two independent biological replicates. Error bars represent SEM. C. (i) Western blots depicting the expression levels of Lamin A/C and Lamin B2 in Lamin A/C, B1 and B2 independent knockdowns. Depletion of Lamin A/C does not impact the expression levels of Lamin B2 and vice

versa. Data shown is a representative result from five independent biological replicates. (ii) Western blot depicting knockdown of Lamin B1 in DLD1 cells. Data shown is a representative result from three independent biological replicates. D. Densitometric quantification of western blots (i) Lamin A (ii) Lamin B2 and (iii) Lamin B1 proteins depicting knockdowns of Lamins (i) A, (ii) B2 and (iii) B1 in DLD1 cells. Data shown is a compilation from 3-4 independent biological replicates. E.Immunostaining for Lamin B1 (green) and Lamin A (red) in control (untreated) and Lamin A/C Kd cells. Scale bar~10μm. F. Fluorescence intensity measurements performed using line scans across nuclei in E. G. Immunostaining for Lamin A/C (green) and Lamin B2 (red) in control (untreated) and Lamin B2 Kd cells. Scale bar~10μm. H. Fluorescence intensity measurements performed using line scans across nuclei in G. Single cell level knockdown of Lamin A/C and Lamin B2 in F and H was ~80-90%, $p<0.0001$, unpaired Student's t – test. I. Representative images depicting nuclear lamina and nuclear shape aberrations in siLamin A/C and siLamin B2 DLD1 cells. Scale bar~5 μm. J. Quantification of the frequency of nuclear shape aberrations in siLamin A/C and siLamin B2 DLD1 cells. Representative result from two independent biological replicates.

---

change ≥ 2.0 fold (on an absolute scale), $p<0.05$ were considered to be significant. Thus, a total of ~300 genes were found to deregulated (inclusive of up and down) upon siLamin A/C (Lamin A/C Kd-128 genes up, 170 genes down and Lamin B2 Kd-169 genes up, 132 genes down) (Fig. 3.2C). Upon Lamin A/C Kd, 276 out of 298 genes were uniquely deregulated, while in Lamin B2 Kd, 279 out of 301 genes were uniquely deregulated (Fig. 3.2C). In both Lamin A/C and B2 depleted cells, 22 genes (~7%) were commonly deregulated (Fig. 3.2C).

3.2.3 Validation of whole genome expression profiling by qRT-PCR

Gene expression levels from expression arrays were independently validated using qRT-PCR for the top deregulated genes (absolute fold change ~2-6 fold) (Fig. 3.3A-B). Two unique primer pairs were used for each gene validation – Primer set A designed from a feature of the transcript that was represented on the microarray, and another independent Primer Set B not represented on the array. This showed a fold change in the same direction as that obtained from the microarray data set (Fig. 3.3A-B). We next performed a recovery assay where DLD1 cells were allowed to recover from the Lamin knockdowns by growing cells up to day 8, well beyond the 48 hour duration of the knockdown. At the end of day 8 there was ~60-70% recovery in the transcript and protein levels of Lamin A/C and B2 respectively (Fig. 3.3C-F). We detected a

Figure 3.2

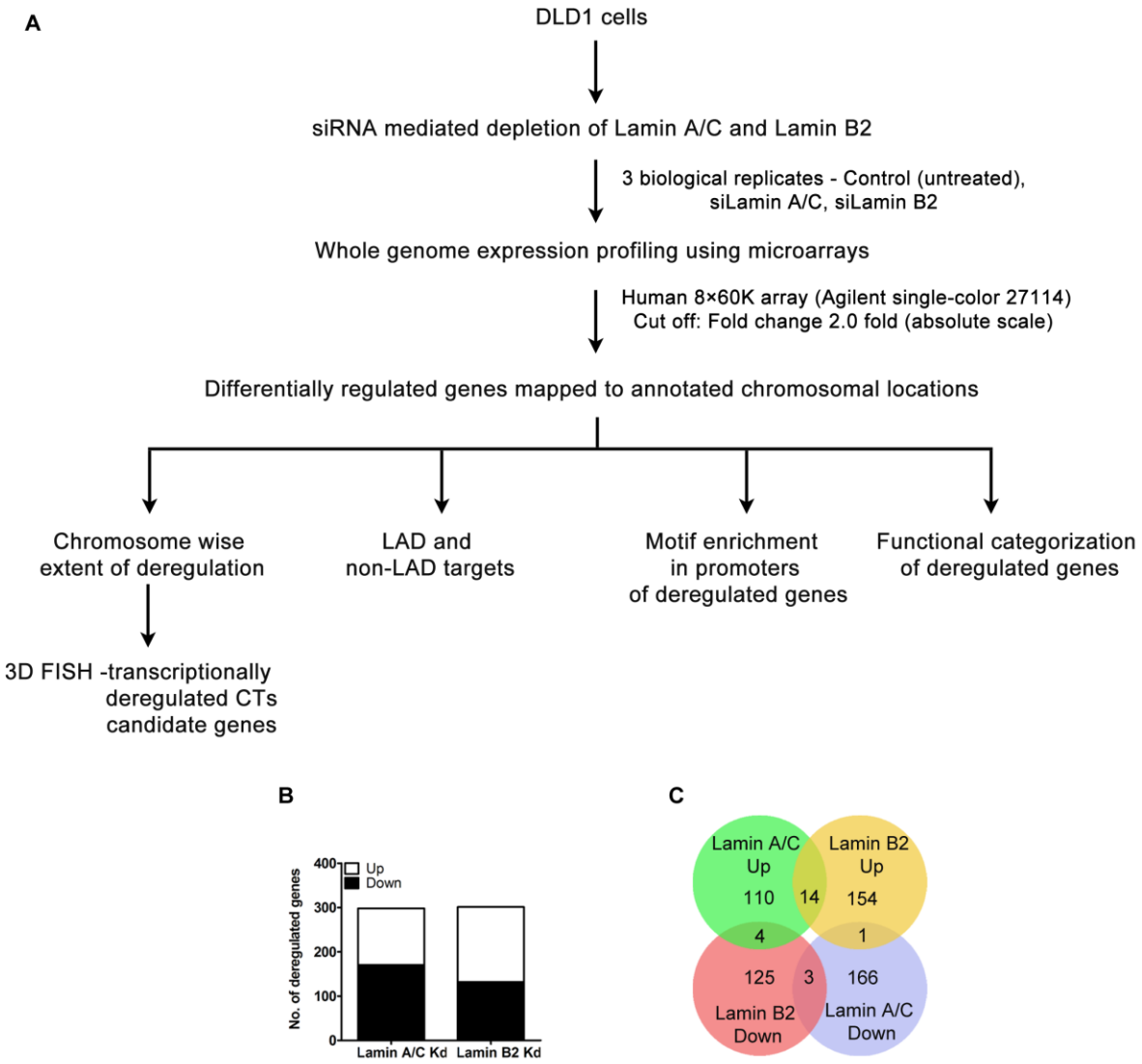

Figure 3.2 Gene expression changes upon depletion of Lamins in DLD1 cells

A. Flowchart representing experiment scheme for gene expression profiling in siLamin A/C and siLamin B2 DLD1 cells. B. Total number of up and down regulated annotated genes (cut off of fold change ≥ 2.0 fold on absolute scale) upon siLamin A/C and siLamin B2 in DLD1 cells. C. Common and uniquely deregulated genes upon Lamin A/C and Lamin B2 depletion in DLD1 cells.

Concomitant and significant recovery in the transcript levels of candidate genes *ABLIM2*, *SMTNL2* upregulated in Lamin A/C Kd and *TMEM14B*, *CDC42* downregulated in Lamin A/C Kd (Fig. 3.3G-H). *REG4*, *PTGS2* were upregulated in Lamin B2 Kd and *MESDC2*, *KRCC1* were downregulated upon Lamin B2 Kd, and recovered in expression levels at day 8 (Fig. 3.3I-J). This recovery profile suggested the dependence of these candidate genes on the levels of Lamin A/C or Lamin B2 for their expression levels.

Figure 3.3

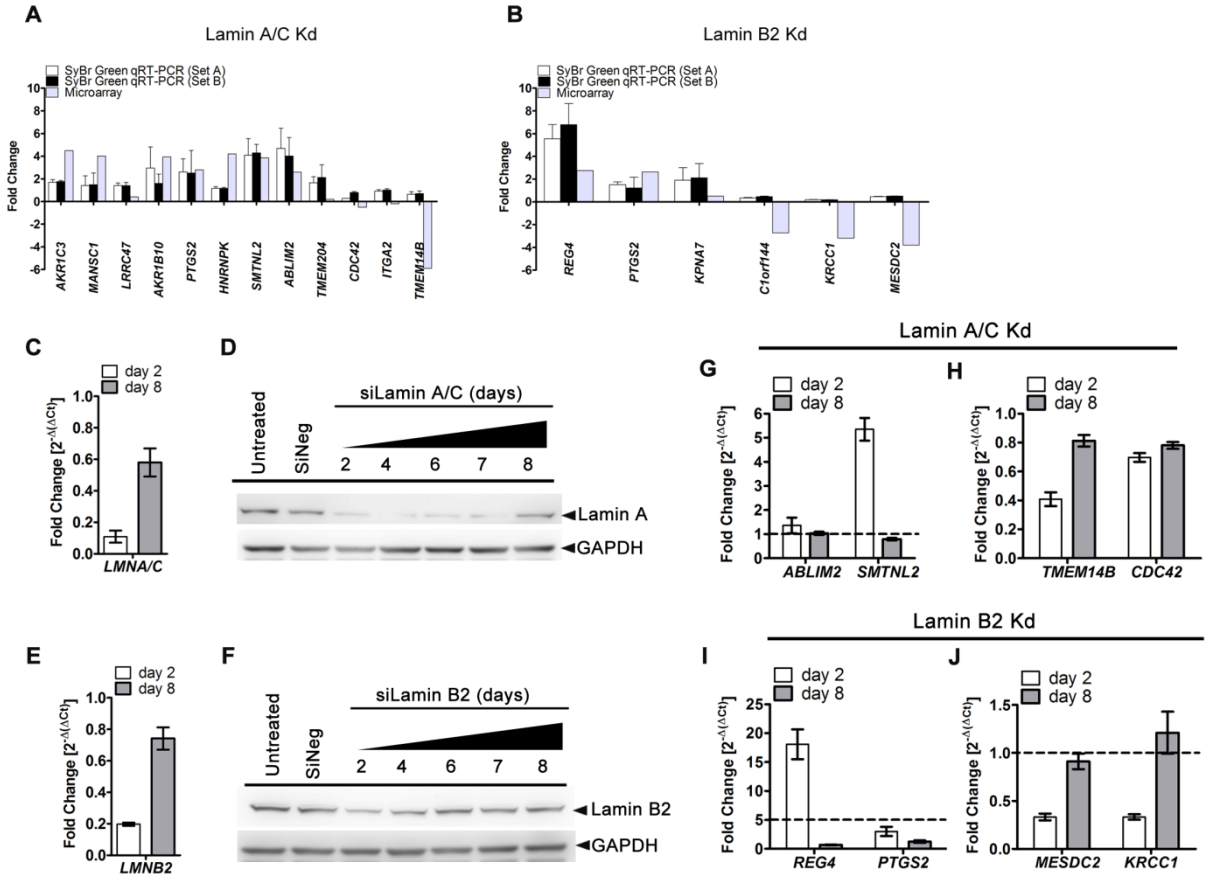

Figure 3.3 Validation of microarray expression data using qRT-PCR

A-B. Validation of microarray data using qRT-PCR for candidate genes from the deregulated gene sets upon (A) Lamin A/C and (B) Lamin B2 depletion in DLD1 cells. Set A: primer sequence from a probe on the array, Set B: primer sequence from a sequence not represented on the array. Data shown is a compilation of three independent biological replicates. Error bars: SEM. C-D. qRT-PCR and Western blots showing recovery in expression level of Lamin A/C at the transcript and protein level respectively at the end of 8 days. E-F. qRT-PCR and Western blots

showing recovery in expression level of Lamin B2 at the transcript and protein level respectively at the end of 8 days. G. Expression levels of candidate upregulated genes upon Lamin A/C depletion (*ABLIM2*, *SMTNL2*) is restored to basal levels at day 8. H. Expression levels of candidate downregulated genes upon Lamin A/C depletion (*TMEM14B*, *CDC42*) is restored to basal levels at day 8. I. Expression levels of candidate upregulated genes upon Lamin B2 depletion (*REG4*, *PTGS2*) is restored to basal levels at day 8. H. Expression levels of candidate downregulated genes upon Lamin B2 depletion (*MESDC2*, *KRCC1*) is restored to basal levels at day 8. qRT-PCRs performed in C, E, G-J are a compilation from two independent biological replicates normalized to expression levels of *ACTIN*.

3.2.4 Chromosome wide gene expression deregulation upon Lamin depletion

Whole genome expression profiling using microarrays from Lamin A mutant (E161K) human cardiomyocytes showed deregulated gene expression levels predominantly from gene poor chromosome 13 (Mewborn et al., 2010). Likewise, mouse fibroblasts lacking a functional Lamin B1 revealed transcriptionally deregulated clusters on the peripherally positioned mouse chromosome 18 (Malhas et al., 2007). We were curious to examine if specific chromosomes were transcriptionally deregulated upon Lamin A/C or B2 depletion. From our expression array data sets independently derived from Lamin A/C and Lamin B2 knockdowns, we calculated the extent of transcriptional deregulation for each chromosome by expressing the total number of deregulated genes on a chromosome as a fraction of the total number of coding genes from that chromosome (Fig. 3.4A). Chromosomes showing >0.7% deregulation in transcript levels were shortlisted since this represented ≥ 50% of the total deregulation per chromosome (~1.5%). Chromosomes showing significant deregulation upon Lamin A/C Kd were Chr.16, 22, 20, 12, 1, 3, 17 and 19 (descending order of expression deregulation), while in Lamin B2 Kd, significantly deregulated genes mapped to Chr.19, 11, 12, 17, X, 8, 3 and 2 (descending order of expression deregulation) (Fig. 3.4A). Comparatively neither Lamin A/C Kd nor Lamin B2 Kd showed a significant transcriptional deregulation from the relatively gene poor chromosomes 13,18 or 7 although these chromosomes are proximal to the nuclear lamina (Fig. 3.4A).

3.2.5 Correlation between transcriptional deregulation and gene density

To examine if chromosomes were selectively deregulated in terms of their transcript levels upon Lamin depletion, we compared properties of chromosomes (viz. chromosome size and gene density) with their extent of transcriptional deregulation. A plot of % transcriptional deregulation against gene density showed a higher correlation with gene density upon Lamin B2 Kd (r^2=0.4629) as compared to Lamin A/C Kd (r^2=0.1823) (Fig. 3.4B-C). No such correlation (r^2 ~ 0.003) was found with chromosome size for the extent of transcriptional deregulation (Fig. 3.4D-E). This reveals an enhanced transcriptional deregulation from gene rich chromosomes upon Lamin B2 Kd as compared to Lamin A/C Kd. Taken together, gene expression profiling of Lamin A/C or B2 depleted cells, uncovered specific chromosomes that were significantly deregulated in their gene expression levels.

3.2.6 ~25 % of deregulated genes upon Lamin knockdown map to constitutive LADs

Genes that were found to be transcriptionally deregulated were assessed for their Lamina association in silico. Genomic sequences of Lamina Associated Domains (LADs) were derived from Dam ID performed for Lamin B1 in Tig3 cells (Guelen et al., 2008). Genes with their promoters within 1.0 kb (±1 Kb) from these LAD sequences were determined. A comparison of these genes with the deregulated genes from siLamin A/C and siLamin B2 datasets was performed to examine the LAD association of the deregulated genes at their promoters. For Lamin A/C Kd, ~19.5% of the upregulated genes and ~11.1% of the downregulated genes were found to map within LADs (Fig. 3.4F). Similarly for Lamin B2 Kd, ~26.6 % of the upregulated genes and ~13.6% of the downregulated genes mapped to LADs (Fig. 3.4G). Thus, in each of Lamin A/C and Lamin B2 Kd, a greater % of upregulated genes were found to map to LADs. This is consistent with an otherwise repressive state of these genes as predicted from LAD association. However, it is important to note that this comparison involves data sets from two different cell types. In addition, only ~11-26% of the total deregulated genes mapped to LADs, suggestive of additional mechanisms alongwith Lamin binding/association in the transcriptional regulation by Lamins.

Figure 3.4

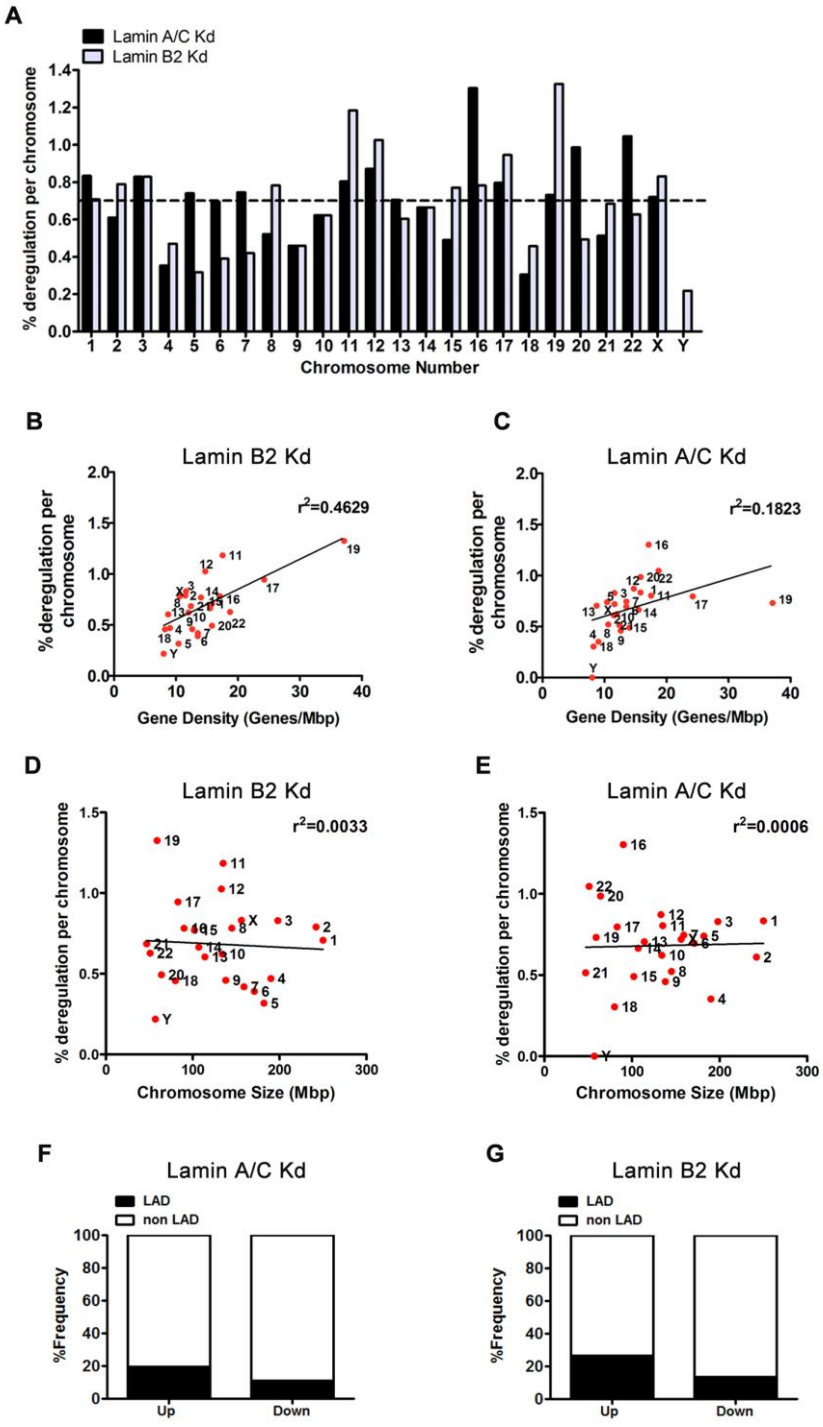

Figure 3.4. Chromosome wise deregulation of transcription upon Lamin A/C and Lamin B2 depletion

A. Chromosome wise extent of % transcriptional deregulation, as determined by normalizing the total number of deregulated genes on a chromosome to the total number of coding genes on that chromosome. B-C. Correlation

between extent of transcriptional deregulation and gene density (no. of genes/Mbp) of chromosomes plotted for (B) Lamin B2 depletion and (C) Lamin A/C depletion. D-E. Correlation between extent of transcriptional deregulation and size (Mbp) of chromosomes plotted for (D) Lamin B2 depletion and (E) Lamin A/C depletion. F-G. % of deregulated genes from (F) Lamin A/C depletion and (G) Lamin B2 depletion that are a part of Lamina associated domains (LADs).

3.2.7 Enrichment of motifs in the promoters of deregulated genes

The gene sets from the Lamin depleted cells yielded an interesting list of genes with potential LAD as well as non LAD associated genes. We were curious to examine if these genes were regulated by a common subset of transcription factors. Alternatively, we examined if these genes were enriched for consensus motifs within their promoter sequences. Toward this end, we performed bioinformatics analysis using Gene Set Enrichment Analysis (GSEA). We compared the enriched gene sets with annotated gene sets for motif searches and associated transcription factors as also micro RNAs. Gene sets from Lamin A/C Kd and Lamin B2 Kd were classified as upregulated and downregulated targets, and each of these lists were compared from gene sets in GSEA Molecular Signature Database (MSigDB). The top 20 enriched motifs and their known binding transcription factors (if any) are documented in Table No 10.1-10.4.

Table 10.1 Motifs/microRNA enriched in promoters of upregulated genes upon Lamin A/C knockdown

No.	TF	Motif	p-value
1	TCF3	CAGGTG	2.86E-09
2	FOXF2	RTAAACA	1.22E-06
3	NFE2	TGCTGAGTCAY	2.42E-06
4	Not known	CTGCAGY	5.42E-06
5	NFE2L2	NTGCTGAGTCAKN	1.64E-05
6	NFE2	TGASTMAG	3.56E-05
7	TCF8	CAGGTA	4.10E-05
8	TCF11	NNNNNATGACTCAGCANTTNNG	4.97E-05
9		MicroRNA TGCACTT	8.65E-05
10	Not known	AACTTT	8.68E-05
11	FOXO3A	TNNTTGTTTACNTW	1.25E-04
12	CEBPA	NNNTKNNGNAAN	1.43E-04
13	FOXC1	NNNNNGTAAATAAACA	1.43E-04
14	Not known	WTGAAAT	1.43E-04
15	Lef1	CTTTGT	1.44E-04
16	FOXF2	NNANNGTAAACAANNN	1.73E-04
17	MLLT7	TTGTTT	2.42E-04
18	NFAT	TGGAAA	2.90E-04
19	CUTL1	NWNATCGATTANYNN	3.75E-04
20		MicroRNA GTGCAAT	4.50E-04

Table 10.2 Motifs/ microRNA enriched in promoters of downregulated genes upon Lamin A/C knockdown

No.	TF	Motif / Micro RNA	p-value
1	unknown	CTTTAAR	2.68E-11
2	MAZ: MYC-associated zinc finger protein (purine-binding transcription factor)	GGGAGGRR	1.10E-08
3	JUN: jun oncogene	TGANTCA	1.28E-08
4	MLLT7	TTGTTT	3.24E-07
5	Sp1	GGGCGGR	7.50E-07
6	MEIS1	TGACAGNY	7.55E-07
7	Not known	NGGGACTTTCCA	8.65E-07
8	Lef1	CTTTGT	1.95E-06
9	Not known	AACTTT	3.43E-06
10		Targets of MicroRNA GTGCCTT,MIR-506	4.93E-06
11	Not known	NGGGGAMTTTCCNN	6.54E-06
12	HNF4A	TGAMCTTTGNCCN	7.97E-06
13		Targets of MicroRNA TGCCTTA,MIR-124A	9.92E-06
14	JUN: jun oncogene	RGTGACTMANN	1.05E-05
15	BACH2	SRTGAGTCANC	1.05E-05
16	TCF8	CAGGTA	1.22E-05
17	FOXA1	TGTTTGY	2.92E-05
18	TFDP1	NCSCGCSAAAN	3.76E-05
19	STAT5B	TTCYNRGAA	4.74E-05
20	YY1	NNNNNCCATNTWNNNWN	4.76E-05

Table 10.3 Motifs/ microRNA enriched in promoters of upregulated genes upon Lamin B2 knockdown

No.	TF	Motif / Micro RNA	p-value
1	Not known	TTANTCA	3.92E-06
2	NR1H4	RRGGTYANTRNM	5.90E-05
3	PITX2	GGATTA	8.90E-05
4	MEF2A	ANKCTAWAAATAGMHNN	1.75E-04
5	TCF3	CAGGTG	1.91E-04
6	FOXD1	CTWAWGTAAACANWGN	2.79E-04
7	STAT5B	TTCYNRGAA	3.08E-04
8	STAT5B	NAWTTCYNGGAAWTN	3.78E-04
9	POU3F1	NNKGAATTAVAVTDN	5.16E-04
10	LEF1	CTTTGT	5.28E-04
11	Not known	AAAYRNCTG	5.93E-04
12	ESRRA	TGACCTY	6.68E-04

Table 10.4 Motifs/ microRNA enriched in promoters of downregulated genes upon Lamin B2 knockdown

No.	TF	Motif / Micro RNA	p-value
1	Sp1	GGGCGGR	4.23E-05
2	FOXF2	RTAAACA	8.51E-05
3	NKX2-5	CWTAATTG	1.27E-04

A comparison of the outputs for siLamin A/C and siLamin B2 sets reveals an interesting pattern of transcription factors with their recognition motifs represented in these target genes. MAZ, Jun, Sp1 are important TFs enriched in Lamin A/C Kd downregulated genes, while the upregulated targets show an enrichment of TCF3, FOXF2 and NFE2 TFs. Lamin B2 Kd data set has a lower annotation of regulatory TFs as compared to Lamin A/C Kd data set. Among the genes downregulated upon Lamin B2 Kd, Sp1, FOXF2 and NKX2-5 were the TFs with their binding motifs represented in the target genes. The upregulated genes upon Lamin B2 Kd showed an enrichment primarily of motifs for NR1H4, PITX2 and MEF2A TFs. There were common TFs and motifs enriched in some of these categories e.g. Lamin A/C and Lamin B2 upregulated genes showed enrichment for motifs of TCF3 and LEF1 TFs, while Lamin A/C kd up and down regulated genes also showed a common set of motifs for TFs MLLT7, TCF8, LEF1. Also, Fox family TFs showed enrichment in both Lamin A/C and Lamin B2 target gene sets. Thus, this analysis revealed a pattern of enrichment of TFs from Sp1, TCF family, LEF family, FOX family that may execute Lamin A/C and/or Lamin B2 dependent transcriptional changes. These TFs were also largely non overlapping between Lamin A/C and Lamin B2 datasets, thereby suggesting a difference in regulation by Lamin A/C and Lamin B2.

In addition to the above analysis involving regulatory sequence motifs and transcriptions factors, we also examined potential TFs enriched in up/downregulated gene sets using Animal Transcription factor data base (Animal TFDB). Different TFs that show transcriptional deregulation upon Lamin depletion are represented in Table No. 11.

3.2.8 Non-overlapping functional categories enriched from deregulated genes upon Lamin A/C and Lamin B2 depletion

We also examined the list of potential biological functions enriched from deregulated genes upon Lamin depletion in DLD1 cells. The differentially regulated gene sets (absolute fold change ≥2.0) from Lamin A/C Kd and Lamin B2 Kd were analyzed using DAVID (Fig. 3.5). Lamin A/C Kd performed on DLD1 cells followed by microarray analyses, revealed clusters of genes that classified into distinct **G**ene **O**ntology categories (Fig. 3.5). A significant ($p<0.05$) downregulation was detected upon

Table 11. Transcription factors deregulated upon Lamin depletion in DLD1 cells

Lamin A/C Kd (Down)	Lamin A/C Kd (Up)	Lamin B2 Kd (Down)	Lamin B2 Kd (Up)
CREM	CRX	ATOH8	CRX
E2F8	FOXF1	HLF	DMRTB1
EGR2	GTF2IRD2B	IRF8	HOXB8
EGR3	HES2	JDP2	HOXC13
GLI1	HOXB8	MYB	POU4F1
MAFK	NFE2	NCOR2	ZIC4
PBX3	PROX1	ZNF837	ZNF540
TFAP4	ZBTB46		ZNF570
	ZFP2		ZNF880
	ZNF362		

Lamin A/C Kd for GO categories: (i) Cell cycle (ii) Signaling (iii) Nuclear and chromosome organization (iv) Cell adhesion and membrane signaling (Fig. 3.5A). The GO categories upregulated upon Lamin A/C Kd include (i) Metabolism (ii) Development and organogenesis (Fig. 3.5B). Downregulated genes upon Lamin B2 Kd predominantly cluster to GO categories of (i) neurological processes (ii) membrane and transport functions and (iii) apoptosis (Fig. 3.5C). Analyses of the GO categories of upregulated targets upon Lamin B2 Kd showed a specific increase in the gene expression levels of (i) neurological processes (ii) membrane associated functions (iii) cellular responses and signaling and (iv) immunological processes (Fig. 3.5D). It would be of interest to examine now the integrative data that emerges from the transcription factor analysis and the functional analysis. Transcription factors that participate in some of these pathways/functions enriched here include Fox family of TFs as also TCF/LEF families. Amongst

these FOX family of TFs is important for cell growth as also cell differentiation and development, while TCF/LEF family TFs participate in Wnt signaling (Cadigan and Waterman, 2012; Hannenhalli and Kaestner, 2009).

Figure 3.5

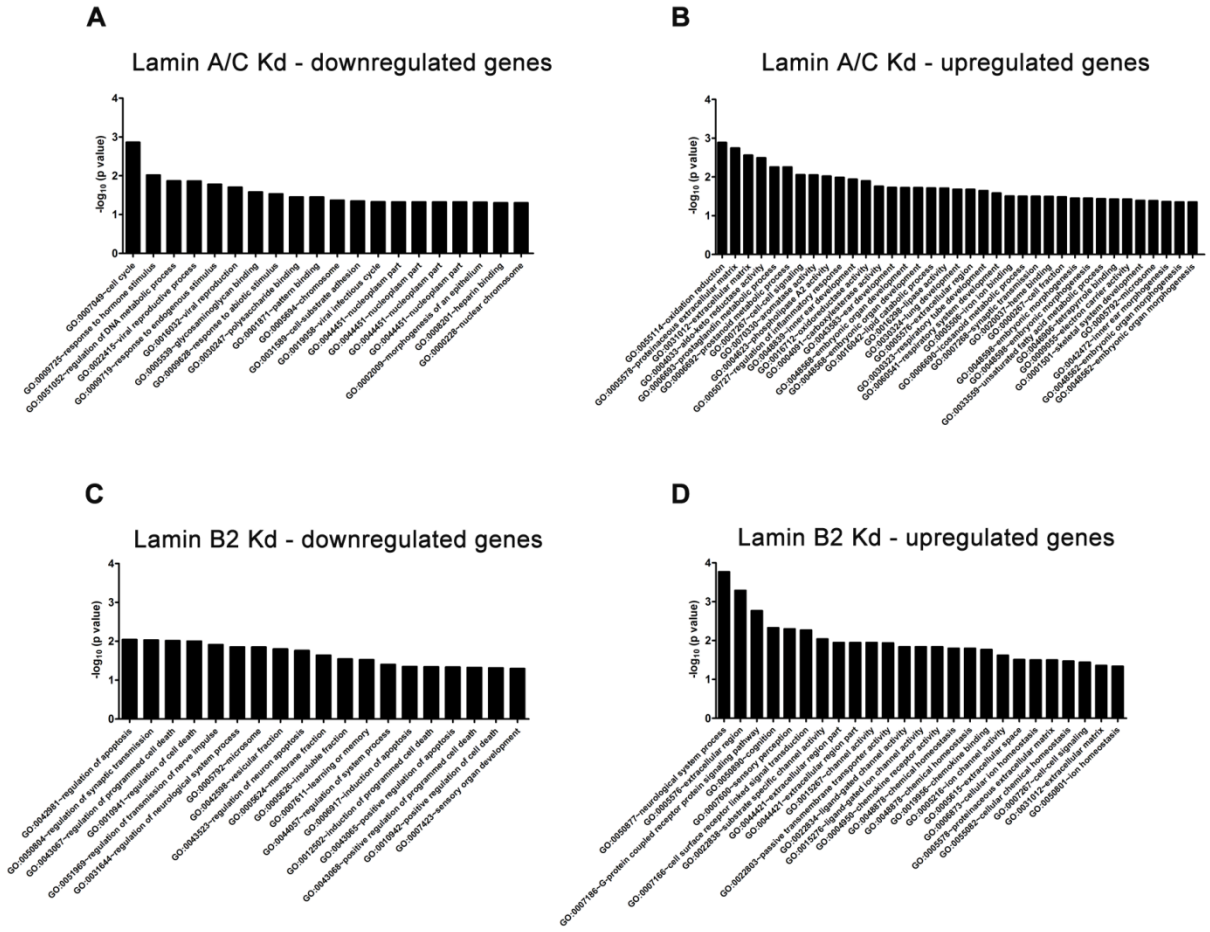

Figure 3.5 Functional categories of deregulated genes upon Lamin A/C and Lamin B2 depletion

A. GO categories (Biological processes, Cellular component, Molecular functional all inclusive) significantly enriched ($p<0.05$) for transcriptionally deregulated gene sets from (A) Lamin A/C – downregulated (B) Lamin A/C – upregulated (C) Lamin B2 – downregulation and (D) Lamin B2 – upregulation categories. Enrichment plotted as – $\log_{10}$ (p value) of shortlisted GO categories.

3.3 Discussion

In this study, we have characterized the gene expression changes elicited in DLD1 cells- a colorectal cancer cell line upon the depletion of Lamin A/C or Lamin B2. We detected a non overlapping profile of gene expression changes upon Lamin A/C and Lamin B2 depletion, with only ~7% genes being commonly deregulated between these data sets. The range of gene expression changes that were captured using microarrays ranged from ~2.0 fold to 6.0 fold on the absolute scale, indicating that the general scale of deregulation of transcription upon Lamin depletion is not very high. This also suggests that Lamin A/C or Lamin B2 depletion may not elicit an overall change in general transcription processes. A loss of general transcription control or transcription stalling would have otherwise resulted in a much greater extent of transcriptional deregulation. A small subset of transcriptionally deregulated genes was also indicative of a greater specificity of the gene expression changes seen. Moreover, the validation of the microarray data, and the recovery assays performed suggest lamin dependence of the gene targets for their expression levels (Fig. 3.3).

The gene expression profiles upon Lamin A/C and Lamin B2 depletion clustered to non overlapping regions of various chromosomes. Lamin A/C and Lamin B2 bind to chromatin at LADs, however the LADs of A and B type lamins across cell types overlap to ~71% (Meuleman et al., 2013). Thus, we speculate that, regions of the genome that are bound by both Lamin A/C and Lamin B2 at LADs may not show gene expression changes when a single lamin protein is knocked down. Alternatively, the presence of Lamin B1, LBR, Emerin, LAP2beta may also be sufficient to anchor and maintain the transcription status of LADs (Amendola and van Steensel, 2015). Hence the spectrum of gene expression changes elicited in Lamin A/C or Lamin B2 knockdown in DLD1 cells might be confined to the small subset of genes that are under direct regulation of either Lamin A/C or Lamin B2 in this case. Comparison of deregulated genes upon Lamin Kd with LADs (Guelen et al., 2008) showed that of the total genes deregulated, only ~25% genes mapped to these LADs. Thus, the remainder of the genes may be a part of facultative LADs for Lamin A/C and/or Lamin B2, which needs to be examined in detail. Alternatively, there may be mechanisms other than direct chromatin binding involved in the regulation of gene expression.

To gain further mechanistic insights into the nature of regulation of these gene targets, we performed bioinformatics analyses to determine sequence motifs and their potential transcription factors. Several important transcription families were enriched in this analysis, with Jun, Maz, Sp1, Lef/TCF families being enriched on targets upon Lamin A/C Kd. Thus, we speculate a model wherein a depletion of Lamin A/C directly or indirectly results in the deregulation of these TFs, which is in turn reflected in a change in gene expression pattern of their target genes. For Lamin B2 as well, Sp1, Fox family, PITX2, Stat, LEF/TCF family TFs were enriched on the promoters of deregulated gene targets. Owing to a lack of sufficient protein binding data for Lamin B2, we cannot comment conclusively on the direct regulation of these factors by Lamin B2. However, we speculate a similar mechanism of regulation by Lamin B2 as for Lamin A/C in this regard. Interestingly, a deregulation of these major family TFs may impinge on key signaling mechanisms in the cell, including developmental cascades, ERK signaling, Wnt signaling since these TFs are important executors of these signaling pathways in cells (Akira, 1999; Cadigan and Waterman, 2012; Hannenhalli and Kaestner, 2009; Tan and Khachigian, 2009). Lamins are shown to sequester TFs at the nuclear periphery and to regulate their activity (Heessen and Fornerod, 2007). Along with this potentially direct mechanism, genes showing transcriptional changes upon Lamin A/C and Lamin B2 depletion also include other transcription factors (Table 11). This could in turn affect the expression status of the target genes of these TFs. Thus, gene regulation by Lamins, whether direct or indirect, involves a complex interplay of several factors. Experimental validation needs to be performed to examine which of these TFs are actually the mediators of the gene expression changes; and which of these are under direct regulatory control of Lamins A/C or B2. It would also be interesting to examine which of these regulatory relationships are cell type specific and are functional only in colorectal cancer cells. However, testing these mechanisms was beyond the scope of this current study; since our preliminary objective in the gene expression profiles was to examine transcription deregulation across different chromosomes and to test if lamin dependent gene expression changes (function) also elicit changes in positioning (structure) of chromosomes and gene loci.

In this study, we found differential gene expression changes on different chromosomes upon Lamin knockdowns. To eliminate any bias from differences in the number of genes present on different chromosomes, we normalized the total number of deregulated genes on each chromosome to the total number of genes present on that chromosome. We compared this

normalized % deregulation per chromosome across chromosomes and noted chromosomes 16 and 19 to be maximally deregulated upon Lamin A/C and Lamin B2 depletion respectively. Other chromosomes that showed significant transcriptional deregulation upon siLamin A/C were 16, 22, 20, 12, 1, 3, 17, and 19 and siLamin B2 were 19, 11, 12, 17, X, 8, 3, and 2, thus indicating a difference between Lamin A/C and Lamin B2 with respect to the chromosomes affected. We next identified chromosomes enriched upon Lamin A/C or Lamin B2 depletion. Comparison of the regression profiles of % deregulation of chromosomes and chromosome size revealed no correlation (r^2 ~0.003) in either Lamin A/C or Lamin B2 depleted cells. % deregulation plotted against gene density of chromosomes revealed an interesting difference between Lamin A/C and Lamin B2. While Lamin A/C depleted cells showed low correlation between these two parameters, Lamin B2 depleted cells showed an increased correlation. This suggests that more gene dense chromosomes were affected in terms of transcription deregulation upon Lamin B2 depletion, while no such trend was noted for Lamin A/C depletion. We used this profile of chromosome wide deregulation and differences between siLamin A/C and siLamin B2 to ask – is this functional deregulation of chromosomes also linked to its structural organization? Is the positioning of transcriptionally deregulated chromosomes different from those that were not transcriptionally affected? We also scaled down from a chromosome territory and asked – are genes that are transcriptionally deregulated due to lamin depletion also organized differently? Some of these questions are dealt with in the following chapter (Chapter 4) of this thesis.

The genes deregulated upon Lamin A/C as well as Lamin B2 depletion clustered functionally to unique non overlapping GO categories. The role of Lamin A/C in development and differentiation has previously been documented in mice as well as human stem cell models (Constantinescu et al., 2006; Solovei et al., 2013; Sullivan et al., 1999; Zuo et al., 2012). Likewise, Lamin B2 has been associated with neurological processes, axon migration and signaling and neuron development (Coffinier et al., 2010; Coffinier et al., 2011; Young et al., 2012). These GO categories were found to be enriched upon Lamin A/C and Lamin B2 depletion respectively, in DLD1 cells. In addition, Lamin A/C depletion showed a downregulation of genes from nuclear and chromosome organization category. An interesting lesser explored category of genes upregulated upon Lamin A/C depletion was of metabolism associated processes. Similarly, for Lamin B2 Kd, upregulated genes clustered to membrane associated processes and signaling; as also a newer category of immunological processes, that has not been examined in detail in

literature. Downregulated genes upon Lamin B2 Kd clustered to apoptosis, signaling and neurological processes; which have been previously described for some kind of cells (Coffinier et al., 2010; Coffinier et al., 2011; Young et al., 2012). Our work has opened up potentially novel pathways of Lamin regulation – primarily of metabolic regulation by Lamin A/C and immunological regulation by Lamin B2. In this work though, our scope has been limited to examining the contribution of Lamins with regard to its role in the nuclear and chromosome organization.

Chapter 4: Spatial organization of transcriptionally deregulated chromosome territories upon Lamin depletion

Results from this chapter are published as a part of the following manuscript:

Ranade, D., Koul, S., Thompson, J., Prasad, K. B. and Sengupta, K. (2016). Chromosomal aneuploidies induced upon Lamin B2 depletion are mislocalized in the interphase nucleus. *Chromosoma*.

4.1 Introduction

The genome wide gene expression profiles determined from the microarray data revealed non-overlapping gene expression changes upon Lamin A/C and Lamin B2 depletion in DLD1 cells. In this chapter we have investigated the nuclear organization of chromosomes that were found to be transcriptionally deregulated upon either Lamin A/C and/or Lamin B2 depletion. However, in addition, both A and B type lamins maintain the mitotic spindle and regulate chromosome numbers. Chromosomal Instability (CIN) is a defining feature of the initiation and progression of several cancers (Bakhoum and Compton, 2012). We report here that Lamin A/C and Lamin B2 depletion reveals multiple chromosome territories in the interphase nucleus, further reiterating the CIN phenotype (Ranade et al., 2016). The mechanistic role of Lamin A in regulating CIN may be attributed to its association with nuclear envelope proteins such as LAP2α and BAF which further stabilize spindle orientation and assembly (Qi et al., 2015). Interestingly, B type Lamins are also a part of the mitotic spindle matrix in *X. laevis* and HeLa cells (Goodman et al., 2010; Tsai et al., 2006). Lamin B2 regulates genomic stability and chromosome segregation in colorectal cancer cells (Kuga et al., 2014). Therefore, Lamins are a unique class of molecules required for genome organization, chromosomal stability and ploidy in mitosis. However, the role for lamins in regulating the spatial organization of diploid and aneuploid chromosomes territories in the interphase nucleus is largely unclear.

Several epithelial cancers as well as developmental disorders are characterized by aneuploidy. Pancreatic cancers, ovarian cancers and breast cancers are characterized by a complex pattern of chromosomal gains and losses and translocations (Bakhoum and Compton, 2012; Thompson and Compton, 2008). Developmental disorders characterized by aneuploidy include Down's Syndrome (chromosome 21 trisomy), Edward's Syndrome (chromosome 18 trisomy) and Patau's Syndrome (chromosome 13 trisomy) (Edwards et al., 1960; Jacobs et al., 1959; Patau et al., 1960). The contribution of aneuploidy to chromosome positioning is not clearly understood as it involves the packaging and organization of more than two chromosome territories in the interphase nucleus. How the cell overcomes these constraints and accommodates extra chromosomes is a mechanism that has not been examined in detail. Artificially introduced gene poor (Chr.7, Chr.18, peripheral) or gene rich (Chr.19, central) chromosomes into colorectal cancer cells, assume conserved locations in the nucleus consistent with their gene densities

(Sengupta et al., 2007). Cancer cells show deviant chromosome positions as compared to normal cells. CT18 and CT19 are more proximal to one another in colon and cervical cancer cell nuclei as compared to normal cells (Cremer et al., 2003).

However, naturally occurring chromosomal aneuploidies in non-cancerous cells largely reveal altered chromosome positioning patterns in cells derived from other diseases. Human X chromosome is altered from a predominantly central to a more peripheral location in X chromosome aneuploidies (XXXXY) (Petrova et al., 2007). In Down's syndrome, 2 copies of chromosome 21 territory have greater proximity as compared to the third copy (Paz et al., 2013). The human embryonic stem cell line (WA09) in culture shows a gain of chromosome 12, which exhibits an altered position of the trisomic chromosome (Shete et al. 2014). Trisomic primary amniocyte cells showed that aneuploid human Chr.18 and 21 territories assume conserved nuclear locations (Hervé et al., 2016). Taken together, these evidences reveal cell type and chromosome specific variations in the positioning of aneuploid chromosome territories. The molecular basis for this however remains elusive. Considering the overarching functions of lamins in regulating ploidy and genome organization, lamins therefore present as important candidates that may regulate genome organization of diploid and aneuploid chromosomes.

Aneuploidy in the form of whole chromosomal gains positively correlates with gene expression levels in cancer cell lines and in cells derived from patient samples (Grade et al., 2007). For instance, gene expression profiling of human Chr.5 and Chr.7 in colorectal cancer cells (HCT116 and DLD1 cells respectively) show enhanced gene expression levels. Moreover, naturally occurring trisomies of Chr.13 (Edward's Syndrome) and Chr.21 (Down's Syndrome) also show transcriptional upregulation from these aneuploid chromosomes by ~1.1-1.5 fold (FitzPatrick et al., 2002; Mao et al., 2003; Stingele et al., 2012; Upender et al., 2004). Interestingly, Lamin A/C or Lamin B2 depleted DLD1 cells showed ~1% deregulation of the transcriptome. In summary, we were intrigued to know if (i) transcriptional deregulation from different chromosomes shows correlations with aneuploidy for those chromosomes (ii) Are lamins involved only in the generation of aneuploidy, or are they also involved in maintenance of positions of aneuploid chromosomes in the interphase?

Here we have examined three interrelated facets associated with chromosome positioning namely (i) Chromosomal instability (ii) lamins A/C and B2 and (iii) transcription. Lamin B2

depletion in the otherwise diploid DLD1 and HCT116 cells showed chromosomal instability (CIN) (Kuga et al., 2014; Ranade et al., 2016). Genesis of diploid and aneuploid subpopulations in Lamin depleted cells enabled us to specifically query for the role of Lamins in positioning of chromosomes in cells showing CIN. We show that specific chromosomes are transcriptionally deregulated upon Lamin A/C and Lamin B2 knockdown. Remarkably, transcriptionally deregulated gene rich or gene poor chromosomes in Lamin depleted diploid cells largely assume conserved chromosome positions as revealed by 3D-FISH. However, aneuploid chromosomes were mislocalized in subpopulations of Lamin B2 and not Lamin A/C depleted cells, suggesting a specific role for Lamin B2 in the maintenance of chromosome positions in aneuploid cells. Consistently, aneuploid cancer cell lines showed a partial loss of gene density based chromosome positioning patterns, as revealed through a reduced spatial separation between gene poor chromosome 18 and gene rich 19. Furthermore, gene loci which are orders of magnitude lower in DNA content than chromosome territories were repositioned upon Lamin depletion, consistent with an increase in their gene expression levels. Taken together, we propose the involvement of Lamin B2 in mechanisms that regulate the spatial organization of aneuploid chromosome territories in the interphase nucleus.

4.2 Results

4.2.1 Chromosomal aneuploidies are induced upon Lamin A/C and Lamin B2 depletion in interphase cells

The gene expression profiles derived from the microarray based expression profiling upon siLamin A/C and siLamin B2 revealed specific chromosomes that showed greater transcriptional deregulation over others (Fig. 3.4A). The pattern of transcriptionally deregulated chromosomes was found to differ between siLamin A/C and siLamin B2 cells. We examined the spatial organization of the transcriptionally deregulated chromosomes. Chromosomes that were found to be transcriptionally deregulated upon Lamin A/C Kd and Lamin B2 Kd were labeled using 3 Dimensional Fluorescence *in situ* hybridization (3D-FISH) to examine their spatial organization (Fig. 4.1). Chromosomes territories 1, 16 were examined upon Lamin A/C depletion and chromosome territories 11 and 17 upon Lamin B2 depletion (Fig. 4.1A-B). Chromosomes 18 and 19 territories were examined upon both Lamin A/C and Lamin B2 depletion (Fig. 4.1C). While control cells (untreated cells and cells treated with siLacZ – non targeting control) showed a consistently diploid population (~95%) for these chromosomes, we detected subpopulations of cells with aneuploid chromosomes showing >2 CTs in siLamin A/C and siLamin B2 cells (Fig. 4.11D-E). While CT18 and CT19 showed aneuploidy in ~ 20-30% of siLamin A/C cells, chromosomes 11,17,18,19 were gained in Lamin B2 Kd cells (3-4 copies) (Fig. 4.11D-E). We verified the extent of Lamin depletion in diploid and aneuploid cells by performing immuno-FISH for Lamin A/C and Lamin B2 with chromosome 18 and 19 respectively (Fig. 4.1F,H). We analyzed copy numbers of CTs and detected a comparable extent of Lamin A and B2 depletion (~75-80%) (Fig. 4.1G,I) in both the diploid and aneuploid subpopulations. In summary, Lamin depletion generated two sub-populations of DLD1 cells – diploid (~75%) and aneuploid (~25%).

Figure 4.1

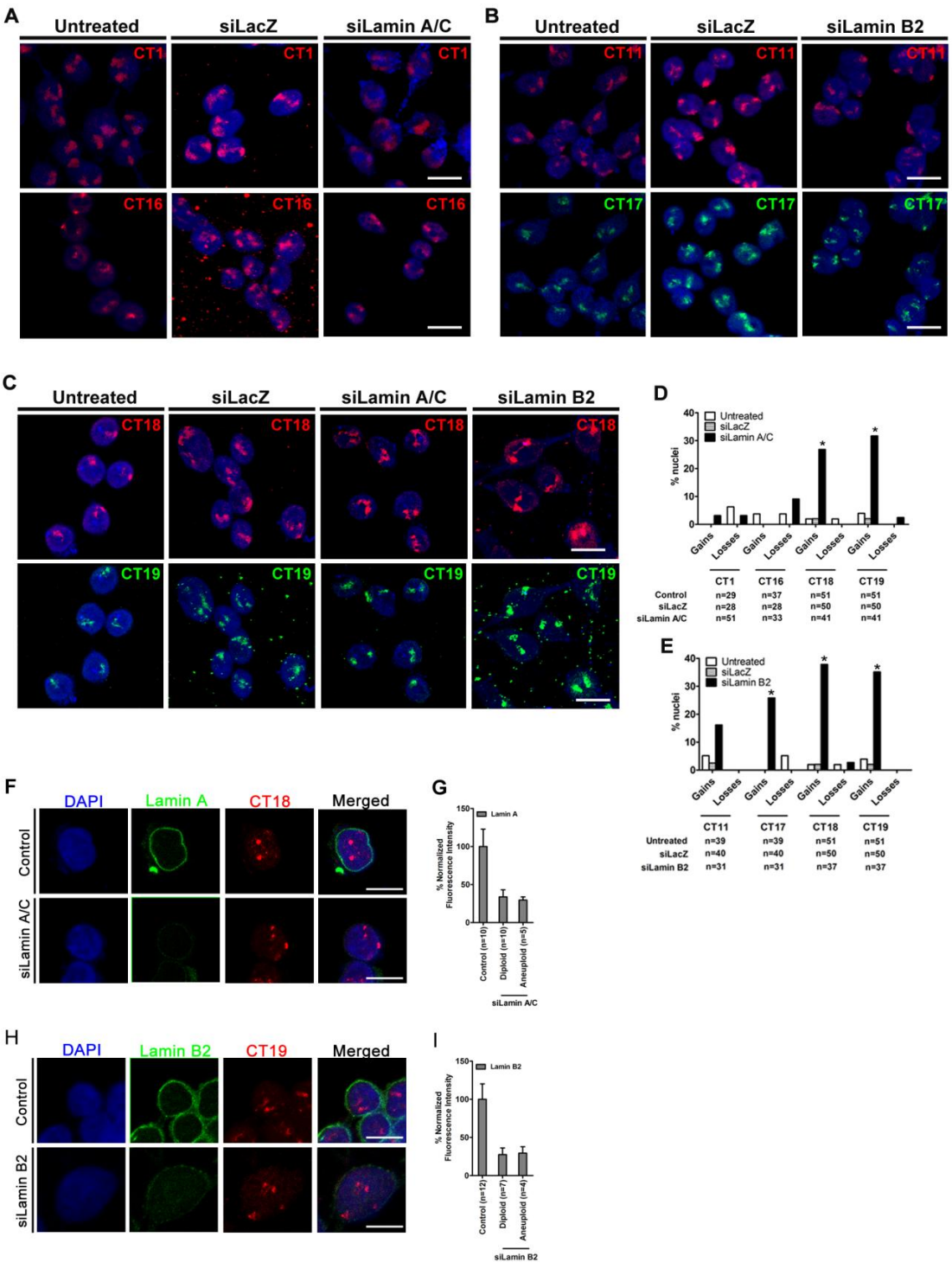

Figure 4.1 Chromosomal aneuploidies are generated upon Lamin A/C and Lamin B2 depletion in DLD1 cells

A-C. Representative 3D FISH images for (A) CT1, CT16 in Control (untreated and siLacZ treated) and siLamin A/C cells (B) CT11, CT17 in Control (untreated and siLacZ treated) and siLamin B2 cells (C) CT18, CT19 in Control (untreated and siLacZ treated), siLamin A/C and siLamin B2 cells. Scale bar~10µm. D-E. Quantification of number of CTs in interphase nuclei of (D) control and siLamin A/C cells, (E) control and siLamin B2 cells. Number of

nuclei scored in each treatment (n) ~28-51. CT18 and CT19 are aneuploid in ~30% cells in Lamin A/C and Lamin B2 depletion. CT11 and CT17 show aneuploidy in ~15-25% cells in Lamin B2 depletion. Data shown is a representative result out of two independent biological replicates. F. ImmunoFISH for Lamin A (green) and CT18 (red) in control and siLamin A/C DLD1 cells. Scale bar~10μm. G. Fluorescence intensity quantification of Lamin A signal at the nuclear periphery performed using line scans in control and siLamin A/C (diploid and aneuploid) cells. H. ImmunoFISH for Lamin B2 (green) and CT19 (red) in control and siLamin B2 DLD1 cells. Scale bar~10μm. G. Fluorescence intensity quantification of Lamin B2 signal at the nuclear periphery performed using line scans in control and siLamin B2 (diploid and aneuploid) cells.

4.2.2 Lamin depletion reveals chromosomal instability (CIN)

We further examined if the extent of aneuploidy detected in interphase cells was also detected at the metaphase stage (Fig. 4.2). Metaphase spreads were generated from control, siLamin A/C and siLamin B2 cells (Fig.4.2A-C). Control cells showed a predominantly pseudo-diploid population (45-46 chromosomes) consistent with the normal ploidy of DLD-1 cells (Fig. 4.2D). However, an increase in the number of cells with chromosomal losses and gains were detected in Lamin A/C Kd ($p=0.0345$) while a predominant increase in chromosomal gains was detected upon Lamin B2 depletion in DLD1 cells ($p=0.018$) (Fig. 4.2D). Thus, chromosomal instability detected in interphase cells was recapitulated in metaphases. Metaphase spreads showed that Lamin A/C depleted cells showed chromosomal losses as well as gains; Lamin B2 depleted cells primarily showed gain of chromosomes.

4.2.3 Lamin depletion induces mitotic aberrations

To further examine the impact of Lamins to address chromosomal instability induced upon Lamin B2 depletion over Lamin A/C depletion, we examined levels of mitotic aberrations and mitotic checkpoint proteins. Cells derived from Lamin B2 knockdowns were fixed every 12 hours in an asynchronous population and stained with DAPI to examine chromosomes in dividing cells (Fig. 4.2E-F).

Figure 4.2

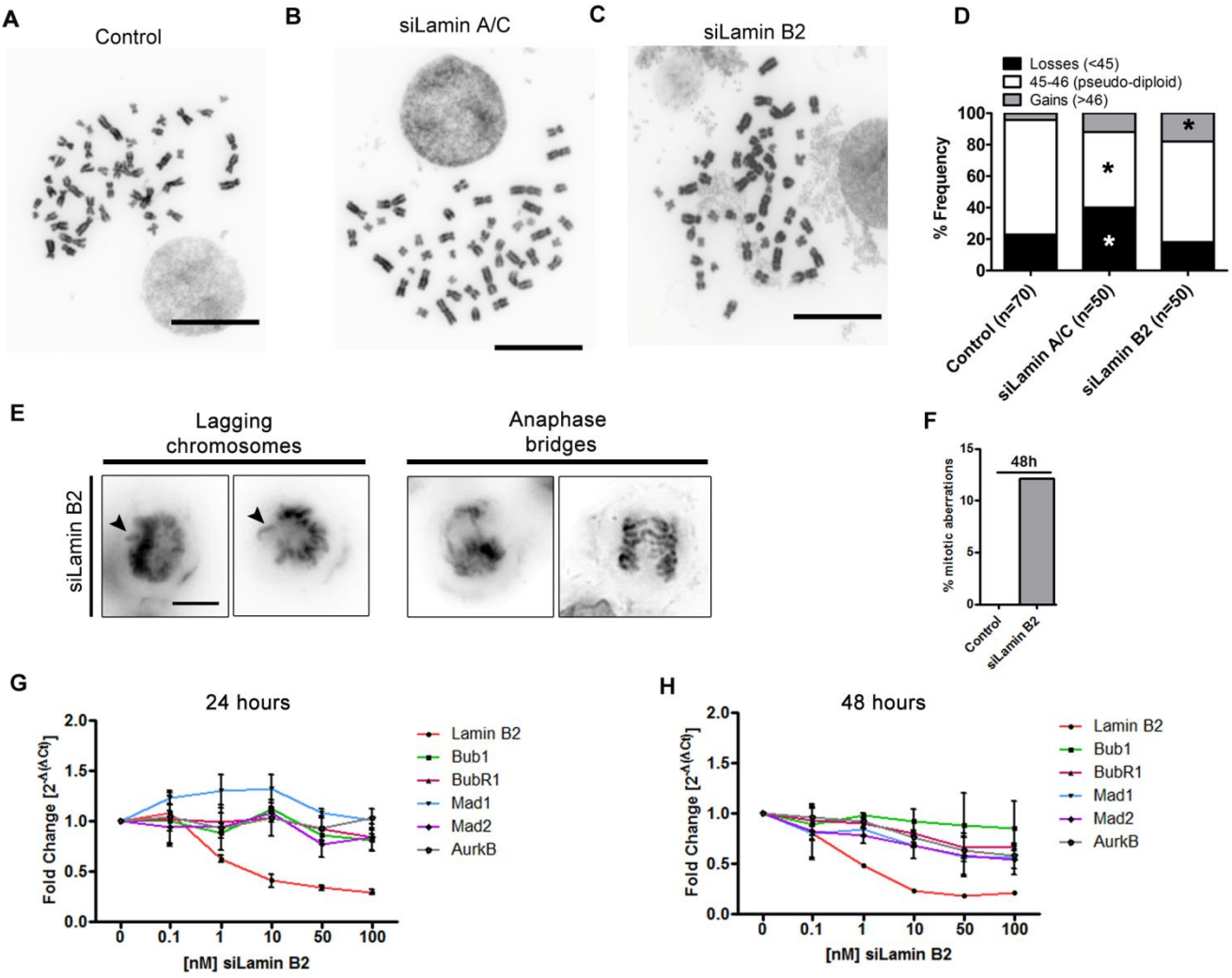

Figure 4.2. Mitotic aberrations and aneuploidy upon Lamin depletion in DLD1 cells

A-C Representative inverted DAPI stained images of metaphase spreads generated from control, Lamin A/C and Lamin B2 depleted cells. Scale bar~10µm. D. Quantification of ploidy (number of chromosomes counted from metaphase spreads) from control, Lamin A/C and Lamin B2 depleted cells. Lamin A/C depleted cells show a decrease in the diploid population, as also an increase in chromosomal gains and losses, while Lamin B2 depleted cells show a predominant gain of chromosomes. E. Representative inverted DAPI stained images of mitotic aberrations – lagging chromosomes, anaphase bridges, spindle defects. F. Quantification of mitotic aberrations at 48 hours post Lamin B2 depletion in DLD1 cells. G-H. qRT-PCR showing expression levels of spindle assembly checkpoint proteins – Bub1, BubR1, Mad1, Mad2, AurkB in a graded level of Lamin B2 depletion in DLD1 cells at (G) 24 hours and (H) 48 hours post knockdown. Data shown is a compilation from two independent biological replicates, normalized to expression levels of *ACTIN*. Error bars: SEM.

Mitotic aberrations included (i) anaphase bridges (ii) lagging chromosomes and (iii) defective spindles (Fig. 4.2E). At 48 hours, we detected ~12-15% cells with mitotic aberrations (Fig. 4.2F).

Furthermore, we also profiled for the transcript levels of major mitotic checkpoint proteins namely Bub1, BubR1, Mad1, Mad2 and Aurora kinase B (Aurk B) upon Lamin B2 depletion (Fig. 4.2G-H). Lamin B2 depletion was performed in a dose response of increasing siRNA concentrations from 0.1nM to 100nM and harvested at 24 hours and 48 hours post knockdown. We detected downregulation (~0.6-0.8 fold) of all these checkpoint factors except Bub1 which showed a marginal increase upon Lamin B2 depletion (Fig. 4.2H). Checkpoints BubR1, Mad1, Mad2 showed a downregulation in expression as a function of time (increasing from 24h to 48h) corresponding to an increase in the extent of Lamin B2 knockdown and the time of occurrence of aneuploidy (Fig. 4.2G-H).

4.2.4 Cell cycle profiles are not severely altered upon Lamin depletion

We next examined if an alteration in chromosome numbers detected by FISH upon Lamin B2 depletion, was also manifested in the cell cycle profiles of cells. FACS analysis was performed using Propidium iodide staining in control and Lamin depleted cells (Fig. 4.3A-D). FACS profiles did not reveal any significant difference between the control and Lamin A/C, B1 or B2 depleted cells suggesting that knockdown of Lamins does not induce an overall change in ploidy from 2n to 3n, but was confined to gains or losses of 1-2 chromosomes as indicated in the metaphase spreads (Fig. 4.3A-D). We also performed western blots to examine the levels of major cell cycle checkpoint proteins Chk1 and Chk2 as also pChk1 and pChk2 upon Lamin depletion in DLD1 cells (Fig. 4.3E-F). No significant change in expression levels was detected for these proteins in Lamin A/C and Lamin B2 depleted cells (Fig. 4.3E-F).

Figure 4.3

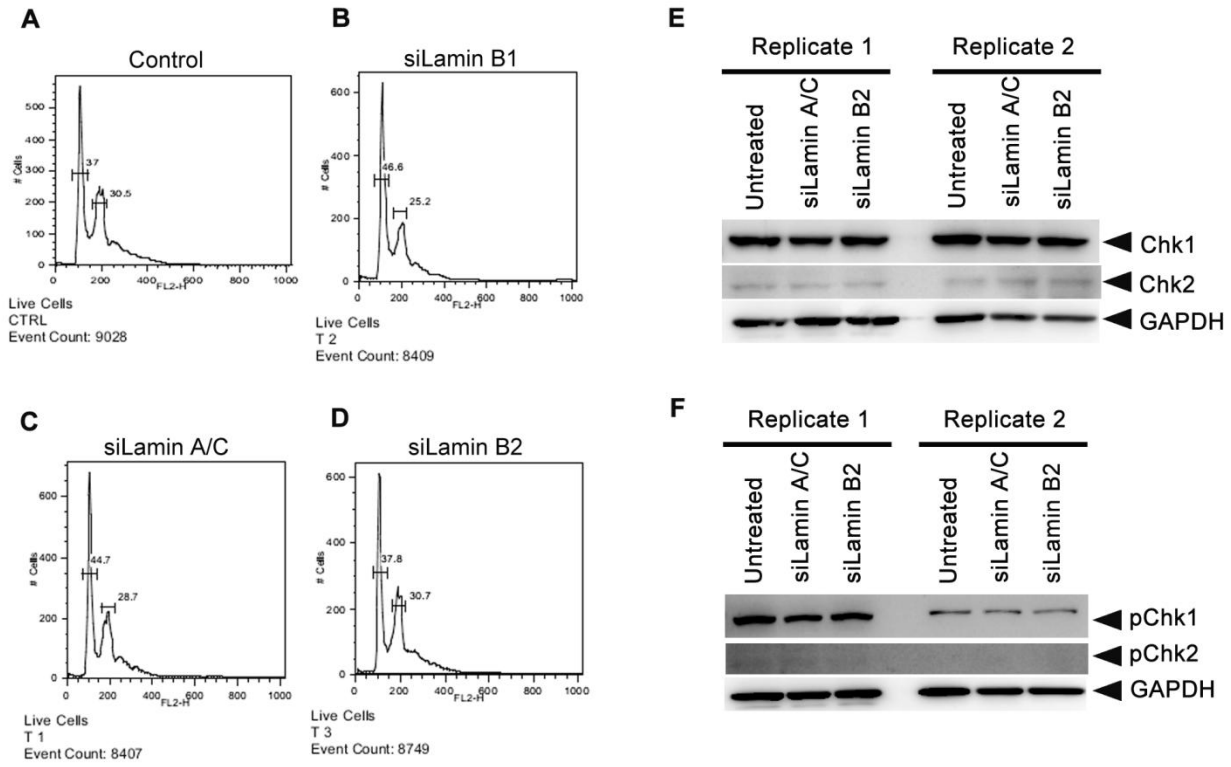

Figure 4.3 Cell cycle profiles are not altered upon Lamin depletion in DLD1 cells

A-D. FACS profiles for (A) Control, (B) Lamin B1, (C) Lamin A/C and (D) Lamin B2 depleted DLD1 cells determined using Propidium iodide staining at the end of 48 hours post knockdown. E-F Western blots depicting expression levels of (E) Chk1, Chk2 and (F) pChk1, pChk2 in control, Lamin A/C and Lamin B2 depleted cells. Loading control: GAPDH.

4.2.5 Lamin B2 overexpression rescues diploid chromosome numbers to DLD1 cells

To confirm the specificity of Lamin B2 dependent induction of chromosomal instability in DLD1 cells, we examined the extent of aneuploidy in DLD1 cells by co expressing a siRNA resistant GFP tagged-Lamin B2 protein (Lamin B2-GFP*) along with Lamin B2 depletion in DLD1 cells (Fig. 4.4). A western blot performed upon transfection of the siRNA sensitive and siRNA resistant Lamin B2 plasmids reveals an increased expression of the siRNA resistant

construct as compared to the siRNA sensitive protein which shows a downregulation due to the effect of siRNA (Fig. 4.4A). We performed 3D-FISH for chromosomes 18 and 19 in these cells and examined the copy numbers of CT18 and CT19 (Fig. 4.4B-C). Cells showing >2 signals were scored as CIN+ i.e. aneuploid for CT18 and/or CT19. We recorded an ~25% CIN phenotype in Lamin B2 depleted cells (Fig. 4.4C). Remarkably, this was rescued by ~50% in Lamin B2-GFP* overexpressing cells (Fig. 4.4C). Essentially, this rescue experiment showed that chromosomal instability (CIN) detected in the otherwise diploid DLD1 cells was dependent on Lamin B2 levels. This finding further corroborates the results from (Kuga et al., 2014), where a depletion of Lamin B2 in the diploid HCT116 cells shows a gain in chromosome numbers.

4.2.6 Chromosomal aneuploidies induced upon Lamin A/C depletion show conserved position in the interphase nucleus

Chromosomes showing transcriptional deregulation upon Lamin A/C and Lamin B2 depletion respectively were examined for their spatial organization in interphase cells using 3D Fluorescence *in situ* hybridization. Chromosomes 1,16 and 11 and 17 were examined upon Lamin A/C and Lamin B2 depletion respectively (Fig. 4.5 and 4.6 respectively). In addition, chromosomes 18 and 19 were examined in both Lamin A/C and Lamin B2 depletion in DLD1 cells (Fig. 4.5 and 4.6). Initially, we performed 3D radial distance measurements and characterized the radial distances of candidate chromosomes (CT1,3,11,16,17,18,19) in control DLD1 cells, and plotted them against their gene density (Fig. 4.5A-B, Table 12). This plot showed a negative correlation between gene density and % radial distance with $r^2 = 0.7228$ (Fig. 4.5B), suggesting that DLD1 cells show a chromosome positioning consistent with gene density. Next we examined 3D radial distance measurements for the diploid (Fig. 4.5C) and aneuploid chromosomes generated in Lamin A/C depleted cells (Fig. 4.5D-K, Table 13). The radial distance measurements were plotted in bins of five nuclear shells of ~20 % of the nuclear sub-volume (0%—nuclear center, 100%—nuclear periphery). The nuclear centre represents the innermost sub-shell and is relatively more transcriptionally active as compared to the peripheral shell. CT1 is a large chromosome territory (gene density ~15.38 genes/Mbp), and shows a predominant localization towards the nuclear periphery (M= 62.27% R.D), while CT16 shows an intermediate chromosome positioning (M =67.42% R.D), concomitant with an intermediate gene

density (10.05 genes/Mbp) (Fig. 4.5D-G). In Lamin A/C depletion, CT1 and CT16 did not show a change in their radial distance distribution profiles (Fig. 4.5E,G). CT18 and CT19 were found to be aneuploid in ~15-20% cells upon Lamin A/C Kd. We next examined the chromosome positioning patterns for CT18 and CT19 in both the diploid and aneuploid subsets of cells upon Lamin A/C Kd (Fig. 4.5H-K). CT18 and CT19 show preferential localization towards the nuclear periphery (Shell IV, RD ~80 %) and nuclear interior (shell III, RD ~60 %) respectively in control DLD1 cells (Fig. 4.5 I,K). Interestingly, CT18 as well as CT19 showed a conserved radial positioning upon Lamin A/C depletion, in both the diploid and aneuploid subsets of cells (Fig. 4.5 I, K). The control siLacZ-treated DLD1 cells showed conserved chromosome positions as compared to untreated control cells (Fig. 4.5E, G, I,K). This suggested that chromosomal aneuploidies do not depend on Lamin A/C for maintenance of their conserved positions in the interphase nucleus.

Figure 4.4

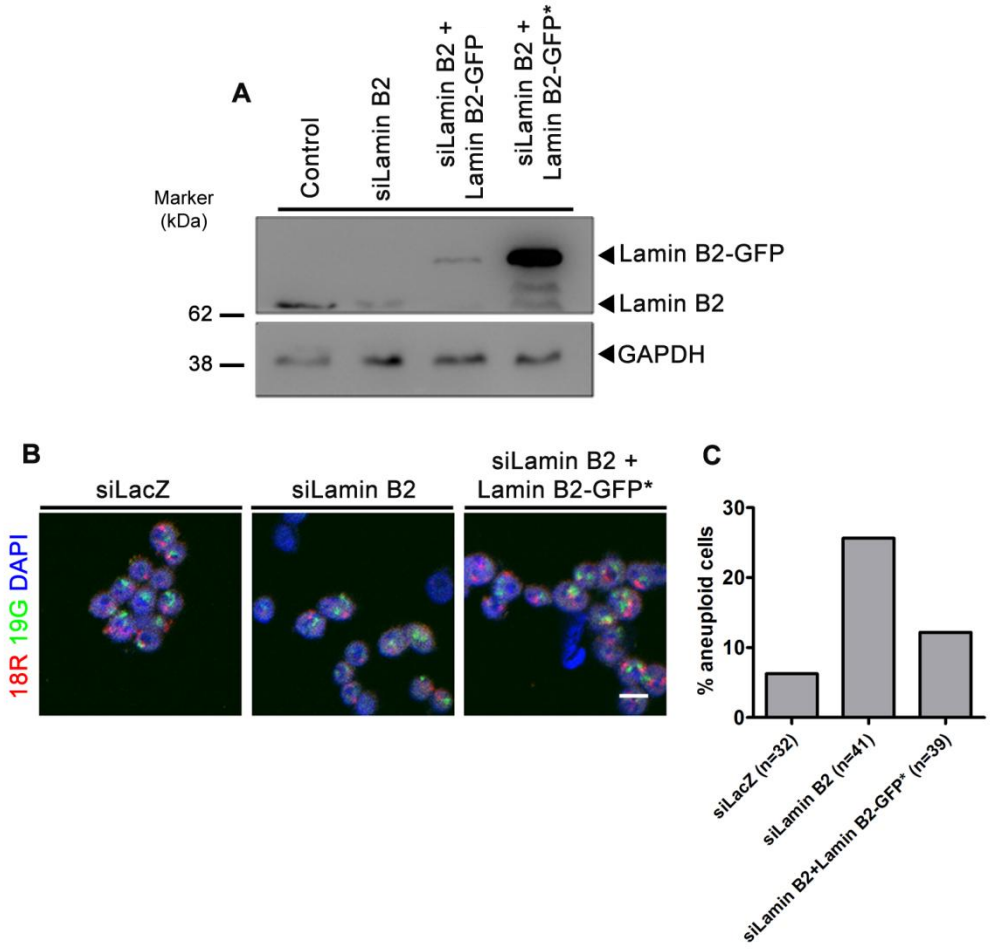

Figure 4.4 Aneuploidy is rescued using a siRNA resistant Lamin B2

A. Western blot showing the expression of siRNA sensitive Lamin B2-GFP and siRNA resistant Lamin B2-GFP* upon co-transfection with siRNA for Lamin B2 in DLD1 cells. Loading control: GAPDH. B. Representative images depicting 3D FISH for CT18 (red), CT19 (green) in siLacZ, siLamin B2 and siLamin B2+ Lamin B2-GFP* DLD1 cells. Scale bar~10µm. C. Quantification of aneuploid cells (aneuploid for either CT18 or CT19) upon overexpression of siRNA resistant Lamin B2-GFP* in DLD1 cells. n=number of cells.

Table 12. Median % Radial Distance (R.D) in DLD1 cells

Chromosome No.	Gene Density	% R.D
CT1	15.38	62.27
CT3	11.58	74.63
CT11	17.5	76.19
CT17	24.21	57.94
CT16	17.05	67.42
CT18	8.21	73.63
CT19	37.08	52.08

4.2.7 Chromosomal aneuploidies induced upon Lamin B2 depletion are mislocalized in the interphase nucleus

We next analyzed the radial distance distributions of chromosomes 11,17,18 and 19 territories, all of which were found to be aneuploid in ~20% of cells upon Lamin B2 Kd in DLD1 cells (Fig. 4.6A, Table 14). Of these, CT11, CT17, CT18 and CT19 showed transcriptional deregulation, while CT18 showed a relatively low transcriptional deregulation (Fig. 3.4A). CT11 shows a peripheral (shell IV: RD ~80 %) nuclear localization in control cells. CT11 is an aberrant chromosome territory which shows a predominant spatial position proximal to the nuclear periphery despite being a gene rich chromosome (Fig. 4.6B-C). This pattern of localization of CT11 has also been reported in mouse fibroblasts and human dermal fibroblasts (Mayer et al., 2005; Schmälter et al., 2014). CT11 in Lamin B2 Kd cells showed a conserved radial distance distribution (predominantly towards the nuclear periphery) in diploid cells (shell IV: RD ~80 %)(Fig 4.6B-C). Aneuploid CT11 also showed a mislocalized sub-population in shell III: RD

Figure 4.5

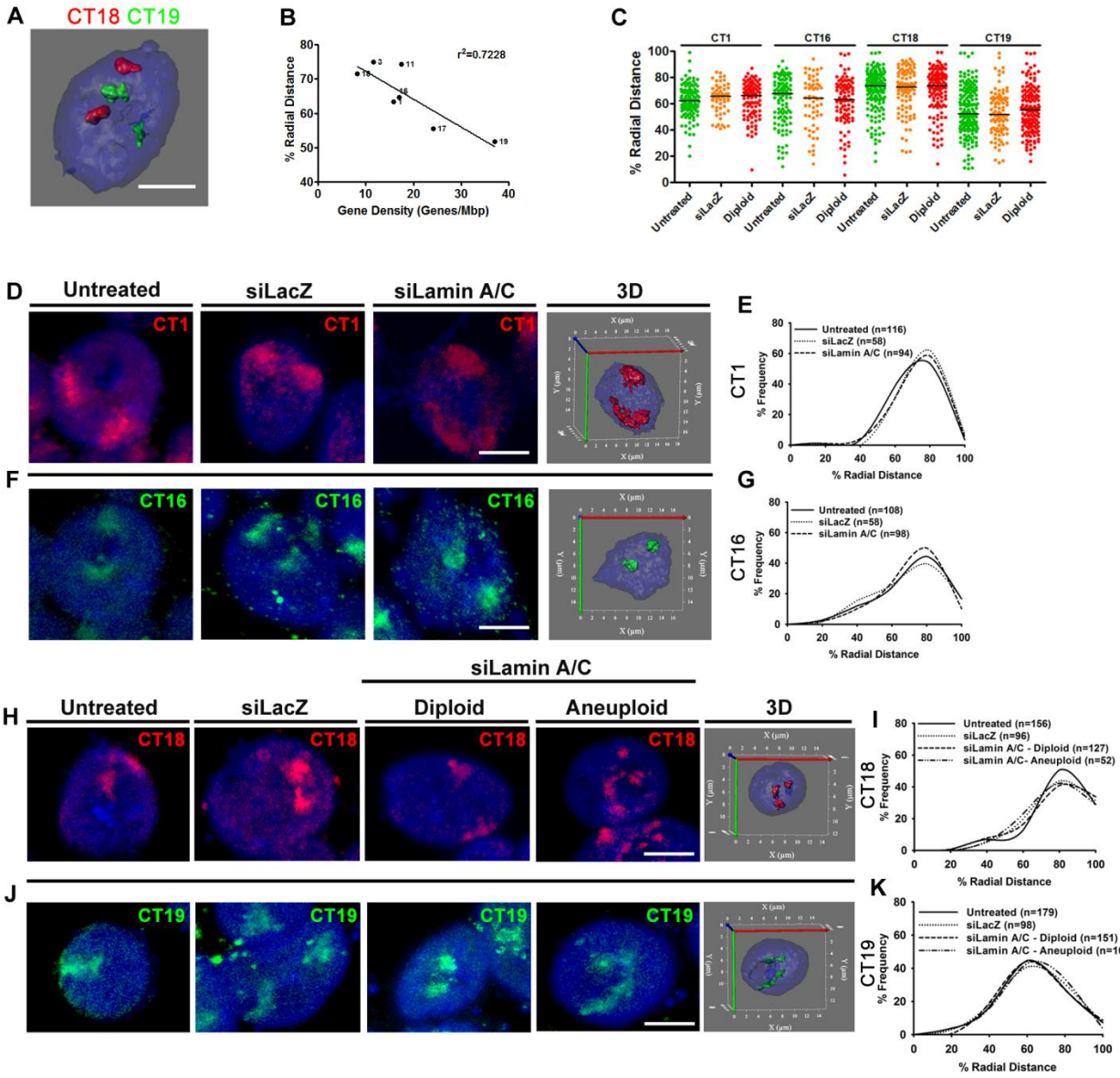

Figure 4.5 Chromsome positioning is conserved in diploid and aneuploid cells upon Lamin A/C depletion in DLD1 cells.

A. Representative 3D reconstruction of control DLD1 cells showing CT18 (red) and CT19 (green). B. Graph showing correlation between % R.D (radial distance) and gene density of candidate chromosomes (CT1,3,11,16,17,18,19) in DLD1 cells. An inverse correlation is seen between the two (r^2=0.7228). C. Dot scatter plots representing radial distances (0%= nuclear centre, 100%= nuclear periphery) of CT1, 16, 18 and 19 in diploid cells generated upon Lamin A/C depletion in DLD1 cells. Horizontal lines represent median. Diploid CTs do not show significant repositioning in Lamin A/C depleted cells. D-K. Representative 3D FISH images and radial

distance distribution profiles for control (untreated and siLacZ treated) and siLamin A/C treated DLD1 cells for (D-E) CT1 (N=1), (F-G) CT16 (N=2), (H-I) CT18 (N=2) and (J-K) CT19 (N=3). Every image panel in D,F,H,J has merged maximum intensity projections for Untreated, siLacZ treated and siLamin A/C treated (with a representative 3D reconstruction). Scale bar~10μm. Graphs in E,G,I,K represent radial distances of CTs binned into 5 nuclear subshells of ~20% radial distance each. No significant repositioning was detected in the distribution profiles for CT1, CT16 (diploid) and CT18, CT19 (diploid and aneuploid)($p>0.05$). Fischer's exact test and chi-square test was used to test the statistical significance of distributions into different sub-shells. N= biological replicate, n= number of CTs analysed, ~50-100 CTs were analysed in each replicate.

~60 % inside the nucleus (Fig. 4.6B-C). CT17 succeeds CT19 in gene density. We next analyzed the spatial organization of CT17 upon siLamin B2 in both its diploid and aneuploid states. The diploid CT17 (gene rich) showed a significant shift toward the nuclear periphery (shell IV: R.D ~80 %) as compared to control cells (shell III: R.D ~60 %) ($p=0.0145$) (Fig.4.6D-E). However, aneuploid CT17 does not show a mislocalization as compared to control cells and remains in shell III (R.D ~60 %) (Fig. 4.6E). We next plotted the radial distance distribution profiles for the gene poor CT18 which shows preferential localization in shell IV (R.D ~80%) upon Lamin B2 Kd in diploid and aneuploid states (Fig. 4.6F-G). Diploid CT18 in Lamin B2 depletion shows a conserved chromosomes positioning towards the nuclear periphery (shell IV: R.D ~80%). Aneuploid CT18 however, shows an increase in the population towards the nuclear interior (shell III, RD~60 %) ($p= 0.0431$) (Fig. 4.6G). Gene-rich CT19 predominantly localized toward the nuclear interior (shell III, RD ~60 %) in control and diploid cells depleted of Lamin B2 (Fig. 4.6H-I). Remarkably, the aneuploid CT19 showed an altered distribution into nuclear sub-shells, where it showed a loss of its conserved chromosome positions towards the nuclear interior (shell III: R.D ~60%), and repositioned further into the nuclear interior (shell II: RD ~40 %) as well as the nuclear periphery (shell IV: RD ~80 %) ($p=0.0157$) (Fig. 4.6I). Control cells (siLacZ-treated DLD1 cells) or untreated cells did not affect the localization of CT11,17,18 and 19 (Fig. 4.6C,E,G,I). Thus, upon Lamin B2 depletion, we detected mislocalized subpopulations of cells with aneuploid chromosome territories for gene rich CT19, CT11 as well as for gene poor CT18, which were not seen in control DLD1 cells.

Figure 4.6

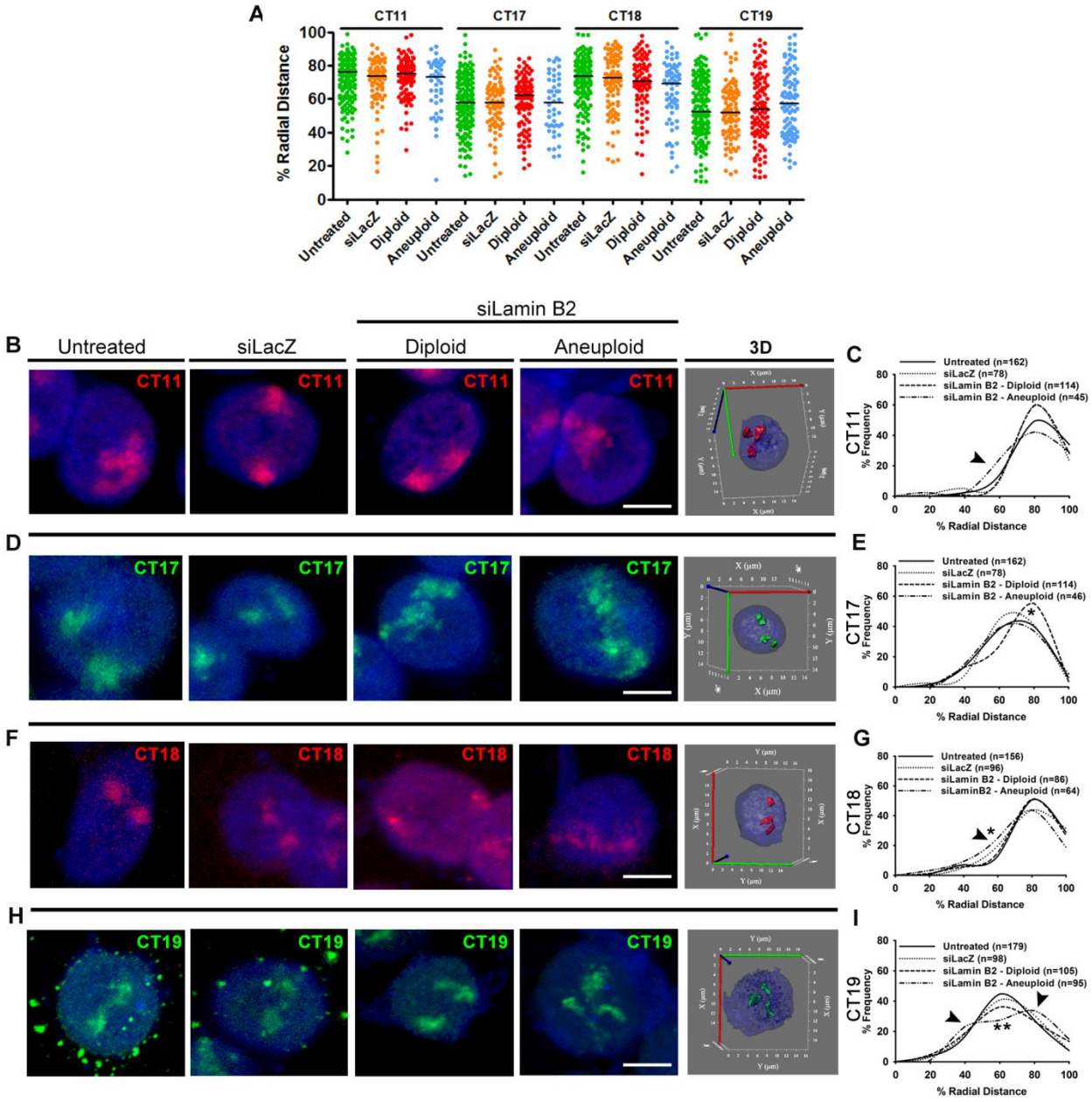

Figure 4.6. Chromosomal aneuploidies induced upon Lamin B2 depletiona are mislocalized in the interphase nucleus

A. Dot scatter plot representing % radial distances of CT11,17,18,19 in diploid and aneuploid cells upon siLamin B2. Horizontal lines represent median. Diploid CTs largely maintain conserved chromosome repositioning upon Lamin B2 depletion. (B-I) Representative 3D FISH images and radial distance (% R.D) distribution profiles for control (untreated and siLacZ treated) and siLamin A/C treated DLD1 cells for (B-C) CT11 (N=2), (D-E) CT17

(N=2), (F-G) CT18 (N=2) and (H-I) CT19 (N=3). Every image panel in A,C,E,G has merged maximum intensity projections for Untreated, siLacZ treated and siLamin B2 treated diploid and aneuploid nuclei (with a representative 3D reconstruction). Scale bar~10µm. Graphs in B,D,F,H represent radial distances of CTs binned into 5 nuclear subshells of ~20% radial distance each. B. Aneuploid CT11 shows an increase in the subpopulation at R.D. 60% over the control. D. Diploid CT17 shows an increase in the subpopulation at R.D 80% as compared to untreated control ($p= 0.0145$). F. Aneuploid CT18 shows an increased subpopulation at R.D. 60% as compared to untreated control cells ($p=0.0431$). H. Aneuploid CT19 shows a significant redistribution into different subshells upon Lamin B2 depletion ($p= 0.0157$). Specifically, it shows a decrease in its population at R.D. 60% ($p=0.0061$) and increase in its internal subpopulation (R.D. 40%) and peripheral subpopulation (R.D. 80%). Fischer's exact test and chi-square test was used to test the statistical significance of distributions into different sub-shells. N= number of biological replicates contributing to the data, n= number of CTs analysed, ~50-100 CTs were analysed in each replicate.

Table 13. Median % Radial Distance (R.D) upon Lamin A/C Kd in DLD1 cells

Chromosome No.	Gene Density (Genes/Mbp)	Untreated		siLacZ		siLamin A/C			
						Diploid		Aneuploid	
		Median	IQR	Median	IQR	Median	IQR	Median	IQR
CT1	15.38	62.27	14.11	65.49	14.98	66.07	19.17	-	-
CT16	17.05	67.42	25.91	64.3	25.31	62.85	22.88	-	-
CT18	8.21	73.63	18.20	72.5	23.61	73.73	22.24	71.14	26.08
CT19	37.08	52.08	27.02	51.73	23.44	54.86	23.8	51.45	23.64

IQR: Inter quartile range

Table 14. Median % Radial Distance (R.D) upon Lamin B2 Kd in DLD1 cells

Chromosome No.	Gene Density (Genes/Mbp)	Untreated		siLacZ		siLamin B2			
						Diploid		Aneuploid	
		Median	IQR	Median	IQR	Median	IQR	Median	IQR
CT11	17.5	76.19	17.25	73.55	16.81	75.06	11.21	73.11	22.73
CT17	24.21	57.94	24.53	57.79	18.84	62.22	14.69	57.6	27.87
CT18	8.21	73.63	18.20	72.5	23.61	70.45	19	69.25	23.3
CT19	37.08	52.08	27.02	51.73	23.44	53.88	29.97	57.23	31.19

IQR: Inter quartile range

4.2.8 Lamin depletion alters volumes of chromosome territories

We next examined if Lamin A/C or B2 depletion affects the volumes of chromosome territories in either diploid or aneuploid cells (Fig. 4.7, Tables 15-16). The nuclear volume showed a significant increase (~1.1 fold) upon Lamin A/C Kd (Fig. 4.7A). Diploid chromosome 1, 18 and 19 territories showed a significant increase in their volumes (~1.2) upon Lamin A/C depletion (Fig. 4.7B,D,E). Chromosome 16 did not show a change in its volume (Fig. 4.7C). Aneuploid CT18 and CT19 also did not show a significant change in volume upon Lamin A/C Kd (Fig. 4.7D-E). This suggests a role for Lamin A/C in either directly or indirectly regulating CT volumes, primarily of specific diploid chromosome territories.

Lamin B2 depletion shows an ~1.2 fold increase in nuclear volume (Fig. 4.7F). We next examined the volumes of diploid and aneuploid CTs in Lamin B2 depleted cells. CT11 and CT17 did not show a change in volume in either in its diploid or aneuploid state (Fig. 4.7G-H). CT18 however showed an increase in volumes (~1.7 fold) in the aneuploid state and CT19 showed an

increase in volume in the diploid (~1.4 fold) as well as aneuploid state (~1.5 fold) (Fig. 4.7I-J). In summary, Lamin A/C and B2 depletion impact nuclear volumes. While Lamin A/C Kd primarily affects volumes of diploid chromosome territories, Lamin B2 Kd impacts volumes of mainly aneuploid chromosome territories.

A change in volumes of aneuploid CTs upon Lamin B2 depletion prompted us to examine whether there exists a correlation between the volume and mislocalization of chromosome territories in aneuploid cells upon Lamin B2 Kd. In other words, do the mislocalized aneuploid chromosome territories show altered volumes in Lamin B2 depleted cells? Towards this end, we examined the volumes of aneuploid CTs across concentric nuclear subshells. A comparison of volumes of CTs in different nuclear subshells did not reveal a significant difference in the volumes of aneuploid chromosome territories whether they were localized towards the nuclear interior or towards the nuclear periphery (Fig. 4.7G'-J'). This suggested that the altered volume of aneuploid CTs analysed may not correlate with its mislocalization into a different nuclear sub-shell. Altered volumes of chromosomes are correlated with changes in compaction of chromatin and greater transcriptional permissiveness (Gilbert et al., 2004). The contribution of altered volumes of chromosomes upon Lamin depletion on the direct transcriptional consequences of chromosomes remains to be examined.

4.2.9 Stable depletion of Lamin B2 mislocalizes aneuploid chromosome territories in the interphase nucleus

We next queried if the effects of Lamin B2 depletion were transient, or were maintained stably across generations. We performed shRNA based stable depletion of Lamin B2 using pLKO-shLamin B2 transfected into DLD1 cells (Fig. 4.8A-B). We ascertained the extent of depletion of Lamin B2 in 3 independent clones by western blotting and immunofluorescence assays to identify the extent of knockdown both at the population level as well as the single cell level

Figure 4.7

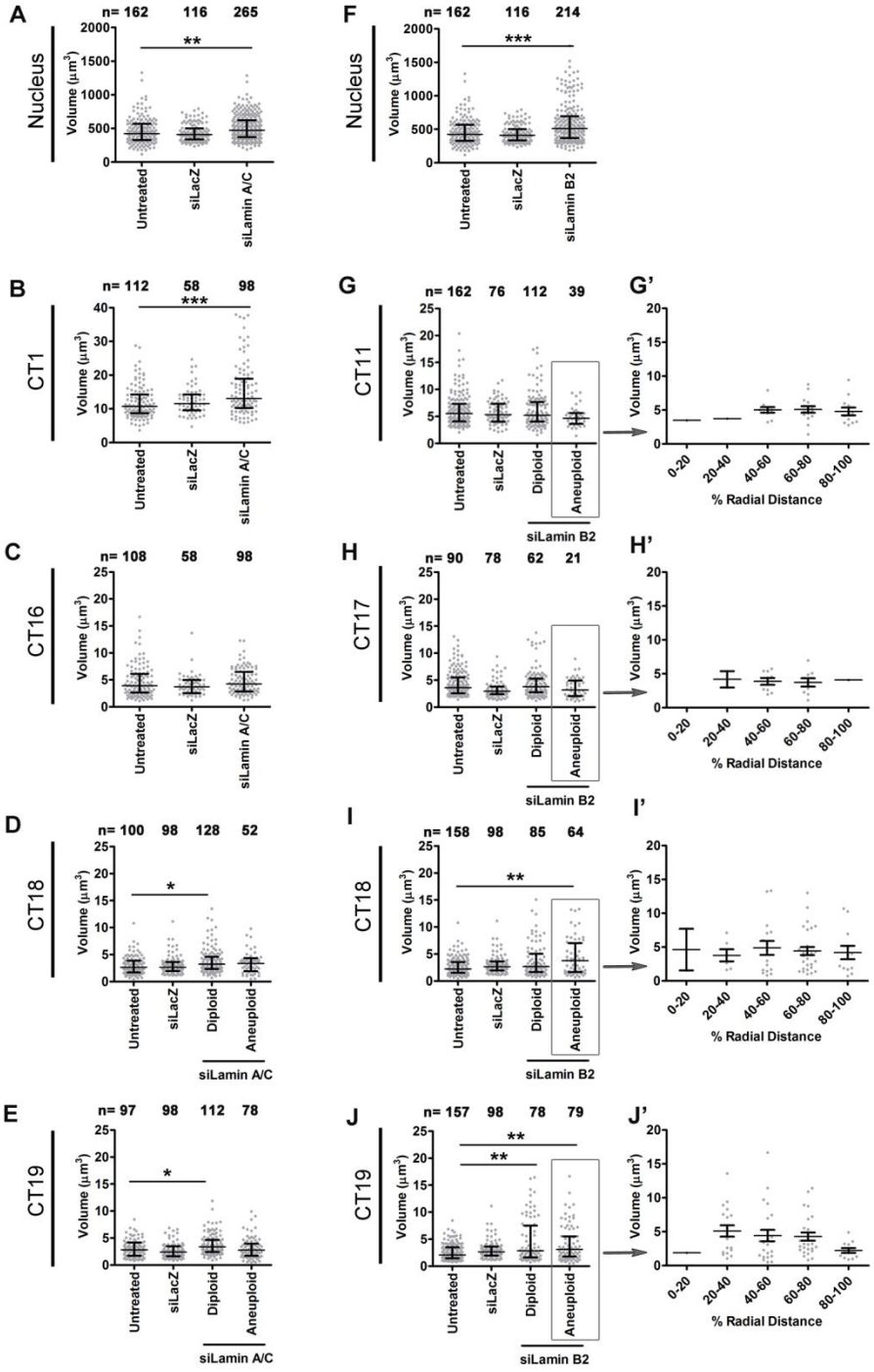

Figure 4.7. Lamin depletion alters volumes of the nucleus and chromosome territories

A-E. Dot scatter plot representing volumes of the nucleus and chromosome territories upon Lamin A/C depletion in DLD1 cells. Horizontal lines indicate median with interquartile range. A. A significant increase in volume of the nucleus (~1.1 fold) upon Lamin A/C depletion (p=0.0001), N=5. B. Volume of CT1 shows a significant increase

upon Lamin A/C depletion (p=0.0009), N=1. C. No significant changes were detected for volumes of CT16 upon Lamin A/C depletion. D-E Diploid CT18 (p=0.0149) and CT19 (p<0.0001) show an increase in volume (N=2 each) while aneuploid CT18 and CT19 do not show a significant change in Lamin A/C depleted cells. F-J.Dot scatter plot representing volumes of the nucleus and chromosome territories upon Lamin B2 depletion in DLD1 cells. Horizontal lines indicate median, with interquartile range. F. Nuclear volume shows a significant increase (~1.2 fold) upon Lamin B2 depletion (p<0.0001). G-H. No significant difference was detected in the volumes of CT11 (N=2) and CT17 (N=1) in diploid and aneuploid states upon Lamin B2 depletion. I. A significant increase in the volume of CT18 (p=0.0019) (N=2). J. Diploid and aneuploid CT19 show a significant increase in volume upon Lamin B2 depletion (p=0.0004) (N=2). G'-J'. Distribution of the volumes of aneuploid CT 11,17,18,19 across nuclear subshells upon Lamin B2 depletion. No significant difference was detected in the volumes across subshells of aneuploid CTs. Kruskal-Wallis test was used to test for statistical significance, N= total no. of biological replicates contributing to the data, n= number of nuclei (A,F) or CTs (B-E, G-J) analysed.

---

in the colony (Fig. 4.8A-B). We selected 3 clones with lowered Lamin B2 levels and presumably of reduced heterogeneity within the colony (Fig. 4.8A-B), and performed 3D FISH for CT18 and CT19 in these clones (Fig. 4.8C). Interestingly, the extent of aneuploidy in the clones stably depleted of Lamin B2 increased from ~25% (in cells treated with siRNA-transient depletion) to ~50-70% (for cells treated with shRNA-stable depletion) (Fig. 4.8D). This suggests that the clones bearing aneuploid chromosomes were selected for across passages of cells, and possibly had a growth advantage over other cells. This also suggested that Lamin B2 depletion induced chromosomal aneuploidies are not just simply a manifestation of transient knockdowns, but a stable feature maintained across passages.

3D FISH and radial distance measurements for CT18 and CT19 in these cells revealed a profile of chromosome positioning very similar to siRNA based depletion of Lamin B2 (Fig. 4.8E-F). Control cells (colonies from empty vector transfection) showed CT 18 positioned proximal to the nuclear periphery (M=71.36% R.D) and CT19 toward the nuclear interior (M=50.00% R.D) (Fig. 4.87E-F). Lamin B2 depleted cells, on the other hand resulted in two sub-populations – diploid and aneuploid for CT18 and CT19 (Fig. 4.8D). While CT18 showed a conserved chromosome positioning profile in both the diploid and aneuploid subpopulations (primarily toward the nuclear periphery at R.D ~80%) (Fig. 4.8E), CT19 showed an altered distribution profile as compared to the control cells. For CT19, we detected a decrease in the population at R.D. ~40% (p=0.0020) and another mislocalized population (R.D ~80%) towards

the nuclear periphery (R.D ~80%) in the aneuploid subpopulation (Fig. 4.8F). The cells diploid for CT19 upon Lamin B2 depletion, maintained their conserved chromosome positions at R.D ~60% (Fig. 4.8F). In summary shRNA mediated knockdown recapitulated the mislocalization of chromosome territories as detected in the siRNA mediated knockdowns.

Table 15. Median Volume of Chromosome Territories upon Lamin A/C Kd in DLD1 cells

Chromosome No.	**Untreated (μm^3)**	**siLacZ (μm^3)**	**siLamin A/C (μm^3)**	
			Diploid	**Aneuploid**
CT1	10.73	11.51	**13.05***	-
CT16	3.89	3.69	4.26	-
CT18	2.65	2.65	**3.21***	3.36
CT19	2.83	2.39	**3.37***	2.75

***significant ($p<0.05$)**

Table 16. Median Volume of Chromosome Territories upon Lamin B2 Kd in DLD1 cells

Chromosome No.	**Untreated (μm^3)**	**siLacZ (μm^3)**	**siLamin B2 (μm^3)**	
			Diploid	**Aneuploid**
CT11	5.53	5.32	5.22	4.64
CT17	2.99	2.94	3.32	4.07
CT18	2.23	2.65	2.66	**3.76***
CT19	2.06	2.65	**2.82***	**3.08***

***significant ($p<0.05$)**

Figure 4.8

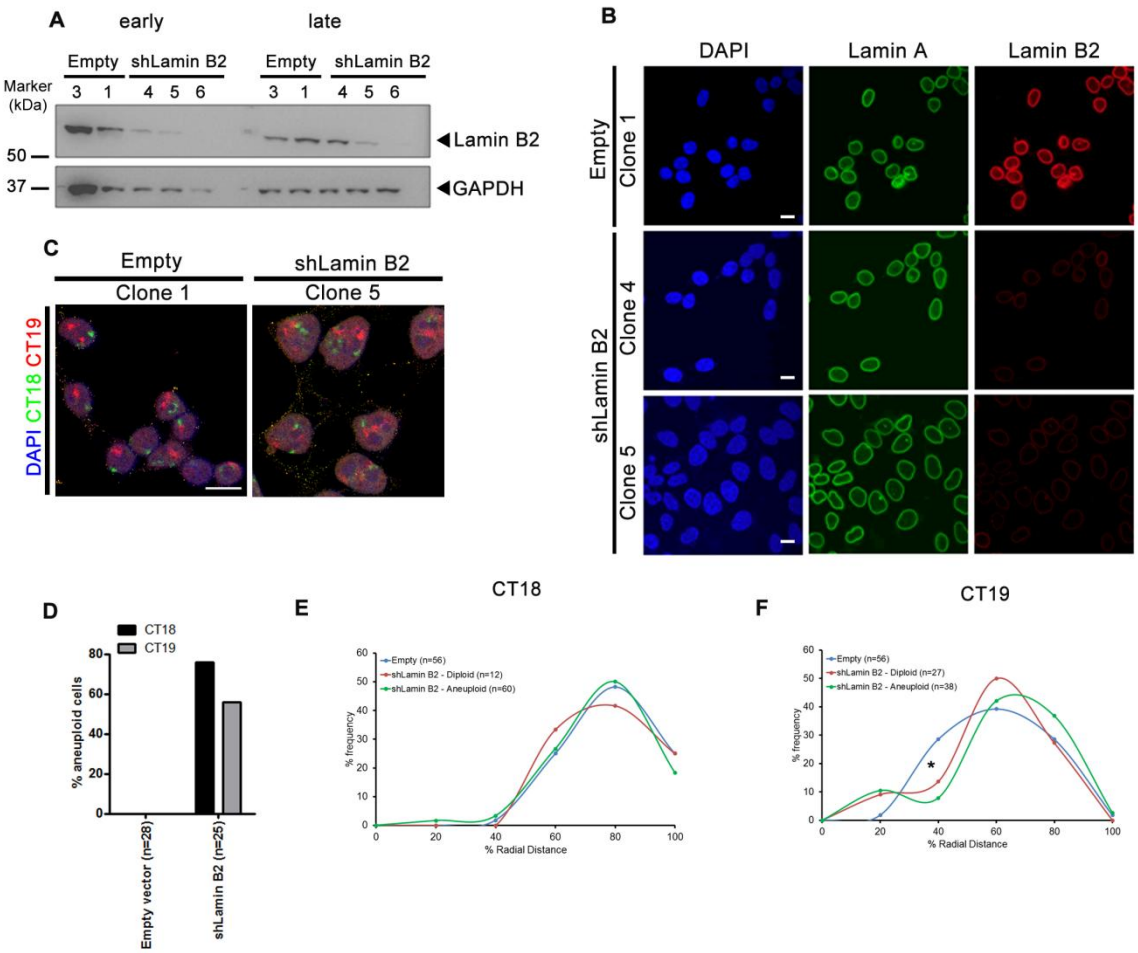

Figure 4.8 shRNA mediated stable depletion of DLD1 cells results in mislocalization of aneuploid chromosome territories

A. Western blot depicting expression levels of Lamin B2 at early (n=3) and late (n=15) passages in clones generated from Empty vector and shLamin B2-pLKO transfected cells. 2 colonies from empty vector transfected cells and 3 colonies with shLamin B2 were selected under Puromycin selection (2µg/mL). B. Immunostaining for Lamin A (green) and Lamin B2 (red) in empty vector and shLamin B2 clones. Scale bar~10µm. C. Representative 3D FISH images for CT18 (green) and CT19 (red) in empty vector (clone 1) and shLamin B2 (clone 5). 3D FISH was performed at an early passage (passage 3) of cells. Scale bar~10µm. D. Quantification of the number of signals for CT18 and CT19 in the interphase nucleus for empty vector and shLamin B2 cells. E-F. Radial distance distribution profiles for (E) CT18 (N=1) and (F) CT19 (N=1) upon shLamin B2 knockdowns. N=number of biological replicates contributing to the data, n= number of CT analysed.

4.2.10 Lamin B2 overexpression rescues mislocalized aneuploid chromosome territories in the interphase nucleus

We detected a specific mislocalization of aneuploid chromosome territories specifically upon Lamin B2 and not Lamin A/C knockdown in DLD1 cells. We sought to examine if these CT positioning changes are reversible and if so, would Lamin B2 overexpression rescue chromosome territory positions.

Towards this end, we first performed siRNA mediated depletion of Lamin B2 in DLD1 cells for 48 hours (Fig. 4.9A). This was followed by overexpression of Lamin B2-GFP, for a further 48 hours. Western Blots were performed to assess the expression levels of Lamin B2 at the end of 48 hours and 96 hours respectively. This revealed an ~80% reduction at the protein levels at the end of 48 hours, which was maintained until ~96 hours, without Lamin B2-GFP overexpression (Fig. 4.9B). Lamin B2-GFP transfected cells showed an increase in the overall levels of Lamin B2 in the control and Lamin B2 Kd cells (Fig. 4.9B). Chromosome positions were assessed at the end of 48 hours and at the end of 96 hours (after Lamin B2 overexpression) (Fig. 4.9C). CT18 and CT19 were aneuploid in ~25% cells as found previously. CT18 did not show a significant difference in its median radial distance at neither 48 hours nor 96 hours (with or without Lamin B2 OE) (Fig. 4.9D,F). Aneuploid CT19 was mislocalized towards the nuclear periphery (M=62.53% R.D) at the end of 48 hours post Lamin B2 Kd as compared to control cells (M=54.93% R.D), and was rescued upon overexpression of Lamin B2-GFP for a further 48 hours (M=55.55% R.D) (p=0.0378) (Fig. 4.9E,G). Remarkably, Lamin B2 knockdown cells (maintained without Lamin B2-GFP overexpression) continued to show a mislocalization of aneuploid CT19 at the end of 96hours (M=65.51% R.D) (Fig. 4.9E, G). Diploid CT19 did not show significant repositioning as compared to control cells at the end of 48 hours (Fig. 4.9E, G), however, at the end of 96 hours post Lamin B2 Kd, diploid CTs show an additional subpopulation toward the nuclear periphery (Fig. 4.9E,G) suggesting that prolonged Lamin B2 depletion may impact the spatial positions of diploid chromosomes territories. Thus, Lamin B2 reintroduction shows a rescue of positions of aneuploid chromosome territories, thereby emphasizing that the levels of Lamin B2 is an important determinant in the maintenance of a gene density dependent chromosome positioning in aneuploid cells.

4.2.11 Lamin depletion in normal colon cells

We performed Lamin A/C and Lamin B2 depletion in cells derived from normal colon epithelium (CRL 1790) and normal colon fibroblasts (CRL 1541). These cells grow as a flat monolayer and show mixed morphologies of epithelial and mesenchymal cells. Lamin expression is low in both these cell types (Fig. 4.10A-D). Lamin B2 is expressed at low levels undetectable on western blots (Fig. 4.2.10B, D) while Lamin A/C expression was robust in CRL 1541 (Fig. 4.10C). We were unable to deplete Lamins in these cells owing to their reduced levels, low proliferation rates and reduced transfection efficiency (Fig. 4.10A-D). However, 3D-FISH performed on CRL1790 cells showed that CT19 occupies a central position similar to that seen in DLD1 cells (Median = 54.28% R.D) (Fig. 4.10E-F).

4.2.12 Gene loci are repositioned away from the lamina in Lamin B2 depleted cells

We detected a mislocalization of aneuploid CTs from their conserved gene density dependent positions upon Lamin B2 depletion in DLD1 cells. We next examined the nuclear organization of gene loci upon Lamin B2 depletion. While it is established that gene loci also assume a non random organization in the interphase nucleus (Chambeyron et al., 2005, Volpi et al., 2000), the organization of gene loci from aneuploid chromosomes has not been investigated. This question assumes significance since gene amplifications are a defining feature of cancer cells and is associated with transcriptional deregulation. Moreover, considering the role of Lamins in regulating the spatial organization of aneuploid chromosome territories, we further asked if Lamin B2 depletion impacts the organization of gene loci in the interphase nucleus.

We selected a candidate gene - *ZNF570* (Chr.19q13.12) owing to chromosomal aneuploidies identified for chromosome 19 aneuploidies upon Lamin B2 knockdown (Fig. 4.11A). An Immuno-FISH experiment was performed to label Lamin A, Lamin B2 and *ZNF570* locus in control and Lamin B2 knockdown cells (Fig. 4.11B). ZNF570 was upregulated upon Lamin B2 Kd as seen from the microarray data (~2.96 fold), and was independently validated using qRT-PCR (Fig. 4.11C). We measured the distance of *ZNF570* gene locus from the nuclear lamina (Lamin A signal) in 3D reconstructed nuclei (Fig. 4.11D). The *ZNF570* gene locus was

Figure 4.9

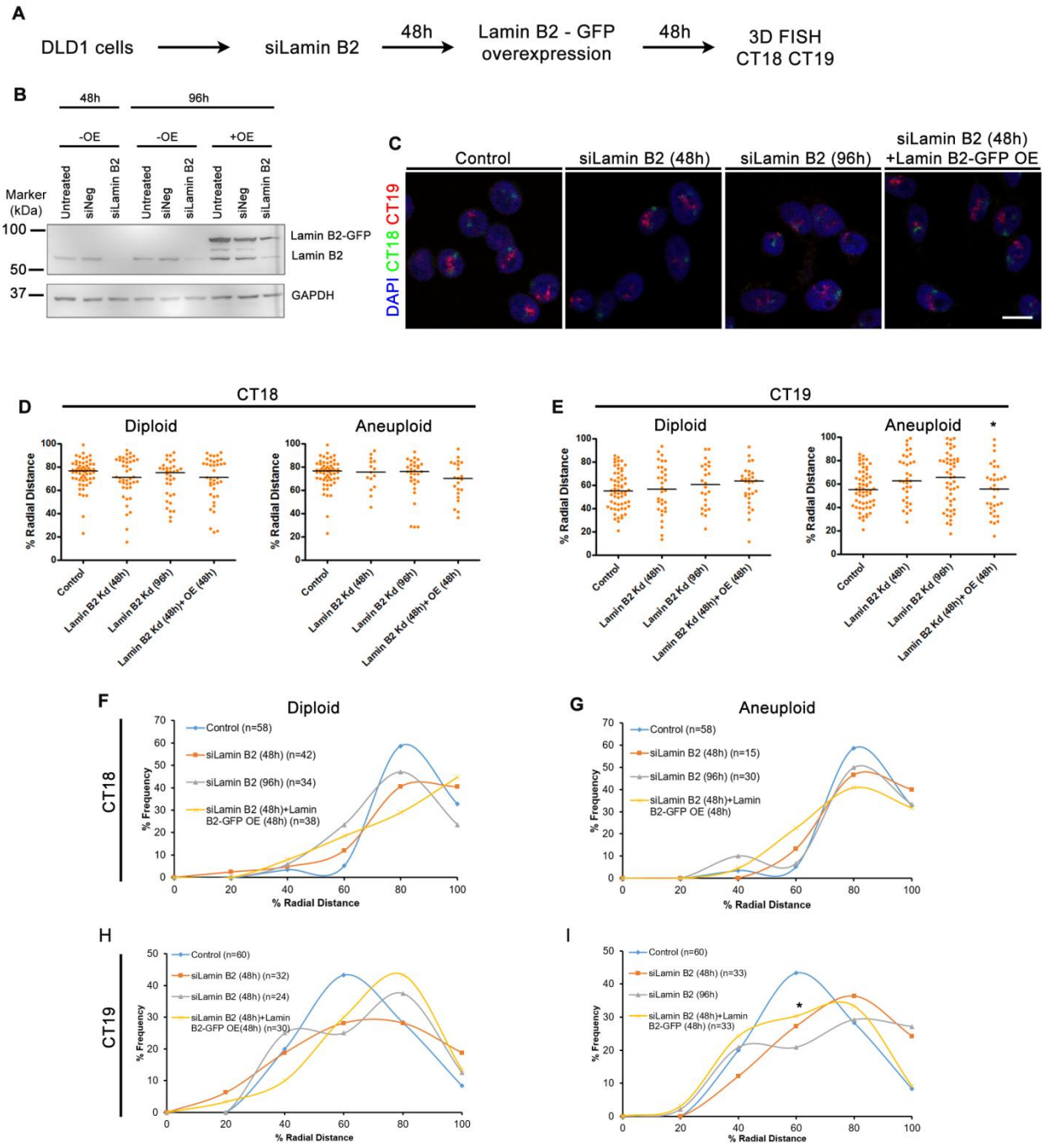

Figure 4.9 Lamin B2 overexpression rescues the positions of aneuploid chromosome territories

A. Experimental scheme for Lamin B2 depletion followed by overexpression. B. Western blot depicting Lamin B2 (endogenous and overexpressed) levels at 48 hours (no overexpression) and at 96 hours (with or without overexpression) in DLD1 cells. Loading control: GAPDH. C. 3D FISH depicting hybridization for CT18 (green), CT19 (red) in controls, Lamin B2 depleted cells with and without overexpression of Lamin B2-GFP. Scale

bar~10µm. D-E. Dot scatter plot representing radial distances of (D) CT18 (N=1) and (E) CT19 (N=1). F-I. % Radial distribution profiles binned into shells of 20% for (F) CT18- diploid, (G) CT18 – aneuploid (H) CT19-diploid (I) CT19 – aneuploid. A significant rescue of CT19 positions was detected upon overexpression of Lamin B2 post Lamin B2 depletion in DLD1 cells. Kruskal-Wallis test was used to test for statistical significance. N= number of biological replicates contributing to the data, n=number of CTs analysed.

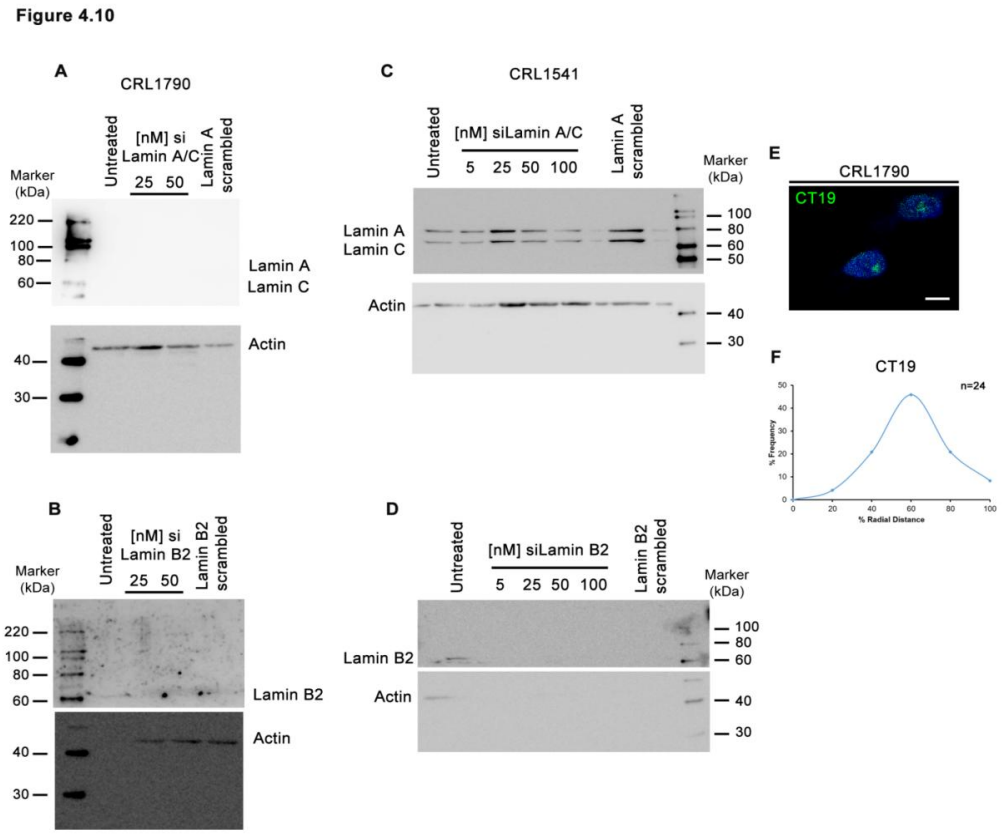

Figure 4.10 Expression of lamins in normal colon fibroblast (CRL1541) and normal colon epithelium (CRL1790) cells

A-B. Western blots depicting the expression levels of (A) Lamin A/C and (B) Lamin B2 in lamin knockdown performed on normal colon fibroblast CRL1790 cells. Loading control: Actin. C-D Western blots depicting the expression levels of (C) Lamin A and (D) Lamin B2 in lamin knockdown performed on normal colon epithelium CRL1451 cells. Loading control: Actin. Very low expression levels of Lamin B2 were detected in both CRL 1451 and CRL1790 cells.E. 3D FISH for CT19 (green) in control CRL1790 cells. Scale bar ~10µm. F. % Radial distance distribution profile for CT19 in CRL1790 cells shows a predominant positioning towards the nuclear interior (Shell III – R.D ~60%).

also found to be aneuploid in ~25% Lamin B2-depleted cells. The distance of the *ZNF570* gene locus was measured with respect to the nuclear lamina (Lamin A) that we considered as the origin, i.e., 0μm. The distance of *ZNF570* gene locus from the lamina was ~0.72 μm in control cells (siLacZ) and was repositioned away from the nuclear lamina upon Lamin B2 depletion (median=1.40μm) (p=0.004) (Fig. 4.11D). The spatial organization of *ZNF570* showed a similar repositioning away from the nuclear lamina, in both diploid and aneuploid Lamin B2 Kd cells (Fig. 4.11D-E). We examined if the altered spatial organization of *ZNF570* correlates with its transcript levels in the interphase nucleus (Fig. 4.11F). We performed RNA-FISH for *ZNF570* transcript and counted the number of RNA signals for *ZNF570*. This revealed an increase *ZNF570* transcript levels upon Lamin B2 depletion (Fig. 4.11G). In summary, Lamin B2 depletion regulates the spatial organization of the candidate gene locus *ZNF570* as well as its transcript levels in the diploid and aneuploid states suggesting that Lamin B2 depletion regulates the organization and transcription of gene loci in both diploid and aneuploid cells.

Figure 4.11

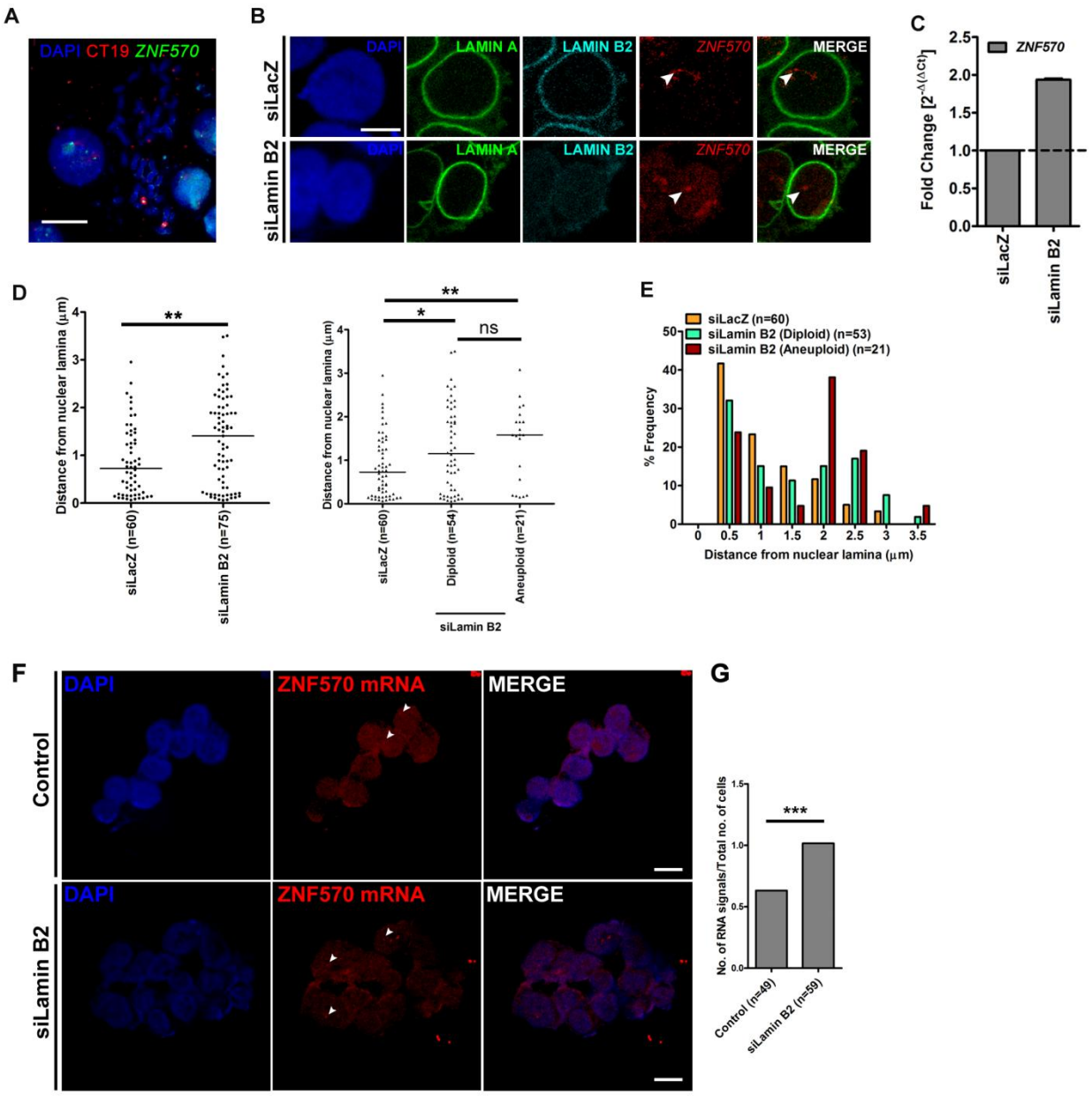

Figure 4.11 Gene loci are repositioned away from the nuclear periphery in Lamin B2 depleted cells

A. 2D FISH on metaphase spreads for *ZNF570* (green) and Chr. 19 (red) in control DLD1 cells. Scale bar ~10 µm. B. 3D immuno-FISH for *ZNF570* (red), Lamin A (green), Lamin B2 (cyan), DAPI (blue) in control (siLacZ) and siLamin B2 DLD1 cells.Arrowheads: *ZNF570* gene locus. Scale bar ~10 µm. C.qRT-PCR showing upregulation of *ZNF570* gene upon Lamin B2 depletion. Data shown is representative out of two independent biological replicates, normalized to internal control *GAPDH*. D. Dot scatter plot showing distance of *ZNF570* from the nuclear lamina in

control (siLacZ), siLamin B2 (diploid and aneuploid subsets). Horizontal lines indicate median. A significant repositioning was detected for *ZNF570* with respect to the lamina in siLamin B2 cells (K-S test, p=0.004). E. Distance of ZNF570 from the nuclear lamina represented as bins of 0.5 µm in control (siLacZ), siLamin B2 (diploid and aneuploid subsets). F. RNA FISH for *ZNF570* (red) in control (untreated) and siLamin B2 cells.G. Quantification of total number of RNA signals in a field normalized to total number of cells in control (untreated) and siLamin B2 cells shows a significant increase in siLamin B2 cells. Scale bar ~10 µm.

4.2.13 Expression levels of lamins is variable in diploid and aneuploid cells

Our data on the mislocalization of chromosome territories upon Lamin B2 depletion prompted us to examine the expression levels of Lamin B2 in naturally occurring aneuploid cells. Aneuploidy is a common feature of several cancers and developmental disorders. We examined the expression levels of Lamins in cancer cells that are characterized by variable levels of ploidy - diploid (DLD1, HCT116, HT1080) and aneuploid (SW480, A549) cells using western blotting (Fig. 4.12A-C). This revealed an interesting trend:

i. The expression of Lamins and LINC proteins is variable across cell types

ii. Maximum variation was seen for Lamin B2 expression across cell types, with DLD1 cells of colorectal cancer subtype showing greater expression of Lamin B2 over HT1080 and SW480 cells. Our data is consistent with that published by (Kuga et al., 2014) (Fig. 4.12D).

iii. The expression of Emerin is comparable across all cell lines examined

Figure 4.12

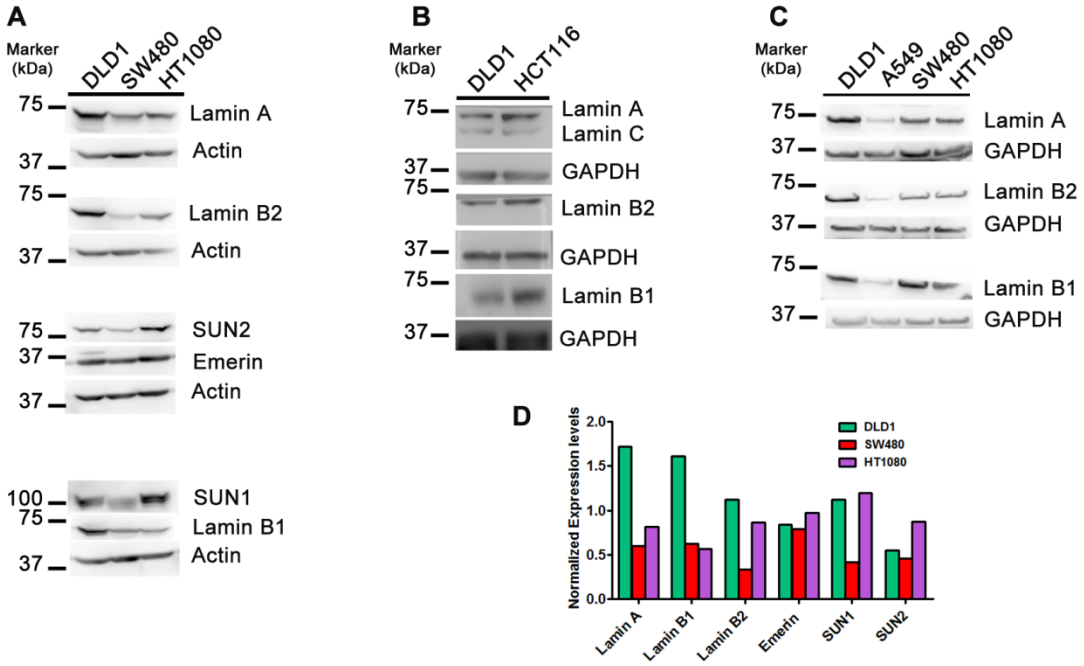

Figure 4.12. Expression of lamins is variable across cell lines

A. Western blots depicting expression levels of Lamins A, B1, B2, SUN1, SUN2, Emerin in DLD1, SW480 and HT1080 cells. Loading control: Actin. B. Western blots depicting expression levels of Lamins A,B1 and B2 in DLD1 and HCT116 cells. Loading control: GAPDH. C. Western blots depicting expression levels of Lamins A,B1 and B2 in DLD1, HT1080, A549, SW480 cells. Loading control: GAPDH. D. Quantification of band intensities in A. Intensity of candidate proteins are normalized to that of loading control Actin. Data shown is representative out of two independent experiments.

4.2.14 Cells with variable ploidy and Lamin B2 levels respond differentially to Lamin B2 depletion – CT18 CT19 positions upon Lamin B2 depletion in HCT116, HT1080, A549, SW480 cell lines

We detected differences in cell lines with regard to their expression levels of lamins as also LINC complex proteins (Fig. 4.12). Amongst the different cell lines that we examined, DLD1, HCT116, HT1080 are stably diploid across generations, while SW480 and A549 are aneuploid

(Table 17). A comparison of the protein expression profiles between these cell lines reveals a difference in expression levels for Lamin B2. Indeed, among colorectal cancer cell lines as well, Lamin B2 was found to be a differentiating factor with lowered Lamin B2 expression in cell lines that show chromosomal instability accompanied by aneuploidy (Kuga et al., 2014). We detected a similar trend between DLD1 and SW480 with higher Lamin B2 expression in DLD1 cells as compared to the aneuploid SW480 cells (Fig. 4.12A). We were curious to examine if the expression levels of Lamin B2 contributes to overall ploidy and chromosome positioning in these cell lines.

Toward this end, we initially examined chromosome 18 and 19 positions in these cell lines. The chromosome copy number and its % radial distance in the control (untreated) cells for CT18 and CT19 was found to be variable. This copy number has been determined on the basis of number of signals for CT18 and CT19 as seen in 3D FISH on interphase cells (~30 cells per cell line), and often represents translocated chromosomes in addition to whole chromosomes as seen through metaphase data.

This has been tabulated in Table 17.

Table 17. Ploidy and median % R.D for CT18 and CT19

Cell Line	Origin	Ploidy (modal chromosome number)	Copy number (signals) of CT18 and CT19		Median % R.D.	
			CT18	**CT19**	**CT18**	**CT19**
DLD1	Colorectal cancer	44-46	2	2	73.63	52.08
HCT116	Colorectal cancer	44	2	2	71.87	49.81
HT1080	Fibrosarcoma	45-46	2	2	69.07	59.23
SW480	Colorectal cancer	57	2-4	2-4	67.98	65.69
A549	Lung carcinoma	66	2-4	2-4	64.70	62.20

The response of different cell lines to Lamin B2 depletion was as follows:

i.HCT116

HCT116 is an aggressive grade III colon cancer cell line, pseudo-diploid with a modal chromosome number of 44-46. Depletion of Lamin B2 induces aneuploidy in these otherwise diploid HCT116 cells (Kuga et al., 2014). This was also corroborated by our results which showed that when Lamin B2 depletion was performed in HCT116 cells, ~25-30% of the cells were aneuploid for CT18 and CT19 (Fig. 4.13A-C). The extent of aneuploidy upon Lamin B2 depletion was similar to that detected in DLD1 cells, thereby suggesting that Lamin B2 regulates chromosomal ploidy in mismatch repair deficient colorectal cancer cells, also as suggested by Kuga et al (2014).

We examined the spatial organization of CT18 and CT19 in the diploid and aneuploid state upon Lamin B2 depletion in HCT116 cells (Fig. 4.13A-B, D-F). The control (siLacZ treated cells) showed a gene density based chromosome positioning, with CT18 being predominantly localized to the nuclear periphery (M=71.87 %R.D) and CT19 (M=49.81 % R.D) toward the nuclear interior with a spatial separation of ~20% R.D between these chromosome territories (Fig. 4.13D-F). In the Lamin B2 depleted cells, both the diploid and aneuploid CT18 and CT19 showed conserved chromosome positioning consistent with gene density (Fig. 4.13D-F). While CT18 and nuclear volume did not show a significant change upon Lamin B2 Kd, CT19 volume showed a marked increase (~1.2 fold) (p=0.0061) (Fig. 4.13G-I). Thus it is likely that Lamin B2 based mechanisms that regulate spatial positions of diploid and aneuploid chromosomes are differentially regulated between DLD1 and HCT116, while the mechanism that involves Lamin B2 and regulates ploidy is conserved between DLD1 and HCT116. A greater in depth analysis of a differential proteome of these two cell lines with regard to proteins of the nuclear structure may yield insights into mechanisms that regulate chromosome positions between these two cell lines which may contribute to differential responses upon Lamin B2 depletion.

ii. HT1080

HT1080 is a stable diploid cell line of fibrosarcoma origin. This cell line is unique since it is of fibroblast origin, but shows an "epithelial-like" pattern of growth. We performed depletion of Lamin B2 in HT1080 cells and examined the positions of CT18 and CT19 in the interphase nucleus (Fig. 4.14A-B). HT1080 has two copies each of CT18 and CT19, which are spatially separated by ~10% R.D in the untreated cells (Fig. 4.14C-F). Thus, CT18 (M=69.07 % R.D) and CT19 (M=59.23 % R.D) are closer to one another in the interphase nucleus as compared to that in DLD1 and HCT116 (Fig. 4.14D-F). This reduced separation of CT may be due to the flatness of the nuclei in these fibroblast-like cells. This morphology is associated with CT18 and CT19 being closer to one another as compared to spherical nuclei (Bolzer et al., 2005). Copy numbers of CT18 and CT19 remained unaltered in HT1080 cells depleted of Lamin B2 (Fig. 4.14C). This suggests that the regulation of ploidy by Lamin B2 is potentially confined to cells of the colorectal cancer sub- type. Both CT18 and CT19 maintained their conserved chromosome positions consistent with gene density, suggesting that Lamin B2 depletion regulates neither the chromosome numbers nor their spatial positions in HT1080 cells (Fig. 4.14C-F). However, an interesting trend was detected for nuclear and chromosome volumes in these cells, with both the nuclear volume and that of CT19 showing a significant decrease (0.63 fold and 0.83 fold respectively, p=0.0001 and p=0.0094 respectively) upon Lamin B2 depletion. CT18 volume remained unaffected (Fig. 4.14G-I).

Figure 4.13

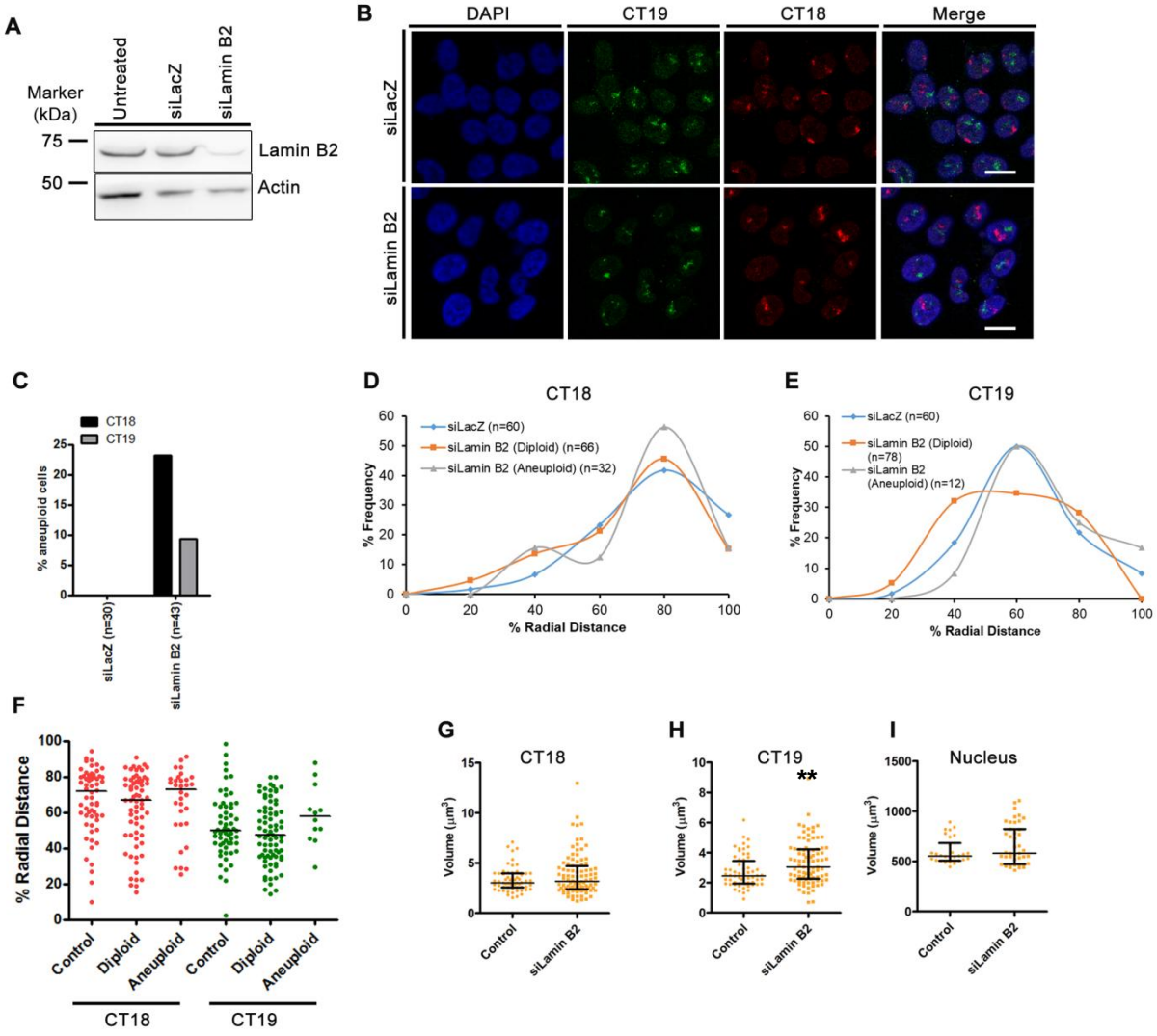

Figure 4.13 Impact of Lamin B2 depletion on the ploidy and spatial positions of CT18 and CT19 in HCT116 cells

A. Western blot depicting knockdown of Lamin B2 in HCT116 cells. Loading control: Actin. B. Representative images depicting 3D FISH for CT18 (red) and CT19 (green) in control (siLacZ) and Lamin B2 depleted HCT116 cells. Scale bar~10 µm. C. Quantification of number of signals (ploidy) for CT18 and CT19 in control and Lamin B2 depletion. D.Dot scatter plot representing % Radial distances (% R.D) of CT18 and CT19 in control and Lamin B2 depleted HCT116 cells. Horizontal lines indicate median. n~30-60 in each category.E. Radial distance

distribution profiles of CT18 (N=1) plotted as % R.D. binned into 5 nuclear subshells of ~20% R.D each for control and siLamin B2 diploid and aneuploid cells. F. Radial distance distribution profiles of CT19 (N=1) plotted as % R.D. binned into 5 nuclear subshells of ~20% R.D each for control and siLamin B2 diploid and aneuploid cells. G-I. Dot scatter plot for the volumes of (G) CT18, (H) CT19 and (I) Nucleus in control and Lamin B2 depleted HCT116 cells (N=1, n~30-60 in each category). N= number of biological replicates contributing to the data, n= number of CTs analysed.

---

iii. A549

A549 is a cell line of lung adenocarcinoma origin. Control cells (untreated cells) show a modal chromosome number of ~66. We performed Lamin B2 depletion in A549 and examined the positions of CT18 and CT19 in the interphase nucleus (Fig. 4.15A-B). The copy numbers of CT18 and CT19 range from 3-4 in each cell (Fig. 4.15C). CT18 and CT19 show a median radial distance of 64.70 % R.D and 62.20% R.D respectively, thereby showing a reduced spatial separation between gene rich CT19 and gene poor CT18. Lamin B2 depletion in A549 cells showed no change in the ploidy of either CT18 or CT19 (Fig. 4.15C). Both CT18 and CT19 upon Lamin B2 Kd showed a predominant population that was more internal toward the nucleus, which was not found to be statistically significant (Fig. 4.15D-F). However, the spatial separation between gene rich CT19 and gene poor CT18 was very low (~2-3%) with median values for CT18 (M=58.06% R.D) and that for CT19 (M=60.44% R.D). The volume of CT18 showed an increase (~1.62 fold, $p<0.0001$) upon Lamin B2 depletion while that of CT19 and the nucleus did not show any change (Fig. 4.15G-I). Thus, the lowering of Lamin B2 did not significantly impact chromosome numbers or positioning for A549 cells.

iv. SW480

SW480 is a colon cancer cell line that belongs to the category of mismatch repair proficient aneuploid colon cancer cell lines with a modal chromosome number of 57, and shows numerous chromosomal aberrations. Predominant subpopulations of these cells show 3 copies of CT18 and CT19, with a translocation T8; 19 or T5:19 (Melcher et al., 2000). We performed Lamin B2 depletion in SW480 cells and examined the spatial organization of CT18 and CT19 (Fig. 4.16A-

B). The expression level of Lamin B2 is relatively low in these cells (Fig. 4.12). In control (untreated) SW480 cells, CT18 showed a predominant localization towards the nuclear periphery (M= 67.98% R.D.), while CT19 showed a localization internal (M=65.69% R.D) as compared to CT18 (Fig. 4.16D-F). The spatial separation between CT18 and CT19 positions in control cells is only 2.29% R.D. This suggests that aneuploid cells show a destabilization of conserved chromosome positions in these cells. We performed Lamin B2 depletion in SW480 cells and detected no differences in the overall ploidy of CT18 and CT19 in SW480 cells (Fig. 4.16C). The spatial positions of CT18 and CT19 however were sensitive to the levels of Lamin B2 in these cells. CT19 showed a more internal localization upon Lamin B2 depletion (M= 56.55% R.D) (p=0.0061) (Fig. 4.16E-F). However, the spatial separation between gene rich CT19 and gene poor CT18 was 7.64% R.D upon Lamin B2 depletion. The volumes of the nucleus as well as CT18 and CT19 were unaffected upon Lamin B2 depletion in SW480 cells (Fig. 4.16G-I).

Thus a comparative study across cell types suggests that there is a variable response to Lamin B2 depletion, in a cell type specific manner. Ploidy of cells, tissue of origin and the relative stoichiometric contribution from other lamin impacts the response of different cell lines to lamin depletion. Regulation of ploidy by Lamin B2 is confined to the colon cancer cell type. Regulation of chromosome positions by Lamin B2 is mainly seen in the aneuploid cells. We next tested if increasing the levels of Lamin B2 impacts gene density dependent chromosome positioning, which otherwise is destabilized in aneuploid cells.

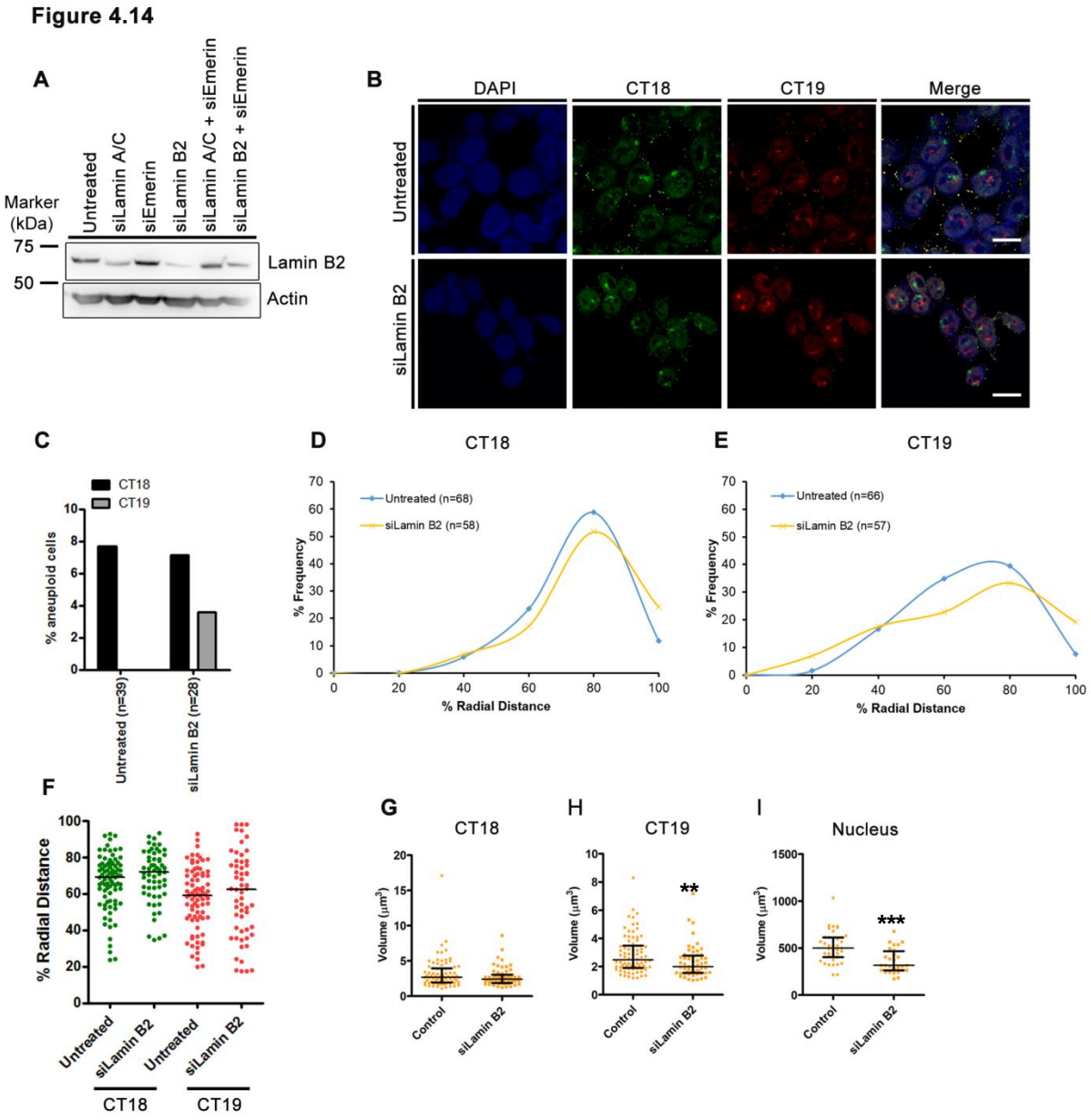

Figure 4.14 Impact of Lamin B2 depletion on the ploidy and spatial positions of CT18 and CT19 in HT1080 cells

A. Western blot depicting knockdown of Lamin B2 in HT1080 cells. Loading control: Actin. B. Representative images depicting 3D FISH for CT18 (green) and CT19 (red) in control (siLacZ) and Lamin B2 depleted HT1080 cells. Scale bar~10 µm. C. Quantification of number of signals (ploidy) for CT18 and CT19 in control and Lamin B2 depletion. D.Dot scatter plot representing % Radial distances (% R.D) of CT18 and CT19 in control and Lamin B2 depleted HT1080 cells. Horizontal lines indicate median. (N=1, n~30-60 in each category) E. Radial distance

distribution profiles of CT18 (N=1) plotted as % R.D. binned into 5 nuclear subshells of ~20% R.D each for control and siLamin B2 diploid and aneuploid cells. F. Radial distance distribution profiles of CT19 (N=1) plotted as % R.D. binned into 5 nuclear subshells of ~20% R.D each for control and siLamin B2 diploid and aneuploid cells. G-I. Dot scatter plot for the volumes of (G) CT18, (H) CT19 and (I) Nucleus in control and Lamin B2 depleted HT1080 cells (N=1, n~30-60 in each category). N= number of biological replicates contributing to the data, n= number of CTs analysed.

4.2.15 Overexpression of Lamin B2 in SW480 cells

Lamin B2 levels are relatively low in the aneuploid cell line SW480, yet a depletion of Lamin B2 repositioned CT19 towards the nuclear interior. We next asked if overexpression of Lamin B2 impacts chromosome positioning patterns in SW480 cells. We overexpressed Lamin B2-GFP in SW480 cells and performed 3D-FISH for CT18 and CT19 in these cells (Fig. 4.16H-I). The ploidy of CT18 and CT19 was not altered upon Lamin B2 overexpression (Fig. 4.16J). The empty vector control showed a median radial position for CT18 at 76.74% R.D, which was not significantly affected upon Lamin B2 overexpression (M= 74.51% R.D) (Fig. 4.16K-L). CT19 also showed conserved chromosome positioning (M=59.99% R.D) in the interphase nucleus as compared to the controls (M=64.61% R.D) (Fig. 4.16K, M). However, plot of binned % radial distance between control and Lamin B2 overexpressing cells shows that majority of CT19 shows a predominant localization proximal to the nuclear interior (R.D. ~60%) while CT18 shows a predominant localization proximal to the nuclear periphery (R.D. ~80%), thereby suggesting that subpopulations of CT18 and CT19 show a difference in their preferential position in the interphase nucleus upon Lamin B2 overexpression.

Figure 4.15

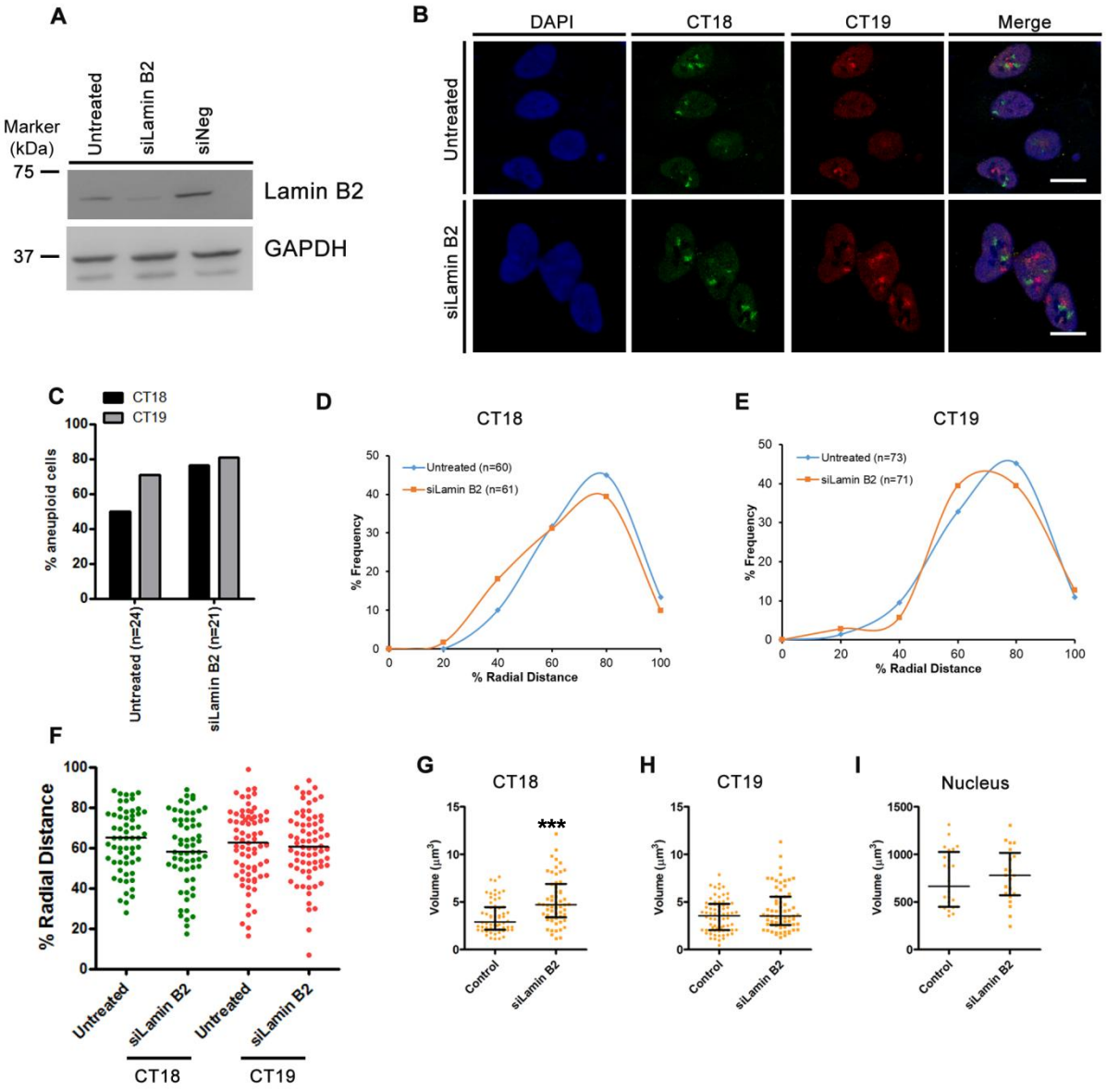

Figure 4.15 Impact of Lamin B2 depletion on the ploidy and spatial positions of CT18 and CT19 in A549 cells

A. Western blot depicting knockdown of Lamin B2 in A549 cells. Loading control: Actin. B. Representative images depicting 3D FISH for CT18 (green) and CT19 (red) in control (siLacZ) and Lamin B2 depleted A549 cells. Scale bar~10 µm. C. Quantification of number of signals (ploidy) for CT18 and CT19 in control and Lamin B2 depletion. D.Dot scatter plot representing % Radial distances (% R.D) of CT18 and CT19 in control and Lamin B2 depleted

A549 cells. Horizontal lines indicate median. (N=1, n~30-60 in each category) E. Radial distance distribution profiles of CT18 (N=1) plotted as % R.D. binned into 5 nuclear subshells of ~20% R.D each for control and siLamin B2 diploid and aneuploid cells. F. Radial distance distribution profiles of CT19 (N=1) plotted as % R.D. binned into 5 nuclear subshells of ~20% R.D each for control and siLamin B2 diploid and aneuploid cells. G-I. Dot scatter plot for the volumes of (G) CT18, (H) CT19 and (I) Nucleus in control and Lamin B2 depleted A549 cells. (N=1, n~30-60 in each category). N= number of biological replicates contributing to the data, n= number of CTs analysed.

Figure 4.16

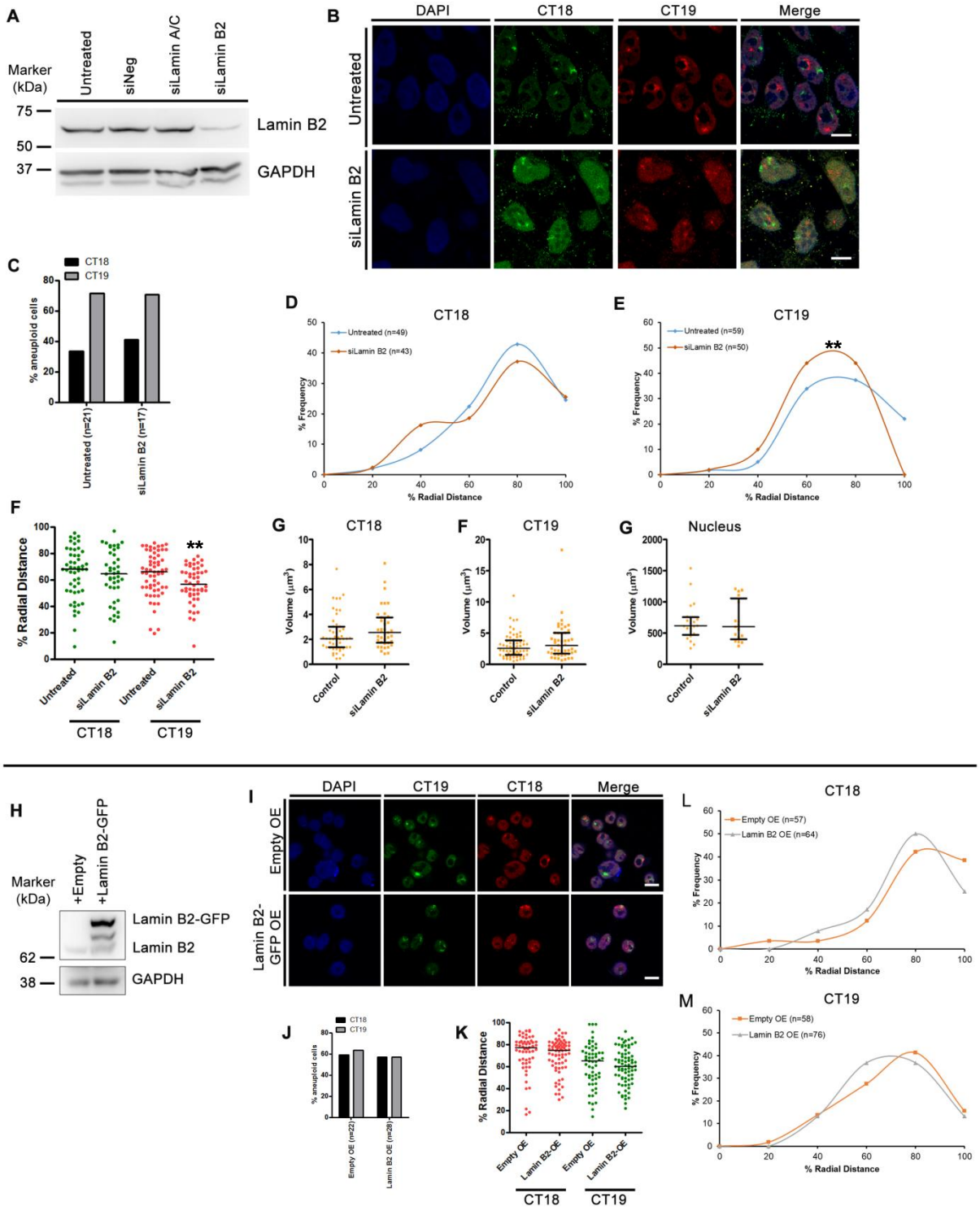

Figure 4.16 Impact of Lamin B2 depletion and overexpression on the ploidy and spatial positions of CT18 and CT19 in SW480 cells

A. Western blot depicting knockdown of Lamin B2 in SW480 cells. Loading control: Actin. B. Representative images depicting 3D FISH for CT18 (green) and CT19 (red) in control (siLacZ) and Lamin B2 depleted SW480 cells. Scale bar~10 µm. C. Quantification of number of signals for CT18 and CT19 in control and Lamin B2 depletion. D.Dot scatter plot representing % Radial distances (% R.D) of CT18 and CT19 in control and Lamin B2 depleted SW480 cells. Horizontal lines indicate median. (N=1, n~30-60 in each category) E. Radial distance distribution profiles of CT18 (N=1) plotted as % R.D. binned into 5 nuclear subshells of ~20% R.D each for control and siLamin B2 diploid and aneuploid cells. F. Radial distance distribution profiles of CT19 (N=1) plotted as % R.D. binned into 5 nuclear subshells of ~20% R.D each for control and siLamin B2 diploid and aneuploid cells. G-I. Dot scatter plot for the volumes of (G) CT18 (H) CT9 and (I) Nucleus in control and Lamin B2 depleted SW480 cells (N=1, n~30-60 in each category). J. Western blot depicting overexpression of Empty vector and Lamin B2-GFP in SW480 cells. Loading control: GAPDH. I. Representative images depicting 3D FISH for CT19 (green) and CT18 (red) in control (Empty vector) and Lamin B2-GFP overexpressing SW480 cells. Scale bar~10 µm. N= number of biological replicates contributing to the data, n= number of CTs analysed.

Table 18. CT18-CT19 positions in cell lines upon Lamin B2 depletion

Cell Line	Origin	Ploidy (modal chromosome number)	Impact upon Lamin B2 depletion	
			Ploidy	**Chromosome Positions**
DLD1	Colorectal cancer	44-46	2n+	Mislocalization of aneuploid CTs
HCT116	Colorectal cancer	44-46	2n+	Conserved positions of aneuploid CTs
HT1080	Fibrosarcoma	45-46	2n	Conserved CT positions
SW480	Colorectal cancer	57	2n	Repositioning of gene rich CT19
A549	Lung adenocarcinoma	66	2n	Conserved CT positions

4.2.16 Interactors of Lamin B2 at mitosis and interphase - Altered localization of LBR at mitosis in Lamin B2 depleted cells

We detected aneuploidy upon Lamin B2 depletion in DLD1 cells. Furthermore, we detected mislocalization of aneuploid CTs in Lamin B2 depleted DLD1 cells, suggesting roles for Lamin B2 at both these stages of the cell cycle. Lamin B2 is a multifunctional protein with different states during mitosis and interphase (Kuga et al., 2014). Depletion of Lamin B2 resulted in mitotic aberrations, aneuploidy; while in the interphase, aneuploid chromosome territories were mislocalized (Fig. 4.1,2,6). Thus, Lamin B2 is unique as it exerts a regulatory function in the interphase and metaphase stages. The two states of Lamin B2 represent a rich interactome of proteins, some of which are unique to the cell cycle phase, and some are interactions that are stable and maintained throughout the cell cycle (Kuga et al., 2014). We were curious to examine if these phenotypes of 'counting' of chromosomes by Lamin B2 are executed through separate or commonly regulated interactors at both these stages.

Lamin B2 associates with the mitotic spindle during mitosis and caps chromatin at condensed chromosomes during nuclear envelope reassembly (Kuga et al., 2014). During interphase, Lamin B2 primarily exists as an ordered polymerized lamina at the nuclear periphery (Shimi et al., 2015) (Fig. 4.17A). In addition, salt extraction methods reveal the presence of fine Lamin B2 structures in the nucleoplasm thereby suggesting the presence of intra nuclear Lamin B2 (Fig. 4.17A). These pools of Lamin B2 in the nuclear interior may have a potential bearing on the role of Lamin B2 in regulating chromosome positions. The biochemical nature and association with the nucleoskeleton for these Lamin B2 pools remains to be examined, since a caveat of the salt extraction followed by DNA digestion method is its inability to distinguish between lamins that have collapsed from the nuclear periphery and those that are associated with the nuclear matrix. At this stage, we interrogated LBR as a potential candidate that may maintain the ploidy and spatial organization of aneuploid chromosomes since Lamin B Receptor (LBR) interacts with Lamin B1/B2 in both mitosis and interphase (Güttinger et al., 2009; Ye and Worman, 1994). LBR binds to heterochromatin domains and HP1 and to Lamin B1 and Lamin B2 (Polioudaki et al., 2001; Ye and Worman, 1994; Ye et al., 1997). LBR is a chromatin capping protein and binds to mitotic chromosomes at early anaphase (Chaudhary and Courvalin, 1993). LBR association potentially functions as a nucleator for the subsequent binding by Lamin B2 in

chromosome segregation (Chaudhary and Courvalin, 1993). Furthermore, LBR is involved in tethering and organization of heterochromatin during development and in interphase cells (Hoffmann et al., 2002; Solovei et al., 2013). Thus, LBR presents an interesting candidate in terms of a mediator of regulation of ploidy (mitosis) and spatial organization (interphase).

We examined the localization of LBR in interphase and mitosis in Lamin B2 depleted cells (Fig.4.17B-F). Immunostaining was performed for LBR in suspension cells to enrich for the mitotic cells (Fig. 4.17B-C). The localization of LBR was differential between control and siLamin B2 cells primarily at the early stages of anaphase (Fig. 4.17B-C). While control DLD1 cells showed a predominant localization of LBR at the periphery of mitotic chromosomes (outlining the mitotic chromosomes – near heterochromatic regions at the outer core of the mitotic chromosomes) at early anaphase, siLamin B2 treated cells showed a delayed recruitment of LBR at early anaphase stages (Fig. 4.17B-C). LBR staining at the outer core of mitotic chromosomes was detected at later stages of anaphase to telophase in both control and Lamin B2 depleted cells (Fig. 4.17B-C). The proportion of cells showing anaphase recruitment for LBR reduced from 80% in controls to ~25% in Lamin B2 depletion (Fig. 4.17D). This suggests that Lamin B2 is an important regulator of the organization of LBR in mitotic cells; since absence of Lamin B2 results in a delayed recruitment of LBR. In interphase cells as well, fluorescence intensity profiles of LBR showed a reduction in peripheral levels of LBR in siLamin B2 cells ($p=0.017$) (Fig. 4.17E-F). The localization of LBR however was unaffected in the interphase cells. Owing to an altered localization of LBR at mitosis and interphase, LBR presents an important regulatory link between Lamin B2 and the effects of its depletion on ploidy and chromosome organization.

Figure 4.17

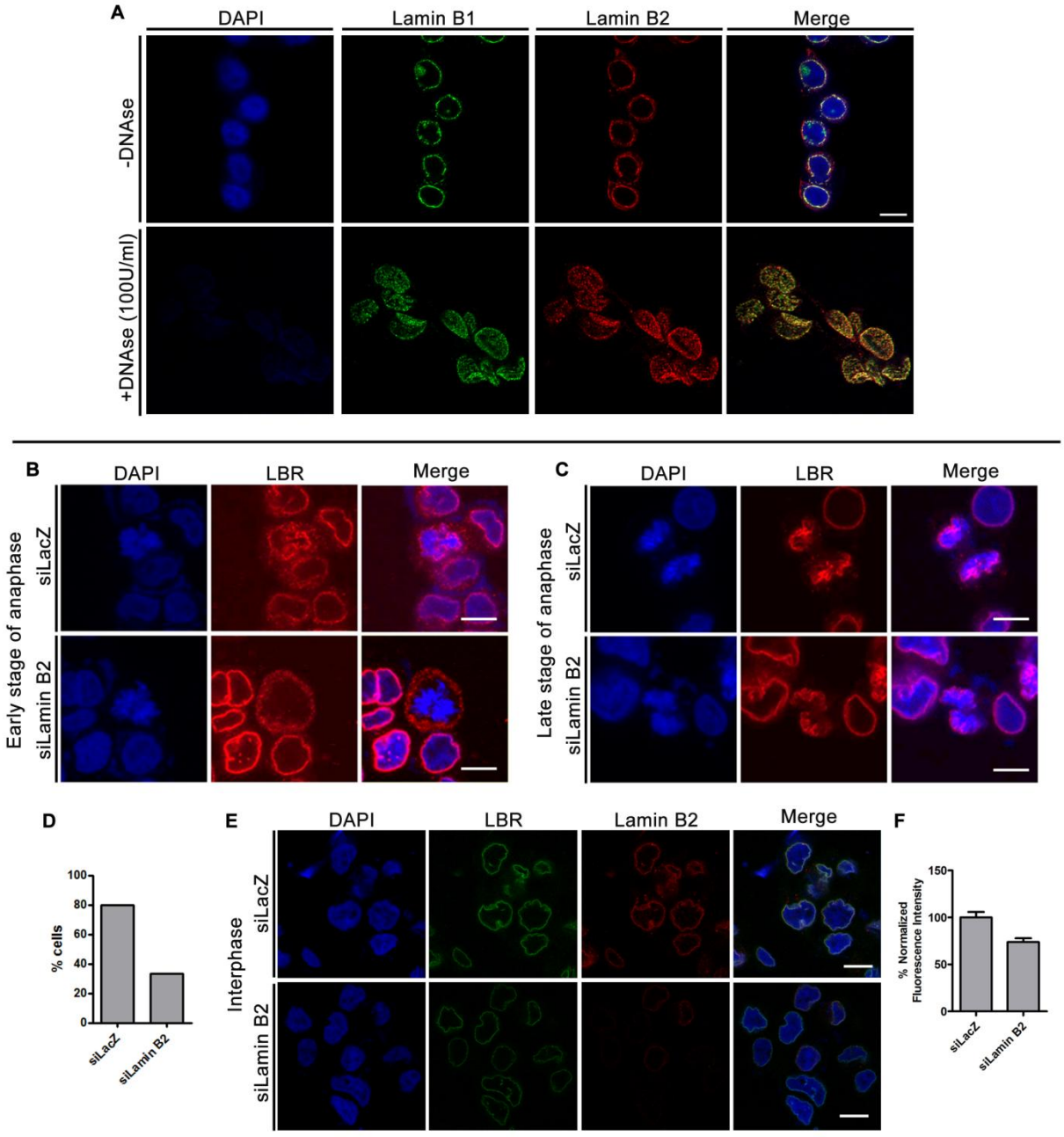

Figure 4.17 Altered localization of LBR upon Lamin B2 depletion in DLD1 cells

A. Immunostaining of Lamin B1 (green) and Lamin B2 (red) in DLD1 cells subjected to salt extraction for nuclear matrix preparation with or without DNAse treatment. Scale bar~10µm. B-C. Immunostaining for Lamin B Receptor (LBR) (red) in mitotic cells in siLacZ and siLamin B2 cells. B. Representative image for LBR staining at early stages of anaphase in siLacZ and siLamin B2 cells. C. Representative image for LBR staining at later stages of

anaphase to telophase in siLacZ and siLamin B2 cells. Scale bar~10µm. D. Quantification of LBR staining profile in mitotic cells of siLacZ and siLamin B2. E. Immunostaining for Lamin B Receptor (LBR) (green) and Lamin B2 (red) in interphase cells in siLacZ and siLamin B2 cells. Scale bar~10µm. F. Mean fluorescence intensity quantification of LBR at the nuclear periphery by performing line scans across nuclei from siLacZ and siLamin B2 cells. Error bars: SEM. A significant decrease was detected in LBR intensity at the nuclear periphery in Lamin B2 depleted DLD1 cells ($p=0.0170$, Unpaired t-test). Scale bar~10µm.

Figure 4.18

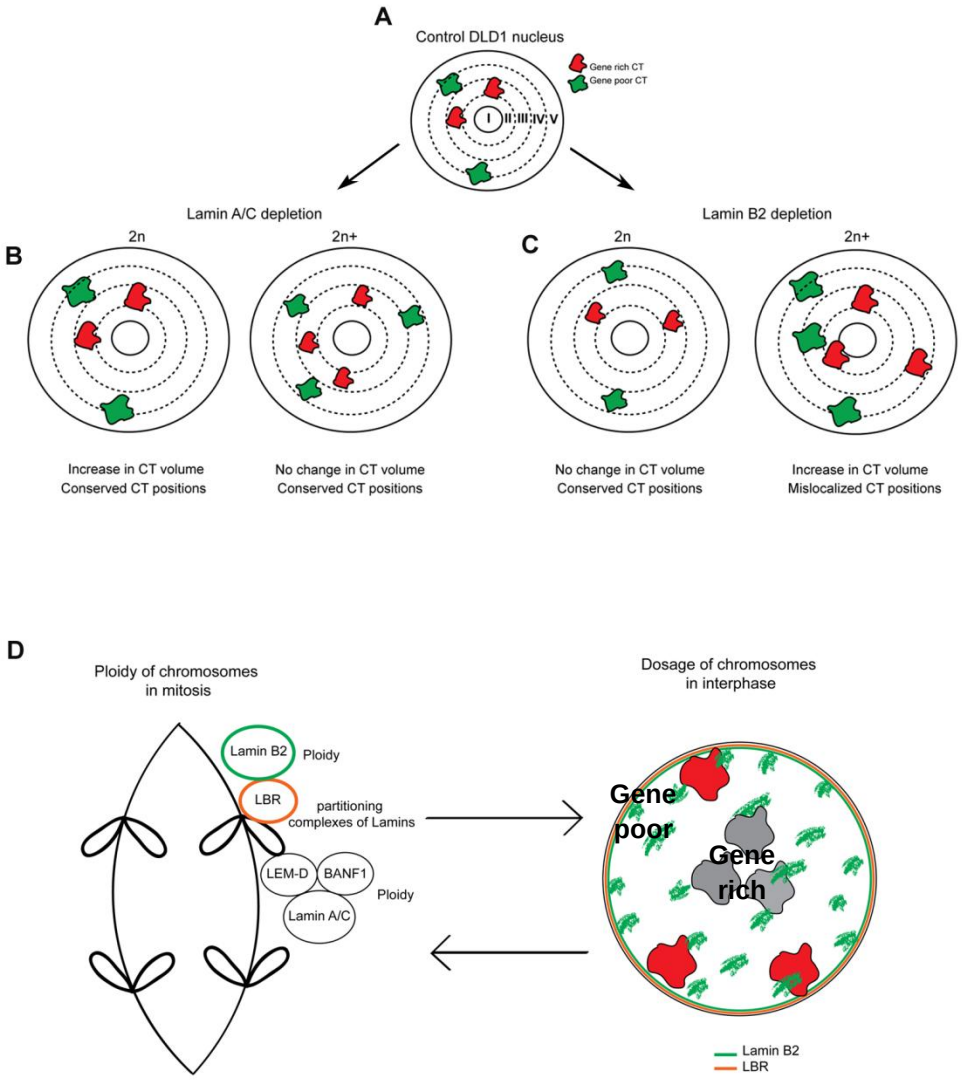

Figure 4.18 Speculative model for Lamin B2 dependent positioning of chromosome territories in the interphase nucleus

A. Control DLD1 cells show distribution of gene rich and gene poor chromosomes into different nuclear sub shells, gene rich (Shell III, R.D ~60%) and gene poor (Shell IV, R.D ~80%). B-C. Depletion of Lamin A/C and Lamin B2 results in generation of aneuploid cells, wherein Lamin B2 and not Lamin A/C depletion results in mislocalization of aneuploid CTs. Nuclear volumes are impacted in both Lamin A/C and Lamin B2 knockdowns, while Lamin A/C impacts the volumes of diploid CTs and Lamin B2 impacts the volumes of aneuploid CTs.

D. Model representing the role of Lamin B2 at mitosis and interphase in association with LBR. Lamin B2 and Lamin A/C form partitioning complexes at anaphase, which regulates ploidy (Qi et al., 2015). In interphase, Lamin B2-LBR interaction may impact the organization of intranuclear Lamin B2 and peripheral LBR levels, which may impinge on spatial positions of aneuploid chromosome territories.

4.3 Discussion

Our results from this chapter suggest a specific requirement for Lamin B2 but not Lamin A/C in the positioning of aneuploid chromosome territories in the nucleus. Lamin B2 is a unique factor since its absence resulted in (i) generation of aneuploidy and (ii) altered positions of aneuploid chromosome territories, while the absence of Lamin A/C resulted only in the generation of aneuploidy but not mislocalization of aneuploid chromosome territories. The aneuploidy was not enriched towards chromosomes showing greater transcriptional deregulation, as seen through a comparable extent of aneuploid for CT19, CT17, CT11 (greater transcriptional deregulation) and CT18 (low transcriptional deregulation).

The specific role of Lamin B2 in regulating chromosomal ploidy and chromosome positioning is difficult to uncouple. While both A and B-type lamins are involved in regulating spindle assembly during mitosis (Goodman et al., 2010; Kuga et al., 2014; Qi et al., 2015; Tsai et al., 2006), lamins are primarily structural proteins that maintain the spatial organization of the genome (Peric-Hupkes and van Steensel, 2010). While both Lamin A/C and Lamin B2 depletion induced CIN, primarily Lamin B2 depletion resulted in a mislocalization of aneuploid CTs (Fig. 4.18). Our study highlights an interesting divergence of the roles for Lamin A/C and Lamin B2. The role of Lamin B2 in the maintenance of genome organization is rather underappreciated. Diploid DLD1 cells, robustly express Lamins A/C, B1 and B2. Owing to this, there may be a compensatory feedback between lamins that maintains conserved chromosome positions in single lamin knockdowns. This is further reiterated in Lamin B1 depleted DLD1 cells, that show a conserved localization of CT18 at the nuclear periphery (Camps et al., 2014). However, in aneuploid cells, an optimum level of Lamin B2 is a likely prerequisite for the correct spatial positioning of chromosome territories (Fig. 4.18A-C).

In this study, we have examined the chromosome positioning patterns in a panel of diploid and aneuploid cell lines, and the impact of Lamin B2 depletion on these patterns. We see that cells diploid for CT18 and CT19 confer to a gene density based chromosome positioning pattern to a greater extent (as measured using the spatial separation between gene rich CT19 and gene poor CT18) as compared to aneuploidies CT18 and/or CT19. The spatial separation between the gene dense and gene poor chromosomes, was relatively higher for diploid cells (~20%), as compared

to aneuploid cell lines (~2-8%). Diploid HT1080 cells with flat growth morphology also showed a reduced spatial separation between CT18 and CT19, owing to their flatter nuclear morphology (Bolzer et al., 2005). SW480 and A549 cells both show lowered Lamin B2 expression levels as compared to diploid DLD1 and HCT116 cells, and show reduced spatial separation between CT18 and CT19. Lamin B2 depletion performed in these cell lines revealed aneuploidy in the otherwise diploid DLD1 and HCT116 cells; but not HT1080 cells. This suggests that the regulation of Lamin B2 at the mitotic spindle is specific to the colon cancer category. DLD1 cells showed a mislocalization of aneuploid CTs, while HCT116 shows aneuploidy upon Lamin B2 depletion, but no mislocalization of aneuploid CTs. Lamin B2 depletion resulted in CT19 localization towards the nuclear interior in SW480 cells. Thus, this screen suggested that Lamin B2 functions to regulate chromosome positions primarily in the background of aneuploidy, in a cell type specific manner. This role of Lamin B2 is largely represented in colon cancers. Our data also leads to further questions of the regulatory role of Lamin B2 during the course of colon cancer progression. It would be interesting to examine the role of Lamin B2 if any, as colon cancers progress and achieve greater aneuploidy. Does a lowering of Lamin B2 present a mechanism for the cells to permit greater mislocalization and hence a greater loss of transcriptional regulation? Some of these questions can be examined in greater details in cellular models of colon cancer progression.

It is plausible that regulation of ploidy and positioning of aneuploid chromosomes is co-regulated by Lamin B2 through its commonly regulated interactors that function during both mitosis and interphase (Fig.4. 18D). One such candidate is the inner nuclear membrane protein SUN1 identified in a screen and which associates with Lamin B2 during mitosis (Kuga et al., 2014). Another interactor that can be a mediator of these functions is the transmembrane protein of the inner nuclear membrane – Lamin B Receptor (LBR) (Ye and Worman, 1994). LBR is an interesting factor that may assist Lamin B2 in mitosis and interphase. We detected a delayed recruitment for LBR in Lamin B2 depleted cells, suggesting this to be a contributing factor to aneuploidy in mitosis. In addition, the role of LBR in interphase cells, in the maintenance of heterochromatin organization has been extensively characterized (Solovei et al., 2009; Solovei et al., 2013). Lamin A/C and LBR are required for tethering heterochromatin, while its absence results in a mislocalization of heterochromatin to the nuclear interior and therefore an inversion in nuclear architecture in murine rod cells (Solovei et al., 2009; Solovei et al., 2013). Our studies

suggest a similar alteration in genome organization as evidenced by the mislocalization of the gene rich CT19 towards the nuclear periphery and gene poor CT18 towards the nuclear interior specifically in Lamin B2 depleted aneuploid cells (Fig. 4.2.6). This suggests a potential involvement of Lamin B2 associated LBR in maintaining conserved CT positions. The absence of LBR results in a loss of order of primarily heterochromatin during development. We speculate that Lamin B2 functions with LBR in sensing the dosage of chromosomes in the interphase (Fig. 4.18D). The Lamin B2-LBR interaction may have a bearing on the organization of intranuclear Lamin B2 as also levels of LBR at the periphery, which may impinge on spatial positions of aneuploid chromosome territories. The functions of Lamin B2 are probably highest represented in colon tissue, and more specific roles are seen in colon cancer, as seen through mass spectrometry and gene expression datasets which show an enrichment of Lamin B2 (Kuga et al., 2014). However, the precise roles of Lamin B2-LBR association remain to be examined further in the context of maintaining the spatial organization of the genome. Moreover, since LBR is primarily localized at the nuclear periphery, the extent to which it contributes to the organization of gene rich chromosomes in the nuclear interior is not clear. It is conceivable that Lamin depletion destabilizes different subsets of Lamin interaction networks at the (i) nuclear periphery (LINC complex) (ii) heterochromatin (iii) nuclear interior and (iv) perinucleolar heterochromatin. Hence, along with LBR, additional Lamin dependent factors are likely to be involved in stabilizing aneuploid chromosomes in the interphase nucleus. A careful biochemical analysis of these nuclear subfractions may provide further insights on these potential interactions with Lamin B2 required for the correct maintenance of CTs in a manner consistent with gene density. Alternatively, the decision to place chromosomes in unique nuclear locations may be initiated during mitosis, where Lamins regulate chromosome segregation (Martin et al., 2010) (Fig. 4.18D).

There are conflicting reports on the expression levels of Lamin A/C in colorectal cancers (Belt et al., 2011; Moss et al., 1999; Willis et al., 2008; Wu et al., 2009). Data from patient samples suggests a general trend of downregulation of Lamin A/C expression in more aggressive colon cancers as compared to less aggressive cancers. However, artificially overexpressing Lamin A in SW480 cells enhances their tumorigenic potential, suggesting an association between increased Lamin A expression and greater invasive properties of tumour cells (Foster et al., 2011). In contrast, Lamin B2 was shown to be a differentially expressed protein between colorectal

cancers with and without CIN – with increase in Lamin B2 expression conferring protection against chromosomal instability (Kuga et al., 2014). It is noteworthy from our results that Chr.17, 18 and 19 (from the specific subset of chromosomes that we examined) were consistently gained independently upon Lamin A/C or Lamin B2 depletion. This is suggestive of a pattern of chromosomal acquisitions potentially relevant for colorectal cancer progression (Tagawa et al., 1996). It remains to be examined if the extent of Lamin stoichiometry correlates with the extent of these chromosomal gains during colorectal cancer progression (Belt et al., 2011; Roth et al., 2010) (Belt et al. 2011; Roth et al. 2010).

Previous studies suggest a remarkable conservation in gene density based chromosome positioning patterns of even aneuploid chromosomes in the interphase nucleus in cancer cells (Cremer et al., 2003). A recent study on primary amniocyte cells show that naturally aneuploid human Chr.18 and 21 territories assume conserved nuclear locations (Hervé et al., 2016). Further, artificially introduced gene poor human Chr.7 or 18 and gene rich Chr.19 into otherwise diploid DLD1 cells, showed a gene density based conservation in their positioning patterns towards the nuclear periphery and nuclear interior respectively (Sengupta et al., 2007). It would be of interest to examine the expression levels of Lamins in these cells which show conserved chromosome territories in trisomies.

It is pertinent to note that lamin depletion induced volume changes of chromosome territories may further impinge on the spatial constraints that position chromosome territories and their transcription potential (Fig. 4.7). Our analysis revealed no correlation between the volumes of aneuploid chromosome territories and the nuclear sub-shells that they occupy (Fig. 4.7). Notably, diploid chromosome territories showed an increase in volume upon Lamin A/C Kd (Fig. 4.7). An interesting target in this regard is SMC1A which is involved in regulation of chromatin architecture (Phillips-Cremins et al., 2013). Microarray based gene expression profiling shows a downregulation of *SMC1A* (~ 2 fold) upon Lamin A/C but not in Lamin B2 knockdown, suggesting that SMC1A could function as a regulator of CT volumes downstream of Lamin A.

Change in spatial positions of the aneuploid chromosomes could potentially have a bearing on its interaction with the nuclear lamina and with neighboring chromosome territories (Branco and Pombo, 2006). Changes in chromatin contacts may also have a bearing on the transcriptional regulation of genes on aneuploid chromosome territories. Changes in ploidy of cells result in

variability in the association patterns of aneuploid chromosomes with the nuclear lamina. This was demonstrated through haploid and diploid KBM7 cells which show variability in their LAD profiles. Thus LAD profiles are sensitive to the ploidy of cells (Kind et al., 2015). It would be useful to compare LAD profiles in diploid versus aneuploid Lamin depleted cells. It would be technically challenging to specifically isolate aneuploid cells and examine chromatin contacts by Hi-C studies and transcriptional profiles by RNA-Seq analyses (Hashimshony et al., 2012; Islam et al., 2012; Nagano et al., 2013). Such an analysis would yield greater insights into the impact of chromosomal aneuploidies on chromatin contact frequencies and transcription.

The correlation between the spatial organization and expression status of gene loci in aneuploid cells is relatively less explored. Amplified *C-MYC* (Chr.8q24) gene loci are localized external to chromosome 8 territory in colon cancer cell line HT-29 (Harnicarová et al., 2006). Interestingly, these loci were found to be transcriptionally active. The nuclear lamina is generally a transcriptionally repressive zone and repositioning of gene loci away from the nuclear lamina is associated with an increase in its gene expression levels (Peric-Hupkes and van Steensel, 2010; Shachar et al., 2015), as shown for artificially targeted reporter genes (LacO gene visualized using LacI-GFP) in single cells (Finlan et al., 2008; Reddy et al., 2008) as well as an endogenous gene *TCRB*, in contact with the nuclear Lamina (Schlimgen et al., 2008; Shachar et al., 2015). In our study, the candidate gene locus *ZNF570* was repositioned away from the nuclear lamina in both diploid and aneuploid coupled with a significant increase in transcript signals in Lamin B2 depleted cells (Fig. 4.11). Thus, our studies reveal altered spatial organization of gene loci consistent with an increase in its expression levels in Lamin B2 depleted cells. A similarity in the organization of gene loci in Lamin B2 depleted diploid as well as aneuploid nuclei is suggestive of a similarity in Lamin B2 dependent transcriptional regulation of gene loci in diploid and aneuploid cells.

Taken together, our studies suggest that aneuploid chromosomes are mislocalized in Lamin depleted cells. This mislocalization may represent a strategy to achieve enhanced transcriptional deregulation by sampling diverse sub-nuclear microenvironments in the interphase nucleus, otherwise maintained by Lamin B2. The presence of Lamin B2 prevents chromosomal aneuploidies and also dampens their positions in the nucleus and may thereby impose further regulation on their transcript levels. The impact of altered spatial organization on the

transcriptional outputs of aneuploid chromosomes would have important consequences on the potential lamin dependent mechanisms of cancer initiation and diseases associated with chromosomal aneuploidies.

Chapter 5: Role of Lamins in genomic stability

Data acknowledgements:

Figure 5.4A-B. Joyce Thompson

5.1 Introduction

The multifunctional lamin family of proteins comprises A and B type lamins which form a filamentous sheath beneath the inner nuclear membrane (Dechat et al., 2008). Along with forming higher order polymers and maintaining the structure and shape of the nucleus, these proteins are also involved in regulation of genomic stability and often called the 'guardians of the genome'.

Lamins are a unique class of proteins that function at multiple scales during the cell cycle. Lamins are involved in mitosis during nuclear envelope reassembly. Both A and B type lamins are disassembled through phosphorylation during mitosis and are dispersed throughout the nucleoplasm in the M phase. Lamins along with other nuclear envelope (NE) associated proteins serve to reform the nuclear envelope post mitosis (Chaudhary and Courvalin, 1993). Lamins reassemble into higher order polymers and form the nuclear lamina. A small fraction of lamins is also found in the nucleoplasm as internal pools of lamins that form a nucleoskeletal veil in the nucleus (Bridger et al., 1993; Broers et al., 1999; Hozák et al., 1995; Moir et al., 2000b; Muralikrishna et al., 2004). The oligomerization state of the nucleoplasmic form of lamins is not completely clear. These two stages of lamins at mitosis and interphase present two different states of the protein and are associated with different regulatory functions of lamins with regard to genomic instability. At the mitotic phase, Lamin B1/B2 and Lamin A/C associate with the mitotic spindle (Goodman et al., 2010; Qi et al., 2015; Tsai et al., 2006). A regulatory role has been ascribed for lamins for maintaining the integrity of the mitotic spindle and ensuring proper chromosome segregation (Kuga et al., 2014; Qi et al., 2015; Tsai et al., 2006). Our previous data also showed an increase in chromosomal instability (CIN) upon depletion of Lamin A/C and Lamin B2 (Ranade et al., 2016). Thus, Lamins A/C and B2 are involved in regulating chromosomal stability of cells by ensuring fidelity of chromosome segregation (Kuga et al., 2014; Qi et al., 2015; Tsai et al., 2006). This increase in CIN upon Lamin knockdowns prompted us to ask whether other aspects of genomic stability in cells were also compromised with depletion of Lamin A/C and/or Lamin B2 in DLD1 cells.

During G1, lamins associate with LADs at the nuclear periphery and act as guardians of the genome at the nuclear periphery. The recruitment and stability of DNA repair proteins to sites of DNA damage is also regulated by Lamins in the interphase of cells, as shown by reduced

efficiency of DNA repair in cells of laminopathy (mutant Lamin A) patients (Liu et al., 2008; Shumaker et al., 2008). Subsequently in S phase, both A and B type lamins act as scaffolding proteins that assist replication machinery protein complexes during DNA duplication (Kennedy et al., 2000; Shumaker et al., 2008; Spann et al., 1997). Thus, the role of lamins in regulation of genomic stability varies with the cell cycle stage under consideration. The different stages and levels of lamin regulation of genomic stability are summarized here:

1. *Chromosomal stability regulation (M phase of cell cycle)*

Lamin A/C, Lamin B1, Lamin B2 associate with the mitotic spindle assembly at the G2-M transition state (Goodman et al., 2010; Kuga et al., 2014; Qi et al., 2015; Tsai et al., 2006). The mitotic spindle matrix contains a matrix of B type lamin filaments dependent on Ran protein gradients as shown in Xenopus cells as well as human HeLa cells (Tsai et al., 2006). Moreover, a colon cancer specific role for regulation of chromosomal stability was demonstrated for Lamin B2 with increased Lamin B2 expression conferring protection against chromosomal instability (Kuga et al., 2014). This role of Lamin B2 was through its localization at the spindle pole during mitosis. The inner nuclear membrane protein SUN1, a part of the LINC complex, was found to be a mitosis specific interacting partner of Lamin B2 and serves to maintain spindle integrity in association with Lamin B2 (Tsai et al., 2006). Depleting the cells of Lamin B1 or Lamin B2 in these studies resulted in incorrectly oriented mitotic spindle, multipolar spindles, anaphase bridges and severe chromosomal segregation defects (Kuga et al., 2014; Tsai et al., 2006). This phenotype is associated with severe aneuploidy. A similar role has been documented for Lamin A/C where a lowered level of Lamin A/C is associated with greater chromosomal instability (aneuploidy) in ovarian and breast cancer cells (Capo-chichi et al., 2011a; Capo-chichi et al., 2011b). In terms of contributing to the mitotic spindle, Lamin A/C forms a complex with LAP2alpha and BAF and loads onto the mitotic spindle. This protein complex associates with acto-myosin axis and microtubules and serves to maintain spindle orientation and integrity (Qi et al., 2015).

Thus, both A and B type lamins contribute to chromosomal stability at the mitotic phase. The molecular nature of regulation by Lamin A/C and Lamins B1 and B2 is different, and probably

influenced by the cell type under consideration. Phenotypically, depletion of both these kinds of lamins has been shown to induce chromosomal instability in terms of aneuploidy in cells, which is reiterated in our studies with DLD1 cells.

2. Genomic Stability – Repair of damaged DNA (G1 phase)

At the end of mitotic phase, Lamins begin to reassemble through polymerization. During this process they associate with chromatin characterized primarily by inactive histone marks (H3K27me3, H3K9me2/3) and are stably associated with heterochromatin at the nuclear periphery (Kind et al., 2013; Kind et al., 2015). Moreover, circulating pools of nucleoplasmic lamins also exist inside the nucleus, which bind to chromatin in the nuclear interior (Lund et al., 2013; Lund et al., 2015). In this stage, lamins contribute to genomic stability by mediating recruitment of DNA repair proteins at the site of damage. The role of lamins in regulating DNA repair machinery is best exemplified through cells from laminopathies – a group of diseases resulting from mutations in Lamin A/C and its interacting proteins at the nuclear periphery (Gonzalo and Kreienkamp, 2015; Schreiber and Kennedy, 2013). Progeroid cells as well as Lamin A/C knockout mice show genomic instability phenotypes characterized by increased telomere dynamics and slower repair of damaged DNA (Gonzalez-Suarez et al., 2009; Huang et al., 2008; Liu et al., 2005; Singh et al., 2013).

Lamin A/C interacts with and stabilizes the DNA repair protein 53BP1 (Gibbs-Seymour et al., 2015). Lamin A/C is important in the recruitment and stability of 53BP1 at sites of DNA double strand breaks (Liu et al., 2008; Redwood et al., 2011). Because 53BP1 is an important molecule involved in both the NHEJ and HR pathways, a reduced stability and recruitment of 53BP1 impacts DNA repair through both these pathways in Lamin A/C deficient cells (Redwood et al., 2011). Lamin A/C also regulates the recruitment of Rad51 and transcript levels of Rad51 and BRCA1- two important molecules in the NHEJ pathway as shown through mouse models of aging and Lamin A deficient mice (Liu et al., 2005; Redwood et al., 2011). Lamins thus function to regulate DNA repair factors transcriptionally, as scaffold proteins as also as signaling molecules. The positional stability of DNA repair foci also depends on the integrity of a Lamin A/C nucleoskeleton (Mahen et al., 2013). In response to several interstrand cross link agents

such as cisplatin, Lamin A/C deficient cells show normal gamma H2Ax foci formation, but delayed repair factors recruitment, suggesting a role for Lamin A/C in maintaining a platform for DNA damage repair pathways. Similarly, the positional stability of DNA repair foci also depends on the integrity of a Lamin A/C nucleoskeleton. Notably, the efficiency of repair through the homologous repair pathway (HR) was not significantly affected in MCF7 cells treated with siLamin A/C (Singh et al., 2013).

B type lamins are also involved in the base excision as well as nucleotide excision repair pathways (Butin-Israeli et al., 2013; Butin-Israeli et al., 2015). Lamin B1 stabilizes Rad51 and thereby regulates Rad51- dependent homologous recombination (Liu et al., 2015). Nucleotide Excision Repair (NER) proteins such as DDB1, CSB and PCNA are downregulated in Lamin B1 depleted cells (Butin-Israeli et al., 2013). Lamin B1 also binds to the promoter of and regulates the expression of key DNA repair proteins including BRCA1 and Rad51 (Butin-Israeli et al., 2015). Taken together, Lamins are involved in various pathways of DNA repair, either as a scaffold that serves to recognize and recruit factors in DNA repair or in epigenetically regulating the transcription of genes involved in DNA repair.

3. Genomic stability during DNA replication (S phase)

DNA replication is a process associated with generation of double strand breaks and DNA lesions during active replication. These replication forks are repaired and resolved with precision, and this requires an efficient recruitment of repair proteins to the sites of replication. Lamins have been implicated in this function of acting as a scaffold for assembly of other proteins during DNA replication. Both A and B type lamins associate with replication foci (Kennedy et al., 2000; Moir et al., 1994). The rate of DNA synthesis has been shown to slow down along with an altered distribution of replication factors in the absence of functional Lamin A (Moir et al., 2000a; Spann et al., 1997). Progeroid cells that harbor a permanently farnesylated Lamin A protein also show defects in DNA replication. Lamin A/C depleted cells showed a delayed replication restart in response to replication stress, as also defective replication foci recruitment. Several DNA damage repair proteins such as Mre11, CtIP, Rad51, RPA, and FANCD2 showed reduced recruitment at DNA damage sites in Lamin A/C depleted cells (Singh

et al., 2013). Moreover, Lamin A/C is also associated with DNA Polymerase subunit ε throughout S phase, suggesting a direct involvement of Lamin A/C in the replication process (Vaara et al., 2012).

B type lamins also associate with DNA Polymerases during the S phase. Moreover, both Lamin B1 and Lamin B2 associate with PCNA during DNA replication (Shumaker et al., 2008) . The rate of replication is reduced in Lamin B1 depleted cells (Butin-Israeli et al., 2015; Camps et al., 2014). Repair of DNA damage foci during replication is also slowed in Lamin B1 depleted cells; suggesting a requirement for Lamin B1 scaffolds in ensuring proper DNA replication (Butin-Israeli et al., 2015). Reduced Lamin B1 expression is also reported to induce a stalling of DNA replication and senescence (Shimi et al., 2011).

Owing to this involvement of both A and B type Lamins in processes associated with DNA repair during G1, S and M phases, it is conceivable that a depletion of Lamin A/C and/or Lamin B2 may compromise genomic stability at various stages of the cell cycle. We previously detected chromosomal instability (CIN) but no cell cycle stalling in DLD1 cells upon single depletion of Lamin A/C and Lamin B2. In this section, we have characterized various genomic instability effects upon Lamin A/C and Lamin B2 depletion. We detected nuclear blebbing, chromosomal aberrations and copy number variations in DLD1 cells upon Lamin depletion.

5.2 Results

5.2.1 Lamin B2 depletion increases the frequency of nuclear blebbing

Lamin depletion performed using siRNA against Lamins A/C, B1 and B2 respectively in colorectal cancer cell line – DLD1 shows an increase in frequency of nuclear shape changes through immunostaining of Lamin depleted nuclei (Refer to Chapter 3 -Fig. 3.1).

Counterstaining of Lamin depleted nuclei with the inactive histone mark H3K27me3 revealed an interesting phenotype of nuclear blebbing upon Lamin depletion in DLD1 cells (Fig. 5.1A). H3K27me3 showed a predominant staining at the nuclear and nucleolar periphery in control DLD1 cells (Fig. 5.1A). These cells also showed a punctate staining of H3K27me3 in the nucleoplasm (Fig. 5.1A). H3K27me3 staining revealed increased incidence of blebbing at the nuclear periphery in Lamin depleted cells. These peripheral nuclear blebs were either continuous (bleb) or discontinuous (micronuclei) (Fig. 5.1A). Quantification of the number of nuclear blebs showed an increase in frequency of nuclear blebbing predominantly upon Lamin B2 knockdown to ~20% as compared to 2-5% in control DLD1 cells (Fig. 5.1B). Lamin A/C or Lamin B1 depletion increased blebbing to only ~10%, suggesting a specific role for Lamin B2 in regulating nuclear bleb formation (Fig. 5.1B).

We next asked if these nuclear blebs generated upon Lamin B2 depletion showed continuity with the nuclear membrane and other lamins. Control and Lamin B2 depleted DLD1 cells were transfected with a plasmid encoding EGFP-Lamin A and imaged in live conditions (Fig. 5.1C). EGFP-Lamin A was found to localize at the periphery of the nuclear bleb/micronucleus, suggesting that the blebs formed showed the presence of Lamin A (Fig. 5.1C). A number of studies previously have documented that the lamina composition is different for the lamina at blebs (Shimi et al., 2008). However, in live DLD1 cells we found a uniformly localized pEGFP-Lamin A signals at the nuclear membrane in control cells as well as in nuclei showing blebs (Fig. 5.1B-C).

We also examined the frequency of nuclear lamina aberrations and nuclear blebs in another diploid cell line – HT1080 (fibrosarcoma origin) (Fig. 5.1D-E). This cell line shows several

nuclear lamina aberrations in the form of (i) discontinuities (differential distribution of Lamin A/C and Lamin B2 in the lamina) as well as (ii) blebs and micronuclei in the untreated control

Figure 5.1

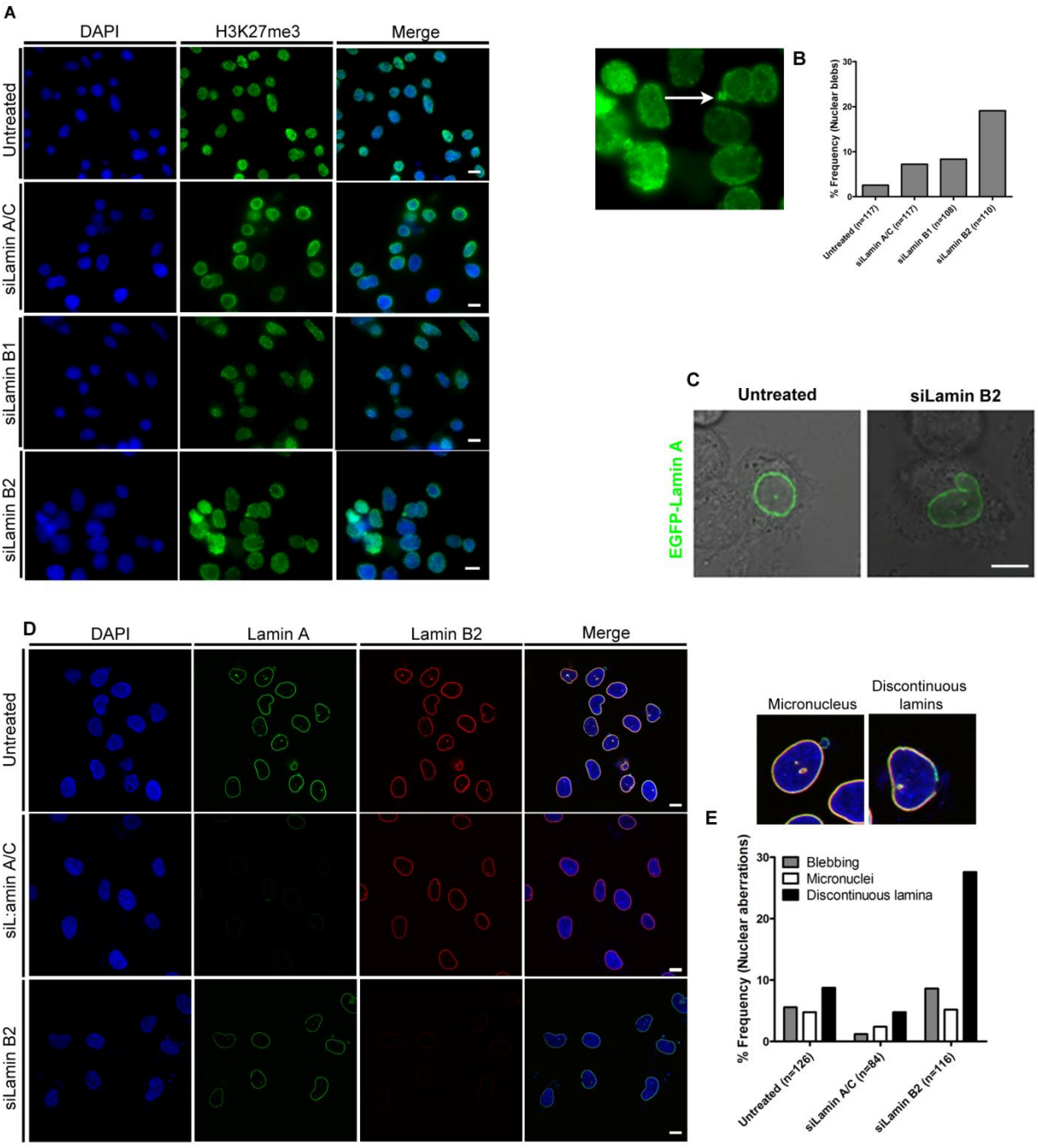

Figure 5.1 Increase in nuclear lamina aberrations upon Lamin depletion

A. Immunostaining for H3K27me3 (green) and Lamin B2 (red) in Control (untreated) and siLamin A/C, siLamin B1 and siLamin B2 cells. Scale bar~10µm. Inset: Enlarged image showing nuclear blebs upon siLamin B2. B. Quantification of number of cells showing nuclear blebbing in Control (untreated) and siLamin A/C, siLamin B1 and siLamin B2 cells. n=number of cells scored. A significant increase was detected in the number of cells with nuclear blebs upon siLamin B2. C. Merged brightfield and fluorescence images from live DLD1 cells (control and siLamin B2) transfected with pEGFP-Lamin A to label the nuclear lamina in live conditions. Nuclear blebs generated in siLamin B2 cells are labeled with EGFP-Lamin A. D. Immunostaining for Lamin A (green) and Lamin B2 (red) in control, siLamin A/C and siLamin B2 treated HT1080 cells. Scale bar~10µm. Insets: Enlarged images showing discontinuous lamina, micronuclei. E. Quantification of nuclear lamina aberrations in control, siLamin A/C and siLamin B2 HT1080 cells. siLamin B2 cells show an increase in the incidence of discontinuous lamina in HT1080 cells.

cells (Fig. 5.1D). In HT1080 cells, a depletion of Lamin B2 was associated with an increase in lamina discontinuities as against the increase in nuclear blebbing seen upon Lamin B2 depletion in DLD1 cells (Fig. 5.1E). On the other hand, depletion of Lamin A/C reduced the frequency of nuclear blebbing in HT1080 cells (Fig. 5.1E). The relative expression levels and stoichiometry of A and B type lamins varies between DLD1 and HT1080 cells (Fig. 4.12). We speculate that depending on the composition of the lamina, the contribution and influence of each Lamin depletion may elicit a different change in the lamina. Lamin B2 is a regulator of nuclear lamina integrity and formation in both DLD1 and HT1080 cells; however, their cell type specificity may determine the precise role of regulation for Lamin B2 in these two cellular backgrounds.

5.2.2 Increase in chromosomal aberrations upon Lamin B2 depletion

Given the increase in number of aneuploid cells (Chapter 4- Fig. 4.1,2), micronuclei and blebbing in Lamin B2 depleted cells (Fig. 5.1), we were curious to ask whether there were any chromosomal aberrations upon Lamin depletion in DLD1 cells. Nuclear blebbing is a classical sign of genomic instability, and these blebs often contain fragmented or excess DNA from cells

Figure 5.2

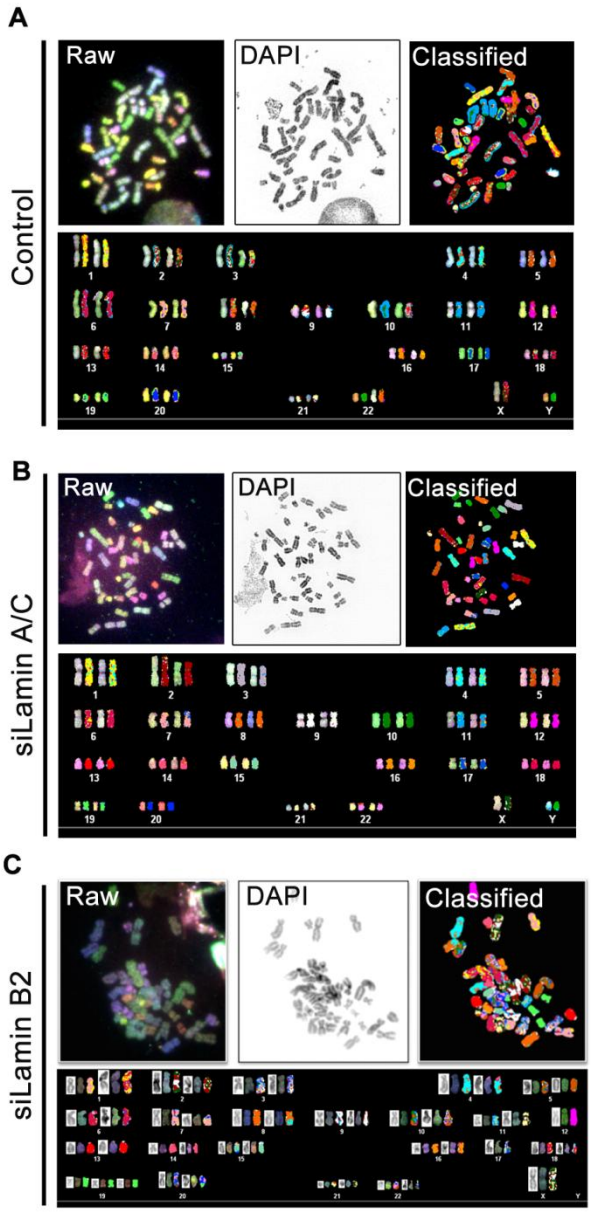

Figure 5.2 Spectral karyotyping on lamin depleted cells

A. Representative spectral karyotyping (SKY) and analysis performed on control (untreated) DLD1 cells. B. Representative spectral karyotyping (SKY) and analysis performed on siLamin A/C DLD1 cells. C. Representative spectral karyotyping (SKY) and analysis performed on siLamin B2 DLD1 cells. Images shown are representative out of two independent biological replicates.

(Shimi et al., 2008). We performed Spectral Karyotyping (SKY) on metaphase spreads generated from Control (untreated), siLamin A/C and siLamin B2 cells (Fig. 5.2). Analyses of SKY images recapitulated aneuploidy and gain of chromosomes upon Lamin B2 knockdown (Fig. 5.2). Chromosomes from Lamin B2 depleted cells revealed a host of chromosomal aberrations. These aberrations included; in addition to gains, chromosomal breaks, non recurrent translocations and in some cases, fragmentation of parts of chromosomes (Fig. 5.2B). These events are listed in Table 19. There was no chromosome specificity in these aberrations. Interestingly, chromosome spreads from Lamin A/C depleted cells did not show obvious chromosomal aberrations. This suggested that like blebbing; chromosomal aberrations are strongly associated with Lamin B2 depletion as compared to Lamin A/C depletion.

Table 19. Chromosomal aberrations detected in siLamin B2 cells using Spectral Karyotyping (Numbers in columns for chromosomal aberrations indicate the chromosomes showing aberrations)

Case No.	Chromosomal aberrations			
	Gains	Losses	Translocations	Others
1	0	0	0	
2	1,6,18,19,	7(-1),9(-2),	0	fragments of 16
3	1	not identified	T (22:5)	
4	18,15(3copies)	7,16,17	T(11:19)	
5	19	12,Y	T(1:18)	break on chromosome 3
6		10,13,Y,20	T(11:19)	
7			T(2:16)	

5.2.3 Lamin B2 depletion results in greater mitotic aberrations

We detected an increase in mitotic aberrations (lagging chromosomes, anaphase bridges, multipolar spindles) upon Lamin B2 depletion in DLD1 cells (Refer to Chapter 4- Fig. 4.2).

5.2.4 Lamin A/C, B1 and B2 depletion shows non overlapping copy number variations (CNVs) in DLD1 cells

We detected an increase in chromosomal instability upon knockdown of Lamin A/C and Lamin B2 in DLD1 cells. This prompted us to examine if the stability of gene loci that are orders of magnitude (~10^5 fold) smaller than whole chromosome territories, is also affected upon Lamin depletion in DLD1 cells. We characterized copy numbers in the genome through Copy Number Variation (CNV) analyses performed using whole genome array hybridization in DLD1 cells (Fig. 5.3). CNV generation is a feature commonly associated with initiation and progression of cancers (Shlien and Malkin, 2009). Genomic DNA from Control and Lamin depleted cells was extracted and subjected to hybridization on an array representing the diploid human genome. CNVs were determined for Control, siLamin A/C, siLamin B1 and siLamin B2 depleted cells. These copy number variations were of the following types:

complete deletion

full copy deletion

single copy insertion

full copy insertion.

LOH – loss of heterozygosity

CNV profiles were initially determined for control DLD1 cells. For this purpose, we examined the CNV profiles for DLD1 cells that were commonly found in the control as well as Lamin depleted cells. A total of 141 CNVs were detected in this analysis (Fig. 5.3A). Predominant among these were LOH (loss of heterozygosity) (seen in ~53% cases), single copy insertions and

deletions (~20% each). LOH was clustered on chromosomes 5,7,14 and Y in DLD1 cells. (Fig. 5.3A) In addition, 42

Figure 5.3

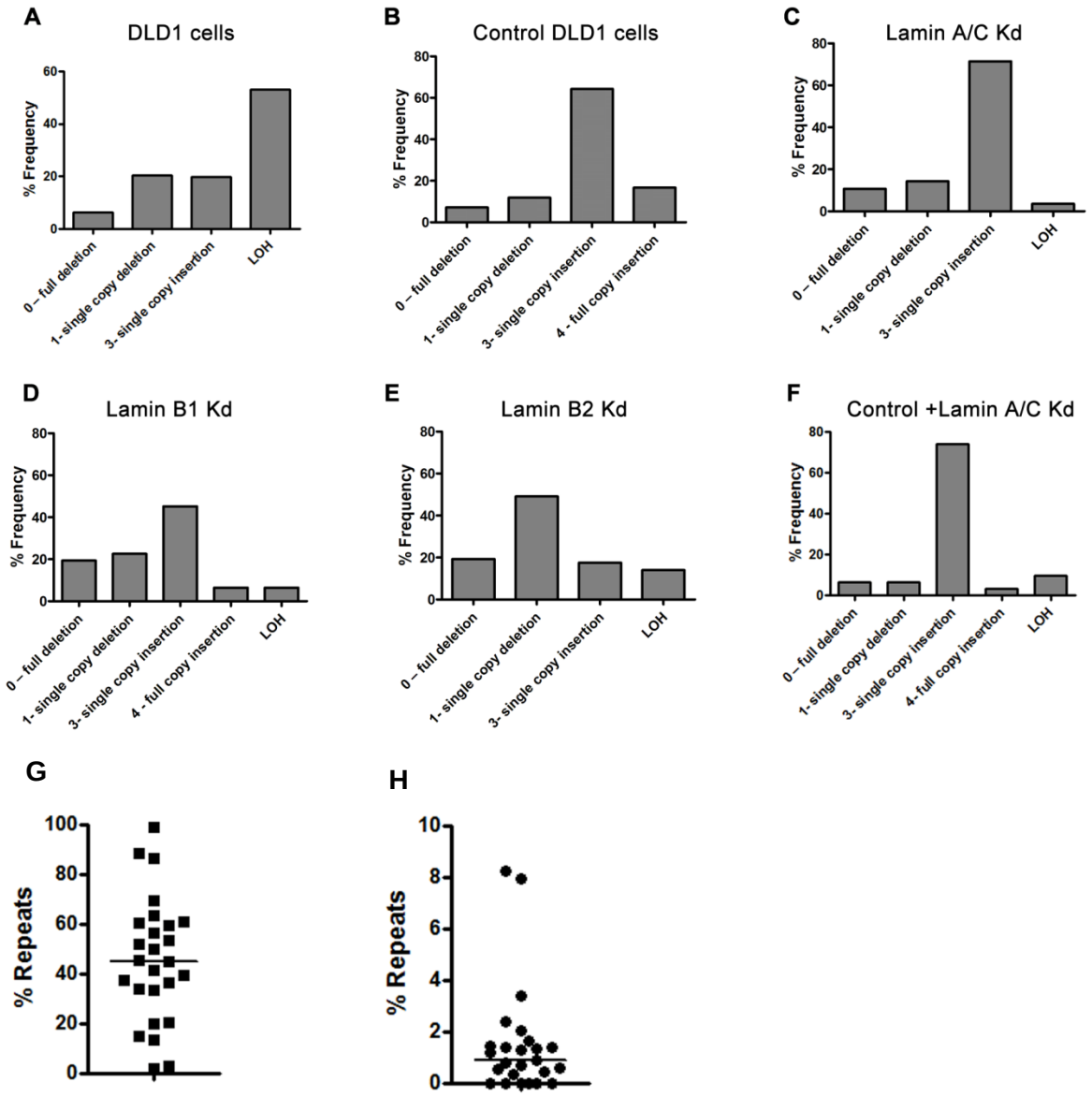

Figure 5.3 Copy number variations in DLD1 cells upon Lamin knockdown

Copy number variations detected in DLD1 cells in the following conditions (A) All the cells in the experiment – Control, siLamin A/C, siLamin B1, siLamin B2. (B) Control cells only (C) siLamin A/C only (D) siLamin B1 only (E) siLamin B2 only (F) common between Control and siLamin A/C. G. % total repeats in the single copy insertions upon siLamin A/C H. % short repeats in the single copy insertions upon siLamin A/C

CNVs were detected only in control cells out of which 64.29 % were single copy insertions (Fig. 5.3B). DLD1 cells belong to the category of microsatellite instability mismatch repair deficient (MSI+ MMR-) category of colorectal cancer cells (Boland and Goel, 2010). They have an active MSI pathway, which results in amplification of mono and di nucleotide microsatellite repeats. These single copy insertions may represent a consequence of microsatellite amplification that is active in DLD1 cells (Boland and Goel, 2010).

Subsequently, we characterized the nature of CNVs that were detected in specifically Lamin depleted cells. A careful examination of the frequency of CNVs in Lamin depleted cells revealed differences in the profiles of siLamin A/C, siLamin B1 and siLamin B2 cells. The predominant type of CNV found in Lamin A/C depleted cells was single copy insertion (71.43% out of total 28 CNVs) (Fig. 5.3C). As against that, the predominant CNV in Lamin B2 depleted cells was single copy deletion (49.12% out of total 57 CNVs) (Fig. 5.3E). Lamin B1 knockdown reveals a profile characterized by numerous kinds of CNVs including both single copy insertion (45.15% out of total 31 CNVs) as also single copy deletions (22.58% out of total 31 CNVs) (Fig. 5.3D). Moreover, CNVs commonly detected between control and siLamin A/C cells also show an increased frequency of single copy insertions (Fig. 5.3F). This is indicative of a difference in the modes of copy number regulation by A and B type lamins. The high frequency of deletion in Lamin B2 depleted cells is corroborated by the high frequency of chromosomal aberrations seen upon Lamin B2 knockdown in DLD1 cells (Fig. 5.2). Moreover, increased nuclear blebbing and micronuclei generation is also associated with greater genomic aberrations, breaks and instability; which was detected in Lamin B2 depleted DLD1 cells.

We further characterized various properties of the CNVs that were detected in Lamin depleted cells. These genomic regions were characterized for their length and chromosomal locations. While Lamin A/C Kd showed a median CNV of length 18.64 Kb, Lamin B1 and Lamin B2 Kd showed CNVs of median length 7.13 Kb and 12.51 Kb respectively. These CNVs did not show predominant clustering to specific chromosomes and were spread over the genome. Comparatively, chromosomes 16, 3 and 6, and 5 and 6 showed greater number of CNVs over other chromosomes in Lamin A/C, Lamin B1 and Lamin B2 Kd respectively.

Next, we examined if the predominant CNVs represented in Lamin A/C and Lamin B2 Kd belong to a particular biological pathway or function. This was done primarily to examine if any

biological function is subjected to regulation by Lamin A/C or Lamin B2 especially with regard to their copy numbers. Cancer cells especially represent CNVs of related/oncogenic targets in their genome. Hence we were curious to examine if the CNV targets contained genes from a particular biological function. Gene Ontology analyses were performed on the gene targets found amplified (predominant CNV in Lamin A/C depleted cells) and on the gene targets deleted (predominant CNV in Lamin B2 depleted cells) using the software DAVID. To our surprise, however, we did not find a significant enrichment ($p<0.05$) for any GO categories in both these data sets. A marginal enrichment ($p=0.05$) was found for the Calcium ion binding category in siLamin A/C cells, and of Olfactory receptor activity in siLamin B2 cells. However, these categories also represented only ~3-4 genes from the total dataset and did not represent a significant enrichment over the others.

The absence of biological (GO category) enrichment reduced the possibility of a biological function bias to the gene targets showing CNVs. We further sought to examine if any other properties of the genome with respect to its sequence properties were associated with the CNV targets. We detected an amplification of gene loci primarily upon Lamin A/C depletion in DLD1 cells. Since amplification of mono/di nucleotide repeats is a feature of the MSI pathway that is functional in DLD1 cells (Boland and Goel, 2010), we sought to examine the extent of sequence repeats in the amplification targets found upon Lamin A/C depletion. The frequency of total repeats in the genomic contigs was determined using Repeat Masker function from UCSC genome browser. We initially examined all repeats found in the contig (without a bias towards microsatellite repeats); and normalized the total to the length of the contig. The median % repeat density (per unit length) was found to be between 40-70% (Fig. 5.3F). Furthermore, we examined the extent of short repeats within these amplified sequences and found that majority of the regions showing genome insertions contained ~ 0.8-1% short repeats (Fig. 5.3G).

5.2.5 Copy number variations for *DNMT1* and not for *WDR8* gene loci

We detected single copy insertions as a predominant CNV upon Lamin A/C depletion in DLD1 cells. In addition, we also examined the copy numbers of candidate gene loci that show robust expression in colorectal cancers as seen through datasets on Oncomine. We chose *DNMT1* (Chr.19p13.2) and *WDR8* (Chr. 1p36.3) which are highly expressed in colorectal cancers as candidate gene loci (Fig. 5.4A-B). The repeat density of *DNMT1* and *WDR8* gene loci showed that *DNMT1* is a repeat rich gene locus, with ~40% total repeats while *WDR8* has ~ 10% total repeats (Fig. 5.4C). DNMT1 contains ~1.9% short repeats while *WDR8* contains ~0.31%. We labeled these gene loci in control and lamin depleted DLD1 cells using BAC clones. We ascertained the chromosomal location of the BAC DNA probes by performing 2D FISH on metaphase spreads generated from control DLD1 cells (Fig. 5.4B). 2D FISH was then performed on metaphase and interphase cells in control and Lamin depleted cells (Fig. 5.4A). The number of FISH signals per nucleus as seen in interphase cells was counted and its frequency distribution was plotted. Interestingly, control DLD1 cells showed ~30% population of cells with 3 copies of *DNMT1* gene locus (Fig. 5.4D). Upon Lamin A/C depletion, the population of DLD1 cells having 2 copies of *DNMT1* gene reduced significantly while that of cells with 3-5 copies of *DNMT1* increased significantly, thereby showing amplification specifically upon Lamin A/C depletion ($p<0.0001$, Fischer's exact test) (Fig. 5.4D). This effect was not seen upon depletion of B type Lamins (Fig. 5.4D). It is important to note that in the genome wide CNV maps siLamin A/C cells showed single copy insertions as the predominant CNV. 2D-FISH was performed for the locus *WDR8* also showed ~ 20% control cells having 3 copies of the gene (Fig. 5.4E). *WDR8* gene locus however did not show any significant amplification in either Lamin A/C or Lamin B2 depleted cells (Fig. 5.4E). Thus, 2D-FISH revealed a differential effect of siLamin A/C (with respect to amplification) on gene loci in different genomic contigs. 2D-FISH detected an amplification of *DNMT1* (having 45% repeats) as against *WDR8* (having 10% repeats).

5.2.6 Lamin A/C depletion in SW480 does not show amplification of *DNMT1*

The single copy insertions detected in DLD1 cells upon Lamin A/C Kd bears resemblance to the accumulation of repeat insertions seen in microsatellite instability seen in control DLD1 cells. To

Figure 5.4

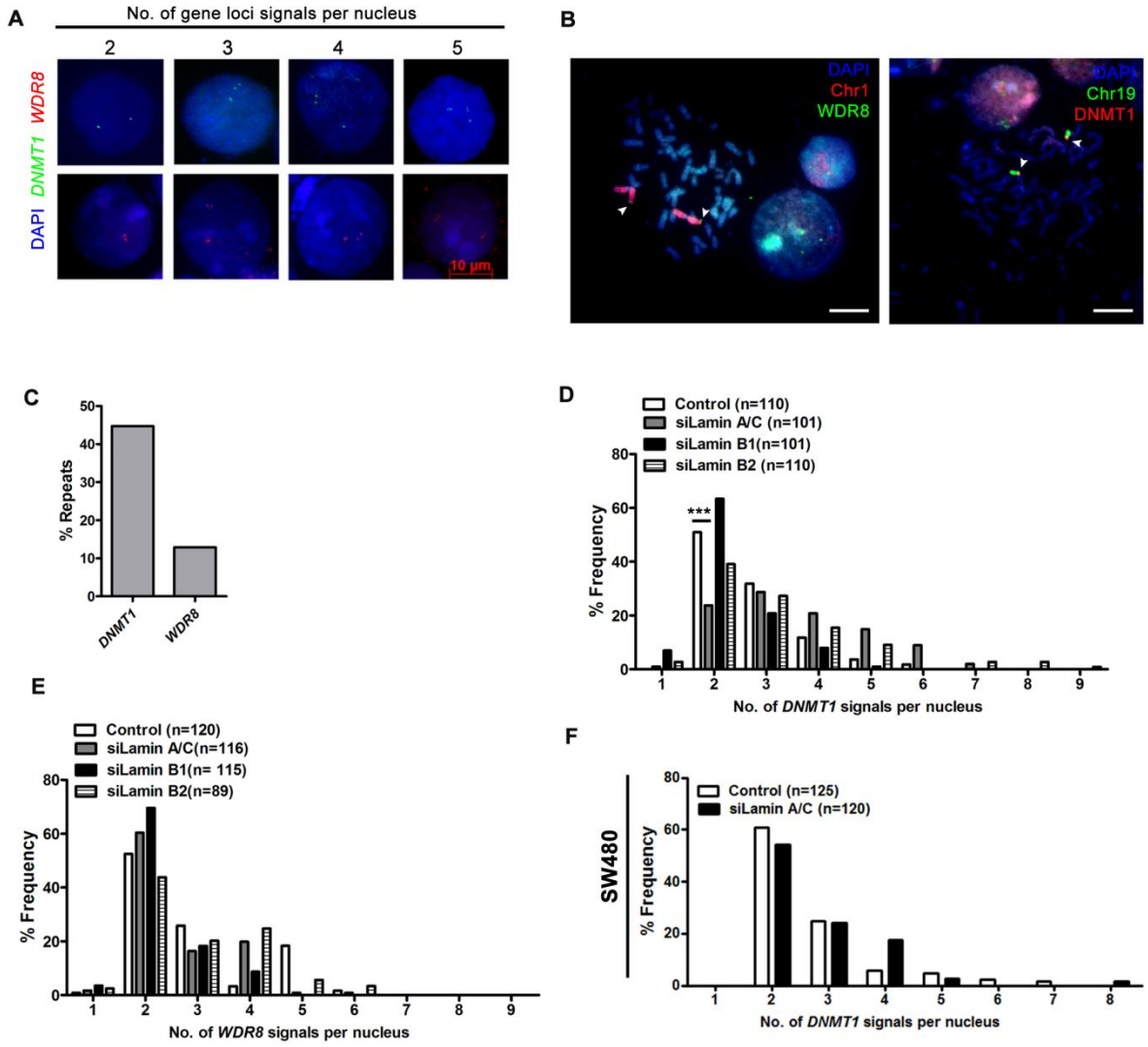

Figure 5.4 Copy number variations for DNMT1 in DLD1 and not SW480 cells upon Lamin depletion

A-B. Representative images for 2D FISH performed on interphase and metaphase DLD1 cells showing copy number variations for genes *DNMT1* (green) and *WDR8* (red). Scale bar~10µm. C. Repeat density for *DNMT1* and *WDR8*. D Quantification of copy numbers of *DNMT1* gene in Control (untreated) and Lamin depleted DLD1 cells. Data shown is a representative out of two independent biological replicates. A significant increase in the population of cells showing amplification (>2 copies) of *DNMT1* seen in siLamin A/C cells ($p<0.0001$, Fischer's exact test). E. Quantification of copy numbers of *WDR8* gene in Control (untreated) and Lamin depleted DLD1 cells. No significant changes were detected in the copy numbers of *WDR8* gene in Lamin depleted cells. F. Quantification of copy numbers of *DNMT1* gene in Control (untreated) and Lamin A/C depleted SW480 cells. No significant changes were detected in the copy numbers of *DNMT1* gene in Lamin A/C depleted SW480 cells. n: number of nuclei analysed.

further examine if there exists a correlation, if any, between the MSI pathway and generation of amplification in Lamin A/C Kd, we performed Lamin A/C Kd and examined the copy numbers of *DNMT1* gene in a cell line SW480 that does not have microsatellite instability (Fig. 5.4F). Lamin A/C Kd was performed in SW480 cells using siRNA for a duration of 48 hours (Fig. 5.4F). The copy numbers of *DNMT1* gene were assessed in control and Lamin A/C depleted cells using 2D FISH (Fig. 5.4F). SW480 cells also showed a population of cells with 3 copies of the *DNMT1* gene in control cells (Fig. 5.4F). However, these cells did not show a significant amplification of the *DNMT1* gene locus (Fig. 5.4F).

5.2.7 Spatial organization of gene loci *DNMT1* and *WDR8* is altered upon Lamin depletion

It is well established that gene loci (~10^3-10^5 fold lower in DNA content as compared to chromosome territories) also exhibit a non-random localization that correlates with its expression levels. Genes with elevated expression levels are "looped-out" of their respective CT, while downregulated genes are sequestered into their CT or associate with repressive nuclear landmarks such as the nuclear lamina (Chambeyron et al., 2005, Volpi et al., 2000). However, the molecular mechanisms that regulate "looping-out" of gene loci from its cognate CT are unclear. We were curious to examine the spatial organization of gene loci that are a part of amplifications generated upon Lamin depletion in DLD1 cells.

We therefore examined the spatial organization of the two candidate genes whose copy numbers were assessed upon Lamin Kd in DLD1 cells- *WDR8* (Chr. 1p36.3) and *DNMT1* (Chr.19p13.2) in the interphase nucleus in the context of Lamin A/C and B2 depletion in DLD1 cells (Fig. 5.5). We have previously seen that while *DNMT1* gene shows amplification upon Lamin A/C Kd, *WDR8* gene did not show amplification. We asked if the spatial organization and gene expression levels of these loci were different between control and Lamin depleted cells. Oncomine analyses showed that these genes are upregulated in colorectal cancer samples. This was also substantiated by qRT-PCR, which demonstrated robust expression levels of these genes in DLD1 cells (Fig. 5.5S). Both these genes were significantly downregulated upon Lamin A/C Kd (*WDR8* - 0.35 fold, *DNMT1*- 0.6 fold) and upon Lamin B2 Kd (*WDR8* - 0.475 fold, *DNMT1*-

Figure 5.5

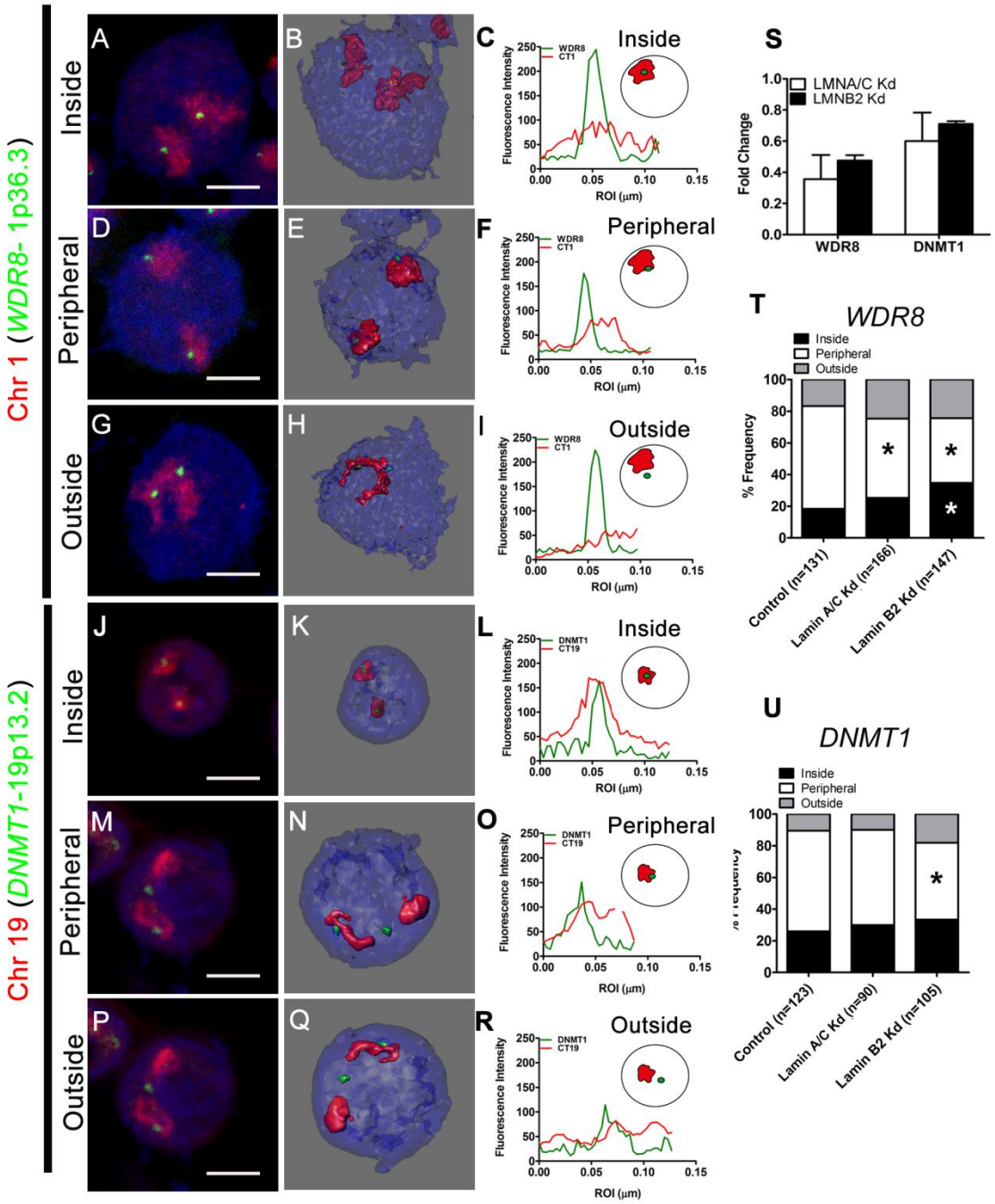

Figure 5.5 Spatial organization of gene loci DNMT1 and WDR8 is altered upon Lamin depletion

Chr.1 ideogram shows location of *WDR8* (1p36.3) BAC contig. (A-I) Spatial organization of *WDR8* gene loci with respect to CT1 in DLD1 cells. Representative maximum intensity projections, 3D reconstructions and line-scans of gene loci (green) and CT1 (red) shows three spatial states of the gene loci with respect to CT1 (i) (A-C) Inside (ii)

(D-F) Peripheral (iii) (G-I) Outside. Blue channel: DAPI stained nuclei, Scale bar ~ 5 µm. (J-R) Chr.19 ideogram shows location of *DNMT1* (19p13.2) BAC contig. Spatial organization of *DNMT1* gene loci with respect to CT19 in DLD1 cells. Representative maximum intensity projections, 3D reconstructions and line-scans of gene loci (green) and CT19 (red) shows three spatial states of the *DNMT1* gene loci with respect to CT19 (i) (J-L) Inside (ii) (M-O) Peripheral (iii) (P-R) Outside. Blue channel: DAPI stained nuclei, Scale bar ~ 5 µm (S) Gene expression levels of *WDR8* and *DNMT1* upon Lamin A/C Kd and Lamin B2 Kd assayed using qRT-PCR. Expression levels normalized to ACTIN (N=3). (T) Quantification of the spatial position of *WDR8* w.r.t CT1 in control, Lamin A/C Kd and Lamin B2 Kd respectively. Significant decrease in the population of cells showing *WDR8* at the periphery of CT1 upon Lamin A ($p=0.009$) and Lamin B2 Kd ($p<0.0001$). A concomitant increase in the population of cells showing an internal localization of *WDR8* w.r.t CT1 was detected only upon Lamin B2 Kd ($p=0.0016$). (U) Quantification of the position of *DNMT1* w.r.t CT19 in control, Lamin A/C Kd and Lamin B2 Kd respectively. A significant decrease in population of cells showing *DNMT1* at the periphery of CT19 upon Lamin B2 Kd ($p=0.0231$).

0.710 fold) (Fig. 5.5S). To examine the spatial organization of these gene loci, we used the chromosome territory as a reference; since transcriptionally overexpressed gene loci are often found to loop out of their CT while repressed ones are found to reside inside the CT (Chambeyron et al., 2005, Volpi et al., 2000). Analyses of 3D reconstructions of nuclei with fluorescently labeled chromosome territories and gene loci revealed that *WDR8* and *DNMT1* gene loci exist (i) inside (ii) outside (iii) peripheral with respect to their chromosome territories 1 and 19 in the interphase nucleus (Fig. 5.5A-R). In control cells, *WDR8* gene locus is predominantly peripheral to CT1 (~65%), while ~18% nuclei show an internal and 17% nuclei show an outside localization of *WDR8* with respect to CT1 (Fig. 5.5T). Lamin A/C Kd as well as Lamin B2 Kd show a significant difference in the positioning of *WDR8* with respect to CT1 ($p=0.0363$ and $p=0.0003$ respectively). A significant decrease in the population of nuclei showing a peripheral localization of *WDR8* gene loci w.r.t CT1 was detected upon Lamin A/C Kd (~65% to ~50%, $p=0.009$) and Lamin B2 Kd (~65% to ~40%, $p<0.0001$) (Fig. 5.5T). A concomitant increase in the population of nuclei showing an internal localization of the *WDR8* w.r.t CT1 was detected only in Lamin B2 Kd cells (~18% to ~35%, $p=0.0016$) but not upon Lamin A/C Kd (Fig. 5.5T). We next examined the spatial organization of *DNMT1* gene loci with respect to CT19. In control cells, *DNMT1* gene loci was predominantly localized peripheral to CT19 (~ 63%), while ~11% nuclei show an external and ~26% nuclei shows an internal location

(Fig. 5.5U). Upon Lamin B2 Kd, a significant decrease in the peripheral population of *DNMT1* gene loci was detected with respect to CT19 (~63% to ~48%, p=0.0231) (Fig. 5.5U). No significant change was detected in the populations of cells showing inside or outside localization of *DNMT1* w.r.t CT19 upon Lamin B2 Kd (Fig. 5.5U). Thus, in summary, Lamin A/C or Lamin B2 depletion affects the spatial organization of *WDR8* and *DNMT1* gene loci with respect to its cognate chromosome territory in the interphase nucleus.

Figure 5.6

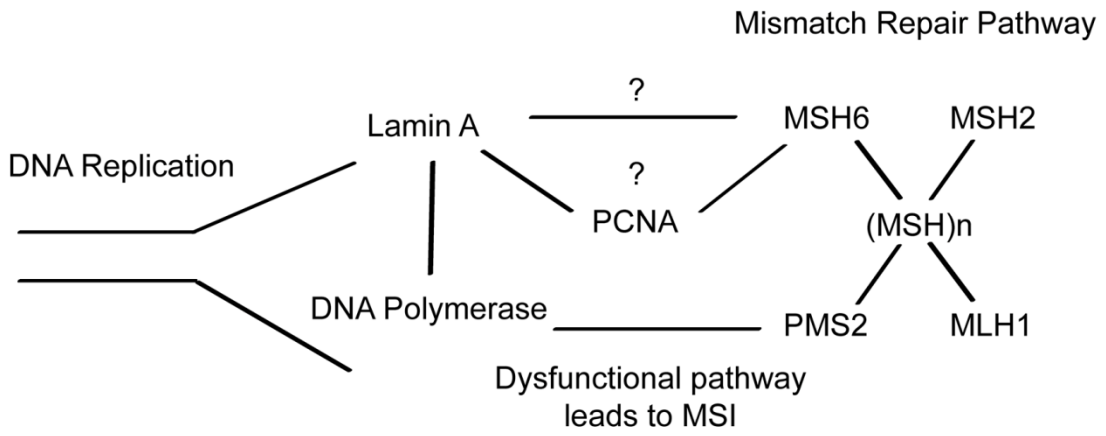

Figure 5.6 Speculative model for a potential cross talk between Lamin A and microsatellite instability pathway

Potential cross talk between components of DNA replication machinery, mismatch repair pathway and Lamin A/C, a deregulation of which may have a bearing on the generation of copy number variations in DLD1 cells

5.3 Discussion

We report here the spectrum of genomic instability effects that are elicited by the depletion of Lamin A/C and Lamin B2 singly and not in combination, in DLD1 cells. In this study, we have confined ourselves to the effects seen on chromosome and gene copy numbers as readouts of genomic instability in the cells. We acknowledge here that several other aspects of genomic instability may also be deregulated upon Lamin A/C and Lamin B2 depletion in DLD1 cells.

There were two major phenotypes noted from the characterization in this study. The first one from these is aneuploidy seen through changes in copies of chromosomes in ~25% of cells upon Lamin A/C or Lamin B2 depletion (Chapter 4 - Fig. 4.1-4.2). Among the candidate chromosomes that we assayed, the gain of chromosomes seen in siLamin A/C cells was confined to chromosomes 18 and 19, while that for siLamin B2 cells was seen for almost all chromosomes examined in this study, viz., 11,17,18,19. This is indicative of a difference in the extent of aneuploidy seen upon Lamin B2 depletion versus Lamin A/C depletion, as also a potential selectivity for the chromosomal gains seen in Lamin A/C depleted against Lamin B2 depleted cells. A selective gain of chromosomes is associated with several cancers. Lamin B2 Kd on the other hand shows an unbiased random gain of chromosomes and a general loss of control over ploidy. In a recent paper that characterised chromosomal instability upon Lamin B2 depletion, differential interactors were reported for Lamin B2 and Lamin A/C that function during mitosis. Qi et al demonstrated the presence of a complex formed by Lamin A/C with LAP2alpha and BAF at the mitotic spindle while Kuga et al showed that Lamin B2 associates with SUN1 specifically during mitosis and maintains the integrity of the spindle (Kuga et al., 2014; Qi et al., 2015). Both these cases suggest a cooperative mechanism that involves both lamins and other associated NE molecules in the regulation of the mitotic spindle.

Regulation of ploidy by either Lamin A/C or Lamin B2 may be cell type specific. Depletion of Lamin B2 in cell types other than colon cancer (Table 17-18) does not result in aneuploidy. We speculate here a mechanism that involves the relative expression levels and stoichiometry of both types of Lamins and their interactors in the maintenance of ploidy (Fig. 4.12). Cell type specificity may contribute to these stoichiometry differences and may be able to explain the cell type specific regulation of ploidy by Lamins. The expression of Lamin B2 is robust and higher in

DLD1 as compared to other cell types of colorectal cancer origin which show chromosomal instability (Kuga et al., 2014). This augmented expression level may be indicative of a stronger control of ploidy vested with Lamin B2. In our experiments, we have also identified Lamin B Receptor (LBR) as a distinguishing Lamin B2 associated factor between diploid and aneuploid cell types. The role of LBR if any in the generation of aneuploidy remains to be investigated.

In addition to a regulation through the protein levels, we also detected a downregulation of aneuploidy checkpoint proteins at the transcript levels upon Lamin B2 knockdown. An altered expression of AurkB, Bub1, BubR1, Mad1, Mad2 in mouse models as well as cell lines has been associated with an increase in aneuploidy (Baker et al., 2004; Dobles et al., 2000; Ricke and van Deursen, 2013; Ricke et al., 2011). Downregulation of transcript levels of these molecules may represent another epigenetic level of regulation between Lamin B2 and aneuploidy, which has not been characterized so far. Previously, a similar role has been documented for Lamin B1 and repair proteins involved in DNA replication (Rad51, BRCA), where Lamin B1 binds to the promoters of these genes and regulates their transcript levels (Butin-Israeli et al., 2015). Further assays are required to examine the promoter occupancy of Lamin B2 on these aneuploidy checkpoint genes to understand if a direct regulatory relationship exists between them.

Another striking feature of Lamin depleted cells that our study shows is the generation of CNVs. Our study reports a possible involvement of Lamins in regulating copy numbers in the genome. The effects shown by Lamin A/C depletion and Lamin B2 depletion on copy numbers of genes were strikingly different. Lamin A/C depletion led to greater single copy insertion of genes while Lamin B2 depletion resulted primarily in deletions. Mechanistically, generation of amplifications (CNVs) could be associated with defects in DNA replication due to the absence of Lamins. SiLamin A/C resulted in an amplification of the repeat rich *DNMT1* locus in DLD1 cells which have MSI and not in SW480 cells which do not have MSI. Moreover, the targets that were found to be amplified in siLamin A/C cells contain about 40-70% of total repeats and 1-2% of short repeats. Thus, the single copy insertion seen in siLamin A/C cells is likely to be associated with repeat rich regions. This is suggestive of the involvement of the MMR/MSI pathway in this phenotype. The mechanisms for the generation of CNVs primarily involve the non homologous end joining and recombination pathways which result in a joining of misaligned DNA fragments, or slippage of polymerases that accumulate mutations and extra nucleotides (Hastings et al.,

2009). The mismatch repair pathway proteins MSH2 and MSH6 are important candidates in sensing mismatched nucleotides and stalling polymerases for repair. DLD1 cells show frameshift mutations in both copies of MSH6 gene resulting in a compromise of its function and correspondingly showing a hypermutable phenotype and microsatellite instability (MSI) (Boland and Goel, 2010; Papadopoulos et al., 1995; Yabuta et al., 2004). We suggest here for the first time a potential regulation by Lamin A/C in this pathway. We propose here a model where, the absence of Lamin A/C may aggravate microsatellite instability and contribute to amplifications during DNA replication (Fig. 5.6). Lamin A/C has been localized at replication foci and interacts with Proliferating cell nuclear antigen (PCNA) (Cobb et al., 2016; Kennedy et al., 2000; Shumaker et al., 2008). PCNA also interacts with components of the mismatch repair pathway - MSH6 and MLH1 as shown in yeast cells (Umar et al., 1996). We surmise that Lamin A/C, PCNA and MSH proteins may form a regulatory complex during DNA replication. The absence of a functional MSH6 protein coupled with a depletion of Lamin A/C may result in an aggravation of the MSI phenotype and manifest as an increase in repeat generation (Fig. 5.6).

Examination of CNVs generated upon Lamin B2 depletion manifested itself as a wide range of chromosomal aberrations and CNVs in the form of deletions of small fragments of the genome. Owing to its involvement in maintaining chromosome segregation during mitosis, an absence of Lamin B2 may contribute to breakages and joining of chromosome fragments thereby resulting in breaks. Alternatively, these breaks could represent persistent DSBs which could not get repaired due to an impaired recruitment of repairing proteins such as 53BP1. Chromosome fragmentation was also noted in the Spectral Karyotyping experiments performed on Lamin B2 depleted cells, which corroborate the losses captured in the CNV experiments. Thus, the operational pathway for Lamin B2 in terms of regulation of genomic stability may be strikingly different from that of Lamin A/C. Lamin B2 depletion resulted in a loss of chromosome integrity as seen through fragmentation and translocations. This also results in greater frequency of nuclear blebbing and micronuclei generation in Lamin B2 depleted cells. Increase in micronuclei is also a classical sign of genomic instability associated particularly with cancers. The increase in generation of translocations is also indicative of a potential cancer associated genomic transition in these cells. The overall implications of the increase in genomic instability upon siLamin A/C and siLamin B2 on the transcriptome and organization of the genome remain to be investigated.

Chapter 6: Role of lamin and its interactors in the maintenance of chromosome positions

Data acknowledgement:

Fig. 6.1D-E: Roopali Pradhan

Fig. 6.7E: Sushmitha Hegde

Results from this chapter are a part of the manuscript:

Ranade, D., Pradhan R., Hegde S., and Sengupta, K. Lamin A/C and Emerin partner to maintain gene rich chromosome territories towards the interior of the interphase nucleus (under review)

6.1 Introduction

The genome is non randomly organized in the interphase nucleus, with gene rich chromosome territories localized predominantly toward the nuclear interior and gene poor toward the nuclear periphery (Cremer et al., 2001; Croft et al., 1999). Such an arrangement is conserved across evolution and across cells (Mayer et al., 2005; Tanabe et al., 2002), and harbors functional significance with regard to organization of transcription in the nucleus (Goetze et al., 2007).

A and B type lamins contribute to maintenance of nuclear structure by associating with numerous proteins and forming stable protein complexes (Gruenbaum and Medalia, 2015; Schirmer and Foisner, 2007). Distinct unique sets of proteins are bound by A and B type lamins at the nuclear periphery and at the nuclear interior (Dechat et al., 2010; Gesson et al., 2016; Schirmer and Foisner, 2007). B type lamins bind predominantly to heterochromatin binding proteins (LBR, HP1, LAP2beta) while A type lamins bind to both heterochromatin binding (at the nuclear periphery- PcG proteins) and euchromatin binding proteins (nuclear interior- LAP2alpha, BANF1) (Cesarini et al., 2015; Dechat et al., 2000; Foisner and Gerace, 1993; Furukawa and Kondo, 1998; Gesson et al., 2016; Worman et al., 1988; Ye and Worman, 1994; Ye et al., 1997). We envisage a role for lamins in the spatial partitioning of the nucleus through their protein-protein interaction networks.

Broadly, Lamin interactors can be classified as stable structural proteins at the nuclear membrane, and transient regulated interactors in the nucleoplasm. In this work, we have confined ourselves to the interactors of Lamins involved in maintenance of nuclear and chromosome structure. The structural stability imparted by Lamins to the nucleus, are executed partly by Lamin interactors. Interaction of Lamins at the lamina with 'Lamina associated domains' (LADs) of chromatin are also partly maintained by interactors of Lamins including Emerin, Lamin B receptor, Lamina associated polypeptide (LAP2B) which also bind to LADs (Amendola and van Steensel, 2015; Guelen et al., 2008). This overlap of binding may also serve as a safeguarding mechanism toward maintenance of chromatin domains in the interphase nucleus.

Some important protein-protein interaction complexes of A type lamins are as follows:

1. LEM-D protein complex – LEM is a domain shared by three transmembrane proteins of the inner nuclear membrane. These proteins are Lamina associated polypeptide 2 alpha

(LAP2A), emerin (EMD) and MAN1. They share the LEM domain and interact with Lamin A on one side, and the barrier to autointegration factor (BANF1) protein on the other. BANF1 is a protein that binds non specifically to chromatin and is a structural organizer for chromatin in the nucleus. Thus LEMD proteins serve as a bridge between Lamin A and chromatin (reviewed by Barton et al., 2015).

2. Nuclear actin-myosin complex – Nuclear cortical actin forms a structure beneath the lamina. Lamin A interacts with nuclear actin directly, as well as through its interaction partner Emerin. Emerin binds to nuclear myosin I and serves as a bridge between Lamin A and nuclear myosins. Emerin interacts with the growing tip of F-actin filaments as also serves as an additional communication between the nucleus and cytoplasm (Holaska and Wilson, 2007; Holaska et al., 2004).

3. LINC Complex – Lamin A forms a connection with the actin cytoskeleton through the Linker to Cytoskeleton (LINC) proteins that harbor the SUN-KASH domains. Lamin A interacts with SUN1 protein that contains the SUN domain. SUN1 interacts with Nesprin protein that harbours the KASH domain; and this in turn interacts with actin. The LINC complex serves as a sensor of mechanical stress to the nucleus (Meinke and Schirmer, 2015).

4. Retinoblastoma protein – Lamin A forms a cell cycle dependent regulatory complex with Retinoblastoma (Rb) protein. This complex is regulated via its binding to LAP2A and primarily localized in the nucleoplasm and serves to regulate cellular transitions to S phase (Ozaki et al., 1994).

5. Transcription factors – c fos, Jun, TAF. Lamin A binds to transcription factors such as c-Fos, Jun, SREBP1, TAFs. This binding often occurs at the nuclear periphery (sequestration) and also in the nucleoplasm when Lamin A acts as a scaffold to dock active transcription factors (Dreuillet et al., 2002; González et al., 2008; Ivorra et al., 2006; Lloyd et al., 2002; Malhas et al., 2009; Ozaki et al., 1994).

6. DNA polymerases and PCNA – Lamin A interacts with DNA polymerase I during early S phase. Lamin A colocalizes with early replication foci in the nuclear interior (Shumaker et al., 2008; Vaara et al., 2012).

7. Lamina associated polypeptide 2 (LAP2A) in the nuclear interior - Soluble fractions of LAP2A interact with Lamin A (Dechat et al., 2000).

Interactors of B type lamins also encompass protein complexes at the nuclear periphery and nuclear interior:

1. Lamin B Receptor (LBR) – Lamin B receptor is a transmembrane protein which binds to heterochromatin marks. Both A and B type Lamins interact with LBR. LBR in turn associates with heterochromatin binding protein1 HP1. The Lamin B – LBR – HP1 complex acts as a heterochromatin organizer (Ye and Worman, 1994; Ye et al., 1997).

2. Lamina associated polypeptide 2 beta (LAP2B) – A transmembrane protein that binds with both Lamin B1 and Lamin B2 at the nuclear membrane.

3. Nucleophosmin (NPM) – Nucleophosmin is a nucleolar protein that interacts with Lamin B1. Lamins are shown to maintain the structure and organization of intra nuclear organelles such as the nucleolus. A direct interaction between Lamin B1 and the structural protein NPM1 serves to impart structural stability to the nucleolus (Martin et al., 2009).

4. PCNA and DNA Polymerase – PCNA (Proliferating Cell nuclear antigen) is a replication associated protein that localizes at replication forks. PCNA interacts with the tail domain of B type lamins which maintain a scaffold like organization of replication factors (Shumaker et al., 2008).

5. Transcription factors and RNA Polymerase – Lamin B1 binds to and sequesters Oct-1 TF at the nuclear periphery (Martin et al., 2009).

6. Actin – Both A and B type lamins are shown to bind to actin in *in vitro* experiments as also in cells. However, whether this interaction with actin includes monomeric actin or polymerized cortical actin in the nucleus is not clear as yet (Simon et al., 2010).

Lamin interactors and protein complexes

Lamin dependent protein complexes are destabilized when Lamin A or Lamin B are depleted from cells or in cells with mutations in Lamins. Often, mutations in Lamin A that result in dystrophies and aging syndromes, affect interaction properties of Lamin A/C in a cell type specific manner and contribute to the phenotype of the disease. Efficient functioning of Lamins depends heavily on the integrity of these interactions. Lamin A mutation G608G results in production of progerin shows an altered interactome of mutant Lamin A as compared to wild type Lamin A. While wild type Lamin A associated primarily with proteins of the nuclear envelope and nucleoplasm, progerin interacts with channel and transmembrane transporter activity proteins. ~50 disease specific interactors have been mapped for the mutant Lamin A delta50 (progerin) which may contribute to disease biology (Kubben et al., 2010).

Lamin dependent protein complexes have not been investigated in detail in cancer cells. The role of these complexes, if any, in partitioning the nucleus has also not been investigated in detail. We speculate that the Lamin meshwork formed at the nuclear periphery and nucleoplasm serves to recruit protein complexes which partition the nucleus into micro environments for accommodating specific chromosome territories. We speculate that Lamin A/C and Lamin B1/B2 may recruit differential interactors and contribute differentially to chromosome organization. While B type lamins bind primarily to heterochromatin organizers, A type lamins form interaction complexes at the nuclear periphery (heterochromatin) as also nucleoplasm (euchromatin). In this study, we have investigated one such protein association of Lamin A with a LEMD protein – Emerin and their role in chromosome positioning. Emerin is a unique interactor of Lamin A given its dual localization in the nucleus and the cytoplasm (Manilal et al., 1996; Ostlund et al., 1999; Salpingidou et al., 2007). Emerin has mechanosensitive properties (Guilluy et al., 2014), and partners with Lamin A to regulate mechanical properties of the lamina, actin dynamics and mechanoresponsiveness of the cell (Bera et al., 2014; Ho et al., 2013). Emerin also associates with nuclear myosin I in the nucleus (Holaska and Wilson, 2007). Nuclear myosin I (NM1) is required for chromatin remodeling activities during transcription by RNA Polymerase I, II and III and functions in long range chromatin movements of gene loci(Chuang et al., 2006; Fomproix and Percipalle, 2004; Percipalle et al., 2006; Pestic-Dragovich et al., 2000). A regulatory complex involving Lamin A-Emerin-NM1 has been

implicated in chromatin organization along with the role of actin in regulating chromatin dynamics at the nuclear interior (Holaska and Wilson, 2007; Kulashreshtha et al., 2016; Mehta et al., 2008; Mehta et al., 2010; Ramdas and Shivashankar, 2015; Toh et al., 2015). Furthermore, NM1 is associated with actin and is involved in orchestrating gene loci movements (Chuang et al., 2006). In this section we detected a transcriptional feedback between Emerin and Lamin A/C. We have further characterized the role of Lamin A/C and Emerin in maintenance of chromosome positions, and found a novel role for Lamin A/C and Emerin in partnering to regulate the positions of gene rich chromosome territories.

6.2 Results

6.2.1 Lamin depletion induces transcriptional deregulation of nuclear architecture genes

Lamin A/C is localized primarily beneath the inner nuclear membrane in the form of higher order polymers that form the nuclear lamina. In addition, Lamin A/C also shows a less polymerized, faster recovering nucleoplasmic pool in the nuclear interior (Moir et al., 2000b). Peripheral and nucleoplasmic pools of Lamin A/C interact with distinct sets of proteins including LEM-D proteins, LINC complex at the nuclear periphery, and proteins such as LAP2alpha, Rb protein, BANF1 among others (Dechat et al., 2010; Gruenbaum and Medalia, 2015). Lamin A/C and Lamin B2 have chromatin binding ability either directly or indirectly through interactors such as BANF1 or HP1 which bind to DNA (Stierlé et al., 2003; Taniura et al., 1995). We reported previously that a depletion of single lamin (either Lamin A/C or Lamin B2) maintains conserved chromosome positions in diploid DLD1 cells, suggesting mechanisms other than lamins in the maintenance of chromosome positioning. We asked if Lamin depletion invokes responses from other Lamin interactors. Towards this end, we profiled the transcription level responses of direct and indirect Lamin interactors using a customized TaqMan based qRT-PCR array (Fig. 6.1A). Lamin depletion was performed using siRNA based approach in a diploid colorectal cancer cell line – DLD1 followed by expression profiling for molecules of nuclear structure (Fig. 6.1A-B). SiRNA mediated gene silencing of *LMNA/C* showed a >80% decrease in the transcript levels of *LMNA* but no significant change in transcript levels of *LMNB1* and *LMNB2* (Fig. 6.1A). This was accompanied by a significant upregulation in the transcript levels of (i) Lamin interactors: *EMD* and *CBX5* (~1.2-1.3 fold) and (ii) Nucleoporin genes: *TMEM48* (~1.2 fold). Genes which showed a significant downregulation were (i) Nucleolar genes: *FBL* (~0.8 fold) and (ii) Nucleoporin genes: *NUP153* and *NUP93* (~0.8 fold), *SEC13*(~0.6 fold) (iii) Lamin interactors: *LBR* (~0.6 fold) and *SUN1* (~0.7 fold), *LEMD3* (MAN1, LEM-D protein) (~0.7 fold) (Fig. 6.1A).

Lamin B2 depletion also invoked transcriptional responses from its associated molecules (Fig. 6.1B). We detected an upregulation of *BCLAF1*, *FOS*, *HOXA7* transcription factors and

Figure 6.1

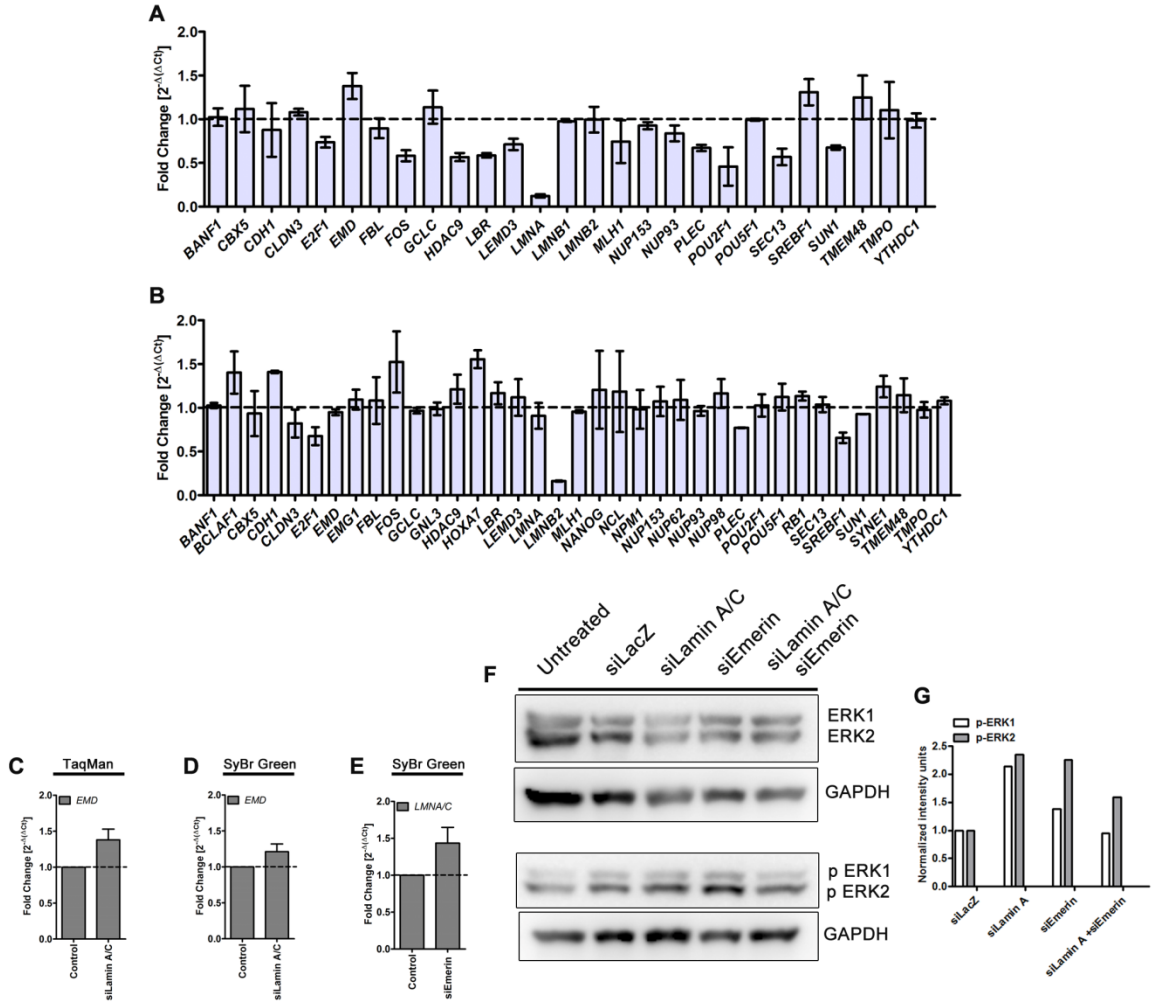

Figure 6.1 Gene expression changes upon Lamin A/C and Lamin B2 depletion in DLD1 cells

A-B. TaqMan qRT-PCR based gene expression profiling for genes coding for nuclear structure and associated proteins at the end of 48 hours post (A) Lamin A/C Kd and (B) Lamin B2 Kd. Data shown is a compilation of two independent biological replicates, normalized to expression levels of *GAPDH*. Error bars indicate SEM. C-D. qRT-PCR with (C) TaqMan probes and (D) SyBr PCR for Emerin expression upon depletion of Lamin A/C at the end of 48 hours post knockdown. E. qRT-PCR for expression of Lamin A/C upon depletion of Emerin in DLD1 cells. Data shown is a compilation from two independent biological replicates normalized to expression levels of *GAPDH*, Error bars = SEM. F. Western blot showing expression levels of ERK 1/2 and pERK 1/2 upon single and combined depletion of Lamin A/C and Emerin in DLD1 cells. Loading control: GAPDH. Data shown is representative out of two independent biological replicates. G. Intensity quantification for levels of pERK 1/2 (normalized to ERK 1/2 respectively) from F. Data shown is representative out of two independent biological replicates.

CDH1. Downregulated genes include *E2F1*, *SREBF1* and *SUN1* (Fig. 6.1B). Thus, in Lamin B2 depleted cells, we detected very few molecules associated with nuclear structure showing transcriptional deregulation. This was an important distinguishing factor for the transcriptional responses between Lamin A/C and Lamin B2. While the transcriptional deregulation profile upon Lamin A/C depletion primarily included molecules that directly contribute to maintenance of the framework (skeleton) of the nucleus, Lamin B2 depletion invoked transcriptional changes primarily from transcription factors. Since our primary interest in this experiment was to investigate if any additional mechanisms along with Lamins are involved in maintaining chromosome and nuclear organization, we focused on molecules that associate with lamins and potentially participate in maintenance of nuclear structure.

6.2.2 Lamin A/C and Emerin show transcriptional feedback

The TaqMan array based qRT-PCR showed an upregulation of Emerin upon Lamin A/C depletion (Fig. 6.1C). This was also corroborated by qRT-PCR performed using SyBr Green (Fig. 6.1D). Likewise, a depletion of Emerin also resulted in an upregulation of Lamin A/C (~1.3 times) at the transcript level (Fig. 6.1E). This is suggestive of a potential transcriptional feedback that operates between these two molecules. The protein levels of these genes in the knockdowns however did not reveal a significant increase in protein expression. It is plausible that a ~1.3-1.5 fold increase in transcript levels is not detectable at the protein level owing to the inherent detection limits of western blotting.

To further characterize the transcriptional deregulation and feedback between Lamin A/C and Emerin, we examined pathways of transcriptional deregulation previously documented for Lamin A/C and Emerin. Lamin A/C and Emerin independently activate ERK signaling, with both p-ERK1/2 showing an increase in Lamin A/C and Emerin knockdowns (Muchir et al., 2009) (Fig. 6.1F-G).

Figure 6.2

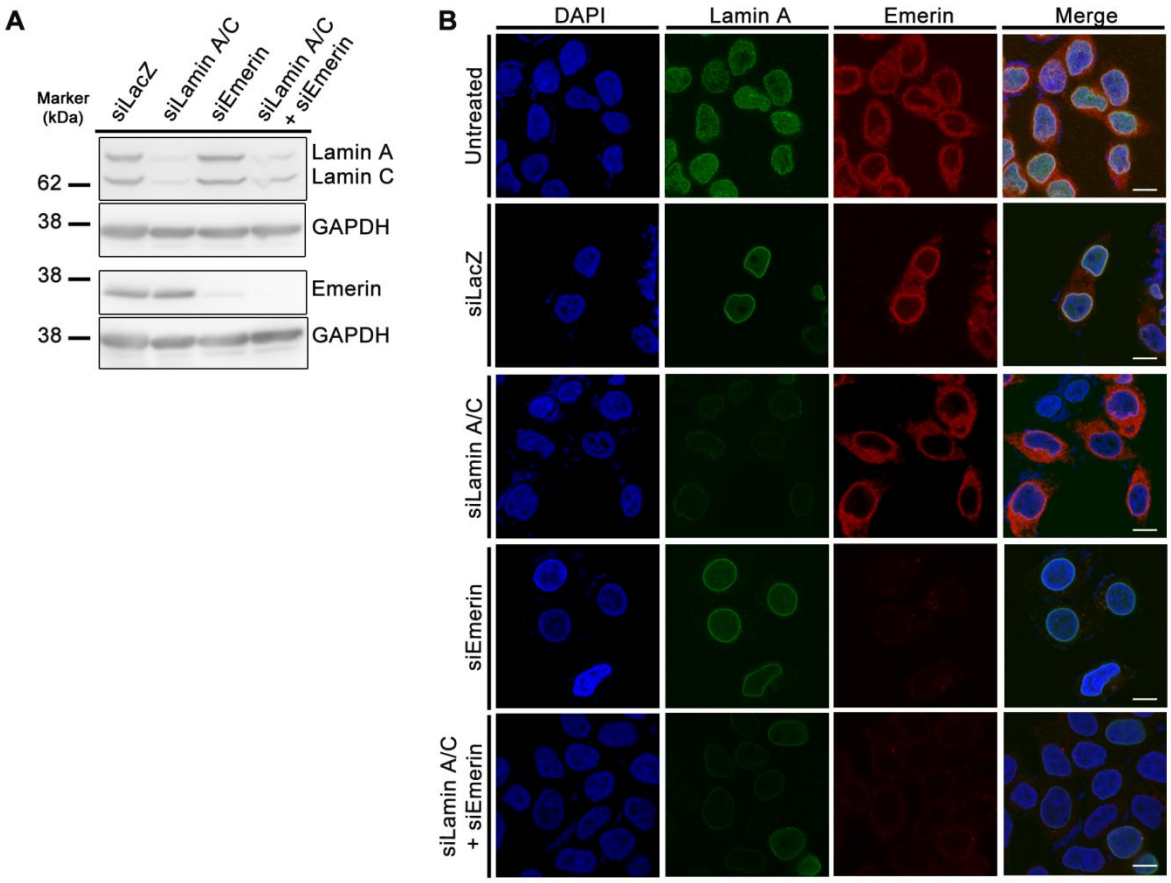

Figure 6. 2. Single and combined depletion of Lamin A/C and Emerin in DLD1 cells

A. Western blots depicting depletion of Lamin A/C, Emerin in single and combination knockdowns in DLD1 cells. Loading control: GAPDH. Data shown is representative out of five independent biological replicates B. Immunofluorescence assay depicting single cell level knockdowns of Lamin A and Emerin in single and combined knockdowns in DLD1 cells. Scale bar ~10µm. Data shown is representative data from two independent biological replicates.

We performed western blotting for p-ERK1/2 and ERK1/2 in Lamin A/C and Emerin depletions. An increase in p-ERK1/2 levels (primarily pERK2 levels) was detected in single and combined Lamin A/C and Emerin depleted cells (Fig. 6.1F-G). Examination of the ERK pathway and its effector transcription factors reveals Elk1, c-Fos, c-Myc, FRA1, SP1, AP-1 as important substrates for ERK (Zhang and Liu, 2002). Some of these TFs act as regulators on the promoters

of Lamin A/C (Muralikrishna and Parnaik, 2001; Okumura et al., 2004). Thus, we speculate that an activation of ERK signaling may impinge on the transcription status of Lamin A/C in Emerin Kd and vice versa.

6.2.3 Depletion of Lamin A/C and Emerin in combination; and not singly repositions gene rich chromosome 19 toward the nuclear periphery

Since we detected a transcriptional feedback between Lamin A/C and Emerin, we were curious to examine if Lamin A/C and Emerin cooperate to perform chromatin associated functions. Both Lamin A/C and Emerin bind to chromatin at 'Lamina associated domains' (LADs) (Amendola and van Steensel, 2015). Emerin is sufficient for maintenance of LADs in the absence of all the lamins A/C, B1 and B2 in mouse stem cells (Amendola and van Steensel, 2015). Single knockdown of Lamin A/C results in conserved chromosome positions for both gene rich and gene poor chromosomes, prompting us to investigate if Emerin functions as an accessory anchor with Lamin A/C to maintain chromosome positions. We performed single and combination knockdowns of Lamin A/C and Emerin in DLD1 cells; and examined the effects on chromosome positions (Fig. 6.2A-B, Table 20). Knockdown efficiency was ~80% as assessed using population level and single cell assays (Fig. 6.2A-B). We used chromosome 18 and 19 as readouts of chromosome positions since these represent highly divergent gene densities and occupy distinct microenvironments in the nucleus (Fig. 6.3A). Chromosome 19 being the most gene rich, occupies the interior of the nucleus and chromosome 18 being gene poor occupies the periphery of the nucleus. Control DLD1 cells (Untreated and siLacZ treated) showed a spatial separation between CT18 and CT19 as previously reported (CT18, M=72.9% and CT19, M=53.05% in untreated cells) (Fig. 6.3B-C). Single depletion of Lamin A/C or Emerin did not show significant difference in chromosome positioning as compared to control cells. However, in the double knockdown of Lamin A/C and Emerin, a significant repositioning was detected primarily for the gene rich chromosome 19 (M= 60.17% R.D) and not the gene poor chromosome 18 (M=75.98% R.D) (Fig. 6.3B-E). Chromosome 19, predominantly localized at the nuclear interior, showed a repositioning toward the nuclear periphery in siLamin A/C + siEmerin cells; and not in control or single lamin knockdown cells (Fig. 6.3B-E).

Figure 6.3

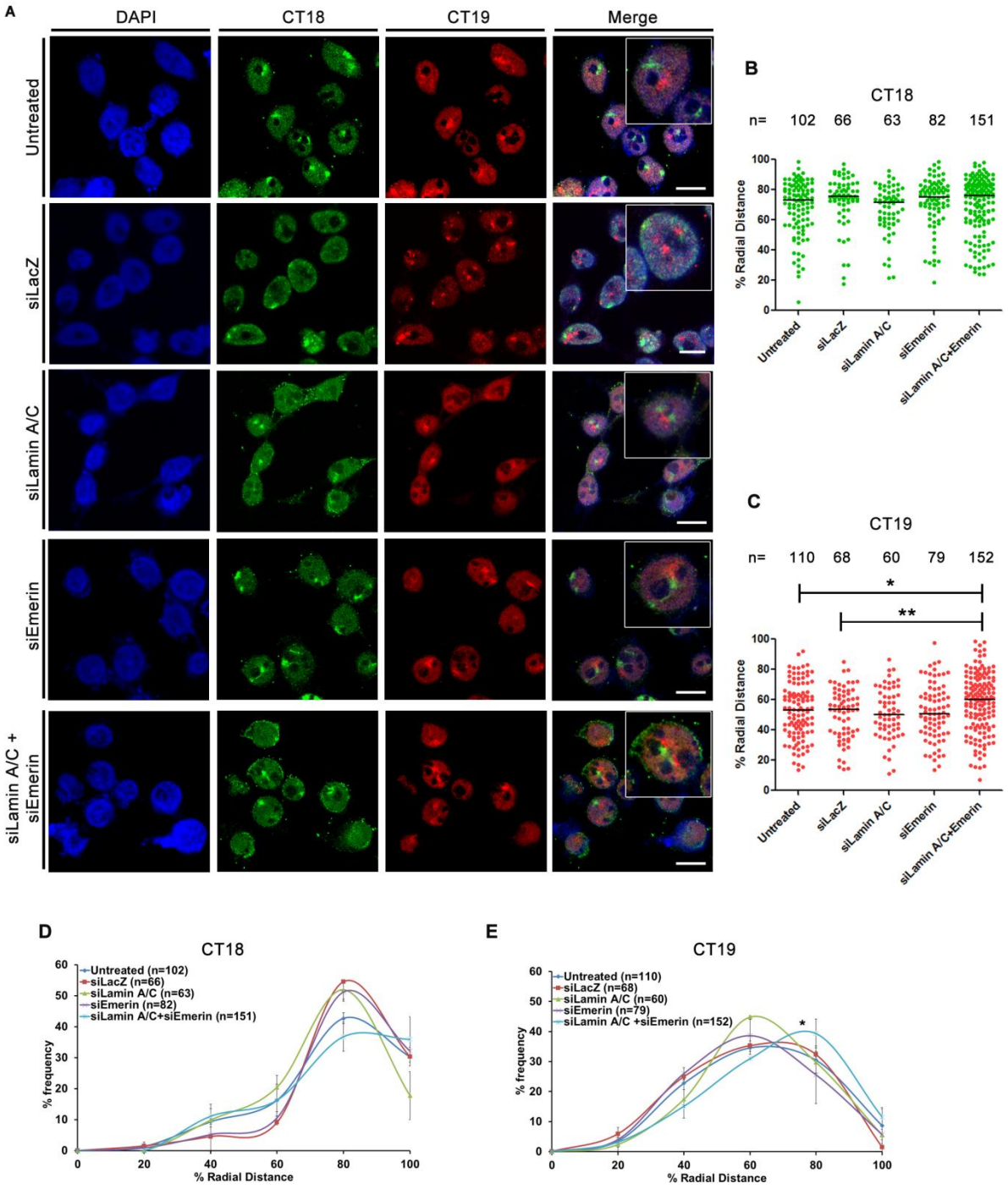

Figure 6.3 Co-depletion of Lamin A/C and Emerin mislocalizes gene rich chromosome 19 territories to the nuclear periphery

A. Representative image for 3D FISH for CT18 (green) and CT19 (red) performed in control (untreated and siLacZ treated) and single and combined depletion of Lamin A/C and Emerin in DLD1 cells. Scale bar ~10µm. Insets: Zoom of single nucleus. B-C. Dot scatter plots representing radial distance measurements (% R.D) for (B) CT18 and (C) CT19 in control (untreated and siLacZ treated) and single and combined depletion of Lamin A/C and Emerin in

DLD1 cells. Horizontal line: median. CT19 shows a repositioning toward the nuclear interior in the co-depletion (p=0.0169, Mann-Whitney test) and not single depletions of Lamin A/C and Emerin in DLD1 cells, n=number of CTs analyzed, Data shown is a compilation from two independent biological replicates. D-E. % Radial distance (% R.D) distribution profiles for (D) CT18 and (E) CT19 plotted as % frequency binned into 5 concentric sub-shells of 20% radial distance each (0%: nuclear centre, 100%: nuclear periphery). Data shown is a compilation from two independent biological replicates, Error bars = SEM.

We compared chromosome positioning for another pair of chromosomes that show divergent positions in the nucleus – CT7 (peripheral) and CT17 (internal) (M=72.15% R.D. and 59.81% R.D respectively) (Fig. 6.4A, Table 21). CT7, a gene poor chromosome predominantly localized toward the nuclear periphery, showed no change in chromosome positions in either the single or combined knockdown of Lamin A/C and Emerin (Fig. 6.4B). CT17, the next most gene rich chromosome second to CT19 is predominantly localized toward the nuclear interior in control cells. This showed a repositioning furthermore toward the nuclear interior upon Lamin A/C knockdown (M=53.96% R.D); which was further aggravated in the combined knockdown of Lamin A/C and Emerin (M=52.51% R.D.) (Fig. 6.4C). This suggested that the chromosomes in the nuclear interior are under regulation by Lamin A/C and Emerin; while chromosomes in the nuclear periphery do not depend exclusively on Lamin A/C and Emerin for their positions.

Figure 6.4

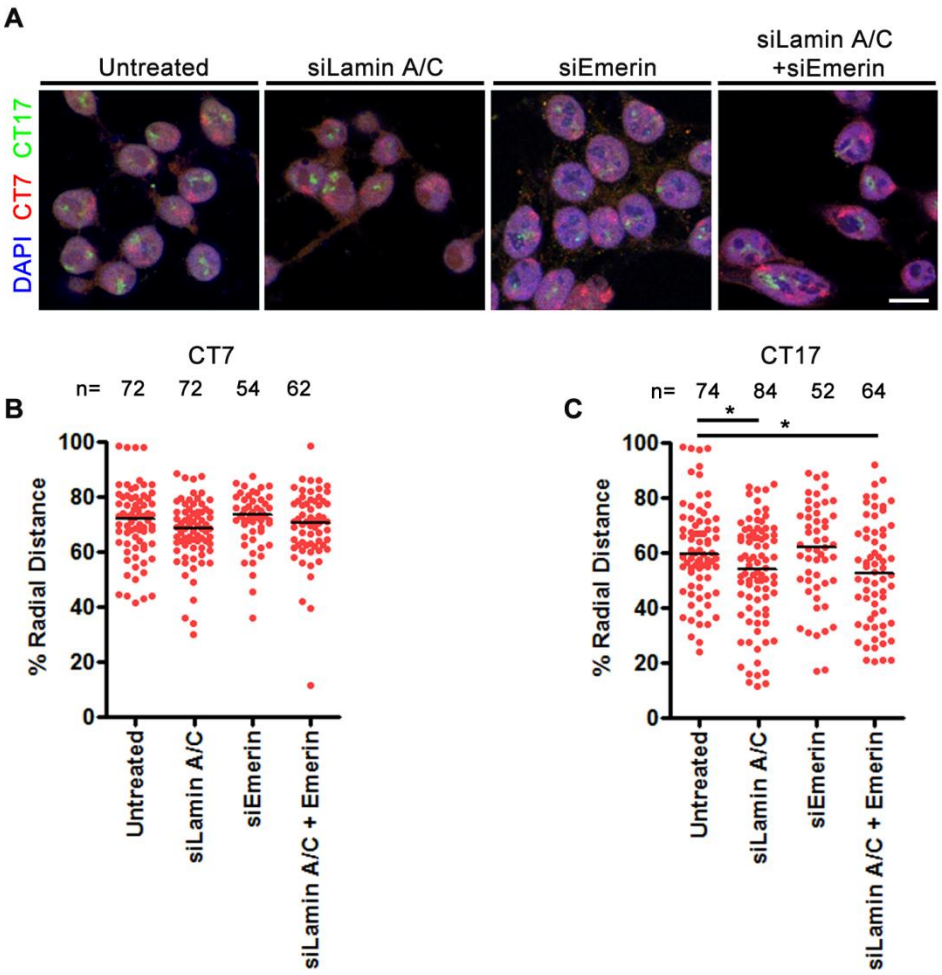

Figure 6.4 Depletion of Lamin A/C singly and co depletion of Lamin A/C and Emerin repositions CT17 to the nuclear interior

A. Representative 3D FISH images for CT7 (red) and CT17 (green) performed in control (untreated) and single and combined depletion of Lamin A/C with Emerin in DLD1. Scale bar ~ 10µm. B-C. Radial distance distribution profiles for (A) CT7 and (B) CT17 in control (untreated) and single and combined depletion of Lamin A/C with Emerin in DLD1. CT17 shows a repositioning toward the nuclear interior in siLamin A/C as well as siLamin A/C + siEmerin cells. Data shown is from a single biological replicate.

Table 20. Median % Radial Distance of CT 18 and CT19 upon co depletion of Lamin A/C and Emerin in DLD1 cells

Chromosome/ Gene Density	Treatment	% Radial Distance (R.D)
CT18 **(8.2 genes/Mbp)**	Untreated	72.9
	siLacZ	75.75
	siLamin A/C	71.34
	siEmerin	74.83
	siLamin A/C + siEmerin	75.98
CT19 **(37.0 genes/Mbp)**	Untreated	53.05
	siLacZ	53.56
	siLamin A/C	49.96
	siEmerin	50.72
	siLamin A/C + siEmerin	**60.17** (p=0.0169)

Table 21. Median % Radial Distance of CT 7 and CT17 upon co depletion of Lamin A/C and Emerin in DLD1 cells

Chromosome/ Gene Density	Treatment	% Radial Distance (R.D)
CT7 **(13.5 genes/Mbp)**	Untreated	72.15
	siLamin A/C	68.40
	siEmerin	73.35
	siLamin A/C + siEmerin	70.81
CT17 **(24.2 genes/Mbp)**	Untreated	59.81
	siLamin A/C	**53.96** (p=0.0202)
	siEmerin	62.00
	siLamin A/C + siEmerin	**52.51** (p=0.0137)

6.2.4 Depletion of Lamin A/C with Emerin does not reposition CT19 in HT1080 cells

We next asked if a depletion of Lamin A/C with Emerin elicits a similar response from another stable diploid cell line of different tissue origin (Fig. 6.5A). We performed single and combination knockdowns of Lamin A/C and Emerin in the fibrosarcoma cell line HT1080 which maintains its stable ploidy of 46 chromosomes (Fig. 6.5). HT1080 cells express lamins at a lower level as compared to DLD1 cells when compared on a western blot (Fig. 4.12).. In HT1080 cells, extensive cell death was noted upon knockdown of Lamin A/C as well as in the combination knockdown of Lamin A/C with Emerin. Due to an inherent lowered level of lamin expression in HT1080 cells, it is plausible that functional compensation between lamins functions at a lower level in HT1080 cells as compared to DLD1 cells, thereby resulting in greater cell death in HT1080 upon Lamin A/C Kd. We assessed the radial positions of chromosomes 18 and 19 in HT1080 cells (Fig. 6.5B). HT1080 cells show a gene density dependent chromosome positioning with CT18 being predominantly toward the nuclear periphery (M=69.07% R.D) and CT19 being predominantly toward the nuclear interior (M=59.23% R.D) (Fig. 6.5B-C). Thus, as compared to DLD1 cells, the extent of spatial separation between CT18 and CT19 was much reduced in HT1080 cells. HT1080 cells show a fibroblast-like growth morphology and a flat nucleus, which may contribute to the relative positioning of CT18 and CT19 in the interphase nucleus. CT18 did not show any significant repositioning from its preferential peripheral position in the nucleus in either single or combined depletion of Lamin A/C with Emerin (Fig. 6.5B). CT19 also maintained its position towards the nuclear interior in single Lamin A/C Kd as also Lamin A/C +Emerin depleted cells (Fig. 6.5C). Thus, Lamin A/C and Emerin regulate chromosome positions in a cell type specific manner. We speculate that the relative expression levels, stoichiometry of lamins and morphological parameters of the nucleus may influence the regulation of chromosome positions via Lamin A/C and Emerin.

Figure 6.5

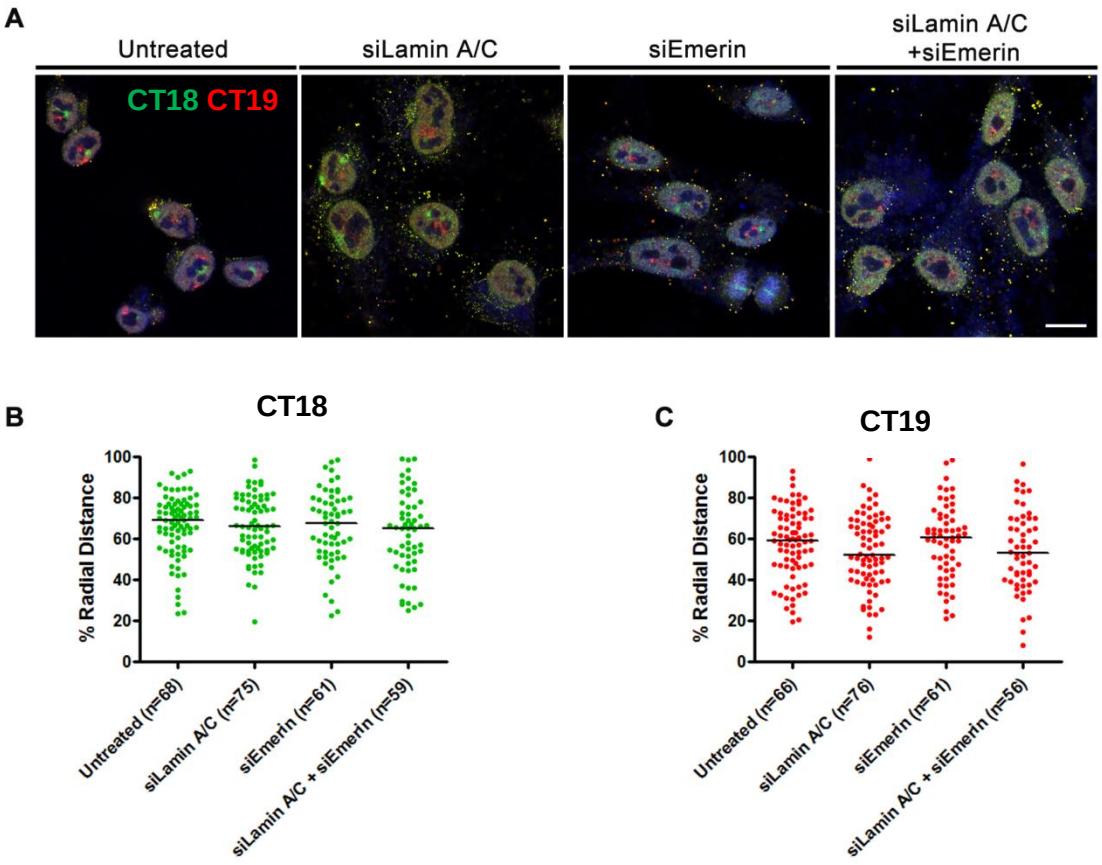

Figure 6.5 CT19 maintains conserved chromosome positioning upon co-depletion of Lamin A/C and Emerin in HT1080 cells

A. Representative 3D FISH images for CT19 (red) and CT18 (green) performed in control (untreated) and single and combined depletion of Lamin A/C with Emerin in HT1080 cells. Scale bar ~ 10µm. B-C. Radial distance distribution profiles for (A) CT18 and (B) CT19 in control (untreated) and single and combined depletion of Lamin A/C with Emerin in DLD1. CT18 and CT19 maintained conserved chromosome positioning. Data shown is from a single biological replicate.

6.2.5 Histone mobility in the nuclear interior increases upon co-depletion of Lamin A/C and Emerin

Lamin A/C binds to chromatin in the nuclear periphery as well as the nuclear interior (Lund et al., 2015). Emerin acts as a supporting partner to assist binding of Lamin A/C to chromatin. While chromatin at the nuclear periphery is bound by the stronger heterochromatin anchors in the form of B type lamins, chromatin in the nuclear interior is primarily under regulation by Lamin A/C and its associated protein complexes (Gesson et al., 2016). Since we detected a repositioning of gene rich chromosome 19 upon Lamin A/C+Emerin depletion in DLD1 cells, we examined whether there was a generalized change in chromatin state in the nuclear interior as compared to nuclear periphery. We used an indirect reporter of chromatin state in the form of mCherry tagged Histone H2A and its kinetics of recovery upon photobleaching as a readout of the same (Fig. 6.6, Table 22). We compared the recovery of mCherry-tagged H2A in the nucleus in the nuclear interior and nuclear periphery using FRAP (Fig. 6.6). Two different ROIs were used for photobleaching, one being in the nuclear interior and one at the nuclear periphery (Fig. 6.6A). We compared the recovery kinetics of H2A-mCherry in single knockdowns of Lamin A/C, Emerin and Lamin A/C+Emerin (Fig. 6.6A). H2A mCherry showed a recovery of ~18% in the internal and peripheral ROIs of the nucleus in control (siLacZ) cells (Fig. 6.6B). Comparison of the mobile fractions of H2A-mCherry in single and combined depletion of Lamin A/C and Emerin showed that the peripheral chromatin recovers at a similar kinetics in the single as well as combination knockdowns (Mobile fractions ~ 18-20%) (Fig. 6.6B). For the internal chromatin (internal ROIs), a reduced mobile fraction was detected for H2A-mCherry in the Lamin A/C depleted cells (~10%) while a greater mobile fraction of H2A-mCherry was detected specifically in Lamin A/C+ Emerin depletion (~38%) (Fig. 6.6B). This is suggestive of a greater mobility and potentially altered condensation of chromatin in the nuclear interior in the combined depletion state. The FRAP recovery curves for the internal and peripheral ROI also supports a greater loss of organization of chromatin in the nuclear interior as compared to nuclear periphery (Fig. 6.6C-D) This is concomitant with a repositioning of chromosomes primarily from the nuclear interior in the combination knockdown (Fig. 6.3). The difference in the impact of Lamin A/C singly and Lamin A/C + Emerin on chromatin in the nuclear interior arises from a multi layered connection that Lamin A/C has with chromatin. A loss of Lamin A/C with Emerin may

relieve spatial constraints on chromatin to a much greater extent as compared to Lamin A/C alone, since this destabilizes several layers of interactions with chromatin, including an

Figure 4.6

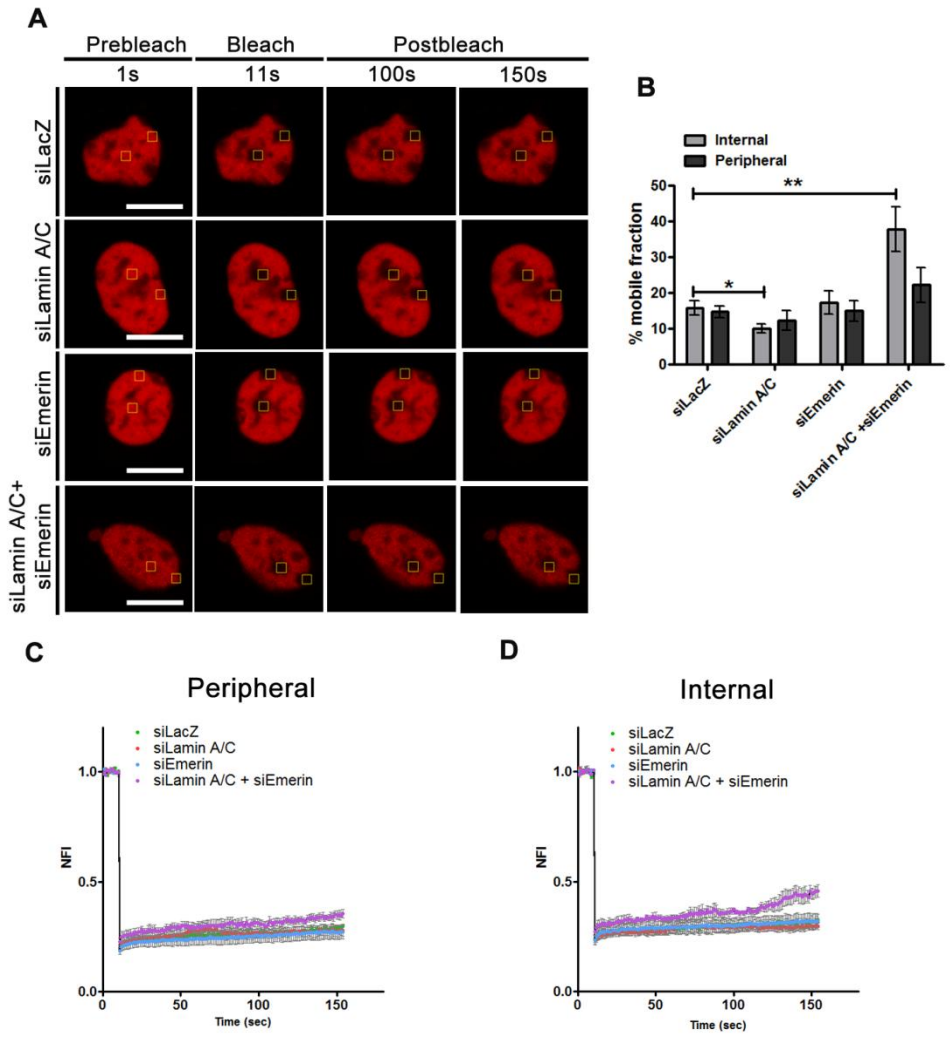

Figure 6.6 Co-depletion of Lamin A/C and Emerin enhances histone mobility at the nuclear interior

A.FRAP profiles for H2A-mCherry in Control (siLacZ), single and combined depletion of Lamin A/C and Emerin in DLD1 cells. Two ROIs were used for the FRAP experiment – one in the interior of the nucleus (Internal) and one proximal to the periphery of the nucleus (Peripheral). B.% mobile fractions for internal and peripheral ROIs for H2A-mCherry in Control (siLacZ), single and combined depletion of Lamin A/C and Emerin in DLD1 cells. Data shown is a compilation from two independent biological replicates, 3-6 nuclei from each replicate, Error bars = SEM. Scale bar ~10 µm. siLamin A/C shows a reduction in the mobile fractions (p=0.03621) while siLamin

A/C+siEmerin shows an increase in mobile fractions of H2A-mCherry (p=0.00677) of the internal ROI. C-D. FRAP recovery curves for (C) peripheral and (D) internal ROIs for H2A-mCherry in Control (siLacZ), single and combined depletion of Lamin A/C and Emerin in DLD1 cells. NFI = normalized fluorescence intensity. Data shown is representative out of two independent experiments, 3-6 nuclei from each replicate, Error bars = SEM.

---

important one with BANF1 – an important chromatin organizer molecule bound by Emerin (Berk et al., 2014; Lee et al., 2001). Our data thus suggests that Lamin A/C and Emerin serve to coregulate the kinetics and organization of chromatin in the nuclear interior; while that in the periphery is not receptive to changes in the levels of Lamin A/C and/or Emerin.

Table 22. % Mobile fractions of H2A-mCherry upon co depletion of Lamin A/C and Emerin in DLD1 cells

	Mean % Mobile Fraction (± SEM)	
	Internal	**Periphery**
siLacZ	15.79± 1.90	14.68±1.64
siLamin A/C	**10.05±1.2** (p=0.03621)	12.27±2.83
siEmerin	17.35±3.21	14.93±2.80
siLamin A/C + siEmerin	**37.72±6.20** (p=0.00677)	22.20±4.95

6.2.6 Lamin A/C regulates the organization of Nuclear Myosin (NM1) in an Emerin dependent manner

Emerin is stably associated with Lamin A at the inner nuclear membrane (Lee et al., 2001). Vaughan et al have previously shown that efficient Emerin localization at the nuclear membrane depends on the presence of the full length Lamin A protein (Vaughan et al., 2001). Since we detected a deregulation of chromosome positions and histone mobility primarily in the nuclear interior in Lamin A/C + Emerin Kd, we were curious to examine the localization and organization of other Emerin interactors in single and combined depletion of Lamin A/C and Emerin. We asked if interactors of Emerin also depend on the presence of Lamin A. Emerin interacts with the nuclear myosin isoform I (NM1) which in turn associates with actin (Holaska and Wilson, 2007; Mehta et al., 2008). We examined the interaction complex involving Lamin A, Emerin, NM1 and actin. We examined this complex in DLD1 cells depleted of Lamin A/C + Emerin using immunostaining and immunoprecipitation (Fig. 6.7). DLD1 cells (control and Lamin A/C + Emerin depleted) were immunostained with anti-MYO1C antibody to examine the organization of NM1 in the intra and extra nuclear compartments (Fig. 6.7A-B). Immuno staining for NM1 in control cells showed a predominant localization at the cell periphery; and intra nuclear speckles (Fig. 6.7B). Immunoprecipitation experiments reiterated the presence of a complex involving Emerin which binds to both NM1 and Lamin A (Fig. 6.7D-E). NM1 (MYO1C) fractions in the nucleus as well as cytoplasm interact with actin (Fig. 6.7F). Depletion of Lamin A results in a mislocalized aggregate of NM1 (MYO1C) in the cytoplasm in ~35% of cells (Fig. 6.7C). This is concomitant with an aggregation of Emerin in the cytoplasm in ~30% cells seen upon Lamin A/C depletion (Vaughan et al., 2001). Co labeling with Emerin in these cells reveals a juxtaposition of Emerin besides the mislocalized NM1 in the cytoplasm (Fig. 6.7B). The overall foci of NM1 in the nucleus also showed an increase in siLamin A/C cells (Fig. 6.7D). This is suggestive of a regulation of the localization of not just Emerin, but also other Emerin dependent interactors by Lamin A/C. Nuclear myosin I (NM1) is a molecular motor involved in the regulation of short as well as long range chromatin movements (Chuang et al.,2006). Our data suggests a dependence of NM1 on the presence of Lamin A (indirectly) and Emerin (directly). Depletion of both Lamin A/C and Emerin resulted in a reduction in this pool of aggregated NM1 in the cytoplasm as also in the pool of intranuclear NM1 foci, suggesting that the retention of this pool of NM1 depends on the presence of Emerin (Fig. 6.7B-C). Depletion of

both Lamin A/C and Emerin did not alter the localization of nuclear myosin in the nucleus or cytoplasm. This suggests a co regulated relationship between Lamin A/C, Emerin and NM1.

Figure 6.7

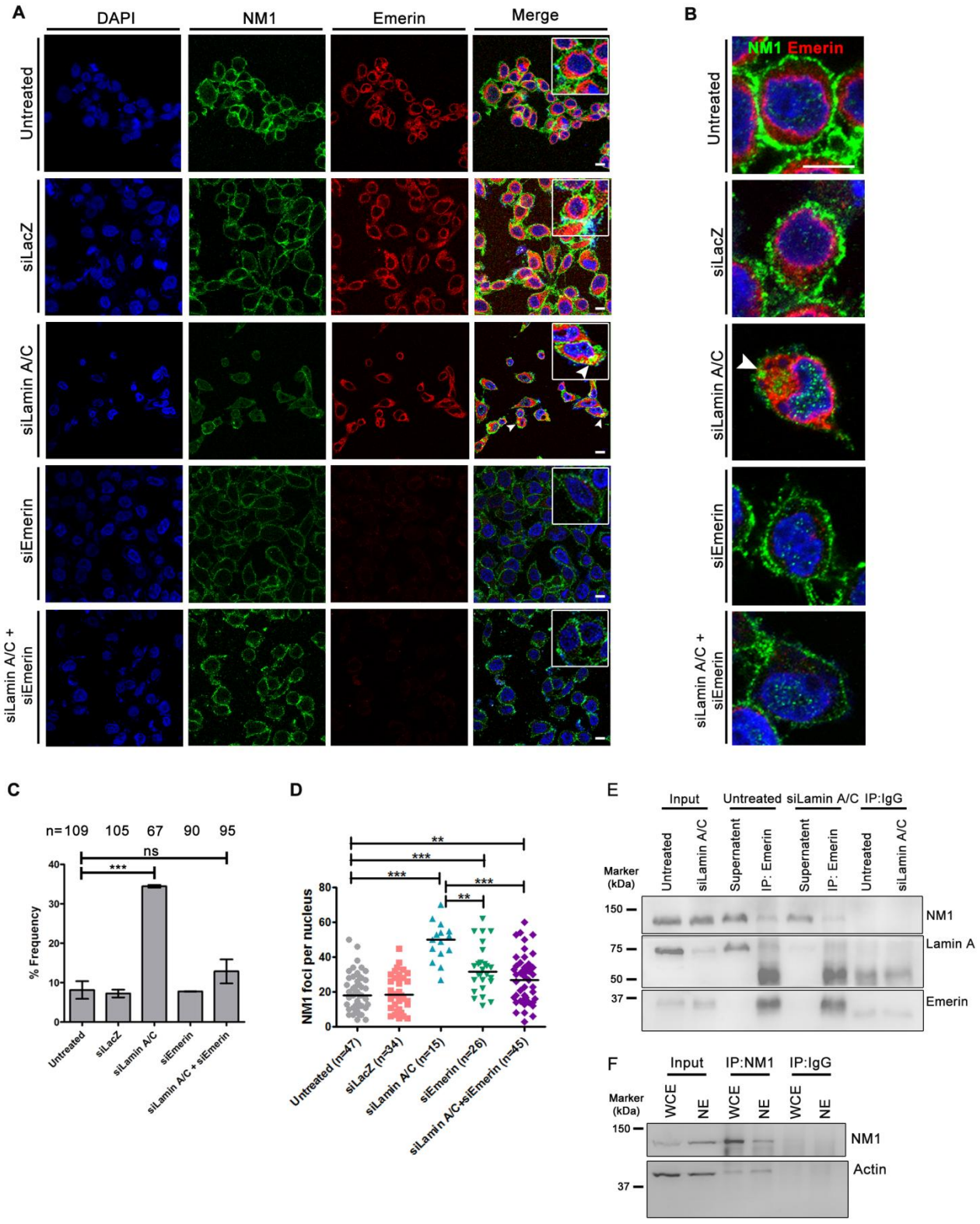
A
DAPI
NM1
Emerin
Merge
Untreated
siLacZ
siLamin A/C
siEmerin
siLamin A/C + siEmerin
B
NM1 Emerin
Untreated
siLacZ
siLamin A/C
siEmerin
siLamin A/C + siEmerin
C
n=109 105 67 90 95
ns
***
% Frequency
Untreated
siLacZ
siLamin A/C
siEmerin
siLamin A/C + siEmerin
D
**
***
***
***
**
NM1 foci per nucleus
Untreated (n=47)
siLacZ (n=34)
siLamin A/C (n=15)
siEmerin (n=26)
siLamin A/C+siEmerin (n=45)
E
Input
Untreated
siLamin A/C
IP:IgG
Untreated
siLamin A/C
Supernatant
IP: Emerin
Supernatant
IP: Emerin
Untreated
siLamin A/C
Marker (kDa)
150
75
50
37
NM1
Lamin A
Emerin
F
Input
IP:NM1
IP:IgG
WCE
NE
WCE
NE
WCE
NE
Marker (kDa)
150
37
NM1
Actin

Figure 6.7 Lamin A/C depletion mislocalizes nuclear myosin I (NMI) and Emerin

A.Immunofluorescence assay for NM1 (green) and Emerin (red) in control (untreated and siLacZ treated) and single and combined depletion of Lamin A/C and Emerin in DLD1 cells. Scale bar ~10 µm. Insets: Zoomed in images showing mislocalization of NM1 in the cytoplasm in Lamin A/C depleted cells. B. Single nuclei showing intranuclear staining for NM1 (green) and Emerin (red) in control (untreated and siLacZ treated) and single and combined depletion of Lamin A/C and Emerin in DLD1 cells. Scale bar ~10 µm. C. Quantification of the frequency of cells showing mislocalized aggregates of NM1 in the cytoplasm. siLamin A/C cells show a significant mislocalization of NM1 in the cytoplasm ($p<0.0001$). Data shown is a compilation from two independent biological replicates, Error bars = SEM. D. Quantification of intanuclear foci of NM1 (mid optical sections) in single and combined depletion of Lamin A/C and Emerin. E. Co-IP performed using anti-Emerin antibody and probed for interaction with NM1 and Lamin A in control and Lamin A/C depleted cells at the end of 48 hours post Lamin A/C Kd. Data shown is representative out of three independent biological replicates F. Co-IP performed on whole cell extracts and nuclear extracts of DLD1 cells using anti NM1 antibody shows a pulldown of actin in both whole cell (WCE) and nuclear extracts (NE).

To further examine if biochemically, Lamin A is involved in maintaining the interaction between Emerin and NM1, we performed a co immunoprecipitation experiment with anti-Emerin antibody in control and Lamin A/C depleted cells (Fig. 6.7E). Depletion of Lamin A/C results in a minor reduction of the extent of pulldown of NM1 with Emerin, again suggesting a co regulation between Lamin A/C, Emerin and NM1; with Lamin A/C being a central molecule regulating the localization and binding between Emerin and NM1 (Fig. 6.7E). We also ascertained that the intanuclear fraction of NM1 associates with actin (Fig. 6.7F). Because NM1 is highly involved in chromatin movements and remodeling of chromatin primarily at gene rich chromatin domains, a regulation by Lamin A/C could potentially explain a greater impact of Lamin A/C depletion on gene rich chromatin in terms of functional deregulation.

6.2.7 Co-depletion of Lamin A/C and Emerin shows increase in actin stress fibres

An important interactor molecule common to Lamin A/C and Emerin is actin (Holaska et al., 2004). Actin is involved in organization of a variety of structures in the cell, including the nucleus and chromatin. Depolymerization of actin is shown to impact the morphology of chromosomes (Ondrej et al., 2008). Emerin is a molecule required for capping and stabilizing the growing tips of F-actin structures, while Lamin A/C binds to and regulates the amount of G-actin in the nucleus (Holaska et al., 2004; Simon et al., 2010). Given this importance of Lamin A/C and Emerin in regulating the biology of nuclear as well as cytoplasmic actin, we examined the organization of actin filaments in the single and combination depletion. Visualization was performed for F actin using Phalloidin staining (Fig. 6.8A). Control (untreated) DLD1 cells showed classical cobble stone growth morphology with staining of phalloidin seen at the plasma membrane (Fig. 6.8A). Very few stress fibres of actin could be seen (in 7% cells), concomitant with reduced spreading of cells. Cells treated with non targeting siRNA also showed very few stress fibres (in ~23% cells) (Fig. 6.8A-B). Depletion of Lamin A/C from DLD1 cells resulted in no significant difference from the control cells in terms of stress fibres (Fig. 6.8B). Loss of Emerin from DLD1 cells however showed an increase in the number of cells showing bundling of actin (37%) and aggregation of stress fibres at the migrating edge of cells (Fig. 6.8B). A combined depletion of Lamin A/C and Emerin further aggravated this phenotype, showing a massive increase in the number of cells with stress fibres (55.8%) (Fig. 6.8B).

It is important to note here that phalloidin staining in DLD1 cells did not stain nuclear actin suggesting a low abundance of F-actin in the nucleus. Hence our methods of evaluation here have largely been confined to the F-actin fraction, primarily in the cytoplasm in DLD1 cells. We performed IFA for actin in the nucleus, using an anti-actin antibody that detects monomeric actin in the nuclear interior (Fig. 6.8C-D). However variability in epitope accessibility did not enable us to quantitatively measure the contribution of intranuclear actin in the Lamin A/C + Emerin depleted cells.

Figure 6.8

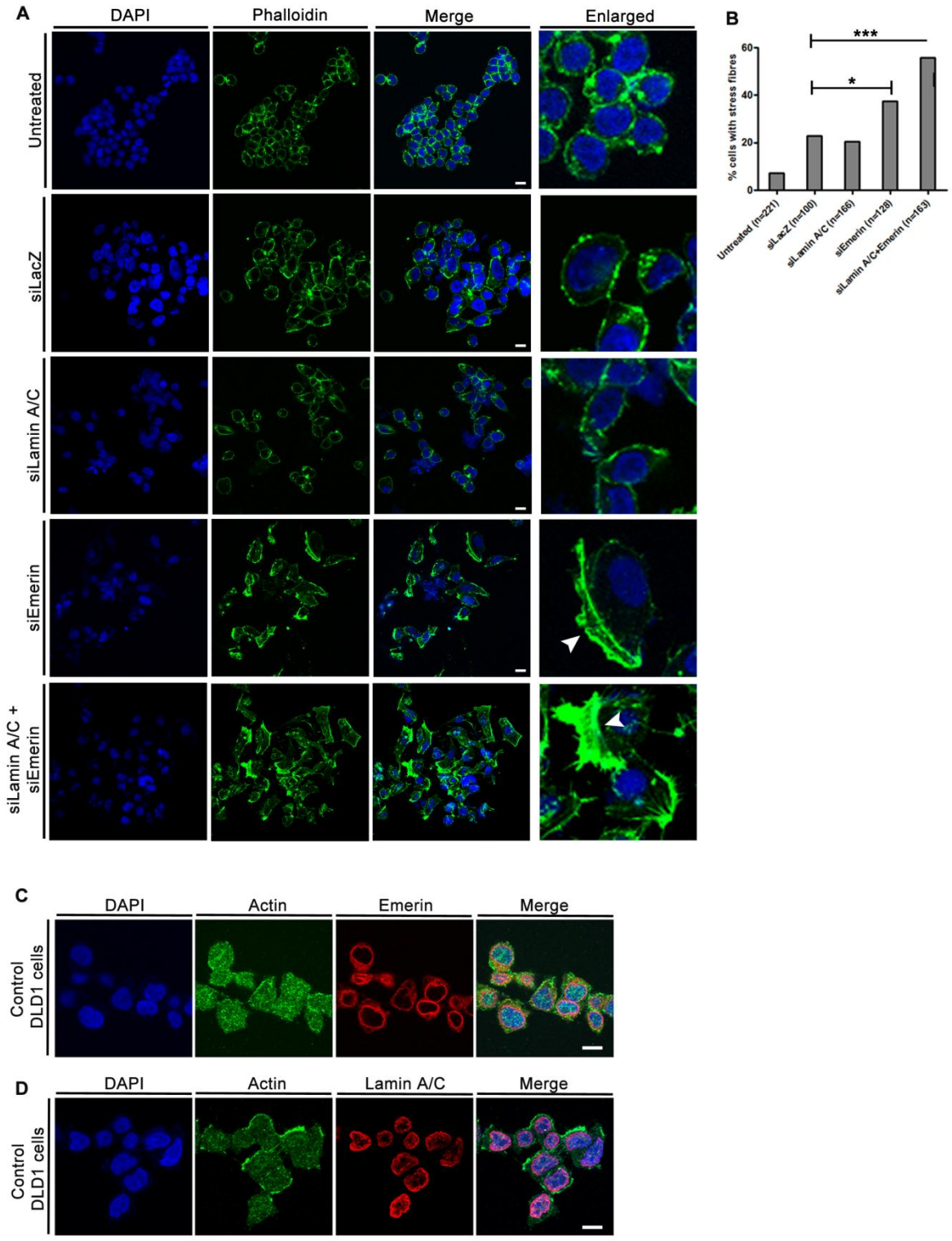

Figure 6.8. Actin stress fibers are enhanced in Lamin A/C and Emerin co-depleted cells

A. Phalloidin staining in control (untreated and siLacZ treated) and single and combined depletion of Lamin A/C and Emerin in DLD1 cells. Scale bar ~10 µm. Enlarged: Zoomed images depicting reorganization of F-actin in the Emerin depleted and Lamin A/C + Emerin depleted cells. B. Quantification of the frequency of cells showing stress

fibers in control (untreated and siLacZ treated) and single and combined depletion of Lamin A/C and Emerin in DLD1 cells. A significant increase was detected in siEmerin ($p=0.0214$) and siLamin A/C + siEmerin cells ($p<0.0001$). Data shown is representative out of two independent biological replicates. C. Immunostaining for actin (green) and Emerin (red) in DLD1 cells. D.Immunostaining for actin (green) and Lamin A/C (red) in DLD1 cells. C and D show intranuclear pool of actin. Scale bar ~ 10µm.

6.2.8 Chromatin mobility (H2A-mCherry) is restored to basal levels upon Latrunculin A treatment

We detected a reorganization of extra nuclear actin filaments upon Lamin A/C + Emerin depletion in DLD1 cells. We next asked if this reorganized actin contributes to the chromatin phenotypes that we previously detected (Fig. 6.9). The influence of actin organization on the topology of chromosomes has been documented previously (Ondrej et al., 2008).

We used Latrunculin A to depolymerize actin in Control (siLacZ treated) and Lamin A/C + Emerin depleted cells and examined histone mobility patterns in the nuclear interior and at the nuclear periphery (Fig. 6.9). Latrunculin A treatment was optimized for the concentration to be used which actively depolymerizes actin but does not grossly impact nuclear morphologies or cell detachment (Fig. 6.9A). A treatment time of 90min with 50nM concentration was found to be optimum (Fig. 6.9A), and we found that cells with Lat A treatment alone did not show histone mobility changes in DLD1 cells (Fig. 6.9B-C). We also examined the protein expression levels of Lamin A/C and Emerin upon depolymerization of actin, and detected an increase in the expression levels of Lamin A/C and a marginal decrease in the levels of Emerin in LatA treated cells (Fig. 6.9D-E). This reiterated a regulatory relationship between levels of Lamin A/C, Emerin and polymerization of actin in DLD1 cells.

Figure 6.9

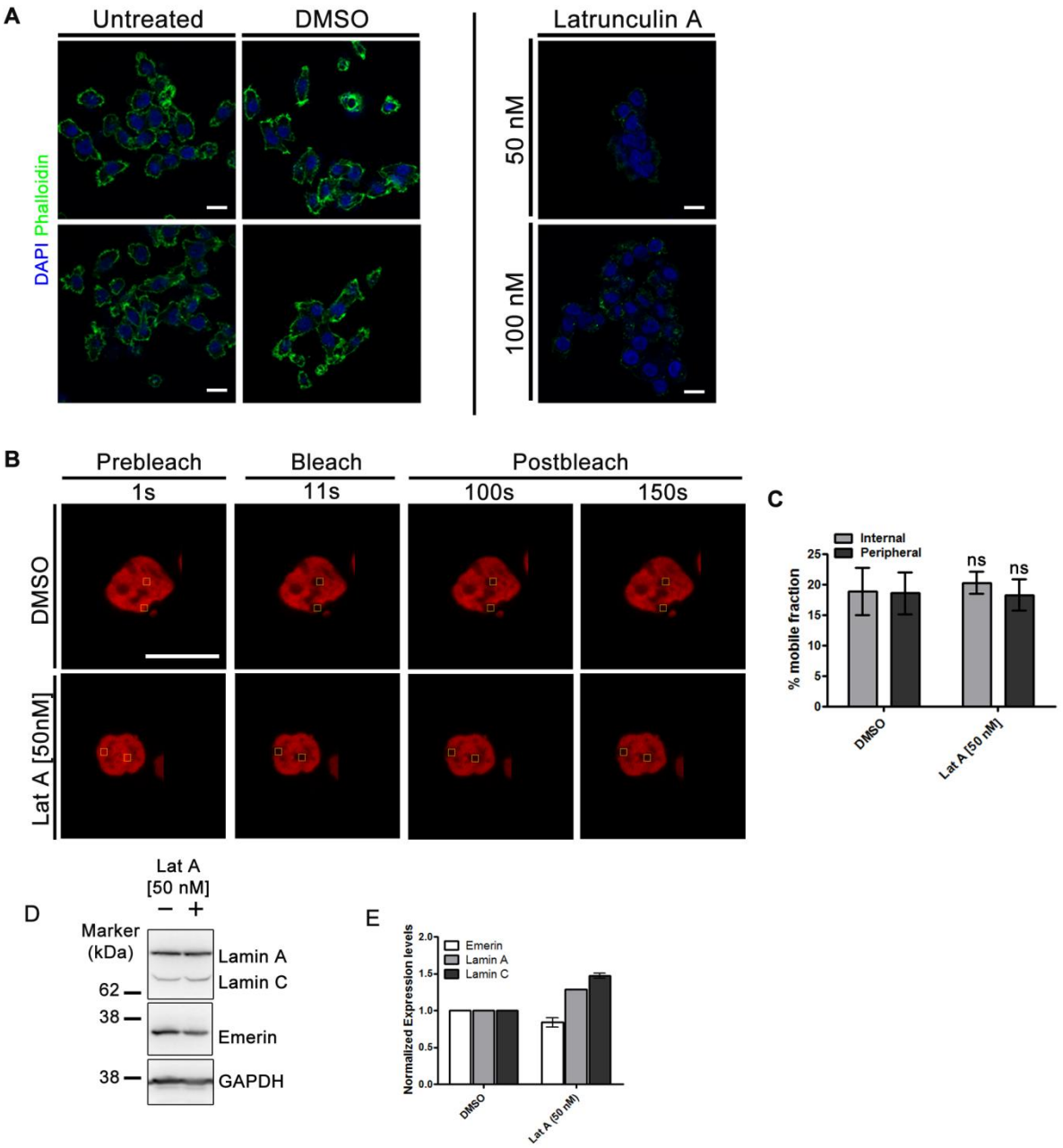

Figure 6.9 Latrunculin A treatment does not impact the mobility of histone H2A-mCherry in the nuclear interior or nuclear periphery

A. Phalloidin staining (green) performed on cells treated with 50nM and 100nM Latrunculin A for 90 min. DMSO treated and untreated cells were used as controls. Depolymerization of actin was ascertained using reduced phalloidin staining upon Lat A treatment. Scale bar ~ 10µm. B. FRAP performed on internal and peripheral H2A-mCherry in control (DMSO) and Lat A (50nM) treated DLD1 cells.~4-5 nuclei were assayed for recovery fractions. C. % mobile fraction for control (DMSO) and Lat A (50nM) treated DLD1 cells. No significant difference was

noted for the mobile fractions of H2A-mCherry in either the intranuclear or peripheral pools upon Lat A (50nM, 90min) treatment. Data shown is from a single biological replicate. D. Western Blot showing expression levels of Lamin A/C, Emerin in LatA treated cells. E. Quantification of intensity profiles from D. D-E. Data shown is a compilation of two independent biological replicates.

Next we compared the mobile fractions of H2A-mCherry in DLD1 cells (siLacZ treated and siLamin A/C +siEmerin cells) upon treatment with LatA (Fig. 6.10). DMSO treated Lamin A/C and Emerin co-depleted cells showed an increased mobile fraction for H2A-mCherry in the nuclear interior and not at the nuclear periphery when compared with control cells (Fig. 6.10A-B). On the other hand, LatA treated cells showed a recovery pattern comparable to the control cells in the nuclear interior and nuclear periphery both (Fig. 6.10B). This suggests that depolymerizing actin in Lamin A/C + Emerin depleted cells rescues the increase in chromatin mobility otherwise seen in the nuclear interior.

Figure 6.10

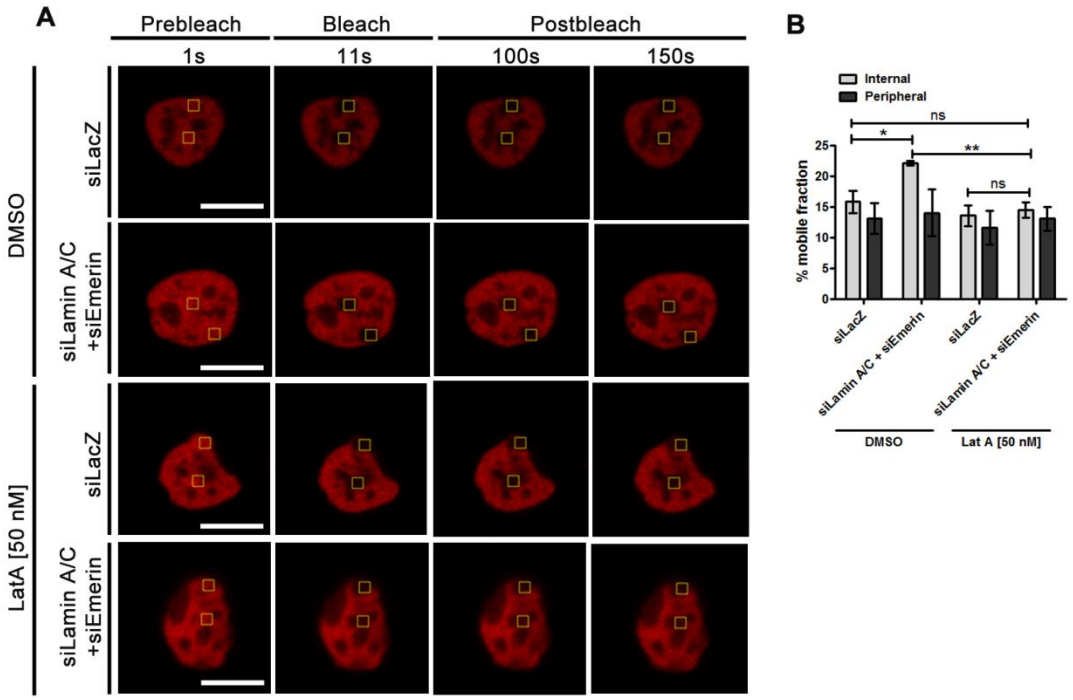

Figure 6.10 Latrunculin A treatment on siLamin A/C + siEmerin cells rescues the effects on chromatin mobility

A. Representative images of FRAP performed on H2A-mCherry in Control (siLacZ), siLamin A/C + siEmerin DLD1 cells with DMSO (control) or Latrunculin A (50nM) treatment. Two ROIs were used for the FRAP experiment – one in the interior of the nucleus (Internal) and one proximal to the periphery of the nucleus (Peripheral). Scale bar ~10 µm. B. % mobile fractions for Internal and peripheral ROIs for H2A-mCherry in Control (siLacZ), siLamin A/C + siEmerin DLD1 cells with DMSO or Latrunculin A (50nM) treatment. Error bars indicate SEM. Data shown is from a single biological replicate, ~3-6 nuclei per category per experiment.

Figure 6.11

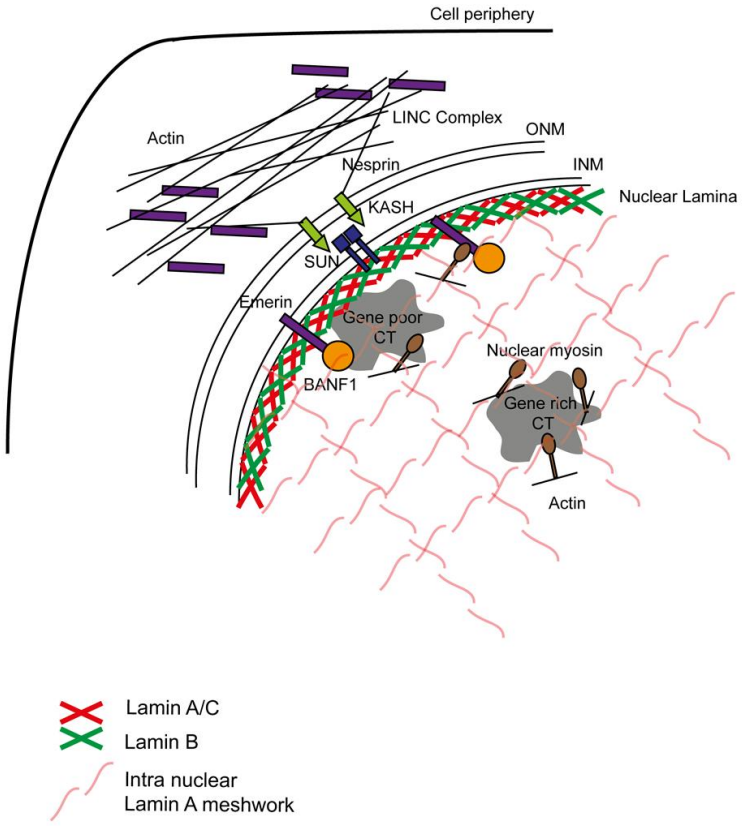

Figure 6.11 Speculative model for regulation of positions of gene rich chromosome territories by Lamin A/C and Emerin.

Lamin A/C maintains an intranuclear meshwork, associates with nuclear actin, forms a complex with Emerin and NM1, and regulates the localization of Emerin and NM1. Emerin associates with NM1 in the nucleus and regulates the organization of extra nuclear F-actin. A combinatorial regulation by Lamin A/C and Emerin functions to organize gene rich chromosome territories at the nuclear interior.

6.3 Discussion

In this study, we report a regulatory mechanism that serves to differentially modulate the organization of chromatin in different sub nuclear compartments. We have identified a role for the nuclear protein Lamin A/C and Emerin in co regulating the spatial positions of gene rich chromosome territories towards the nuclear interior.

A specific repositioning was detected for gene rich CT 19 in cells depleted of Lamin A/C and Emerin. Concomitantly, a greater mobile fraction was detected for tagged histone H2A-mCherry in Lamin A/C and Emerin codepletion specifically for chromatin in the nuclear interior and not at the nuclear periphery. These evidences are suggestive of a greater dependence of gene rich chromatin in the nuclear interior (as against gene poor chromatin in the nuclear periphery) on Lamin A/C and Emerin. Mechanistically, we speculate a differential contribution of Lamin A/C and Emerin on three aspects of nuclear structure and function (Fig. 6.11).

1. *Consequences of the potential loss of Lamin A/C and Emerin dependent interactions at the periphery and in the nuclear interior*
2. *Re-organization of perinuclear actin into F-actin stress fibers*
3. *Regulation of nuclear motor – Nuclear Myosin I*

Consequences of the potential loss of Lamin A/C and Emerin dependent interactions at the periphery and in the nuclear interior

Lamin A/C predominantly forms coiled coil polymers beneath the inner nuclear membrane (Gruenbaum and Medalia, 2015). In addition to the nuclear membrane, Lamin A/C also shows a nucleoplasmic localization throughout the nucleus (Moir et al., 2000b). This interphase nucleoplasmic pool contains phosphorylated fractions of Lamin A/C, the contribution of which to genome organization is unknown (Kochin et al., 2014; Torvaldson et al., 2015). Lamin A/C network in the nuclear interior has been shown to constrain the motion and diffusion of an artificially integrated LacO gene locus in the nuclear interior (Bronshtein et al., 2015). Moreover,

when stem cells differentiate, an increase in Lamin A/C expression also corroborates with a decrease in chromatin mobility in the nucleus (Melcer et al., 2012). The nucleoplasmic veil of Lamin A/C is proposed to regulate the binding and organization of chromatin in the nuclear interior, either directly or through its interacting partners such as BANF1, LEM-D proteins. In our case, single knockdown of Lamin A/C results in a decrease in chromatin mobility in the nuclear interior, thereby suggesting that additional anchoring mechanisms exist for chromatin, which may also regulate its mobility. We speculate that the nucleoskeletal veil of Lamin A/C filaments in the nuclear interior is maintained by Lamin A/C at the periphery in conjunction with its peripheral interactors such as Emerin and LAP2alpha (Dechat et al., 2010). We speculate that the intranuclear Lamin meshwork is maintained by the pools of Lamin A/C at the nuclear periphery in conjunction with its interactors such as Emerin (also at the periphery) and LAP2α-BAF (at the nuclear interior) (Lee et al., 2001). LEM-D protein interactors may partition Lamin A/C at the nuclear periphery and nuclear interior respectively. Chromatin from the nuclear periphery is bound by both A and B type Lamins, Emerin, Lamin B Receptor, Lamina associated polypeptide (LAP) whereas that in the nuclear interior is bound primarily by the nucleoplasmic fraction of Lamin A/C (Gesson et al., 2016; Guelen et al., 2008). The mobility of genes in the nuclear interior has reduced constraints on its dynamics as compared to those at the nuclear periphery which are associated with stronger anchors of both A and B type lamins (Chubb et al., 2002). We surmise that a potential stoichiometric destabilization of intranuclear chromatin interactors owing to a loss of Lamin A/C and Emerin renders internal chromatin more susceptible to organizational changes than peripheral chromatin. In addition, Lamin A-Emerin combined depletion may alter the epigenetic landscape of the nucleus; which may have a bearing on chromatin mobility. The impact of epigenetic regulation and chromatin remodeling in the regulation of H2A mobility needs further investigation specifically in the Lamin A/C-Emerin combined depletion. It is quite likely that the combination knockdown impacts the activity of chromatin remodeling enzyme machineries and histone modifying enzymes such as SWI/SNF complex, HAT CBP/p300 which may in turn impacts chromatin mobility (Jaskelio€ et al., 2000; Whitehouse et al., 1999, Annunziato and Hansen, 2000).

Re-organization of perinuclear actin into F-actin stress fibers

Lamin A/C binds to G-Actin in the nucleus (Simon et al., 2010). Emerin is an actin binding protein that caps the growing tips of F-actin filaments (Ho et al., 2013; Holaska et al., 2004). In addition, Emerin also interacts with non-muscle myosin IIA which is involved in bundling of F-actin into stress fibers (Le et al., 2016). We report here that a loss of Emerin reorganizes cytoplasmic actin into fibers that are perinuclear and also extend across the length of the cell. This is similar to a reorganization of actin under mechanical stress, which is regulated by Emerin (Le et al., 2016). However, this effect is in contrast to the increased polymerization of actin upon Emerin overexpression (Ho et al., 2013). We surmise that the increased F-actin bundling in DLD1 cells upon Emerin depletion may be a re-organizational change and not altered polymerization of actin. In the combined depletion of Lamin A/C and Emerin, the number of cells with actin stress fibers increases. This suggests that the organization of F-actin filaments in the cell is regulated by Lamin A/C and Emerin; with a dominant regulatory role for Emerin supported by Lamin A/C. Reorganization of perinuclear F-actin shows a reduced fraction of G-Actin inside the nucleus (Le et al., 2016). The importance of G-actin inside the nucleus is supported by the finding that RNA Polymerase II utilizes actin for transcription (Qi et al., 2011). We speculate that a reorganization of perinuclear F-actin mediated by the depletion of Emerin, and aggravated by Lamin A/C impinges on the levels and organization of G-actin inside the nucleus. This disruption of the actin network may perturb the activity and organization of euchromatin in the nucleus, since euchromatin is rapidly remodeled assisted by G actin during transcription (Qi et al., 2011). Alternatively, F-actin reorganization in the cell may impact mechanical properties such as stiffness, pliability of the nucleus that results in the loosening of an intact nucleoskeleton (Tojkander et al., 2012). The enhanced chromatin mobility in the nuclear interior upon Lamin A/C and Emerin depletion was rescued upon Latrunculin A treatment, suggesting a significant contribution of actin in the spatial organization of chromatin in the nuclear interior. Our results are thus in agreement with the reported impact of cytoskeletal reorganization on nuclear structure and histone mobility (Ramdas and Shivashankar, 2015; Toh et al., 2015). Interestingly, perturbation of actin organization impinges on chromosome territory topology (Ondrej et al., 2008; Spichal et al., 2016). Actin impacts the mobility and diffusion of chromatin through contributions from both its nuclear and cytoplasmic fractions (Spichal et al., 2016). Our study is confined to the evaluation of the cytoplasmic fraction of actin. We detect a

localization of actin at the nuclear periphery along with Emerin and Lamin A/C, and in the nuclear interior. Dissecting the contribution of nuclear actin by high resolution imaging and biochemical approaches will provide mechanistic insights into the regulatory aspects between actin and chromatin.

Regulation of nuclear motor – Nuclear Myosin I

The major chromatin remodeling events during transcription by RNA Polymerases as well as independent short and long range chromatin movements are executed in the nucleus by the nuclear isoform of a non-muscle myosin – NM1 (Hofmann et al., 2006). Previous studies have identified an interaction between NM1 and Emerin (Holaska and Wilson, 2007). However the functional relevance of such an interaction has not been investigated in detail. Interestingly, Lamin A/C depletion showed a mislocalization of Emerin and NM1 in ~25% of cells, further NM1 showed a mislocalized cytoplasmic aggregate in the cells. NM1 foci increased in the nucleus in Lamin A/C depleted cells. These observations suggest that Lamin A/C regulates the organization of Emerin and NM1 in the nucleus. A combined depletion of Lamin A/C and Emerin does not show cytoplasmic aggregation of NM1 suggesting that the organization of NM1 also depends on Emerin. Thus, Emerin may regulate the distribution of NM1 in the nucleus and cytoplasm. Moreover the association of gene rich chromosomes with NM1 in the nucleus is significantly higher as compared to other chromosomes (Almuzzaini et al., 2015; Kulashreshtha et al., 2016); suggesting a greater requirement for binding and activity of NM1 to gene rich chromosomes. It remains to be examined if the activity of NM1 is altered with a depletion of Emerin. We speculate that a combined depletion of Lamin A/C with Emerin may impinge on the organization and activity of NM1. Since NM1 is enriched on chromatin that undergoes remodeling, we speculate that a deregulation of NM1 function may manifest itself as a loss of organization primarily of gene rich chromatin.

The functional significance of the mislocalization of gene rich chromosome territories upon Lamin A/C and Emerin depletion is unclear and remains to be investigated. Mislocalization of gene rich chromosomes in the nucleus is likely to reorganize (i) Topologically associated domains (TADs) and (ii) Lamina associated domains (LADs) of chromatin which may be

revealed by Dam-ID and Hi-C based approaches that map the frequency of chromatin contacts at the sub-chromosomal level (Dixon et al., 2012; Guelen et al., 2008; Kind et al., 2013). Fine mapping of these reorganized domains may reveal if specific subdomains of gene rich chromosomes are under stronger regulation by Lamin A/C and Emerin.

We speculate that nuclear myosin and actin represent a level of regulation of chromatin organization imposed by Lamin A/C and Emerin in the nucleus. We speculate that a gradient of gene density (from nuclear interior to the nuclear periphery) overlaps with a gradient of Lamin A/C responsiveness, further fine-tuned by Lamin A/C dependent interactors. Additional levels of chromatin regulation imposed by B type lamins in association with its interactors such as Lamin B Receptor (LBR) are likely to organize subdomains of heterochromatin in the nucleus. A and B type lamins potentially partition the nucleus into specific sub domains through their interactors.

Chapter 7: Discussion - Insights into chromosome positioning and lamin functions

The work presented in this thesis discusses various new facets of lamin functions that we have uncovered for Lamin A/C and Lamin B2 in human cells. Notwithstanding the large body of literature documenting the cellular and molecular functions of lamins, our studies highlight rather unappreciated but divergent roles for Lamin A/C and B2 that regulate chromosome organization in conjunction with its effects on regulating ploidy and cytoskeletal dynamics.

7.1 Non-overlapping transcriptional deregulation by Lamin A/C and Lamin B2

Here we detected non overlapping transcriptional changes upon Lamin A/C and Lamin B2 depletion in DLD1cells. This suggests that a perturbation to different components of the nuclear lamina does not invoke a similar responding set of genes. We speculate that a differential binding of Lamin A/C and Lamin B2 in the genome may contribute to this difference in regulatory regions of the genome.

Both Lamin A/C and B2 depletion impacted ~1% of the transcriptome. However, chromosome positions were largely conserved in Lamin depleted diploid cells. Thus, it is unclear as to how many targets downstream of lamins are effectively required to impact chromosome positions. Studies prior to ours have identified chromosome positioning changes upon Lamin A/C depletion, however the extent of transcriptional deregulation required to elicit such a chage has been examined in very few studies (Mewborn et al., 2010; Malhas et al., 2007). Thus, whether lamin dependent organization of chromosomes impinges on transcriptional regulation and chromosome positioning through two different mechanisms or whether the two converge is not clear. Loss of function mutants of Lamins which inhibit either of these functions will further be required to dissect this mechanism.

7.2 Crosstalk between mechanisms that regulate aneuploidy and chromosome positioning in the interphase nucleus

The organization of chromosomes is dictated by the gene density of chromosomes with gene rich chromosomes preferentially localized towards the nuclear interior and gene poor toward the nuclear periphery (Croft et al., 1999). Additional factors that affect radial positioning of

chromosomes include chromosome size, gene density and replication timing of chromatin. Chromosome size is found to be an important factor for chromosome positioning in relatively flatter nuclei, with smaller chromosomes being clustered toward the nuclear interior, and larger ones occupying the nuclear peripheral volumes; which have greater space for accommodating larger chromosome territories (Bolzer et al., 2005). With regard to replication timing as well, early replicating foci localize in the nuclear interior (Jackson and Pombo, 1998; Zink et al., 1999). Thus, the positioning of a chromosome territory is influenced by a tug-of-war between these various physical factors. Moreover, the contents of the nucleus are not solely confined to chromatin and include numerous other entities such as the nuclear lamina, nucleolus, Cajal bodies among others; which function as nuclear landmarks. Further, nuclear matrix components impose constraints on the organization of chromosomes. Heride et al suggested the concept of positioning constraints for chromosomes and that chromosome gene density /size show a positive correlation with the radial positions of chromosome territories (Heride et al., 2010). Indeed, spatial positioning inside the nucleus is subject to numerous constraints. Our data unravels the role of chromosomal ploidy in imposing spatial constraints on positioning chromosomes in the interphase nucleus.

Chromosomal aneuploidy in cells with gains or losses of chromosomes are a defining feature of >90% of cancers of epithelial origin. Aneuploidy also poses a packaging problem inside the nucleus. A question that is not completely addressed so far in literature is how does the nucleus accommodate extra copies of chromosomes in the nucleus? Does the nucleus adapt to obtain greater flexibility to accommodate extra chromosomes? Do cancer cells represent a "floppy" nucleus capable of accommodating additional copies of chromosomes? Although some of these questions have been addressed in literature; the molecular basis for the same remains unanswered. Our data for the first time shows that Lamin B2 is involved in maintaining spatial positions of aneuploid chromosome territories. We detected a partial loss of gene density dependent chromosome positioning in naturally occurring aneuploid cancer cell lines which had lower Lamin B2 expression (SW480, A549); wherein CT18 and CT19 were proximal to one another as compared to that in diploid cells. However, the positioning of aneuploid CTs that were artificially introduced was conserved in a gene density dependent manner (Sengupta et al., 2007). Therefore we surmise that there are cellular mechanisms which regulate the spatial positions of even aneuploid chromosome territories in the interphase nucleus. The molecular

details of such a mechanism, if any are not clearly understood. Our studies reveal that the spatial organization of aneuploid chromosomes is altered in Lamin B2 depleted cells (Ranade et al., 2016). Thus, it is likely that in cells with artificially introduced chromosomes, Lamin B2 is robustly expressed which potentially maintains the spatial localization of chromosome territories. This was further substantiated by a modulating the levels of Lamin B2 in naturally occurring aneuploid cancer cell lines which also resulted in alteration of chromosome positions, thereby suggesting that chromosome positions were sensitive to the overall levels of Lamin B2 in cells. It is important to note that these functions of Lamin B2 are best represented in colorectal cancer cells. Indeed Lamin B2 distinguishes the CIN+ MSI- category of colon cancers from CIN-MSI+ stably diploid colon cancer cells (Kuga et al., 2014). It is quite likely that Lamin B2 functions to coregulate ploidy and chromosome positioning in a cell type specific manner.

We speculate that Lamin B2 interactors may serve to function as sensors of chromosome 'dosage' in cells. This tripartite interaction between Lamin B2, Lamin interactors and chromatin is established during early anaphase in mitosis which is sustained throughout interphase. We speculate that Lamin B2 associated complexes formed during mitosis not only assist in chromosome segregation but also in interphase chromosome positioning. At this stage, it is important to note that during mitosis, distinct and unique sub-complexes are formed by Lamins – the outer core of chromatin is bound by LBR – HP1 alpha – Lamin B; while the inner core is bound by LAP2- Emerin – BANF - Lamin A (Foisner,2003) . These complexes involve three main components – Lamin (either A or B type), a lamin interactor and chromatin. E.g. Lamin B1/B2 form a complex with LBR/HP1 which is in turn bound to heterochromatin (Ye and Worman, 1994). Lamin A bind to LAP2α/Emerin which are bound to BANF1 which in turn binds to euchromatin (Qi et al., 2015). Both A and B type lamin dependent complexes serve to regulate chromosomal ploidy; and this is supported by the depletion of either Lamin A/C or Lamin B2 resulting in aneuploidy in DLD1 cells. These complexes regulate chromosomal ploidy and may nucleate chromosome organization. This could explain in part the observation that cells which show stable ploidy across generations also show stable chromosome positioning in interphase. On the other hand, sensing dosage of chromosomes in interphase may be a function uniquely performed by Lamin B2 and its interactors. Our data for the first time suggests that mechanisms that regulate chromosomal ploidy and gene density dependent chromosome positioning may converge; via lamin dependent mechanisms. Cell type specificities may alter the

course and specificities of these interactions. We have examined one such component of Lamin B2 dependent interactions in mitosis and interphase – Lamin B Receptor (LBR). Whether these mechanisms distinguish gene rich and gene poor chromosomes or simply senses the dosage (copy number) of chromosomes through direct/indirect binding is not known. A more high-throughput study in colon cancer cells may enable identification of differential interactors of Lamin B2 in diploid and aneuploid cells both at mitosis and interphase, which may be involved in generation and maintenance of aneuploidy in colon cancer cells.

7.3 Lamin A/C dependent mechanisms involving the cytoskeleton impinge on chromosome organization

Here we show a role for Lamin A/C which is executed through its interacting partner Emerin and impinges on the organization of the cytoskeletal components. We have uncovered a potential mechanism involving Lamin A – Emerin – Actin that differentially impacts the spatial organization of gene rich (euchromatin rich) and gene poor (heterochromatin rich) chromosomes. We detected a reorganization of nuclear myosin and actin which reversibly impacted chromatin mobility in DLD1 cells. The role of the cytoskeleton (primarily actin) in maintaining chromatin architecture and function has been documented. Depolymerization of actin by Latrunculin A impacted chromosome morphology as well chromatin mobility in the nucleus (Ondrej et al., 2008). Here we show that a combined regulation of actin and nuclear myosin by Emerin and nuclear Lamin A/C impacts the behavior of chromatin, primarily in the nuclear interior. The presence of a complex involving Lamin A-Emerin-NM1-Actin has been previously discussed in literature (Mehta et al., 2008). Chromosome positioning is altered upon serum starvation, is dependent on the presence and activity of NM1 and actin (Mehta et al., 2007). The chromatin in the nuclear interior (gene rich) shows lesser constraints in motion as compared to that proximal to the nuclear periphery (gene poor)(Chubb et al., 2002). Such an arrangement may have evolved due to a greater requirement for transcriptional permissiveness in the nuclear interior. Therefore, it is conceivable that the impact of nuclear myosin and actin (nuclear and cytoplasmic) would be perceived by euchromatin to a greater extent than heterochromatin. Here we show that Lamin A/C and Emerin together regulate the organization of actin, which in turn impacts chromatin mobility in the nuclear interior. Concomitantly gene rich chromosome 19 was repositioned

towards the nuclear periphery specifically upon Lamin A/C + Emerin depletion but not in single depletions of Lamin A/C and or Emerin. Owing to the impact of Lamin A/C and Emerin on the acto-myosin machinery and its subsequent regulation on chromatin, we speculate that Lamin A/C and Emerin may impact chromosome positions in a similar manner. This mechanism distinguishes between gene rich and gene poor chromosomes and further re-iterates the difference in regulation between Lamin A/C and Lamin B2 in terms of impacting chromatin in different microenvironments inside the nucleus. A mechanism involving nuclear acto-myosin corroborates an activity dependent segregation employed to model the intra nuclear organization of chromosomes through several simulation models (Ganai et al., 2014). We show for the first time a mechanism of chromosome positioning that is potentially biased towards the gene rich chromosome territories. Our data provides evidence for an influence of cytoskeletal and nucleoskeletal factors in regulating the positions of chromosomes primarily in the nuclear interior. Emerin is a unique interactor of Lamin A given its dual localization in the nucleus and cytoplasm (Manilal et al., 1996; Ostlund et al., 1999; Salpingidou et al., 2007). Moreover, due to its role in perceiving mechanical signals and relaying them to the nucleus, Emerin may also serve the function of integrating the influence of extranuclear cytoskeleton on chromatin (Guilluy et al., 2014). We further aim to investigate the sub-domains of Lamin A and Emerin in regulating nuclear myosin and actin organization respectively. We speculate that nuclear myosin and actin represent one level of regulation of chromatin organization imposed by Lamin A/C and Emerin in the nucleus. We propose that a gradient of gene density (from nuclear interior to the nuclear periphery) may overlaps with a gradient of Lamin A/C responsiveness to chromosome positions (highest for chromosomes with greater gene density in the nuclear interior), further fine tuned by Lamin A/C dependent interactors. Additional levels of chromatin regulation imposed by B type lamins in association with its interactors such as Lamin B Receptor (LBR) are likely to organize subdomains of heterochromatin in the nucleus. A and B type lamins are potentially associated with independent and interdependent sets of interactomes required for the overall maintenance of the structural and functional organization of the genome.

7.4 The multifunctional lamin family – A versus B type lamins

Assembly-disassembly kinetics of lamins contribute to the multifunctionality of lamins. The highly polymerized lamins in the lamina form a structure that binds to different structural as well as regulatory proteins, primarily in interphase. On the other hand, the disassembled forms of lamins provide access to newer binding sites and function during mitosis and in the nucleoplasm in the nuclear interior.

A and B type lamins assemble into higher order filaments in a unique manner with the assembly kinetics and mesh sizes being different for each of the lamins (Shimi et al; 2015). There is interdependence between lamins for their efficient assembly into the nuclear lamina, with a more dominating role for Lamin B1 which influences the organization of Lamin A/C and Lamin B2 (Guo et al; 2014,Shimi et al; 2015). However, it has also been demonstrated in literature that a robust expression of lamins enables an independent assembly of the lamin filament for each lamin sub type (Guo et al; 2014). Since the expression of all four lamins is robust in DLD1 cells, the knockdown of one does not appreciably affect the protein expression and localization of the other lamins, thereby making it possible to selectively examine the function of a particular lamin protein. However, further characterization and super resolution imaging should be performed to study the impact of Lamin A/C or Lamin B2 depletion on the polymerization kinetics and mesh sizes and localization of other lamins.

In this study, we have uncovered functions that are common as well as largely unique to lamins A/C and B2.

Common: Both Lamin A/C and Lamin B2 regulate ploidy of DLD1 cells. In addition, Lamin A/C and Lamin B2 regulate the expression of a specific subset of genes.

Unique: Lamin B2 regulates chromosome positions of aneuploid chromosome territories, as well as overall chromosome stability.

Lamin A/C associates with Emerin to regulate actin-myosin organization and spatial positions of gene rich chromosomes, as also independently regulates copy number amplifications.

These unique functions may be executed through different domains of lamins A/C and B2. Potential interactors involved in these are as follows:

Table 23. Potential lamin interactors that regulate chromosome positioning and genomic stability

	Phenotype	Potential Interactors
Lamin A/C	Regulation of cellular ploidy	LAP2α-BAF (Qi et al., 2015)
	Generation of amplifications as CNV	DNA Polymerases, PCNA (Shumaker et al., 2008)
	Regulation of chromosome positions of gene rich CTs	Emerin, Actin, Chromatin (Lee et al., 2001; Simon et al., 2010)
Lamin B2	Regulation of cellular ploidy	SUN1 (Kuga et al., 2014), Lamin B Receptor (Ye and Worman, 1994)
	Regulation of positions of aneuploid chromosomes	Lamin B Receptor (Ye and Worman, 1994)

Greater characterization of interactions domains of Lamins A/C and B2 with regard to the above interactors will provide insights into the mechanistic basis of these functions for Lamin A/C or Lamin B2.

7.5 Involvement of Lamin A/C, Lamin B2 in cancer associated genomic instability

In this study, we have uncovered non overlapping roles for Lamin A/C and Lamin B2 in regulating various facets of nuclear organization and function. The changes elicited in DLD1 cells upon Lamin A/C or Lamin B2 knockdown closely resemble those seen in progression of cancers. The correlation between Lamin expression and cancer initiation and progression is weak. Data mining across databases (GENT- Gene Expression across Normal and Tumor tissue, CCLE- Cancer Cell Line Encyclopedia) (Fig.7.1-2) suggest that Lamin A/C expression is lower in cancer cells as compared to normal cells for most cell types notably colon, brain, breast, ovary.

In colon tissue particularly, a decrease in expression of Lamin A/C is seen for cancer cells as compared to normal cells, seen through cell lines as also patient sample data. This reduced Lamin A expression is often correlated with increased proliferation activity of colon cells, which enhances the tumor formation capacity of these cells. On the other hand, examination of Lamin B2 expression in colon cells shows an increase in expression in cancer cells as compared to normal cells (Kuga et al., 2014). This is also reiterated through examination of normal (CRL1541, CRL1790) colon fibrobast cells as compared to colon cancer (DLD1, SW480) cells which show a greater expression of Lamin B2 in the cancer cells. It is quite likely that this increase in expression of Lamin B2 results in an enhanced organization of Lamin B2 in the nuclear periphery and interior of these cells, and may contribute to the organizational aspects of the nuclei in cancer cells. Furthermore, a modulation of Lamin levels may be correlative to changes in cancer progression, which can be examined in cancer progression cell culture models.

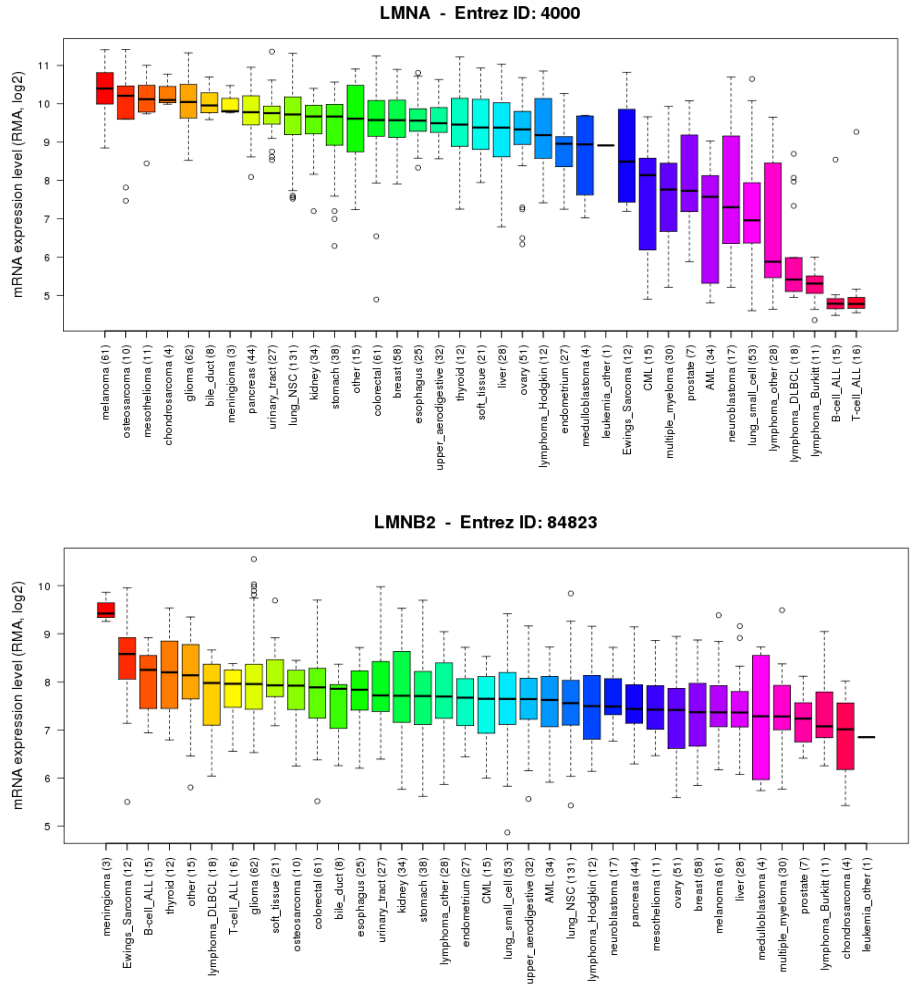

Fig. 7.1 CCLE outputs for expression of Lamin A and Lamin B2 across cancer types

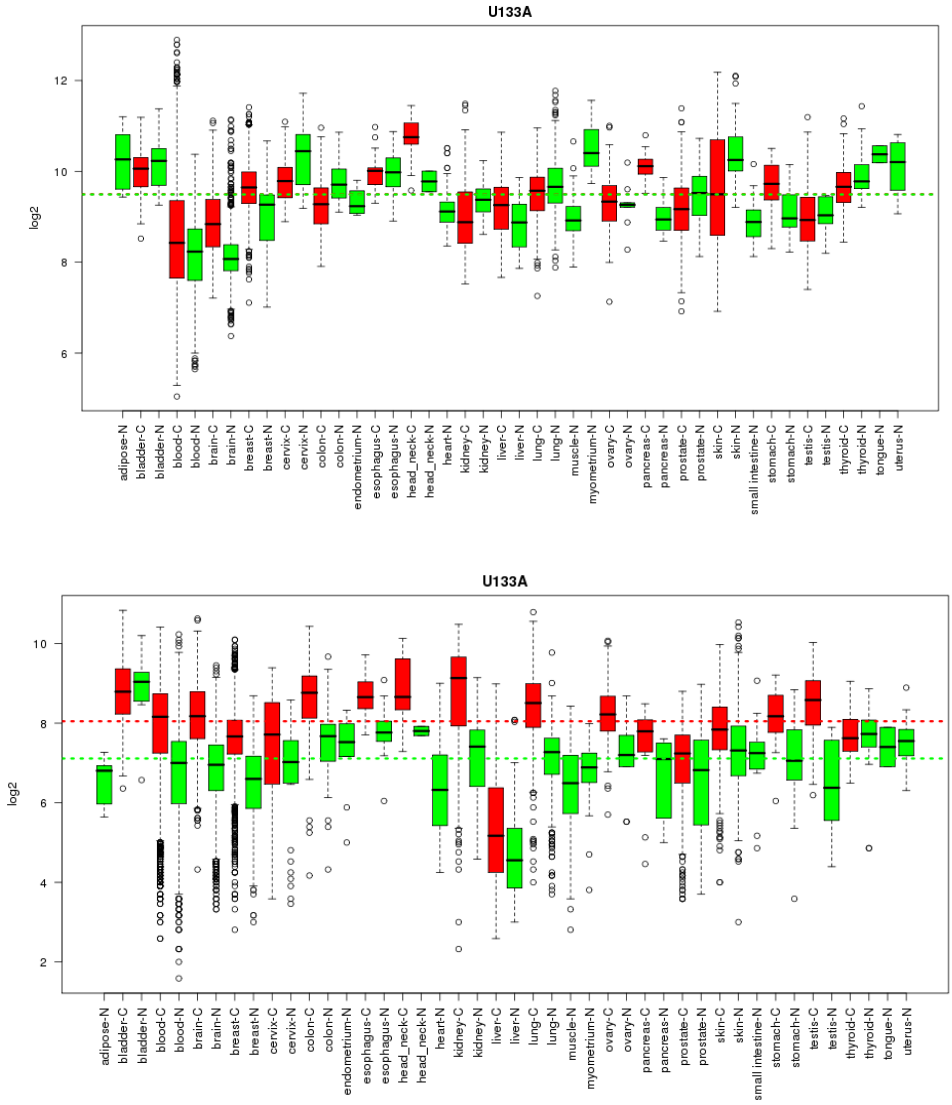

Fig. 7.2 GENT outputs for expression of Lamin A and Lamin B2 across normal and cancer cells

Genomic instability phenotypes upon Lamin A/C depletion include aneuploidy, amplifications and CNVs, while Lamin B2 depleted cells show chromosomal aberrations, aneuploidy and mislocalization of aneuploid chromosomes. Thus, Lamin A/C and B2 may serve to confer a protective action to the genome through non overlapping pathways. These changes are often associated with aggressive cancers. Loss of lamins may represent a mechanism for cells to attain an enhanced genomic instability, associated with cancer progression. It remains to be examined, as to how does this kind of nuclear structure change impinge on transcription (functional) state of cells. Cancer cells may achieve enhanced transcriptional deregulation profiles by enabling the

genome to sample diverse nuclear microenvironments. The presence of lamins may otherwise serve to guard the genome against not just copy number changes but also against spatial excursions of the genome to non conserved locations. It will be interesting to test altered chromatin contacts in the genome upon generation of CNVs and upon mislocalization of aneuploid chromosomes using chromatin proximity ligation methods such as Hi-C. The functional consequences of the same can be mapped using using RNA-sequencing. We envisage that these changes in the structure of the genome inside the nucleus are likely to have far reaching effects on the functional (transcriptional) organization of chromosomes and impact the biology of cells.

7.6 Limitations of the present study

Potential limitations of this study

1. Cell type specific effects of Lamins: Owing to the cell type specific effects exerted upon Lamin depletion, these studies have been largely confined to colorectal cancer cells and therefore the implications of the downstream effects of Lamin depletion cannot be generalized across other cell types. Furthermore, Lamin depletion in certain cell lines HCT116 (Lamin A/C depletion resulted in cell death), HeLa showed extensive cell death further reiterating the cell type specificity of lamin function.
2. Visualization of chromosome territories and gene loci have been performed on fixed cells, which provide a single snapshot of the effects of Lamin depletion on chromosome territories and gene loci. These studies are being complemented independently using live-imaging visualization of gene loci using CRISPR-dCAS9 based approaches.
3. The uncoupling of lamin effects on transcription and chromosome positioning has been difficult to uncouple in our present study. In other words, the extents of downstream targets of lamins that are effectively required to impact chromosome positions are unclear.
4. Analyses methods: Radial distance measurements offer a useful means to quantify relative distances of chromosome territories from the nuclear center where the nucleus is approximated to a sphere. These analyses do not factor in variations in nuclear shapes (i)

Flat ellipsoid (ii) Spherical (iii) flattened (fibroblasts) (iv) lobulate. This is a difficult problem to address and will involve additional mathematical operations to examine the specific contributions of nuclear topologies to the spatial organization of chromosome territories in the interphase nucleus.

Appendix

Appendix I

CLUSTAL W (1.83) multiple sequence alignment

```
sp|P02545-2|LMNA_HUMAN  METPSQ--RRATR----------SGAQASSTPLSPTRITRLQEKEDL
sp|P02545|LMNA_HUMAN    METPSQ--RRATR----------SGAQASSTPLSPTRITRLQEKEDL
sp|P20700|LMNB1_HUMAN   MATATPVPPRM----------GSRAGGPTTPLSPTRLSRLQEKEEL
sp|Q03252|LMNB2_HUMAN   MSPPSPGRRREQRRPRAAATMATPLPGRAGGPATPLSPTRLSRLQEKEEL
                        * ..:   *           . * ..:*******::******.*

sp|P02545-2|LMNA_HUMAN  QELNDRLAVYIDRVRSLETENAGLRLRITESEEVVSREVSGIKAAYEAEL
sp|P02545|LMNA_HUMAN    QELNDRLAVYIDRVRSLETENAGLRLRITESEEVVSREVSGIKAAYEAEL
sp|P20700|LMNB1_HUMAN   RELNDRLAVYIDKVRSLETENSALQLQVTEREEVRGRELTGLKALYETEL
sp|Q03252|LMNB2_HUMAN   RELNDRLAHYIDRVRALELENDRLLLKISEKEEVTTREVSGIKALYESEL
                        :******* ***:**:** **  * *:::* ***  **::*:** **:**

sp|P02545-2|LMNA_HUMAN  GDARKTLDSVAKERARLQLELSKVREEFKELKARNTKKEGDLIAAQARLK
sp|P02545|LMNA_HUMAN    GDARKTLDSVAKERARLQLELSKVREEFKELKARNTKKEGDLIAAQARLK
sp|P20700|LMNB1_HUMAN   ADARRALDDTARERAKLQIELGKCKAEHDQLLLNYAKKESDLNGAQIKLR
sp|Q03252|LMNB2_HUMAN   ADARRVLDETARERARLQIEIGKLRAELDEVNKSAKKREGELTVAQGRVK
                        .***:.**..*:***:**:*:.* : * .::    *:*.:*  ** :::

sp|P02545-2|LMNA_HUMAN  DLEALLNSKEAALSTALSEKRTLEGELHDLRGQVAKLEAALGEAKKQLQD
sp|P02545|LMNA_HUMAN    DLEALLNSKEAALSTALSEKRTLEGELHDLRGQVAKLEAALGEAKKQLQD
sp|P20700|LMNB1_HUMAN   EYEAALNSKDAALATALGDKKSLEGDLEDLKDQIAQLEASLAAAKKQLAD
sp|Q03252|LMNB2_HUMAN   DLESLFHRSEVELAAALSDKRGLESDVAELRAQLAKAEDGHAVAKKQLEK
                        : *: :: .:. *::**.:*: **.:: :*: *:*: * . . ***** .

sp|P02545-2|LMNA_HUMAN  EMLRRVDAENRLQTMKEELDFQKNIYSEELRETKRRHETRLVEIDNGKQR
sp|P02545|LMNA_HUMAN    EMLRRVDAENRLQTMKEELDFQKNIYSEELRETKRRHETRLVEIDNGKQR
```

```
sp|P20700|LMNB1_HUMAN   ETLLKVDLENRCQSLTEDLEFRKSMYEEEINETRRKHETRLVEVDSGRQI
sp|Q03252|LMNB2_HUMAN   ETLMRVDLENRCQSLQEELDFRKSVFEEEVRETRRRHERRLVEVDSSRQQ
                        * * :** *** *:: *:*:*:*.::.**:.**:*:** ****:*..:*

sp|P02545-2|LMNA_HUMAN  EFESRLADALQELRAQHEDQVEQYKKELEKTYSAKLDNARQSAERNSNLV
sp|P02545|LMNA_HUMAN    EFESRLADALQELRAQHEDQVEQYKKELEKTYSAKLDNARQSAERNSNLV
sp|P20700|LMNB1_HUMAN   EYEYKLAQALHEMREQHDAQVRLYKEELEQTYHAKLENARLSSEMNTSTV
sp|Q03252|LMNB2_HUMAN   EYDFKMAQALEELRSQHDEQVRLYKLELEQTYQAKLDSAKLSSDQNDKAA
                        *:: ::*:**.*:* **: **. ** ***:** ***:.*: *:: * . .

sp|P02545-2|LMNA_HUMAN  GAAHEELQQSRIRIDSLSAQLSQLQKQLAAKEAKLRDLEDSLARERDTSR
sp|P02545|LMNA_HUMAN    GAAHEELQQSRIRIDSLSAQLSQLQKQLAAKEAKLRDLEDSLARERDTSR
sp|P20700|LMNB1_HUMAN   NSAREELMESRMRIESLSSQLSNLQKESRACLERIQELEDLLAKEKDNSR
sp|Q03252|LMNB2_HUMAN   SAAREELKEARMRLESLSYQLSGLQKQASAAEDRIRELEEAMAGERDKFR
                        .:*:*** ::*:*::*** *** ***:  *   ::::**: :* *:*. *

sp|P02545-2|LMNA_HUMAN  RLLAEKEREMAEMRARMQQQLDEYQELLDIKLALDMEIHAYRKLLEGEEE
sp|P02545|LMNA_HUMAN    RLLAEKEREMAEMRARMQQQLDEYQELLDIKLALDMEIHAYRKLLEGEEE
sp|P20700|LMNB1_HUMAN   RMLTDKEREMAEIRDQMQQQLNDYEQLLDVKLALDMEISAYRKLLEGEEE
sp|Q03252|LMNB2_HUMAN
KMLDAKEQEMTEMRDVMQQQLAEYQELLDVKLALDMEINAYRKLLEGEEE
                        ::*  **:**:*:*  ***** :*::***:******** **********

sp|P02545-2|LMNA_HUMAN  RLRLSPSPTSQRSRGRASSHSSQT--QG-GGSVTKKRKLESTESR-----
sp|P02545|LMNA_HUMAN    RLRLSPSPTSQRSRGRASSHSSQT--QG-GGSVTKKRKLESTESR-----
sp|P20700|LMNB1_HUMAN   RLKLSPSPSSRVTVSRASSSRSVR--TT-R---GKRKRVDVEESEA----
sp|Q03252|LMNB2_HUMAN   RLKLSPSPSSRVTVSRATSSSSGSLSATGRLGRSKRKRLEVEEPLGSGPS
                        **:*****:*: : .**:*  *         *::::  *.

sp|P02545-2|LMNA_HUMAN  ---------S--SFSQHARTSGRVAVEEVDEEGKFVRLRNKSNEDQSMGN
sp|P02545|LMNA_HUMAN    ---------S--SFSQHARTSGRVAVEEVDEEGKFVRLRNKSNEDQSMGN
```

```
sp|P20700|LMNB1_HUMAN   --------SSSVSISHSASATGNVCIEEIDVDGKFIRLKNTSEQDQPMGG
sp|Q03252|LMNB2_HUMAN   VLGTGTGGSGGFHLAQQASASGSVSIEEIDLEGKFVQLKNNSDKDQSLGN
                        .  ::: * ::* *.:**:* :***::*:*.*::**.:*.

sp|P02545-2|LMNA_HUMAN  WQIKRQNGDDPLLTYRFPPKFTLKAGQVVTIWAAGAGATHSPPTDLVWKA
sp|P02545|LMNA_HUMAN    WQIKRQNGDDPLLTYRFPPKFTLKAGQVVTIWAAGAGATHSPPTDLVWKA
sp|P20700|LMNB1_HUMAN   WEMIRKIGDT-SVSYKYTSRYVLKAGQTVTIWAANAGVTASPPTDLIWKN
sp|Q03252|LMNB2_HUMAN   WRIKRQVLEGEEIAYKFTPKYILRAGQMVTVWAAGAGVAHSPPSTLVWKG
                *.: *:  :  ::*::...:: *:*** **:***.**.: ***: *:**

sp|P02545-2|LMNA_HUMAN  QNTWGCGNSLRTALINSTGEEVAMRKLVRSVTVVEDDE-DEDG------D
sp|P02545|LMNA_HUMAN    QNTWGCGNSLRTALINSTGEEVAMRKLVRSVTVVEDDE-DEDG------D
sp|P20700|LMNB1_HUMAN   QNSWGTGEDVKVILKNSQGEEVAQRSTVFKTTIPEEEE-EEEEAAGVVVE
sp|Q03252|LMNB2_HUMAN   QSSWGTGESFRTVLVNADGEEVAMRTVKKSSVMRENENGEEEEEEAEFGE
                *.:** *:..:. * *: ***** *.   . .: *::: :*:      :

sp|P02545-2|LMNA_HUMAN  DLLHHHHVS----------------------------------------
sp|P02545|LMNA_HUMAN    DLLHHHHGSHCSSSGDPAEYNLRSRTVLCGTCGQPADKASASGSGAQVGG
sp|P20700|LMNB1_HUMAN   EELFHQQG----------------------------------------
sp|Q03252|LMNB2_HUMAN   EDLFHQQG----------------------------------------
                : *.*::

sp|P02545-2|LMNA_HUMAN  ------------------------------------------------
sp|P02545|LMNA_HUMAN    PISSGSSASSVTVTRSYRSVGGSGGGSFGDNLVTRSYLLGNSSPRTQSPQ
sp|P20700|LMNB1_HUMAN   ----------------------------------------TPRAS-NR
sp|Q03252|LMNB2_HUMAN   ----------------------------------------DPRTT-SR


sp|P02545-2|LMNA_HUMAN  -GSRR
sp|P02545|LMNA_HUMAN    NCSIM
```

sp|P20700|LMNB1_HUMAN SCAIM

sp|Q03252|LMNB2_HUMAN GCYVM

Appendix II

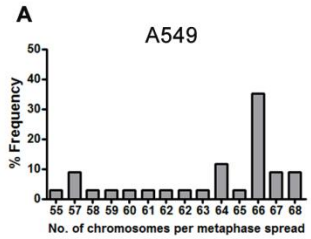
A
A549
% Frequency
0
10
20
30
40
50
55 57 58 59 60 61 62 62 63 64 65 66 67 68
No. of chromosomes per metaphase spread

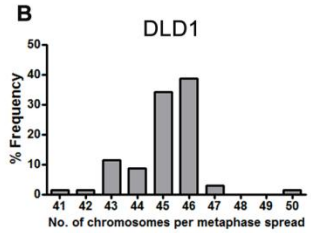
B
DLD1
% Frequency
0
10
20
30
40
50
41 42 43 44 45 46 47 48 49 50
No. of chromosomes per metaphase spread

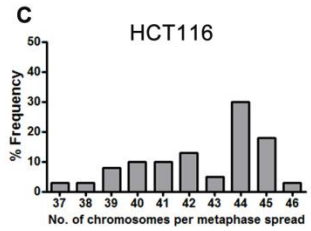
C
HCT116
% Frequency
0
10
20
30
40
50
37 38 39 40 41 42 43 44 45 46
No. of chromosomes per metaphase spread

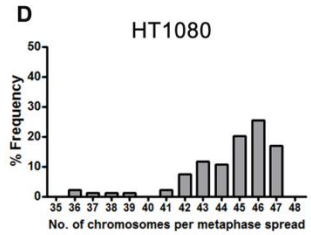
D
HT1080
% Frequency
0
10
20
30
40
50
35 36 37 38 39 40 41 42 43 44 45 46 47 48
No. of chromosomes per metaphase spread

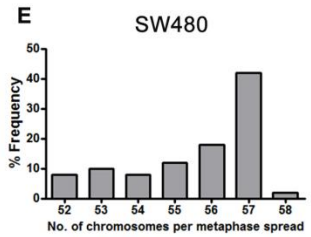
E
SW480
% Frequency
0
10
20
30
40
50
52 53 54 55 56 57 58
No. of chromosomes per metaphase spread

Appendix III

A

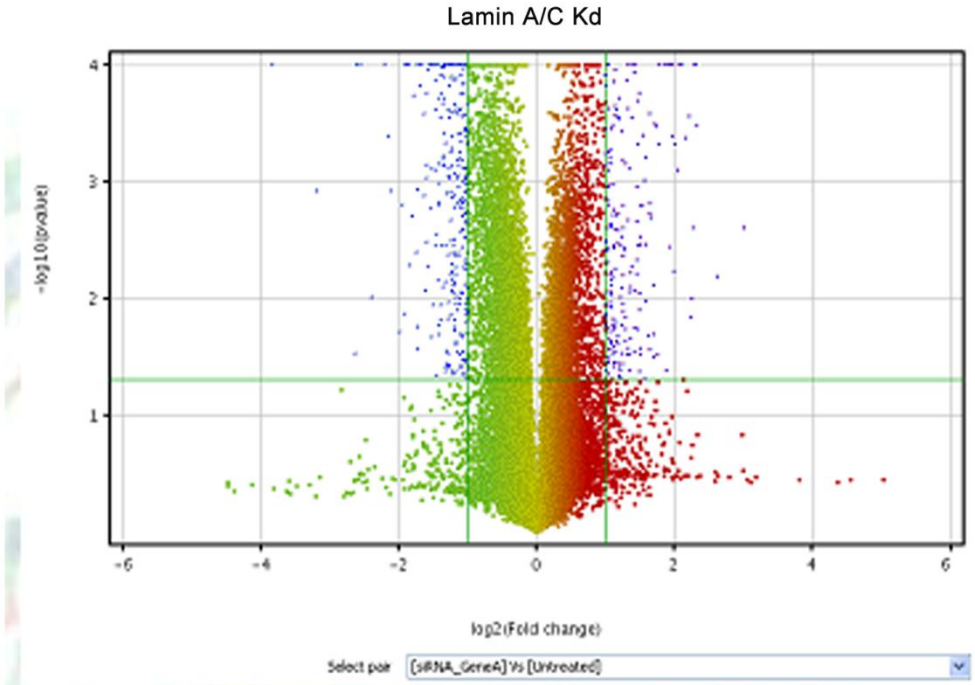

B

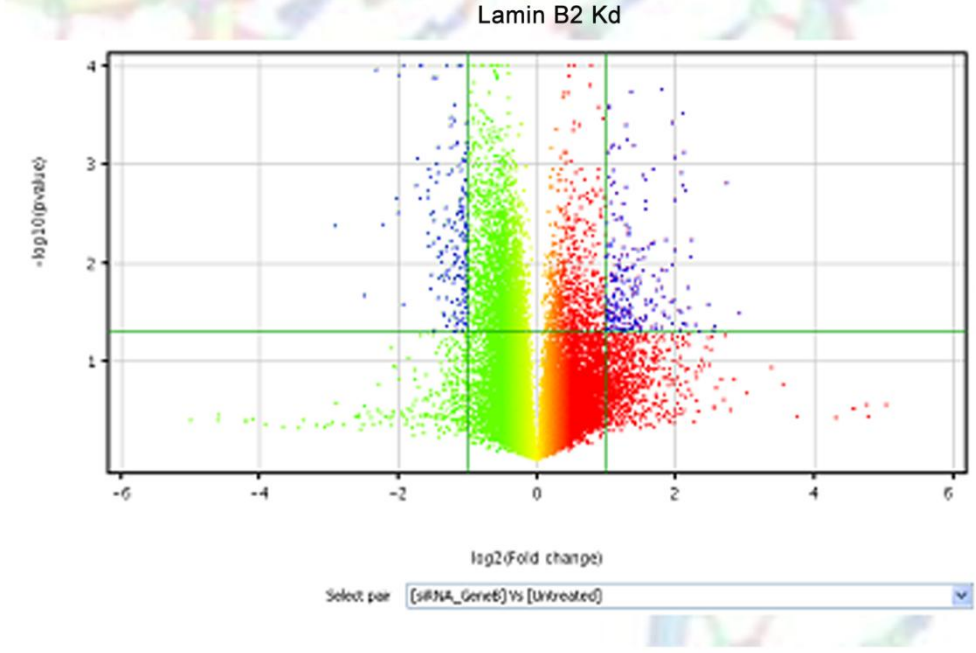

Appendix IV

List of all qRT-PCR primers used in this study

Gene Name	Primer sequences	Efficiency determined at 60ºC
LMNA	F- 5' CCGCAAGACCCTTGACTCA 3' R- 5' TGGTATTGCGCGCTTTCAG 3'	1.0
LMNB2	F- 5' AGTTCACGCCCAAGTACATC 3' R- 5' CTTCACAGTCCTCATGGCC 3'	1.0
ACTIN	F- 5' GATTCCTATGTGGGCGAC 3' R-5' GGTAGTCAGTCAGGTCCCG 3'	0.88
AKR1C3-A	F- 5' GCATGAGGTCTGCCAGAAG 3' R- 5' ACCAGCATAGAGCCATCCTC 3'	1.00
AKR1C3-B	F- 5' TGGGAGGCCATGGAGAAG 3' R- 5' GAAGTTTGACACCCCAATGGA 3'	1.23
MANSC1-A	F- 5' CCGCAGGAAACGTTACTCA 3' R – 5' ACTCATTGCATTTGGGCTTC 3'	1
MANSC1-B	F – 5' TGAAACCAGCAAAAGGACTTATGA 3' R - 5' TCTTGGCTTGGCAAATTTCTG 3'	1
LRRC47-A	F-5' GGATGCCCTCATTCTGAAAA 3' R – 5' GTGGGATCTGGAAGTTGTCC 3'	1.01
LRRC47-B	F- 5' GGCCTGCACAGATACCTTCAC 3' R- 5' CATCCACAAGACACGGGTAATTT 3'	1.0
AKR1B10-A	F – 5' AAACTGGAGGGCCTTTGACT 3' R – 5' TTCTGCATCGAAGGGAAAGT 3'	1.03
AKR1B10-B	F- 5' TGGAAGTCTCCTCTTGGCAAA 3' R – 5' TGTGCCGATATCCTGCATCA 3'	1.11
PTGS2-A	F – 5' CTATGTGCTAGCCCACAAAGAA 3' R – 5' GGTCAGTCTTATGGCACATTCA 3'	1.0
PTGS2-B	F- 5' TGAGTGTGGGATTTGACCAGTATAA 3' R – 5' ATTCCGGTGTTGAGCAGTTTTC 3'	1.0
HNRPK-A	F – 5' ATGGTGATCTTGGTGGACCT 3' R – 3' TTAATCCGCTGACCACCTTT 3'	1.04
HNRPK-B	F – 5' TGGAAAAGGAGGCAAGAATATTAAG 3' R – 5' TGCTGTCTGGGACTGAAACACT 3'	1.05
SMTNL2-A	F – 5' TTCCCTCTGGTGAATTCGAT 3' R – 5' ACCTACAATCGCGTGAGGAA 3'	0.87
SMTNL2-B	F – 5' GGCCAGAGTTTGGATCACGAT 3' R – 5' GATGCAGGAGTTTGAGGTCTTTC 3'	1.0
ABLIM2-A	F- 5' AAAGTGTTTCAATGTGACAGGA 3' R – 5' AACACATCATCATTTCCAAGC 3'	1.23
ABLIM2-B	F- 5' TGTCAGGTGCGGCCAGAT 3' R – 5' CGCCGGATGCCAGATG 3'	1.26
TMEM204-A	F – 5' GGATGAGTCTGGGTGACCTC 3'	1.39

	R – 5’ CCGACATAACAGTAAACGCACA 3’	
TMEM204-B	F – 5’ CCATGGCCGCTGCATT 3’ R – 5’ AAAGTCACGAGCCCGATGAC 3’	1.23
CDC42-A	F- 5’ ATTTTGGTTGCAGTTTCCAA 3’ R – 5’ TTTGGGAAGGTGGGAAAGAT 3’	1.10
CDC42-B	F – 5’ AGAAAAGTGGGTGCCTGAGATAAC 3’ R – 5’ GAGTCCCAACAAGCAAGAAAGG 3’	1.08
ITGA2-A	F- 5’ AAGCCGAAGTACCAACAGGA 3’ R – 5’ GCCGAGCTTCCATAAAATTG 3’	1.1
ITGA2-B	F- 5’ TGCCCCGAGCACATCAT 3’ R – 5’ ACGCAAATCCAAAGAGTTGACA 3’	1.0
TMEM14B-A	F – 5’ AACGTTTGGGGTTTCCTAGC 3’ R – 5’ CAAACTGGCACCTGCAATTA 3’	1.391
TMEM14B-B	F- 5’ CTTTGGCTACACAGCACTGGTT 3’ R – 5’ GCACGCTGCCTGTTTTTACA 3’	1.23
REG4-A	F – 5’ CCGTCCTCTTCCTTTCTGCT 3’ R – 5’ TGCTAGGTTTCCCCTCTGAA 3’	1
REG4-B	F – 5’ GGTTTTACCACAAGTCCAATTGC 3’ R – 5’ ACTCGAGCTCGGCATCAGA 3’	1
KPNA7-A	F – 5’ GAAAGAGGCTGTCTGGATGG 3’ R – 5’ AGATTCACCAGTGGCTCCAG 3’	1.1
KPNA7-B	F – 5’ CCACCCTGCCGATCACAT 3’ R – 5’ TTCGGCACAGATTCGACAAG 3’	1.1
C1orf144-A	F- 5’ GCAATTTTTAGCCAGGGACA 3’ R – 5’ TGGTACATTTCCTGTGTGCAA 3’	1.12
C1orf144-B	F- 5’ CACAAAAAGAGAGCAGGAAATCC 3’ R- 5’ GGCTATCGTCCTGAATCACAATG 3’	1.2
KRCC1-A	F- 5’ ATCCGTGTTCATACCACTTTT 3’ R – 5’ TCTTTAACTTCTAACAAAGGC 3’	1.2
KRCC1-B	F- 5’ CCAGACCCACGTATAGAATGTTTG 3’ R- 5’ TCTTGGGTAGGTCTGGATGGTT 3’	1.0
MESDC2-A	F – 5’ GGGGTTCTGTTTTGTTTCCTT 3’ R – 5’ CATATAACCCCTCGACACCAG 3’	1.08
MESDC2-B	F – 5’ CAGCCTTTTCAATGCCAACTATG 3’ R – 5’ GCATGAAGATAGCACGGTCTGA 3’	1.07
ZNF570	F - 5' GGCTGGGAGCCTATATGTGA 3’ R- 5' CTTCCTTGAAACACGCCTTC 3'	
GAPDH	F - 5'-CGAGATCCCTCCAAAATCAAG-3' R - 5'-GCAGAGATGATGACCCTTTTG-3'	0.81
EMD	F - 5’ CAGAGCAAGGGCTACAATGA 3’ R- 5’ CGTCAGCATCTGGGAATGAA 3’	0.99

List of all SDM primers used in the study

Name	Sequence of primer
LMNB2 siRNA resistant	F- 5’ATGCTGGACGCCAAGGAACAAGAAATGACAGAAATGCGGGACGTGATGCA 3’
LMNA siRNA resistant	F- 5’CTGGACAATGCCAGGCAATCCGCCGAAAGAAAUAGCAACCTGGTGGGG 3’
LMNA R453W	F- 5’ GAGGAGGTGGATGAGGAGGGCAAGTTTGTCUGGCTGCGCAACAAGTCCAATGAGGACCAGTCC 3’

References

Aebi, U., Cohn, J., Buhle, L. and Gerace, L. (1986). The nuclear lamina is a meshwork of intermediate-type filaments. *Nature* **323**, 560–564.

Akira, S. (1999). Functional roles of STAT family proteins: lessons from knockout mice. *Stem Cells* **17**, 138–146.

Almuzzaini, B., Sarshad, A. A., Farrants, A.-K. Ö. and Percipalle, P. (2015). Nuclear myosin 1 contributes to a chromatin landscape compatible with RNA polymerase II transcription activation. *BMC Biol* **13**, 35.

Alsheimer, M. and Benavente, R. (1996). Change of karyoskeleton during mammalian spermatogenesis: expression pattern of nuclear lamin C2 and its regulation. *Exp Cell Res* **228**, 181–188.

Amendola, M. and van Steensel, B. (2015). Nuclear lamins are not required for lamina-associated domain organization in mouse embryonic stem cells. *EMBO Rep* **16**, 610–617.

Annunziato, A. T. and Hansen, J. C. (2000). Role of histone acetylation in the assembly and modulation of chromatin structures. *Gene Expr* **9**, 37–61.

Athar, F. and Parnaik, V. K. (2015). Association of lamin A/C with muscle gene-specific promoters in myoblasts. *Biochemistry and Biophysics Reports* **4**, 76–82.

Baker, D. J., Jeganathan, K. B., Cameron, J. D., Thompson, M., Juneja, S., Kopecka, A., Kumar, R., Jenkins, R. B., de Groen, P. C., Roche, P., et al. (2004). BubR1 insufficiency causes early onset of aging-associated phenotypes and infertility in mice. *Nat Genet* **36**, 744–749.

Bakhoum, S. F. and Compton, D. A. (2012). Chromosomal instability and cancer: a complex relationship with therapeutic potential. *J Clin Invest* **122**, 1138–1143.

Barrowman, J., Hamblet, C., George, C. M. and Michaelis, S. (2008). Analysis of prelamin A biogenesis reveals the nucleus to be a CaaX processing compartment. *Mol Biol Cell* **19**, 5398–5408.

Barton, L. J., Soshnev, A. A. and Geyer, P. K. (2015). Networking in the nucleus: a spotlight on LEM-domain proteins. *Curr Opin Cell Biol* **34**, 1–8.

Beck, L. A., Hosick, T. J. and Sinensky, M. (1990). Isoprenylation is required for the processing of the lamin A precursor. *J Cell Biol* **110**, 1489–1499.

Beliveau, B. J., Boettiger, A. N., Avendaño, M. S., Jungmann, R., McCole, R. B., Joyce, E. F., Kim-Kiselak, C., Bantignies, F., Fonseka, C. Y., Erceg, J., et al. (2015). Single-molecule super-resolution imaging of chromosomes and in situ haplotype visualization using Oligopaint FISH probes. *Nat Commun* **6**, 7147.

Bell, E. S. and Lammerding, J. (2016). Causes and consequences of nuclear envelope alterations in tumour progression. *Eur J Cell Biol* **95**, 449–464.

Belt, E. J. T., Fijneman, R. J. A., van den Berg, E. G., Bril, H., Delis-van Diemen, P. M., Tijssen, M., van Essen, H. F., de Lange-de Klerk, E. S. M., Beliën, J. A. M., Stockmann, H. B. A. C., et al. (2011). Loss of lamin A/C expression in stage II and III colon cancer is associated with disease recurrence. *Eur J Cancer* **47**, 1837–1845.

Benson, E. K., Lee, S. W. and Aaronson, S. A. (2010). Role of progerin-induced telomere dysfunction in HGPS premature cellular senescence. *J Cell Sci* **123**, 2605–2612.

Bercht Pfleghaar, K., Taimen, P., Butin-Israeli, V., Shimi, T., Langer-Freitag, S., Markaki, Y., Goldman, A. E., Wehnert, M. and Goldman, R. D. (2015). Gene-rich chromosomal regions are preferentially localized in the lamin B deficient nuclear blebs of atypical progeria cells. *Nucleus* **6**, 66–76.

Bera, M., Kotamarthi, H. C., Dutta, S., Ray, A., Ghosh, S., Bhattacharyya, D., Ainavarapu, S. R. K. and Sengupta, K. (2014). Characterization of unfolding mechanism of human lamin A Ig fold by single-molecule force spectroscopy-implications in EDMD. *Biochemistry* **53**, 7247–7258

Berk, J. M., Simon, D. N., Jenkins-Houk, C. R., Westerbeck, J. W., Grønning-Wang, L. M., Carlson, C. R. and Wilson, K. L. (2014). The molecular basis of emerin-emerin and emerin-BAF interactions. *J Cell Sci* **127**, 3956–3969.

Biamonti, G., Giacca, M., Perini, G., Contreas, G., Zentilin, L., Weighardt, F., Guerra, M., Della Valle, G., Saccone, S. and Riva, S. (1992). The gene for a novel human lamin maps at a highly transcribed locus of chromosome 19 which replicates at the onset of S-phase. *Mol Cell Biol* **12**, 3499–3506.

Boland, C. R. and Goel, A. (2010). Microsatellite instability in colorectal cancer. *Gastroenterology* **138**, 2073–2087.e3.

Bolzer, A., Kreth, G., Solovei, I., Koehler, D., Saracoglu, K., Fauth, C., Müller, S., Eils, R., Cremer, C., Speicher, M. R., et al. (2005). Three-dimensional maps of all chromosomes in human male fibroblast nuclei and prometaphase rosettes. *PLoS Biol* **3**, e157.

Booth, E. A., Spagnol, S. T., Alcoser, T. A. and Dahl, K. N. (2015). Nuclear stiffening and chromatin softening with progerin expression leads to an attenuated nuclear response to force. *Soft Matter* **11**, 6412–6418.

Boyle, S., Gilchrist, S., Bridger, J. M., Mahy, N. L., Ellis, J. A. and Bickmore, W. A. (2001). The spatial organization of human chromosomes within the nuclei of normal and emerin-mutant cells. *Hum Mol Genet* **10**, 211–219.

Branco, M. R. and Pombo, A. (2006). Intermingling of chromosome territories in interphase suggests role in translocations and transcription-dependent associations. *PLoS Biol* **4**, e138.

Bridger, J. M., Kill, I. R., O'Farrell, M. and Hutchison, C. J. (1993). Internal lamin structures within G1 nuclei of human dermal fibroblasts. *J Cell Sci* **104 (Pt 2)**, 297–306.

Broers, J. L., Machiels, B. M., Kuijpers, H. J., Smedts, F., van den Kieboom, R., Raymond, Y. and Ramaekers, F. C. (1997). A- and B-type lamins are differentially expressed in normal human tissues. *Histochem Cell Biol* **107**, 505–517.

Broers, J. L., Machiels, B. M., van Eys, G. J., Kuijpers, H. J., Manders, E. M., van Driel, R. and Ramaekers, F. C. (1999). Dynamics of the nuclear lamina as monitored by GFP-tagged A-type lamins. *J Cell Sci* **112 (Pt 20)**, 3463–3475.

Bronshtein, I., Kepten, E., Kanter, I., Berezin, S., Lindner, M., Redwood, A. B., Mai, S., Gonzalo, S., Foisner, R., Shav-Tal, Y., et al. (2015). Loss of lamin A function increases chromatin dynamics

in the nuclear interior. *Nat Commun* **6**, 8044.

Brosig, M., Ferralli, J., Gelman, L., Chiquet, M. and Chiquet-Ehrismann, R. (2010). Interfering with the connection between the nucleus and the cytoskeleton affects nuclear rotation, mechanotransduction and myogenesis. *Int J Biochem Cell Biol* **42**, 1717–1728.

Burke, B. and Stewart, C. L. (2002). Life at the edge: the nuclear envelope and human disease. *Nat Rev Mol Cell Biol* **3**, 575–585.

Burke, B. and Stewart, C. L. (2013). The nuclear lamins: flexibility in function. *Nat Rev Mol Cell Biol* **14**, 13–24.

Butin-Israeli, V., Adam, S. A. and Goldman, R. D. (2013). Regulation of nucleotide excision repair by nuclear lamin b1. *PLoS ONE* **8**, e69169.

Butin-Israeli, V., Adam, S. A., Jain, N., Otte, G. L., Neems, D., Wiesmüller, L., Berger, S. L. and Goldman, R. D. (2015). Role of lamin b1 in chromatin instability. *Mol Cell Biol* **35**, 884–898.

Buxboim, A., Swift, J., Irianto, J., Spinler, K. R., Dingal, P. C. D. P., Athirasala, A., Kao, Y.-R. C., Cho, S., Harada, T., Shin, J.-W., et al. (2014). Matrix elasticity regulates lamin-A,C phosphorylation and turnover with feedback to actomyosin. *Curr Biol* **24**, 1909–1917.

Cadigan, K. M. and Waterman, M. L. (2012). TCF/LEFs and Wnt signaling in the nucleus. *Cold Spring Harb Perspect Biol* **4**,.

Camps, J., Wangsa, D., Falke, M., Brown, M., Case, C. M., Erdos, M. R. and Ried, T. (2014). Loss of lamin B1 results in prolongation of S phase and decondensation of chromosome territories. *FASEB J* **28**, 3423–3434.

Capo-chichi, C. D., Cai, K. Q., Simpkins, F., Ganjei-Azar, P., Godwin, A. K. and Xu, X.-X. (2011a). Nuclear envelope structural defects cause chromosomal numerical instability and aneuploidy in ovarian cancer. *BMC Med* **9**, 28.

Capo-chichi, C. D., Cai, K. Q., Smedberg, J., Ganjei-Azar, P., Godwin, A. K. and Xu, X.-X. (2011b). Loss of A-type lamin expression compromises nuclear envelope integrity in breast cancer. *Chin J Cancer* **30**, 415–425.

Caron, H., van Schaik, B., van der Mee, M., Baas, F., Riggins, G., van Sluis, P., Hermus, M. C., van Asperen, R., Boon, K., Voûte, P. A., et al. (2001). The human transcriptome map: clustering of highly expressed genes in chromosomal domains. *Science* **291**, 1289–1292.

Cesarini, E., Mozzetta, C., Marullo, F., Gregoretti, F., Gargiulo, A., Columbaro, M., Cortesi, A., Antonelli, L., Di Pelino, S., Squarzoni, S., et al. (2015). Lamin A/C sustains PcG protein architecture, maintaining transcriptional repression at target genes. *J Cell Biol* **211**, 533–551.

Chaudhary, N. and Courvalin, J. C. (1993). Stepwise reassembly of the nuclear envelope at the end of mitosis. *J Cell Biol* **122**, 295–306.

Chaumeil, J., Augui, S., Chow, J. C. and Heard, E. (2008). Combined immunofluorescence, RNA fluorescent in situ hybridization, and DNA fluorescent in situ hybridization to study chromatin changes, transcriptional activity, nuclear organization, and X-chromosome inactivation. *Methods Mol Biol* **463**, 297–308.

Chelsky, D., Sobotka, C. and O'Neill, C. L. (1989). Lamin B methylation and assembly into the nuclear

envelope. *J Biol Chem* **264**, 7637–7643.

Chen, C.-Y., Chi, Y.-H., Mutalif, R. A., Starost, M. F., Myers, T. G., Anderson, S. A., Stewart, C. L. and Jeang, K.-T. (2012). Accumulation of the inner nuclear envelope protein Sun1 is pathogenic in progeric and dystrophic laminopathies. *Cell* **149**, 565–577.

Chojnowski, A., Ong, P. F., Wong, E. S. M., Lim, J. S. Y., Mutalif, R. A., Navasankari, R., Dutta, B., Yang, H., Liow, Y. Y., Sze, S. K., et al. (2015). Progerin reduces LAP2α-telomere association in Hutchinson-Gilford progeria. *elife* **4**,.

Chuang, C.-H., Carpenter, A. E., Fuchsova, B., Johnson, T., de Lanerolle, P. and Belmont, A. S. (2006). Long-range directional movement of an interphase chromosome site. *Curr Biol* **16**, 825–831.

Chubb, J. R., Boyle, S., Perry, P. and Bickmore, W. A. (2002). Chromatin motion is constrained by association with nuclear compartments in human cells. *Curr Biol* **12**, 439–445.

Cobb, A. M., Murray, T. V., Warren, D. T., Liu, Y. and Shanahan, C. M. (2016). Disruption of PCNA-lamins A/C interactions by prelamin A induces DNA replication fork stalling. *Nucleus* **7**, 498–511.

Coffinier, C., Chang, S. Y., Nobumori, C., Tu, Y., Farber, E. A., Toth, J. I., Fong, L. G. and Young, S. G. (2010). Abnormal development of the cerebral cortex and cerebellum in the setting of lamin B2 deficiency. *Proc Natl Acad Sci U S A* **107**, 5076–5081.

Coffinier, C., Jung, H.-J., Nobumori, C., Chang, S., Tu, Y., Barnes, R. H., Yoshinaga, Y., de Jong, P. J., Vergnes, L., Reue, K., et al. (2011). Deficiencies in lamin B1 and lamin B2 cause neurodevelopmental defects and distinct nuclear shape abnormalities in neurons. *Mol Biol Cell* **22**, 4683–4693.

Constantinescu, D., Gray, H. L., Sammak, P. J., Schatten, G. P. and Csoka, A. B. (2006). Lamin A/C expression is a marker of mouse and human embryonic stem cell differentiation. *Stem Cells* **24**, 177–185.

Cremer, T., Cremer, C., Schneider, T., Baumann, H., Hens, L. and Kirsch-Volders, M. (1982). Analysis of chromosome positions in the interphase nucleus of Chinese hamster cells by laser-UV-microirradiation experiments. *Hum Genet* **62**, 201–209.

Cremer, T. and Cremer, C. (2001). Chromosome territories, nuclear architecture and gene regulation in mammalian cells. *Nat Rev Genet* **2**, 292–301.

Cremer, M., von Hase, J., Volm, T., Brero, A., Kreth, G., Walter, J., Fischer, C., Solovei, I., Cremer, C. and Cremer, T. (2001). Non-random radial higher-order chromatin arrangements in nuclei of diploid human cells. *Chromosome Res* **9**, 541–567.

Cremer, M., Küpper, K., Wagler, B., Wizelman, L., von Hase, J., Weiland, Y., Kreja, L., Diebold, J., Speicher, M. R. and Cremer, T. (2003). Inheritance of gene density-related higher order chromatin arrangements in normal and tumor cell nuclei. *J Cell Biol* **162**, 809–820.

Cremer, M., Grasser, F., Lanctôt, C., Müller, S., Neusser, M., Zinner, R., Solovei, I. and Cremer, T. (2008). Multicolor 3D fluorescence in situ hybridization for imaging interphase chromosomes. *Methods Mol Biol* **463**, 205–239.

Croft, J. A., Bridger, J. M., Boyle, S., Perry, P., Teague, P. and Bickmore, W. A. (1999). Differences

in the localization and morphology of chromosomes in the human nucleus. *J Cell Biol* **145**, 1119–1131.

Dahl, K. N., Scaffidi, P., Islam, M. F., Yodh, A. G., Wilson, K. L. and Misteli, T. (2006). Distinct structural and mechanical properties of the nuclear lamina in Hutchinson-Gilford progeria syndrome. *Proc Natl Acad Sci U S A* **103**, 10271–10276.

Dechat, T., Korbei, B., Vaughan, O. A., Vlcek, S., Hutchison, C. J. and Foisner, R. (2000). Lamina-associated polypeptide 2alpha binds intranuclear A-type lamins. *J Cell Sci* **113 Pt 19**, 3473–3484.

Dechat, T., Pfleghaar, K., Sengupta, K., Shimi, T., Shumaker, D. K., Solimando, L. and Goldman, R. D. (2008). Nuclear lamins: major factors in the structural organization and function of the nucleus and chromatin. *Genes Dev* **22**, 832–853.

Dechat, T., Gesson, K. and Foisner, R. (2010). Lamina-independent lamins in the nuclear interior serve important functions. *Cold Spring Harb Symp Quant Biol* **75**, 533–543.

Decker, M. L., Chavez, E., Vulto, I. and Lansdorp, P. M. (2009). Telomere length in Hutchinson-Gilford progeria syndrome. *Mech Ageing Dev* **130**, 377–383.

Delbarre, E., Tramier, M., Coppey-Moisan, M., Gaillard, C., Courvalin, J.-C. and Buendia, B. (2006). The truncated prelamin A in Hutchinson-Gilford progeria syndrome alters segregation of A-type and B-type lamin homopolymers. *Hum Mol Genet* **15**, 1113–1122.

De Vos, W. H., Houben, F., Hoebe, R. A., Hennekam, R., van Engelen, B., Manders, E. M. M., Ramaekers, F. C. S., Broers, J. L. V. and Van Oostveldt, P. (2010). Increased plasticity of the nuclear envelope and hypermobility of telomeres due to the loss of A-type lamins. *Biochim Biophys Acta* **1800**, 448–458.

Dhe-Paganon, S., Werner, E. D., Chi, Y.-I. and Shoelson, S. E. (2002). Structure of the globular tail of nuclear lamin. *J Biol Chem* **277**, 17381–17384.

Dittmer, T. A. and Misteli, T. (2011). The lamin protein family. *Genome Biol* **12**, 222.

Dixon, J. R., Selvaraj, S., Yue, F., Kim, A., Li, Y., Shen, Y., Hu, M., Liu, J. S. and Ren, B. (2012). Topological domains in mammalian genomes identified by analysis of chromatin interactions. *Nature* **485**, 376–380.

Dobles, M., Liberal, V., Scott, M. L., Benezra, R. and Sorger, P. K. (2000). Chromosome missegregation and apoptosis in mice lacking the mitotic checkpoint protein Mad2. *Cell* **101**, 635–645.

Dorner, D., Vlcek, S., Foeger, N., Gajewski, A., Makolm, C., Gotzmann, J., Hutchison, C. J. and Foisner, R. (2006). Lamina-associated polypeptide 2alpha regulates cell cycle progression and differentiation via the retinoblastoma-E2F pathway. *J Cell Biol* **173**, 83–93.

Dreuillet, C., Tillit, J., Kress, M. and Ernoult-Lange, M. (2002). In vivo and in vitro interaction between human transcription factor MOK2 and nuclear lamin A/C. *Nucleic Acids Res* **30**, 4634–4642.

Eckersley-Maslin, M. A., Bergmann, J. H., Lazar, Z. and Spector, D. L. (2013). Lamin A/C is expressed in pluripotent mouse embryonic stem cells. *Nucleus* **4**, 53–60.

Edwards, J. H., Harnden, D. G., Cameron, A. H., Crosse, V. M. and Wolff, O. H. (1960). A new

trisomic syndrome. *Lancet* **1**, 787–790.

Farnsworth, C. C., Wolda, S. L., Gelb, M. H. and Glomset, J. A. (1989). Human lamin B contains a farnesylated cysteine residue. *J Biol Chem* **264**, 20422–20429.

Federico, C., Scavo, C., Cantarella, C. D., Motta, S., Saccone, S. and Bernardi, G. (2006). Gene-rich and gene-poor chromosomal regions have different locations in the interphase nuclei of cold-blooded vertebrates. *Chromosoma* **115**, 123–128.

Ferrera, D., Canale, C., Marotta, R., Mazzaro, N., Gritti, M., Mazzanti, M., Capellari, S., Cortelli, P. and Gasparini, L. (2014). Lamin B1 overexpression increases nuclear rigidity in autosomal dominant leukodystrophy fibroblasts. *FASEB J* **28**, 3906–3918.

Finlan, L. E., Sproul, D., Thomson, I., Boyle, S., Kerr, E., Perry, P., Ylstra, B., Chubb, J. R. and Bickmore, W. A. (2008). Recruitment to the nuclear periphery can alter expression of genes in human cells. *PLoS Genet* **4**, e1000039.

Fisher, D. Z., Chaudhary, N. and Blobel, G. (1986). cDNA sequencing of nuclear lamins A and C reveals primary and secondary structural homology to intermediate filament proteins. *Proc Natl Acad Sci U S A* **83**, 6450–6454.

FitzPatrick, D. R., Ramsay, J., McGill, N. I., Shade, M., Carothers, A. D. and Hastie, N. D. (2002). Transcriptome analysis of human autosomal trisomy. *Hum Mol Genet* **11**, 3249–3256.

Foisner, R. and Gerace, L. (1993). Integral membrane proteins of the nuclear envelope interact with lamins and chromosomes, and binding is modulated by mitotic phosphorylation. *Cell* **73**, 1267–1279.

Foisner, R. (2003). Cell cycle dynamics of the nuclear envelope. *ScientificWorldJournal* **3**, 1–20.

Fomproix, N. and Percipalle, P. (2004). An actin-myosin complex on actively transcribing genes. *Exp Cell Res* **294**, 140–148

Foster, H. A., Abeydeera, L. R., Griffin, D. K. and Bridger, J. M. (2005). Non-random chromosome positioning in mammalian sperm nuclei, with migration of the sex chromosomes during late spermatogenesis. *J Cell Sci* **118**, 1811–1820.

Foster, C. R., Robson, J. L., Simon, W. J., Twigg, J., Cruikshank, D., Wilson, R. G. and Hutchison, C. J. (2011). The role of Lamin A in cytoskeleton organization in colorectal cancer cells: a proteomic investigation. *Nucleus* **2**, 434–443.

Freund, A., Laberge, R.-M., Demaria, M. and Campisi, J. (2012). Lamin B1 loss is a senescence-associated biomarker. *Mol Biol Cell* **23**, 2066–2075.

Furukawa, K. and Hotta, Y. (1993). cDNA cloning of a germ cell specific lamin B3 from mouse spermatocytes and analysis of its function by ectopic expression in somatic cells. *EMBO J* **12**, 97–106.

Furukawa, K. and Kondo, T. (1998). Identification of the lamina-associated-polypeptide-2-binding domain of B-type lamin. *Eur J Biochem* **251**, 729–733.

Furukawa, K., Inagaki, H. and Hotta, Y. (1994). Identification and cloning of an mRNA coding for a germ cell-specific A-type lamin in mice. *Exp Cell Res* **212**, 426–430.

Galiová, G., Bártová, E. and Kozubek, S. (2004). Nuclear topography of beta-like globin gene cluster in IL-3-stimulated human leukemic K-562 cells. *Blood Cells Mol Dis* **33**, 4–14.

Ganai, N., Sengupta, S. and Menon, G. I. (2014). Chromosome positioning from activity-based segregation. *Nucleic Acids Res* **42**, 4145–4159.

Georgatos, S. D., Maroulakou, I. and Blobel, G. (1989). Lamin A, lamin B, and lamin B receptor analogues in yeast. *J Cell Biol* **108**, 2069–2082.

Gerace, L. and Blobel, G. (1980). The nuclear envelope lamina is reversibly depolymerized during mitosis. *Cell* **19**, 277–287.

Gerace, L., Blum, A. and Blobel, G. (1978). Immunocytochemical localization of the major polypeptides of the nuclear pore complex-lamina fraction. Interphase and mitotic distribution. *J Cell Biol* **79**, 546–566.

Gesson, K., Rescheneder, P., Skoruppa, M. P., von Haeseler, A., Dechat, T. and Foisner, R. (2016). A-type lamins bind both hetero- and euchromatin, the latter being regulated by lamina-associated polypeptide 2 alpha. *Genome Res* **26**, 462–473.

Gibbs-Seymour, I., Markiewicz, E., Bekker-Jensen, S., Mailand, N. and Hutchison, C. J. (2015). Lamin A/C-dependent interaction with 53BP1 promotes cellular responses to DNA damage. *Aging Cell* **14**, 162–169.

Gieffers, C. and Krohne, G. (1991). In vitro reconstitution of recombinant lamin A and a lamin A mutant lacking the carboxy-terminal tail. *Eur J Cell Biol* **55**, 191–199.

Gilbert, N., Boyle, S., Fiegler, H., Woodfine, K., Carter, N. P. and Bickmore, W. A. (2004). Chromatin architecture of the human genome: gene-rich domains are enriched in open chromatin fibers. *Cell* **118**, 555–566.

Gilbert, N., Gilchrist, S. and Bickmore, W. A. (2005). Chromatin organization in the mammalian nucleus. *Int Rev Cytol* **242**, 283–336.

Glass, C. A., Glass, J. R., Taniura, H., Hasel, K. W., Blevitt, J. M. and Gerace, L. (1993). The alpha-helical rod domain of human lamins A and C contains a chromatin binding site. *EMBO J* **12**, 4413–4424.

Goetze, S., Mateos-Langerak, J., Gierman, H. J., de Leeuw, W., Giromus, O., Indemans, M. H. G., Koster, J., Ondrej, V., Versteeg, R. and van Driel, R. (2007). The three-dimensional structure of human interphase chromosomes is related to the transcriptome map. *Mol Cell Biol* **27**, 4475–4487.

Goldberg, M. W., Huttenlauch, I., Hutchison, C. J. and Stick, R. (2008). Filaments made from A- and B-type lamins differ in structure and organization. *J Cell Sci* **121**, 215–225.

Goldman, A. E., Maul, G., Steinert, P. M., Yang, H. Y. and Goldman, R. D. (1986). Keratin-like proteins that coisolate with intermediate filaments of BHK-21 cells are nuclear lamins. *Proc Natl Acad Sci U S A* **83**, 3839–3843.

González, J. M., Navarro-Puche, A., Casar, B., Crespo, P. and Andrés, V. (2008). Fast regulation of AP-1 activity through interaction of lamin A/C, ERK1/2, and c-Fos at the nuclear envelope. *J Cell Biol* **183**, 653–666.

Gonzalez-Suarez, I., Redwood, A. B., Perkins, S. M., Vermolen, B., Lichtensztejin, D., Grotsky, D. A., Morgado-Palacin, L., Gapud, E. J., Sleckman, B. P., Sullivan, T., et al. (2009). Novel roles for A-type lamins in telomere biology and the DNA damage response pathway. *EMBO J* **28**, 2414–2427.

Gonzalo, S. and Kreienkamp, R. (2015). DNA repair defects and genome instability in Hutchinson-Gilford Progeria Syndrome. *Curr Opin Cell Biol* **34**, 75–83.

Goodman, B., Channels, W., Qiu, M., Iglesias, P., Yang, G. and Zheng, Y. (2010). Lamin B counteracts the kinesin Eg5 to restrain spindle pole separation during spindle assembly. *J Biol Chem* **285**, 35238–35244.

Grade, M., Hörmann, P., Becker, S., Hummon, A. B., Wangsa, D., Varma, S., Simon, R., Liersch, T., Becker, H., Difilippantonio, M. J., et al. (2007). Gene expression profiling reveals a massive, aneuploidy-dependent transcriptional deregulation and distinct differences between lymph node-negative and lymph node-positive colon carcinomas. *Cancer Res* **67**, 41–56.

Gruenbaum, Y. and Medalia, O. (2015). Lamins: the structure and protein complexes. *Curr Opin Cell Biol* **32**, 7–12.

Guelen, L., Pagie, L., Brasset, E., Meuleman, W., Faza, M. B., Talhout, W., Eussen, B. H., de Klein, A., Wessels, L., de Laat, W., et al. (2008). Domain organization of human chromosomes revealed by mapping of nuclear lamina interactions. *Nature* **453**, 948–951.

Guilluy, C., Osborne, L. D., Van Landeghem, L., Sharek, L., Superfine, R., Garcia-Mata, R. and Burridge, K. (2014). Isolated nuclei adapt to force and reveal a mechanotransduction pathway in the nucleus. *Nat Cell Biol* **16**, 376–381.

Guo, Y., Kim, Y., Shimi, T., Goldman, R. D. and Zheng, Y. (2014). Concentration-dependent lamin assembly and its roles in the localization of other nuclear proteins. *Mol Biol Cell* **25**, 1287–1297.

Güttinger, S., Laurell, E. and Kutay, U. (2009). Orchestrating nuclear envelope disassembly and reassembly during mitosis. *Nat Rev Mol Cell Biol* **10**, 178–191.

Hannenhalli, S. and Kaestner, K. H. (2009). The evolution of Fox genes and their role in development and disease. *Nat Rev Genet* **10**, 233–240.

Haque, F., Lloyd, D. J., Smallwood, D. T., Dent, C. L., Shanahan, C. M., Fry, A. M., Trembath, R. C. and Shackleton, S. (2006). SUN1 interacts with nuclear lamin A and cytoplasmic nesprins to provide a physical connection between the nuclear lamina and the cytoskeleton. *Mol Cell Biol* **26**, 3738–3751.

Harnicarová, A., Kozubek, S., Pacherník, J., Krejci, J. and Bártová, E. (2006). Distinct nuclear arrangement of active and inactive c-myc genes in control and differentiated colon carcinoma cells. *Exp Cell Res* **312**, 4019–4035.

Harr, J. C., Luperchio, T. R., Wong, X., Cohen, E., Wheelan, S. J. and Reddy, K. L. (2015). Directed targeting of chromatin to the nuclear lamina is mediated by chromatin state and A-type lamins. *J Cell Biol* **208**, 33–52.

Hashimshony, T., Wagner, F., Sher, N. and Yanai, I. (2012). CEL-Seq: single-cell RNA-Seq by multiplexed linear amplification. *Cell Rep* **2**, 666–673.

Hastings, P. J., Lupski, J. R., Rosenberg, S. M. and Ira, G. (2009). Mechanisms of change in gene copy number. *Nat Rev Genet* **10**, 551–564.

Heald, R. and McKeon, F. (1990). Mutations of phosphorylation sites in lamin A that prevent nuclear lamina disassembly in mitosis. *Cell* **61**, 579–589.

Heessen, S. and Fornerod, M. (2007). The inner nuclear envelope as a transcription factor resting place. *EMBO Rep* **8**, 914–919.

Heitlinger, E., Peter, M., Häner, M., Lustig, A., Aebi, U. and Nigg, E. A. (1991). Expression of chicken lamin B2 in Escherichia coli: characterization of its structure, assembly, and molecular interactions. *J Cell Biol* **113**, 485–495.

Heitlinger, E., Peter, M., Lustig, A., Villiger, W., Nigg, E. A. and Aebi, U. (1992). The role of the head and tail domain in lamin structure and assembly: analysis of bacterially expressed chicken lamin A and truncated B2 lamins. *J Struct Biol* **108**, 74–89.

Heride, C., Ricoul, M., Kiêu, K., von Hase, J., Guillemot, V., Cremer, C., Dubrana, K. and Sabatier, L. (2010). Distance between homologous chromosomes results from chromosome positioning constraints. *J Cell Sci* **123**, 4063–4075

Hervé, B., Coussement, A., Gilbert, T., Dumont, F., Jacques, S., Cuisset, L., Chicard, M., Hizem, S., Bourdoncle, P., Letourneur, F., et al. (2016). Aneuploidy: the impact of chromosome imbalance on nuclear organization and overall genome expression. *Clin Genet* **90**, 35–48.

Ho, C. Y., Jaalouk, D. E., Vartiainen, M. K. and Lammerding, J. (2013). Lamin A/C and emerin regulate MKL1-SRF activity by modulating actin dynamics. *Nature* **497**, 507–511.

Hoffmann, K., Dreger, C. K., Olins, A. L., Olins, D. E., Shultz, L. D., Lucke, B., Karl, H., Kaps, R., Müller, D., Vayá, A., et al. (2002). Mutations in the gene encoding the lamin B receptor produce an altered nuclear morphology in granulocytes (Pelger-Huët anomaly). *Nat Genet* **31**, 410–414.

Hofmann, W. A., Johnson, T., Klapczynski, M., Fan, J.-L. and de Lanerolle, P. (2006). From transcription to transport: emerging roles for nuclear myosin I. *Biochem Cell Biol* **84**, 418–426.

Höger, T. H., Zatloukal, K., Waizenegger, I. and Krohne, G. (1990). Characterization of a second highly conserved B-type lamin present in cells previously thought to contain only a single B-type lamin. *Chromosoma* **100**, 67–69.

Holaska, J. M. and Wilson, K. L. (2007). An emerin "proteome": purification of distinct emerin-containing complexes from HeLa cells suggests molecular basis for diverse roles including gene regulation, mRNA splicing, signaling, mechanosensing, and nuclear architecture. *Biochemistry* **46**, 8897–8908.

Holaska, J. M., Kowalski, A. K. and Wilson, K. L. (2004). Emerin caps the pointed end of actin filaments: evidence for an actin cortical network at the nuclear inner membrane. *PLoS Biol* **2**, E231.

Holtz, D., Tanaka, R. A., Hartwig, J. and McKeon, F. (1989). The CaaX motif of lamin A functions in conjunction with the nuclear localization signal to target assembly to the nuclear envelope. *Cell* **59**, 969–977.

Hozák, P., Sasseville, A. M., Raymond, Y. and Cook, P. R. (1995). Lamin proteins form an internal nucleoskeleton as well as a peripheral lamina in human cells. *J Cell Sci* **108 (Pt 2)**, 635–644.

Huang, S., Risques, R. A., Martin, G. M., Rabinovitch, P. S. and Oshima, J. (2008). Accelerated telomere shortening and replicative senescence in human fibroblasts overexpressing mutant and wild-type lamin A. *Exp Cell Res* **314**, 82–91.

Huang, D. W., Sherman, B. T. and Lempicki, R. A. (2009a). Systematic and integrative analysis of large gene lists using DAVID bioinformatics resources. *Nat Protoc* **4**, 44–57.

Huang, D. W., Sherman, B. T. and Lempicki, R. A. (2009b). Bioinformatics enrichment tools: paths toward the comprehensive functional analysis of large gene lists. *Nucleic Acids Res* **37**, 1–13.

Islam, S., Kjällquist, U., Moliner, A., Zajac, P., Fan, J.-B., Lönnerberg, P. and Linnarsson, S. (2012). Highly multiplexed and strand-specific single-cell RNA 5' end sequencing. *Nat Protoc* **7**, 813–828.

Ivorra, C., Kubicek, M., González, J. M., Sanz-González, S. M., Alvarez-Barrientos, A., O'Connor, J.-E., Burke, B. and Andrés, V. (2006). A mechanism of AP-1 suppression through interaction of c-Fos with lamin A/C. *Genes Dev* **20**, 307–320.

Jackson, D. A. and Pombo, A. (1998). Replicon clusters are stable units of chromosome structure: evidence that nuclear organization contributes to the efficient activation and propagation of S phase in human cells. *J Cell Biol* **140**, 1285–1295.

Jacobs, P. A., Baikie, A. G., Court Brown, W. M. and Strong, J. A. (1959). The somatic chromosomes in mongolism. *Lancet* **1**, 710.

Jagatheesan, G., Thanumalayan, S., Muralikrishna, B., Rangaraj, N., Karande, A. A. and Parnaik, V. K. (1999). Colocalization of intranuclear lamin foci with RNA splicing factors. *J Cell Sci* **112 (Pt 24)**, 4651–4661.

Jaskelioff, M., Gavin, I. M., Peterson, C. L. and Logie, C. (2000). SWI-SNF-mediated nucleosome remodeling: role of histone octamer mobility in the persistence of the remodeled state. *Mol Cell Biol* **20**, 3058–3068.

Ji, J. Y., Lee, R. T., Vergnes, L., Fong, L. G., Stewart, C. L., Reue, K., Young, S. G., Zhang, Q., Shanahan, C. M. and Lammerding, J. (2007). Cell nuclei spin in the absence of lamin b1. *J Biol Chem* **282**, 20015–20026.

Kalhor, R., Tjong, H., Jayathilaka, N., Alber, F. and Chen, L. (2011). Genome architectures revealed by tethered chromosome conformation capture and population-based modeling. *Nat Biotechnol* **30**, 90–98.

Kennedy, B. K., Barbie, D. A., Classon, M., Dyson, N. and Harlow, E. (2000). Nuclear organization of DNA replication in primary mammalian cells. *Genes Dev* **14**, 2855–2868.

Kim, J. B. and Spiegelman, B. M. (1996). ADD1/SREBP1 promotes adipocyte differentiation and gene expression linked to fatty acid metabolism. *Genes Dev* **10**, 1096–1107.

Kind, J., Pagie, L., Ortabozkoyun, H., Boyle, S., de Vries, S. S., Janssen, H., Amendola, M., Nolen, L. D., Bickmore, W. A. and van Steensel, B. (2013). Single-cell dynamics of genome-nuclear lamina interactions. *Cell* **153**, 178–192.

Kind, J., Pagie, L., de Vries, S. S., Nahidiazar, L., Dey, S. S., Bienko, M., Zhan, Y., Lajoie, B., de Graaf, C. A., Amendola, M., et al. (2015). Genome-wide maps of nuclear lamina interactions in

single human cells. *Cell* **163**, 134–147.

Kochin, V., Shimi, T., Torvaldson, E., Adam, S. A., Goldman, A., Pack, C.-G., Melo-Cardenas, J., Imanishi, S. Y., Goldman, R. D. and Eriksson, J. E. (2014). Interphase phosphorylation of lamin A. *J Cell Sci* **127**, 2683–2696.

Kolb, T., Maass, K., Hergt, M., Aebi, U. and Herrmann, H. (2011). Lamin A and lamin C form homodimers and coexist in higher complex forms both in the nucleoplasmic fraction and in the lamina of cultured human cells. *Nucleus* **2**, 425–433.

Kong, L., Schäfer, G., Bu, H., Zhang, Y., Zhang, Y. and Klocker, H. (2012). Lamin A/C protein is overexpressed in tissue-invading prostate cancer and promotes prostate cancer cell growth, migration and invasion through the PI3K/AKT/PTEN pathway. *Carcinogenesis* **33**, 751–759.

Korfali, N., Wilkie, G. S., Swanson, S. K., Srsen, V., de Las Heras, J., Batrakou, D. G., Malik, P., Zuleger, N., Kerr, A. R. W., Florens, L., et al. (2012). The nuclear envelope proteome differs notably between tissues. *Nucleus* **3**, 552–564.

Krimm, I., Ostlund, C., Gilquin, B., Couprie, J., Hossenlopp, P., Mornon, J.-P., Bonne, G., Courvalin, J.-C., Worman, H. J. and Zinn-Justin, S. (2002). The Ig-like structure of the C-terminal domain of lamin A/C, mutated in muscular dystrophies, cardiomyopathy, and partial lipodystrophy. *Structure* **10**, 811–823.

Kubben, N., Voncken, J. W., Demmers, J., Calis, C., van Almen, G., Pinto, Y. and Misteli, T. (2010). Identification of differential protein interactors of lamin A and progerin. *Nucleus* **1**, 513–525

Kuga, T., Nie, H., Kazami, T., Satoh, M., Matsushita, K., Nomura, F., Maeshima, K., Nakayama, Y. and Tomonaga, T. (2014). Lamin B2 prevents chromosome instability by ensuring proper mitotic chromosome segregation. *Oncogenesis* **3**, e94.

Kulashreshtha, M., Mehta, I. S., Kumar, P. and Rao, B. J. (2016). Chromosome territory relocation during DNA repair requires nuclear myosin 1 recruitment to chromatin mediated by ϒ-H2AX signaling. *Nucleic Acids Res* **44**, 8272–8291.

Kumaran, R. I. and Spector, D. L. (2008). A genetic locus targeted to the nuclear periphery in living cells maintains its transcriptional competence. *J Cell Biol* **180**, 51–65.

Kumaran, R. I., Muralikrishna, B. and Parnaik, V. K. (2002). Lamin A/C speckles mediate spatial organization of splicing factor compartments and RNA polymerase II transcription. *J Cell Biol* **159**, 783–793.

Lammerding, J., Schulze, P. C., Takahashi, T., Kozlov, S., Sullivan, T., Kamm, R. D., Stewart, C. L. and Lee, R. T. (2004). Lamin A/C deficiency causes defective nuclear mechanics and mechanotransduction. *J. Clin. Invest.* **113**, 370–378.

Lammerding, J., Fong, L. G., Ji, J. Y., Reue, K., Stewart, C. L., Young, S. G. and Lee, R. T. (2006). Lamins A and C but not lamin B1 regulate nuclear mechanics. *J Biol Chem* **281**, 25768–25780.

Le, H. Q., Ghatak, S., Yeung, C.-Y. C., Tellkamp, F., Günschmann, C., Dieterich, C., Yeroslaviz, A., Habermann, B., Pombo, A., Niessen, C. M., et al. (2016). Mechanical regulation of transcription controls Polycomb-mediated gene silencing during lineage commitment. *Nat Cell Biol* **18**, 864–875.

Lee, K. K., Haraguchi, T., Lee, R. S., Koujin, T., Hiraoka, Y. and Wilson, K. L. (2001). Distinct

functional domains in emerin bind lamin A and DNA-bridging protein BAF. *J Cell Sci* **114**, 4567–4573.

Lehner, C. F., Stick, R., Eppenberger, H. M. and Nigg, E. A. (1987). Differential expression of nuclear lamin proteins during chicken development. *J Cell Biol* **105**, 577–587.

Lin, F. and Worman, H. J. (1993). Structural organization of the human gene encoding nuclear lamin A and nuclear lamin C. *J Biol Chem* **268**, 16321–16326.

Lin, F. and Worman, H. J. (1995). Structural organization of the human gene (LMNB1) encoding nuclear lamin B1. *Genomics* **27**, 230–236.

Liu, B., Wang, J., Chan, K. M., Tjia, W. M., Deng, W., Guan, X., Huang, J., Li, K. M., Chau, P. Y., Chen, D. J., et al. (2005). Genomic instability in laminopathy-based premature aging. *Nat Med* **11**, 780–785.

Liu, Y., Wang, Y., Rusinol, A. E., Sinensky, M. S., Liu, J., Shell, S. M. and Zou, Y. (2008). Involvement of xeroderma pigmentosum group A (XPA) in progeria arising from defective maturation of prelamin A. *FASEB J* **22**, 603–611.

Liu, N.-A., Sun, J., Kono, K., Horikoshi, Y., Ikura, T., Tong, X., Haraguchi, T. and Tashiro, S. (2015). Regulation of homologous recombinational repair by lamin B1 in radiation-induced DNA damage. *FASEB J* **29**, 2514–2525.

Live Cell Imaging: A Laboratory Manual, Second Edition *Live Cell Imaging: A Laboratory Manual, Second Edition*.

Lloyd, D. J., Trembath, R. C. and Shackleton, S. (2002). A novel interaction between lamin A and SREBP1: implications for partial lipodystrophy and other laminopathies. *Hum Mol Genet* **11**, 769–777.

Loewinger, L. and McKeon, F. (1988). Mutations in the nuclear lamin proteins resulting in their aberrant assembly in the cytoplasm. *EMBO J* **7**, 2301–2309.

Lund, E., Oldenburg, A. R., Delbarre, E., Freberg, C. T., Duband-Goulet, I., Eskeland, R., Buendia, B. and Collas, P. (2013). Lamin A/C-promoter interactions specify chromatin state-dependent transcription outcomes. *Genome Res* **23**, 1580–1589.

Lund, E. G., Duband-Goulet, I., Oldenburg, A., Buendia, B. and Collas, P. (2015). Distinct features of lamin A-interacting chromatin domains mapped by ChIP-sequencing from sonicated or micrococcal nuclease-digested chromatin. *Nucleus* **6**, 30–39.

Lutz, R. J., Trujillo, M. A., Denham, K. S., Wenger, L. and Sinensky, M. (1992). Nucleoplasmic localization of prelamin A: implications for prenylation-dependent lamin A assembly into the nuclear lamina. *Proc Natl Acad Sci U S A* **89**, 3000–3004.

Machiels, B. M., Zorenc, A. H., Endert, J. M., Kuijpers, H. J., van Eys, G. J., Ramaekers, F. C. and Broers, J. L. (1996). An alternative splicing product of the lamin A/C gene lacks exon 10. *J Biol Chem* **271**, 9249–9253.

Maeno, H., Sugimoto, K. and Nakajima, N. (1995). Genomic structure of the mouse gene (Lmnb1) encoding nuclear lamin B1. *Genomics* **30**, 342–346.

Mahen, R., Hattori, H., Lee, M., Sharma, P., Jeyasekharan, A. D. and Venkitaraman, A. R. (2013).

A-type lamins maintain the positional stability of DNA damage repair foci in mammalian nuclei. *PLoS ONE* **8**, e61893.

Malhas, A., Lee, C. F., Sanders, R., Saunders, N. J. and Vaux, D. J. (2007). Defects in lamin B1 expression or processing affect interphase chromosome position and gene expression. *J Cell Biol* **176**, 593–603.

Malhas, A. N., Lee, C. F. and Vaux, D. J. (2009). Lamin B1 controls oxidative stress responses via Oct-1. *J Cell Biol* **184**, 45–55.

Manilal, S., Nguyen, T. M., Sewry, C. A. and Morris, G. E. (1996). The Emery-Dreifuss muscular dystrophy protein, emerin, is a nuclear membrane protein. *Hum Mol Genet* **5**, 801–808.

Manuelidis, L. (1985). Individual interphase chromosome domains revealed by in situ hybridization. *Hum Genet* **71**, 288–293.

Mao, R., Zielke, C. L., Zielke, H. R. and Pevsner, J. (2003). Global up-regulation of chromosome 21 gene expression in the developing Down syndrome brain. *Genomics* **81**, 457–467.

Martin, C., Chen, S., Maya-Mendoza, A., Lovric, J., Sims, P. F. G. and Jackson, D. A. (2009). Lamin B1 maintains the functional plasticity of nucleoli**.** ***J Cell Sci*** **122, 1551–1562.**

Martin, C., Chen, S. and Jackson, D. A. (2010). Inheriting nuclear organization: can nuclear lamins impart spatial memory during post-mitotic nuclear assembly? *Chromosome Res* **18**, 525–541.

Matsumoto, A., Hieda, M., Yokoyama, Y., Nishioka, Y., Yoshidome, K., Tsujimoto, M. and Matsuura, N. (2015). Global loss of a nuclear lamina component, lamin A/C, and LINC complex components SUN1, SUN2, and nesprin-2 in breast cancer. *Cancer Med* **4**, 1547–1557.

Mayer, R., Brero, A., von Hase, J., Schroeder, T., Cremer, T. and Dietzel, S. (2005). Common themes and cell type specific variations of higher order chromatin arrangements in the mouse. *BMC Cell Biol* **6**, 44.

McCord, R. P., Nazario-Toole, A., Zhang, H., Chines, P. S., Zhan, Y., Erdos, M. R., Collins, F. S., Dekker, J. and Cao, K. (2013). Correlated alterations in genome organization, histone methylation, and DNA-lamin A/C interactions in Hutchinson-Gilford progeria syndrome. *Genome Res* **23**, 260–269.

McKeon, F. D., Kirschner, M. W. and Caput, D. (1986). Homologies in both primary and secondary structure between nuclear envelope and intermediate filament proteins. *Nature* **319**, 463–468.

Meaburn, K. J., Levy, N., Toniolo, D. and Bridger, J. M. (2005). Chromosome positioning is largely unaffected in lymphoblastoid cell lines containing emerin or A-type lamin mutations. *Biochem Soc Trans* **33**, 1438–1440.

Meaburn, K. J., Cabuy, E., Bonne, G., Levy, N., Morris, G. E., Novelli, G., Kill, I. R. and Bridger, J. M. (2007). Primary laminopathy fibroblasts display altered genome organization and apoptosis. *Aging Cell* **6**, 139–153.

Mehta, I. S., Figgitt, M., Clements, C. S., Kill, I. R. and Bridger, J. M. (2007). Alterations to nuclear architecture and genome behavior in senescent cells. *Ann N Y Acad Sci* **1100**, 250–263.

Mehta, I. S., Elcock, L. S., Amira, M., Kill, I. R. and Bridger, J. M. (2008). Nuclear motors and

nuclear structures containing A-type lamins and emerin: is there a functional link? *Biochem Soc Trans* **36**, 1384–1388.

Mehta, I. S., Kulashreshtha, M., Chakraborty, S., Kolthur-Seetharam, U. and Rao, B. J. (2013). Chromosome territories reposition during DNA damage-repair response. *Genome Biol* **14**, R135.

Melcer, S., Gruenbaum, Y. and Krohne, G. (2007). Invertebrate lamins. *Exp Cell Res* **313**, 2157–2166.

Melcer, S., Hezroni, H., Rand, E., Nissim-Rafinia, M., Skoultchi, A., Stewart, C. L., Bustin, M. and Meshorer, E. (2012). Histone modifications and lamin A regulate chromatin protein dynamics in early embryonic stem cell differentiation. *Nat Commun* **3**, 910.

Melcher, R., Steinlein, C., Feichtinger, W., Müller, C. R., Menzel, T., Lührs, H., Scheppach, W. and Schmid, M. (2000). Spectral karyotyping of the human colon cancer cell lines SW480 and SW620. *Cytogenet Cell Genet* **88**, 145–152.

Meuleman, W., Peric-Hupkes, D., Kind, J., Beaudry, J.-B., Pagie, L., Kellis, M., Reinders, M., Wessels, L. and van Steensel, B. (2013). Constitutive nuclear lamina-genome interactions are highly conserved and associated with A/T-rich sequence. *Genome Res* **23**, 270–280.

Mewborn, S. K., Puckelwartz, M. J., Abuisneineh, F., Fahrenbach, J. P., Zhang, Y., MacLeod, H., Dellefave, L., Pytel, P., Selig, S., Labno, C. M., et al. (2010). Altered chromosomal positioning, compaction, and gene expression with a lamin A/C gene mutation. *PLoS ONE* **5**, e14342.

Moir, R. D., Montag-Lowy, M. and Goldman, R. D. (1994). Dynamic properties of nuclear lamins: lamin B is associated with sites of DNA replication. *J Cell Biol* **125**, 1201–1212.

Moir, R. D., Spann, T. P., Herrmann, H. and Goldman, R. D. (2000a). Disruption of nuclear lamin organization blocks the elongation phase of DNA replication. *J Cell Biol* **149**, 1179–1192.

Moir, R. D., Yoon, M., Khuon, S. and Goldman, R. D. (2000b). Nuclear lamins A and B1: different pathways of assembly during nuclear envelope formation in living cells. *J Cell Biol* **151**, 1155–1168.

Montes de Oca, R., Shoemaker, C. J., Gucek, M., Cole, R. N. and Wilson, K. L. (2009). Barrier-to-autointegration factor proteome reveals chromatin-regulatory partners. *PLoS ONE* **4**, e7050.

Mootha, V. K., Lindgren, C. M., Eriksson, K.-F., Subramanian, A., Sihag, S., Lehar, J., Puigserver, P., Carlsson, E., Ridderstråle, M., Laurila, E., et al. (2003). PGC-1alpha-responsive genes involved in oxidative phosphorylation are coordinately downregulated in human diabetes. *Nat Genet* **34**, 267–273.

Moss, S. F., Krivosheyev, V., de Souza, A., Chin, K., Gaetz, H. P., Chaudhary, N., Worman, H. J. and Holt, P. R. (1999). Decreased and aberrant nuclear lamin expression in gastrointestinal tract neoplasms. *Gut* **45**, 723–729.

Muchir, A., Wu, W. and Worman, H. J. (2009). Reduced expression of A-type lamins and emerin activates extracellular signal-regulated kinase in cultured cells. *Biochim Biophys Acta* 1792, 75–81

Muralikrishna, B. and Parnaik, V. K. (2001). SP3 and AP-1 mediate transcriptional activation of the lamin A proximal promoter. *Eur J Biochem* **268**, 3736–3743.

Muralikrishna, B., Thanumalayan, S., Jagatheesan, G., Rangaraj, N., Karande, A. A. and Parnaik, V. K. (2004). Immunolocalization of detergent-susceptible nucleoplasmic lamin A/C foci by a novel monoclonal antibody. *J Cell Biochem* **91**, 730–739.

Nabbi, A. and Riabowol, K. (2015). Rapid Isolation of Nuclei from Cells In Vitro. *Cold Spring Harb Protoc* **2015**, 769–772.

Nagano, T., Lubling, Y., Stevens, T. J., Schoenfelder, S., Yaffe, E., Dean, W., Laue, E. D., Tanay, A. and Fraser, P. (2013). Single-cell Hi-C reveals cell-to-cell variability in chromosome structure. *Nature* **502**, 59–64.

Neusser, M., Schubel, V., Koch, A., Cremer, T. and Müller, S. (2007). Evolutionarily conserved, cell type and species-specific higher order chromatin arrangements in interphase nuclei of primates. *Chromosoma* **116**, 307–320.

Okumura, K., Hosoe, Y. and Nakajima, N. (2004). c-Jun and Sp1 family are critical for retinoic acid induction of the lamin A/C retinoic acid-responsive element. *Biochem Biophys Res Commun* **320**, 487–492.

Ondrej, V., Lukásová, E., Krejcí, J., Matula, P. and Kozubek, S. (2008). Lamin A/C and polymeric actin in genome organization. *Mol Cells* **26**, 356–361.

Ostlund, C., Folker, E. S., Choi, J. C., Gomes, E. R., Gundersen, G. G. and Worman, H. J. (2009). Dynamics and molecular interactions of linker of nucleoskeleton and cytoskeleton (LINC) complex proteins. *J Cell Sci* **122**, 4099–4108.

Ozaki, T., Saijo, M., Murakami, K., Enomoto, H., Taya, Y. and Sakiyama, S. (1994). Complex formation between lamin A and the retinoblastoma gene product: identification of the domain on lamin A required for its interaction. *Oncogene* **9**, 2649–2653.

Pajerowski, J. D., Dahl, K. N., Zhong, F. L., Sammak, P. J. and Discher, D. E. (2007). Physical plasticity of the nucleus in stem cell differentiation. *Proc Natl Acad Sci U S A* **104**, 15619–15624.

Papadopoulos, N., Nicolaides, N. C., Liu, B., Parsons, R., Lengauer, C., Palombo, F., D'Arrigo, A., Markowitz, S., Willson, J. K. and Kinzler, K. W. (1995). Mutations of GTBP in genetically unstable cells. *Science* **268**, 1915–1917.

Patau, K., Smith, D. W., Therman, E., Inhorn, S. L. and Wagner, H. P. (1960). Multiple congenital anomaly caused by an extra autosome. *Lancet* **1**, 790–793.

Paz, N., Zabala, A., Royo, F., García-Orad, Á., Zugaza, J. L. and Parada, L. A. (2013). Combined fluorescent-chromogenic in situ hybridization for identification and laser microdissection of interphase chromosomes. *PLoS ONE* **8**, e60238.

Pekovic, V., Harborth, J., Broers, J. L. V., Ramaekers, F. C. S., van Engelen, B., Lammens, M., von Zglinicki, T., Foisner, R., Hutchison, C. and Markiewicz, E. (2007). Nucleoplasmic LAP2alpha-lamin A complexes are required to maintain a proliferative state in human fibroblasts. *J Cell Biol* **176**, 163–172.

Percipalle, P., Fomproix, N., Cavellán, E., Voit, R., Reimer, G., Krüger, T., Thyberg, J., Scheer, U., Grummt, I. and Farrants, A.-K. O. (2006). The chromatin remodelling complex WSTF-SNF2h interacts with nuclear myosin 1 and has a role in RNA polymerase I transcription. *EMBO Rep* **7**, 525–530.

Pestic-Dragovich, L., Stojiljkovic, L., Philimonenko, A. A., Nowak, G., Ke, Y., Settlage, R. E., Shabanowitz, J., Hunt, D. F., Hozak, P. and de Lanerolle, P. (2000). A myosin I isoform in the

nucleus. *Science* **290**, 337–341.

Peric-Hupkes, D. and van Steensel, B. (2010). Role of the nuclear lamina in genome organization and gene expression. *Cold Spring Harb Symp Quant Biol* **75**, 517–524.

Peric-Hupkes, D., Meuleman, W., Pagie, L., Bruggeman, S. W. M., Solovei, I., Brugman, W., Gräf, S., Flicek, P., Kerkhoven, R. M., van Lohuizen, M., et al. (2010). Molecular maps of the reorganization of genome-nuclear lamina interactions during differentiation. *Mol Cell* **38**, 603–613.

Peter, M., Nakagawa, J., Dorée, M., Labbé, J. C. and Nigg, E. A. (1990). In vitro disassembly of the nuclear lamina and M phase-specific phosphorylation of lamins by cdc2 kinase. *Cell* **61**, 591–602.

Petrova, N. V., Yakutenko, I. I., Alexeevski, A. V., Verbovoy, V. A., Razin, S. V. and Iarovaia, O. V. (2007). Changes in chromosome positioning may contribute to the development of diseases related to X-chromosome aneuploidy. *J Cell Physiol* **213**, 278–283.

Phillips-Cremins, J. E., Sauria, M. E. G., Sanyal, A., Gerasimova, T. I., Lajoie, B. R., Bell, J. S. K., Ong, C.-T., Hookway, T. A., Guo, C., Sun, Y., et al. (2013). Architectural protein subclasses shape 3D organization of genomes during lineage commitment. *Cell* **153**, 1281–1295.

Polioudaki, H., Kourmouli, N., Drosou, V., Bakou, A., Theodoropoulos, P. A., Singh, P. B., Giannakouros, T. and Georgatos, S. D. (2001). Histones H3/H4 form a tight complex with the inner nuclear membrane protein LBR and heterochromatin protein 1. *EMBO Rep* **2**, 920–925.

Qi, T., Tang, W., Wang, L., Zhai, L., Guo, L. and Zeng, X. (2011). G-actin participates in RNA polymerase II-dependent transcription elongation by recruiting positive transcription elongation factor b (P-TEFb). *J Biol Chem* **286**, 15171–15181.

Qi, R., Xu, N., Wang, G., Ren, H., Li, S., Lei, J., Lin, Q., Wang, L., Gu, X., Zhang, H., et al. (2015). The lamin-A/C-LAP2α-BAF1 protein complex regulates mitotic spindle assembly and positioning. *J Cell Sci* **128**, 2830–2841.

Ramdas, N. M. and Shivashankar, G. V. (2015). Cytoskeletal control of nuclear morphology and chromatin organization. *J Mol Biol* **427**, 695–706.

Ranade, D., Koul, S., Thompson, J., Prasad, K. B. and Sengupta, K. (2016). Chromosomal aneuploidies induced upon Lamin B2 depletion are mislocalized in the interphase nucleus. *Chromosoma*.

Reddy, K. L., Zullo, J. M., Bertolino, E. and Singh, H. (2008). Transcriptional repression mediated by repositioning of genes to the nuclear lamina. *Nature* **452**, 243–247.

Redwood, A. B., Perkins, S. M., Vanderwaal, R. P., Feng, Z., Biehl, K. J., Gonzalez-Suarez, I., Morgado-Palacin, L., Shi, W., Sage, J., Roti-Roti, J. L., et al. (2011). A dual role for A-type lamins in DNA double-strand break repair. *Cell Cycle* **10**, 2549–2560.

Ricke, R. M. and van Deursen, J. M. (2013). Aneuploidy in health, disease, and aging. *J Cell Biol* **201**, 11–21.

Ricke, R. M., Jeganathan, K. B. and van Deursen, J. M. (2011). Bub1 overexpression induces aneuploidy and tumor formation through Aurora B kinase hyperactivation. *J Cell Biol* **193**, 1049–1064.

Röber, R. A., Weber, K. and Osborn, M. (1989). Differential timing of nuclear lamin A/C expression in the various organs of the mouse embryo and the young animal: a developmental study. *Development* **105**, 365–378.

Roth, U., Razawi, H., Hommer, J., Engelmann, K., Schwientek, T., Müller, S., Baldus, S. E., Patsos, G., Corfield, A. P., Paraskeva, C., et al. (2010). Differential expression proteomics of human colorectal cancer based on a syngeneic cellular model for the progression of adenoma to carcinoma. *Proteomics* **10**, 194–202.

Saarinen, I., Mirtti, T., Seikkula, H., Boström, P. J. and Taimen, P. (2015). Differential Predictive Roles of A- and B-Type Nuclear Lamins in Prostate Cancer Progression. *PLoS ONE* **10**, e0140671.

Salpingidou, G., Smertenko, A., Hausmanowa-Petrucewicz, I., Hussey, P. J. and Hutchison, C. J. (2007). A novel role for the nuclear membrane protein emerin in association of the centrosome to the outer nuclear membrane. *J Cell Biol* **178**, 897–904.

Schardin, M., Cremer, T., Hager, H. D. and Lang, M. (1985). Specific staining of human chromosomes in Chinese hamster x man hybrid cell lines demonstrates interphase chromosome territories. *Hum Genet* **71**, 281–287.

Schirmer, E. C. and Foisner, R. (2007). Proteins that associate with lamins: many faces, many functions. *Exp Cell Res* **313**, 2167–2179.

Schirmer, E. C. and Gerace, L. (2004). The stability of the nuclear lamina polymer changes with the composition of lamin subtypes according to their individual binding strengths. *J Biol Chem* **279**, 42811–42817.

Schirmer, E. C., Guan, T. and Gerace, L. (2001). Involvement of the lamin rod domain in heterotypic lamin interactions important for nuclear organization. *J Cell Biol* **153**, 479–489.

Schlimgen, R. J., Reddy, K. L., Singh, H. and Krangel, M. S. (2008). Initiation of allelic exclusion by stochastic interaction of Tcrb alleles with repressive nuclear compartments. *Nat Immunol* **9**, 802–809.

Schmälter, A.-K., Kuzyk, A., Righolt, C. H., Neusser, M., Steinlein, O. K., Müller, S. and Mai, S. (2014). Distinct nuclear orientation patterns for mouse chromosome 11 in normal B lymphocytes. *BMC Cell Biol* **15**, 22.

Schreiber, K. H. and Kennedy, B. K. (2013). When lamins go bad: nuclear structure and disease. *Cell* **152**, 1365–1375.

Sengupta, K., Upender, M. B., Barenboim-Stapleton, L., Nguyen, Q. T., Wincovitch, S. M., Garfield, S. H., Difilippantonio, M. J. and Ried, T. (2007). Artificially introduced aneuploid chromosomes assume a conserved position in colon cancer cells. *PLoS ONE* **2**, e199.

Shachar, S., Voss, T. C., Pegoraro, G., Sciascia, N. and Misteli, T. (2015). Identification of Gene Positioning Factors Using High-Throughput Imaging Mapping. *Cell* **162**, 911–923.

Shah, P. P., Donahue, G., Otte, G. L., Capell, B. C., Nelson, D. M., Cao, K., Aggarwala, V., Cruickshanks, H. A., Rai, T. S., McBryan, T., et al. (2013). Lamin B1 depletion in senescent cells triggers large-scale changes in gene expression and the chromatin landscape. *Genes Dev* **27**, 1787–1799.

Shete, A., Rao, P., Pati, D. and Merchant, F. (2014). Spatial quantitation of FISH signals in diploid versus aneuploid nuclei. *Cytometry A* **85**, 339–352.

Shimi, T., Pfleghaar, K., Kojima, S., Pack, C.-G., Solovei, I., Goldman, A. E., Adam, S. A., Shumaker, D. K., Kinjo, M., Cremer, T., et al. (2008). The A- and B-type nuclear lamin networks: microdomains involved in chromatin organization and transcription. *Genes Dev* **22**, 3409–3421.

Shimi, T., Butin-Israeli, V., Adam, S. A., Hamanaka, R. B., Goldman, A. E., Lucas, C. A., Shumaker, D. K., Kosak, S. T., Chandel, N. S. and Goldman, R. D. (2011). The role of nuclear lamin B1 in cell proliferation and senescence. *Genes Dev* **25**, 2579–2593.

Shimi, T., Kittisopikul, M., Tran, J., Goldman, A. E., Adam, S. A., Zheng, Y., Jaqaman, K. and Goldman, R. D. (2015). Structural organization of nuclear lamins A, C, B1, and B2 revealed by superresolution microscopy. *Mol Biol Cell* **26**, 4075–4086.

Shlien, A. and Malkin, D. (2009). Copy number variations and cancer. *Genome Med* **1**, 62

Shumaker, D. K., Solimando, L., Sengupta, K., Shimi, T., Adam, S. A., Grunwald, A., Strelkov, S. V., Aebi, U., Cardoso, M. C. and Goldman, R. D. (2008). The highly conserved nuclear lamin Ig-fold binds to PCNA: its role in DNA replication. *J Cell Biol* **181**, 269–280.

Simon, D. N. and Wilson, K. L. (2013). Partners and post-translational modifications of nuclear lamins. *Chromosoma* **122**, 13–31.

Simon, D. N., Zastrow, M. S. and Wilson, K. L. (2010). Direct actin binding to A- and B-type lamin tails and actin filament bundling by the lamin A tail. *Nucleus* **1**, 264–272.

Sinensky, M., Fantle, K., Trujillo, M., McLain, T., Kupfer, A. and Dalton, M. (1994). The processing pathway of prelamin A. *J Cell Sci* **107 (Pt 1)**, 61–67.

Singh, M., Hunt, C. R., Pandita, R. K., Kumar, R., Yang, C.-R., Horikoshi, N., Bachoo, R., Serag, S., Story, M. D., Shay, J. W., et al. (2013). Lamin A/C depletion enhances DNA damage-induced stalled replication fork arrest. *Mol Cell Biol* **33**, 1210–1222.

Smeets, D., Markaki, Y., Schmid, V. J., Kraus, F., Tattermusch, A., Cerase, A., Sterr, M., Fiedler, S., Demmerle, J., Popken, J., et al. (2014). Three-dimensional super-resolution microscopy of the inactive X chromosome territory reveals a collapse of its active nuclear compartment harboring distinct Xist RNA foci. *Epigenetics Chromatin* **7**, 8.

Solovei, I., Kreysing, M., Lanctôt, C., Kösem, S., Peichl, L., Cremer, T., Guck, J. and Joffe, B. (2009). Nuclear architecture of rod photoreceptor cells adapts to vision in mammalian evolution. *Cell* **137**, 356–368.

Solovei, I., Wang, A. S., Thanisch, K., Schmidt, C. S., Krebs, S., Zwerger, M., Cohen, T. V., Devys, D., Foisner, R., Peichl, L., et al. (2013). LBR and lamin A/C sequentially tether peripheral heterochromatin and inversely regulate differentiation. *Cell* **152**, 584–598.

Spann, T. P., Moir, R. D., Goldman, A. E., Stick, R. and Goldman, R. D. (1997). Disruption of nuclear lamin organization alters the distribution of replication factors and inhibits DNA synthesis. *J Cell Biol* **136**, 1201–1212.

Spann, T. P., Goldman, A. E., Wang, C., Huang, S. and Goldman, R. D. (2002). Alteration of nuclear lamin organization inhibits RNA polymerase II-dependent transcription. *J Cell Biol* **156**, 603–608.

Spichal, M., Brion, A., Herbert, S., Cournac, A., Marbouty, M., Zimmer, C., Koszul, R. and Fabre, E. (2016). Evidence for a dual role of actin in regulating chromosome organization and dynamics in yeast. *J Cell Sci* **129**, 681–692.

Stick, R. (1992). The gene structure of Xenopus nuclear lamin A: a model for the evolution of A-type from B-type lamins by exon shuffling. *Chromosoma* **101**, 566–574.

Stick, R. (1994). The gene structure of B-type nuclear lamins of Xenopus laevis: implications for the evolution of the vertebrate lamin family. *Chromosome Res* **2**, 376–382.

Stierlé, V., Couprie, J., Ostlund, C., Krimm, I., Zinn-Justin, S., Hossenlopp, P., Worman, H. J., Courvalin, J.-C. and Duband-Goulet, I. (2003). The carboxyl-terminal region common to lamins A and C contains a DNA binding domain. *Biochemistry* **42**, 4819–4828.

Stingele, S., Stoehr, G., Peplowska, K., Cox, J., Mann, M. and Storchova, Z. (2012). Global analysis of genome, transcriptome and proteome reveals the response to aneuploidy in human cells. *Mol Syst Biol* **8**, 608.

Stuurman, N., Heins, S. and Aebi, U. (1998). Nuclear lamins: their structure, assembly, and interactions. *J Struct Biol* **122**, 42–66.

Subramanian, A., Tamayo, P., Mootha, V. K., Mukherjee, S., Ebert, B. L., Gillette, M. A., Paulovich, A., Pomeroy, S. L., Golub, T. R., Lander, E. S., et al. (2005). Gene set enrichment analysis: a knowledge-based approach for interpreting genome-wide expression profiles. *Proc Natl Acad Sci U S A* **102**, 15545–15550.

Sullivan, T., Escalante-Alcalde, D., Bhatt, H., Anver, M., Bhat, N., Nagashima, K., Stewart, C. L. and Burke, B. (1999). Loss of A-type lamin expression compromises nuclear envelope integrity leading to muscular dystrophy. *J Cell Biol* **147**, 913–920.

Sun, S., Xu, M. Z., Poon, R. T., Day, P. J. and Luk, J. M. (2010). Circulating Lamin B1 (LMNB1) biomarker detects early stages of liver cancer in patients. *J Proteome Res* **9**, 70–78.

Swift, J., Ivanovska, I. L., Buxboim, A., Harada, T., Dingal, P. C. D. P., Pinter, J., Pajerowski, J. D., Spinler, K. R., Shin, J.-W., Tewari, M., et al. (2013). Nuclear lamin-A scales with tissue stiffness and enhances matrix-directed differentiation. *Science* **341**, 1240104.

Szczerbal, I., Foster, H. A. and Bridger, J. M. (2009). The spatial repositioning of adipogenesis genes is correlated with their expression status in a porcine mesenchymal stem cell adipogenesis model system. *Chromosoma* **118**, 647–663.

Tagawa, Y., Sawai, T., Nakagoe, T., Morinaga, M., Yasutake, T., Ayabe, H. and Tomita, M. (1996). Numerical aberrations of chromosomes 11 and 17 in colorectal adenocarcinomas. *Surg Today* **26**, 869–874.

Taimen, P., Pfleghaar, K., Shimi, T., Möller, D., Ben-Harush, K., Erdos, M. R., Adam, S. A., Herrmann, H., Medalia, O., Collins, F. S., et al. (2009). A progeria mutation reveals functions for lamin A in nuclear assembly, architecture, and chromosome organization. *Proc Natl Acad Sci U S A* **106**, 20788–20793.

Tan, N. Y. and Khachigian, L. M. (2009). Sp1 phosphorylation and its regulation of gene transcription. *Mol Cell Biol* **29**, 2483–2488.

Tanabe, H., Müller, S., Neusser, M., von Hase, J., Calcagno, E., Cremer, M., Solovei, I., Cremer, C. and Cremer, T. (2002). Evolutionary conservation of chromosome territory arrangements in cell nuclei from higher primates. *Proc Natl Acad Sci U S A* **99**, 4424–4429.

Tang, C. W., Maya-Mendoza, A., Martin, C., Zeng, K., Chen, S., Feret, D., Wilson, S. A. and Jackson, D. A. (2008). The integrity of a lamin-B1-dependent nucleoskeleton is a fundamental determinant of RNA synthesis in human cells. *J Cell Sci* **121**, 1014–1024.

Taniura, H., Glass, C. and Gerace, L. (1995). A chromatin binding site in the tail domain of nuclear lamins that interacts with core histones. *J Cell Biol* **131**, 33–44.

Theodor Boveri, 1909 *Theodor Boveri, 1909*.

Thompson, S. L. and Compton, D. A. (2008). Examining the link between chromosomal instability and aneuploidy in human cells. *J Cell Biol* **180**, 665–672.

Toh, K. C., Ramdas, N. M. and Shivashankar, G. V. (2015). Actin cytoskeleton differentially alters the dynamics of lamin A, HP1α and H2B core histone proteins to remodel chromatin condensation state in living cells. *Integr Biol (Camb)* **7**, 1309–1317.

Tojkander, S., Gateva, G. and Lappalainen, P. (2012). Actin stress fibers--assembly, dynamics and biological roles. *J Cell Sci* **125**, 1855–1864.

Torvaldson, E., Kochin, V. and Eriksson, J. E. (2015). Phosphorylation of lamins determine their structural properties and signaling functions. *Nucleus* **6**, 166–171.

Towbin, B. D., González-Aguilera, C., Sack, R., Gaidatzis, D., Kalck, V., Meister, P., Askjaer, P. and Gasser, S. M. (2012). Step-wise methylation of histone H3K9 positions heterochromatin at the nuclear periphery. *Cell* **150**, 934–947.

Tsai, M.-Y., Wang, S., Heidinger, J. M., Shumaker, D. K., Adam, S. A., Goldman, R. D. and Zheng, Y. (2006). A mitotic lamin B matrix induced by RanGTP required for spindle assembly. *Science* **311**, 1887–1893.

Umar, A., Buermeyer, A. B., Simon, J. A., Thomas, D. C., Clark, A. B., Liskay, R. M. and Kunkel, T. A. (1996). Requirement for PCNA in DNA mismatch repair at a step preceding DNA resynthesis. *Cell* **87**, 65–73.

Upender, M. B., Habermann, J. K., McShane, L. M., Korn, E. L., Barrett, J. C., Difilippantonio, M. J. and Ried, T. (2004). Chromosome transfer induced aneuploidy results in complex dysregulation of the cellular transcriptome in immortalized and cancer cells. *Cancer Res* **64**, 6941–6949.

Vaara, M., Itkonen, H., Hillukkala, T., Liu, Z., Nasheuer, H.-P., Schaarschmidt, D., Pospiech, H. and Syväoja, J. E. (2012). Segregation of replicative DNA polymerases during S phase: DNA polymerase ε, but not DNA polymerases α/δ, are associated with lamins throughout S phase in human cells. *J Biol Chem* **287**, 33327–33338.

Van Berkum, N. L., Lieberman-Aiden, E., Williams, L., Imakaev, M., Gnirke, A., Mirny, L. A., Dekker, J. and Lander, E. S. (2010). Hi-C: a method to study the three-dimensional architecture of genomes. *J Vis Exp*.

Vaughan, A., Alvarez-Reyes, M., Bridger, J. M., Broers, J. L., Ramaekers, F. C., Wehnert, M., Morris, G. E., Whitfield WGF and Hutchison, C. J. (2001). Both emerin and lamin C depend on

lamin A for localization at the nuclear envelope. *J Cell Sci* **114**, 2577–2590.

Vergnes, L., Péterfy, M., Bergo, M. O., Young, S. G. and Reue, K. (2004). Lamin B1 is required for mouse development and nuclear integrity. *Proc Natl Acad Sci U S A* **101**, 10428–10433.

Willis, N. D., Cox, T. R., Rahman-Casañs, S. F., Smits, K., Przyborski, S. A., van den Brandt, P., van Engeland, M., Weijenberg, M., Wilson, R. G., de Bruïne, A., et al. (2008). Lamin A/C is a risk biomarker in colorectal cancer. *PLoS ONE* **3**, e2988.

Whitehouse, I., Flaus, A., Cairns, B. R., White, M. F., Workman, J. L. and Owen-Hughes, T. (1999). Nucleosome mobilization catalysed by the yeast SWI/SNF complex. *Nature* **400**, 784–787.

Worman, H. J., Yuan, J., Blobel, G. and Georgatos, S. D. (1988). A lamin B receptor in the nuclear envelope. *Proc Natl Acad Sci U S A* **85**, 8531–8534.

Wu, Z., Wu, L., Weng, D., Xu, D., Geng, J. and Zhao, F. (2009). Reduced expression of lamin A/C correlates with poor histological differentiation and prognosis in primary gastric carcinoma. *J Exp Clin Cancer Res* **28**, 8.

Yabuta, T., Shinmura, K., Yamane, A., Yamaguchi, S., Takenoshita, S. and Yokota, J. (2004). Effect of exogenous MSH6 and POLD1 expression on the mutation rate of the HPRT locus in a human colon cancer cell line with mutator phenotype, DLD-1. *Int J Oncol* **24**, 697–702.

Yang, S. H., Jung, H.-J., Coffinier, C., Fong, L. G. and Young, S. G. (2011). Are B-type lamins essential in all mammalian cells? *Nucleus* **2**, 562–569.

Ye, Q. and Worman, H. J. (1994). Primary structure analysis and lamin B and DNA binding of human LBR, an integral protein of the nuclear envelope inner membrane. *J Biol Chem* **269**, 11306–11311.

Ye, Q., Callebaut, I., Pezhman, A., Courvalin, J. C. and Worman, H. J. (1997). Domain-specific interactions of human HP1-type chromodomain proteins and inner nuclear membrane protein LBR. *J Biol Chem* **272**, 14983–14989.

Young, S. G., Jung, H.-J., Coffinier, C. and Fong, L. G. (2012). Understanding the roles of nuclear A- and B-type lamins in brain development. *J Biol Chem* **287**, 16103–16110.

Zhang, H.-M., Chen, H., Liu, W., Liu, H., Gong, J., Wang, H. and Guo, A.-Y. (2012). AnimalTFDB: a comprehensive animal transcription factor database. *Nucleic Acids Res* **40**, D144–9.

Zhang, W. and Liu, H. T. (2002). MAPK signal pathways in the regulation of cell proliferation in mammalian cells. *Cell Res* **12**, 9–18.

Zhen, Y.-Y., Libotte, T., Munck, M., Noegel, A. A. and Korenbaum, E. (2002). NUANCE, a giant protein connecting the nucleus and actin cytoskeleton. *J Cell Sci* **115**, 3207–3222.

Zhong, Z., Wilson, K. L. and Dahl, K. N. (2010). Beyond lamins other structural components of the nucleoskeleton. *Methods Cell Biol* **98**, 97–119.

Zink, D., Bornfleth, H., Visser, A., Cremer, C. and Cremer, T. (1999). Organization of early and late replicating DNA in human chromosome territories. *Exp Cell Res* **247**, 176–188.

Zorn, C., Cremer, T., Cremer, C. and Zimmer, J. (1976). Laser UV microirradiation of interphase nuclei and post-treatment with caffeine. A new approach to establish the arrangement of interphase chromosomes. *Hum Genet* **35**, 83–89.

Zorn, C., Cremer, C., Cremer, T. and Zimmer, J. (1979). Unscheduled DNA synthesis after partial UV irradiation of the cell nucleus. Distribution in interphase and metaphase. *Exp Cell Res* **124**, 111–119.

Zullo, J. M., Demarco, I. A., Piqué-Regi, R., Gaffney, D. J., Epstein, C. B., Spooner, C. J., Luperchio, T. R., Bernstein, B. E., Pritchard, J. K., Reddy, K. L., et al. (2012). DNA sequence-dependent compartmentalization and silencing of chromatin at the nuclear lamina. *Cell* **149**, 1474–1487.

Zuo, B., Yang, J., Wang, F., Wang, L., Yin, Y., Dan, J., Liu, N. and Liu, L. (2012). Influences of lamin A levels on induction of pluripotent stem cells. *Biol Open* **1**, 1118–1127.

Zwerger, M., Roschitzki-Voser, H., Zbinden, R., Denais, C., Herrmann, H., Lammerding, J., Grütter, M. G. and Medalia, O. (2015). Altering lamina assembly reveals lamina-dependent and -independent functions for A-type lamins. *J Cell Sci* **128**, 3607–3620.

Chromosoma
DOI 10.1007/s00412-016-0580-y

RESEARCH ARTICLE

Chromosomal aneuploidies induced upon Lamin B2 depletion are mislocalized in the interphase nucleus

Devika Ranade[1] · **Shivsmriti Koul**[1] · **Joyce Thompson**[1] · **Kumar Brajesh Prasad**[1] · **Kundan Sengupta**[1]

Received: 30 May 2015 / Revised: 28 January 2016 / Accepted: 9 February 2016

Abstract Chromosome territories assume non-random positions in the interphase nucleus with gene-rich chromosomes localized toward the nuclear interior and gene-poor chromosome territories toward the nuclear periphery. Lamins are intermediate filament proteins of the inner nuclear membrane required for the maintenance of nuclear structure and function. Here, we show using whole-genome expression profiling that Lamin A/C or Lamin B2 depletion in an otherwise diploid colorectal cancer cell line (DLD1) deregulates transcript levels from specific chromosomes. Further, three-dimensional fluorescence in situ hybridization (3D-FISH) analyses of a subset of these transcriptionally deregulated chromosome territories revealed that the diploid chromosome territories in Lamin-depleted cells largely maintain conserved positions in the interphase nucleus in a gene-density-dependent manner. In addition, chromosomal aneuploidies were induced in ~25 % of Lamin A/C or Lamin B2-depleted cells. Sub-populations of these aneuploid cells consistently showed a mislocalization of the gene-rich aneuploid chromosome 19 territory toward the nuclear periphery, while gene-poor aneuploid chromosome 18 territory was mislocalized toward the nuclear interior predominantly upon Lamin B2 than Lamin A/C depletion. In addition, a candidate gene locus *ZNF570* (Chr.19q13.12) significantly overexpressed upon Lamin B2 depletion was remarkably repositioned away from the nuclear lamina. Taken together, our studies strongly implicate an overarching role for Lamin B2 in the maintenance of nuclear architecture since loss of Lamin B2 relieves the spatial positional constraints required for maintaining conserved localization of aneuploid chromosome territories in the interphase nucleus.

Keywords Aneuploidy · Chromosome territories · Lamins · Transcription · Cancer cells · Nucleus · Chromosome positioning

Electronic supplementary material The online version of this article (doi:10.1007/s00412-016-0580-y) contains supplementary material, which is available to authorized users.

✉ Kundan Sengupta
kunsen@iiserpune.ac.in

[1] Biology, Indian Institute of Science Education and Research, Pune, Main Building, Homi Bhabha Road, Pashan, Pune, Maharashtra 411008, India

Introduction

Chromosome territories (CTs) assume a unique sub-volume in the three-dimensional interphase nucleus. Gene-rich CTs are positioned toward the nuclear interior, while gene-poor chromosomes are closer to the nuclear periphery (Cremer et al. 2001; Croft et al. 1999). Human CTs 18 (~80 Mbp) and 19 (~59 Mbp) are of comparable DNA content, but of divergent gene densities of ~8.2 genes/Mbp and ~37.0 genes/Mbp, respectively. Chr.18 is peripheral, while Chr.19 is located toward the nuclear center in the interphase nucleus (Cremer et al. 2001; Croft et al. 1999). Such an arrangement is conserved in evolution, suggesting a functional significance for non-random chromosome positions (Neusser et al. 2007; Tanabe et al. 2002). Chromosome positioning is altered in biological processes such as senescence, adipocyte differentiation, spermatogenesis, immune responses, and DNA damage (Foster et al. 2005; Galiova et al. 2004; Mehta et al. 2007, 2013; Szczerbal et al. 2009).

The organization of CTs has been corroborated by high-throughput genomic approaches that map the physical proximity of chromatin contacts as a function of their ligation frequencies (van Berkum et al. 2010). Chromosome

Published online: 27 February 2016

conformation capture studies (3C, 4C, 5C, and Hi-C) revealed enhanced *cis* interactions of sub-genomic regions of a chromosome in the nucleus, as opposed to interactions in *trans*, thereby also suggesting a territorial confinement of chromosomes (Kalhor et al. 2012). Moreover, computational contour maps from chromatin contact frequencies recapitulate a greater enrichment of gene-rich chromosomes toward the nuclear center (Kalhor et al. 2012; Lieberman-Aiden et al. 2009).

Gene loci are significantly smaller (~10^4–10^6-fold) than CTs and exhibit a non-random organization, since overexpressed genes typically "loop-out" of their CT (Chambeyron and Bickmore 2004; Volpi et al. 2000). Hi-C data revealed that the genome is organized in ~1 Mb sized topologically associated domains (TADs) that showed a higher cross-linking frequency with each other as compared to other regions of the genome (Dixon et al. 2012). Gene loci within a TAD have increased proximity in the human X chromosome as shown by three-dimensional fluorescence in situ hybridization (3D-FISH) (Nora et al. 2012), which suggested a concordance between single-cell imaging and 5C. However, the 3D localization of the Hox gene cluster as revealed by 3D-FISH showed a greater decompaction as compared to 5C approaches, suggesting a disagreement between single-cell versus population assays and reiterating the fundamental importance of microscopy-based single-cell assays in a context-specific manner (Williamson et al. 2014).

The molecular mechanisms that regulate chromosome positioning and genome organization in the interphase nucleus are largely unclear. Lamins, Lamin B receptor (LBR), emerin, actin, and CCCTC-binding Factor (CTCF) have been implicated in the maintenance of chromosome organization and chromatin contacts (Malhas et al. 2007; Meaburn et al. 2007; Ondrej et al. 2008; Phillips-Cremins et al. 2013; Shimi et al. 2008; Solovei et al. 2013; Taimen et al. 2009). Lamins serve to maintain nuclear structure and genome organization. Lamins are type V intermediate filaments that form coiled coil structures beneath the inner nuclear membrane (Goldman et al. 1986). In higher eukaryotes, A-type Lamins are encoded by a single gene *LMNA* (that codes for two splice variants—Lamin A and Lamin C) and B type (Lamin B1 and B2 are encoded by two different genes—*LMNB1* and *LMNB2*, respectively) (Hoger et al. 1990; Zewe et al. 1991). B-type Lamins are expressed during all stages of development, while A-type Lamins are expressed primarily in differentiated cells (Constantinescu et al. 2006; Rober et al. 1989). Laminopathies are a group of diseases due to mutations in Lamins, which show altered nuclear shapes, gene expression, and chromatin organization (Burke and Stewart 2002; Taimen et al. 2009). Both A- and B-type Lamins are involved in wide range of cellular processes such as replication, transcription, cell division, DNA damage repair, differentiation, and senescence (Butin-Israeli et al. 2015; Martin et al. 2010; Shimi et al. 2011; Shumaker et al. 2008; Spann et al. 2002; Swift et al. 2013; Tang et al. 2008). Furthermore, Lamins exhibit cell-type-specific expression levels and function (de Las Heras et al. 2013; Swift et al. 2013; Yang et al. 2011). In addition, the relative stoichiometry of A- and B-type Lamins is often cell-type specific and the ratio of A/B-type Lamins determines mechanical properties of nuclei (Swift et al. 2013).

Nuclear Lamins contribute to the organization of CTs by associating with chromatin in 'Lamina-associated domains' (LADs) during interphase (Guelen et al. 2008). LADs are enriched in Lamina-associated sequences (LASs) and are ~0.1–10-Mb regions characterized by low density of coding genes, high density of repetitive sequences, and inactive histone mark H3K9me2/3 (Belmont et al. 1993; Guelen et al. 2008; Harr et al. 2015; Towbin et al. 2012; Zullo et al. 2012). Constitutive LADs are conserved across cell types and correlate with a repressive state of chromatin (Meuleman et al. 2013). Live imaging assays performed on LADs using a fluorescently coupled m6A-Tracer reveal that they are dynamic, stochastic, and not solely confined to the nuclear periphery, suggesting roles for Lamins in the nuclear interior and periphery (Kind et al. 2013). CTs are mislocalized in cells expressing mutant Lamin A in progeria and cardiomyopathies (Meaburn et al. 2007; Mewborn et al. 2010). Lamin A and B1 depletion in fibroblasts and HeLa cells also showed mislocalized CTs (Malhas et al. 2007; Meaburn et al. 2007; Shimi et al. 2008; Tang et al. 2008).

Furthermore, Lamin A forms a complex with LAP2α and BAF and is involved in proper spindle orientation and assembly (Qi et al. 2015). B-type Lamins are also a part of the mitotic spindle matrix in *Xenopus laevis* and human cells (Goodman et al. 2010; Tsai et al. 2006). Lamin B2 maintains genomic stability and chromosome segregation in colorectal cancer cells (Kuga et al. 2014). Thus, Lamins are unique, since they are required for genome organization, chromosomal stability, and ploidy in mitosis. However, a rather unappreciated role for Lamins is in the spatial organization of diploid and aneuploid chromosome territories in the interphase nucleus.

Aneuploidy is a hallmark of several cancer and developmental disorders. In general, chromosomes assume a gene-density-based positioning pattern in cancer cells (Cremer et al. 2003). More specifically, cancer cells from several epithelial cancers are characterized by aneuploidy with a complex pattern of chromosomal gains and losses (Cimini and Degrassi 2005) that may show changes in chromosome positioning. Notably, CT18 and CT19 are more proximal to one another in colon and cervical cancer cell nuclei as compared to normal cells (Cremer et al. 2003). Chromosomal trisomies generated by artificial introduction of either gene-poor (Chr.7, Chr.18, peripheral) or gene-rich (Chr.19, central) chromosomes assume conserved locations in the nucleus consistent with their gene densities (Sengupta et al. 2007). Human X

chromosome is altered from a predominantly central to a more peripheral location in X chromosome aneuploidies (XXXXY) (Petrova et al. 2007). Interestingly, while two copies of chromosome 21 territory are in closer proximity as compared to the third copy in cells derived from Down's syndrome patients (Paz et al. 2013), spontaneous trisomy for Chr.12 in human embryonic stem cell line (WA09) also shows an altered position of the trisomic chromosome (Shete et al. 2014). However, given the overarching function of Lamins in regulating ploidy and genome organization, the specific role of Lamins in the spatial organization of aneuploid CTs is largely unclear.

Here, we have studied the role of Lamins in regulation of transcription and spatial organization of the genome in diploid DLD1 cells. Lamin B2 depletion in DLD1 cells shows chromosomal instability (CIN) (Kuga et al. 2014). We show that specific chromosomes are transcriptionally deregulated upon Lamin A/C and Lamin B2 knockdown. Remarkably, transcriptionally deregulated gene-rich or gene-poor chromosomes in Lamin-depleted diploid cells largely assume conserved chromosome positions as revealed by 3D-FISH. However, aneuploid chromosomes were mislocalized in subpopulations of Lamin B2 and not Lamin A/C-depleted cells. In addition, candidate gene loci were repositioned upon Lamin B2 depletion, consistent with an increase in their gene expression levels. Taken together, we propose the involvement of Lamin B2 in mechanisms that regulate spatial organization of aneuploid CTs in the interphase nucleus.

Materials and methods

Cell culture

DLD1 colorectal adenocarcinoma cells were obtained from the lab of Thomas Ried, NCI/NIH, Bethesda, USA, and karyotyped independently by 4′,6-diamidino-2-phenylindole (DAPI) to ascertain karyotypic stability across passages. DLD1 cells were grown in RPMI 1640 media (Invitrogen, Cat. No. 11875) supplemented with 10 % fetal bovine serum (FBS, Invitrogen, Cat. No. 6140-079 Carlsbad, USA) and antibiotics penicillin (100 U/mL) and streptomycin (100 μg/mL) (Invitrogen, Cat. No. 15070-063) at 37 °C with 5 % CO_2.

Small interfering RNA transfection

The sequences of the small interfering RNA (siRNA) oligonucleotides targeting Lamins are as follows: *LMNA/C*: 5′-CAGUCUGCUGAGAGGAACA-3′, *LMNB2*: 5′- GAGCA GGAGAUGACGGAGA-3′, *LMNB1*: 5′- AGACAA AGAGAGAGAGAUG-3′ and *LMNB2* scrambled: 5′-GG AAGCGUAGACGGAAGAG-3′. DLD1 cells were transfected with 100 nM siRNA oligonucleotide using Lipofectamine RNAiMax (Invitrogen 13778-075) in media with reduced serum (OptiMEM, Invitrogen Cat. No. 31985-070). Control siRNAs used were On-target Plus non-targeting siRNA controls (Dharmacon-D-001810-01-20, D-001810-02-20) or siLacZ: 5′-CGUACGCGGAAUACUUCGA-3′; positive control is a siRNA against the gene *PLK1* (si*PLK1*)—polo-like kinase—5′-UGACCUACAUCGA CGAGAA-3′. The uptake of transfection mix was for 6 h, followed by replenishment of complete growth medium. The total duration of the knockdown was for 48 h at 37 °C.

Western blotting

Cell lysates were prepared using radioimmunoprecipitation assay (RIPA) buffer and quantified using bicinchoninic acid (BCA) kit (Pierce, Cat. No. 23225). Equal amounts of the protein were boiled in 4× Laemmli buffer and resolved on a 10 % acrylamide–bisacrylamide gel. The protein was transferred to an activated PVDF membrane at a constant voltage of 90 V for 90 min. The membrane was blocked in 5 % non-fat dried milk prepared in 1× Tris-buffered saline–Tween 20 (1× TBST) for 1 h at room temperature (RT). Primary antibodies used were as follows: Rabbit anti-Lamin A/C (Epitomics (2966-S), 1:5000), Rabbit anti-Lamin B1 (Abcam (ab16048), 1:1000), Mouse anti-Lamin B2 (Abcam (ab8983), 1:400), Mouse anti-Actin (Abcam (ab3280), 1:400), and Rabbit anti-GAPDH (Sigma (G9545), 1:5000). Antibody dilutions were prepared in 0.5 % non-fat dried milk in 1× TBST and incubated overnight at 4 °C or for 3 h at RT. Secondary antibodies used were sheep anti-mouse IgG–horseradish peroxidase (HRP) (GE cat no NA9310V, 1:5000) and donkey anti-rabbit IgG HRP (GE NA9340V, 1:10,000) for 1 h at RT. Blots were developed using chemiluminescent substrate GE ECL Prime (89168-782), Thermo ECL Western Blot Substrate (32132), and images were acquired at incremental exposures of 10 s under a chemiluminescence system (LAS4000, GE).

Immunofluorescence assay

Cells grown on coverslips (18 × 18 or 22 × 22 mm^2) were briefly washed using 1× phosphate-buffered saline (PBS, pH 7.4) (5 min, twice at RT) followed by cold cytoskeletal (CSK) buffer (0.1 M NaCl, 0.3 M sucrose, 3 mM $MgCl_2$, 10 mM PIPES (pH 7.4), 0.5 % Triton X-100) treatment on ice for 5 min. Cells were fixed in 4 % paraformaldehyde (PFA) (prepared in 1× PBS, pH 7.4) for 10 minutes at RT followed by permeabilization in 0.5 % Triton X-100 (prepared in 1× PBS) for 10 min. Blocking was performed for 30 min using 1 % bovine serum albumin (BSA) in 1× PBS at RT. Primary antibodies used were as follows: Rabbit anti-Lamin A/C (Epitomics (2966-S), 1:300), Rabbit anti-Lamin A (Abcam (ab26300), 1:500), Rabbit anti-Lamin B1 (Abcam (ab16048), 1:500), Mouse anti-Lamin B2 (Abcam (ab8983),

1:600), and Mouse anti-Lamin A (Abcam (ab8980), 1:500). Antibody dilutions were prepared in 0.5 % BSA in 1× PBS and incubated for 90 min at RT. Secondary antibodies used were goat anti-rabbit IgG–Alexa 488 (Invitrogen (A-11034) 1:1000) and goat anti-mouse IgG–Alexa 568 (Invitrogen (A-11004) 1:1000) for 1 h at RT. Cells were counter stained with DAPI for 2 min at RT, washed in 1× PBS, mounted in Slowfade Gold Antifade (Invitrogen S36937), and stored in 4 °C until they were imaged. Quantification of fluorescence intensities of the acquired images was performed using ImageJ with line scans manually drawn across nuclei.

Three-dimensional fluorescence in situ hybridization—chromosome territories

Fixation and permeabilization

Cells were grown to a confluency of ~30–40 % on glass coverslips (18 × 18 or 22 × 22 mm^2) placed in single wells of a six-well plate and were subjected to siRNA knockdown (Kd). Cells were washed three times in 1× PBS for 5 min each at RT. The cells were incubated on ice for 5 min in pre-chilled CSK buffer and immediately fixed in 4 % paraformaldehyde (PFA, prepared in 1× PBS (pH 7.4)) for 7 min at RT. The cells were washed in 0.1 M Tris-HCl (pH 7.4) followed by two washes with 1× PBS for 5 min each at RT. The cells were repermeabilized in 0.5 % Triton X-100 (prepared in 1× PBS) for 10 min and incubated in 20 % glycerol (prepared in 1× PBS) for 60 min followed by four freeze–thaw cycles in liquid nitrogen. The cells were washed three times in 1× PBS for 5 min each and incubated in 0.1 N HCl for 10 min followed by three washes in 1× PBS for 5 min each. The cells were stored in 50 % formamide (FA)/2× saline sodium citrate (SSC) (pH 7.4) overnight at 4 °C or until used for hybridization.

Hybridization

Chromosome painting probes were obtained from Applied Spectral Imaging (ASI), Israel, or MetaSystems, USA. Probes were equilibrated at 37 °C for 5 min followed by denaturation at 80 °C for 5 min and quick chilled on ice for 2 min followed by a pre-annealing at 37 °C for 30 min. This denatured probe (3–4 μL) was spotted onto fixed cells, sealed, and subjected to co-denaturation at 80 °C for 5 min. Hybridization was for 48 h in a humidified box at 37 °C.

Detection

Post hybridization, coverslips were washed in 50 % FA/2× SSC (pH 7.4), thrice for 5 min each at 45 °C, followed by three washes for 5 min each in 0.1× SSC at 60 °C with gentle agitation. Coverslips were briefly rinsed in 0.1 % Tween 20/4× SSC and counterstained with DAPI for 2 min, washed in 2× SSC and mounted in Slowfade Gold Antifade (Invitrogen S36937), and stored at 4 °C until they were imaged.

Imaging

Image acquisition was performed on a Zeiss LSM 710 or 780 confocal microscope (Carl Zeiss, Thornwood, NJ, USA) with a ×63 Plan-Apochromat 1.4 NA oil immersion objective using scan zoom of 2.5. Acquisition of Z-stacked images (voxel size of 0.105 μm × 0.105 μm × 0.34 μm) was at 512 × 512 pixels per frame using 8-bit pixel depth for each channel. The line averaging was set to 4, and images were collected sequentially in a three-channel mode.

Three-dimensional immunofluorescence in situ hybridization-gene loci

Preparation of bacterial artificial chromosome DNA probes

Bacterial artificial chromosome (BAC) DNA was extracted from clones purchased from CHORI BACPAC Resources (using Hi-Pure Plasmid DNA Extraction Kit (Invitrogen K210017). BAC clones used were RP11-1134K12 for *ZNF570* gene. This DNA was nick translated using fluorescently labeled dUTP (Abbott) and Nick Translation Mix (Roche 11 745 808 910). Labeling reaction was at 15 °C for 90 min, followed by termination of reaction using 0.5 M EDTA (pH 8.0) at 65 °C for 10 min. The DNA was precipitated using ethanol and 3 M sodium acetate and resuspended using deionized FA and Master Mix containing dextran sulfate and 2× saline sodium citrate (SSC) buffer.

Fixation and permeabilization of cells

Cells grown on coverslips and siRNA treated for 48 h were washed twice (5 min each) with 1× PBS (pH 7.4) followed by permeabilization on ice using ice-cold CSK buffer containing 0.5 % Triton X-100 for 5 min. Cells were subsequently fixed in 4 % paraformaldehyde (PFA) solution prepared in 1× PBS for 5–7 min at RT. The fixation protocol followed was the same as that for 3D-FISH (described above in 3D-FISH for visualizing CTs).

Immunostaining followed by hybridization

Previously fixed coverslips were subjected to two washes with 1× PBS (5 min each). Blocking was performed for 30 min using 1 % bovine serum albumin (BSA) in 1× PBS at RT. Primary antibodies used were as follows: Mouse anti-Lamin B2 (Abcam (ab8983), 1:600) and Rabbit anti-Lamin A (Abcam (ab26300), 1:500). Antibody dilutions were prepared in 0.5 % BSA in 1× PBS and incubated for 90 min at RT. Secondary

antibodies used were goat anti-mouse IgG–Alexa 633 (Invitrogen (A-21052) 1:1000) and goat anti-rabbit IgG–Alexa 488 (Invitrogen (A-11034) 1:1000) for 1 h at RT. Post fixation and post permeabilization were subsequently performed with 4 % PFA (5 min RT) and 0.5 % Triton X-100 in 1× PBS (5 min RT), respectively. This was followed by two washes each with 1× PBS (5 min each) and 50 % FA/2× SSC (pH 7.4). The probe for *ZNF570* was equilibrated at 37 °C for 5 min followed by denaturation at 80 °C for 5 min and quick chilled on ice for 2 min. Pre-annealing was performed at 37 °C for 30–40 min. This denatured probe (3–4 μL) was spotted onto the fixed cells that were subjected to immunostaining for Lamin A and Lamin B2 and subjected to co-denaturation at 80 °C for 5 min. Hybridization was for 48 h in a humidified box at 37 °C.

Post hybridization washes

Post hybridization, coverslips were washed in 50 % FA/2× SSC (pH 7.4), thrice for 5 min each at 45 °C, followed by three washes for 5 min each in 0.1× SSC at 60 °C with gentle agitation. Coverslips were stained with DAPI and mounted with Antifade and stored in 4 °C until they were imaged. The images were acquired on Zeiss LSM 710 or 780 confocal microscope similarly as for CT hybridizations, using a zoom = 2.0.

Radial distance measurements of chromosome territories

Three-dimensional distance measurements of CTs were performed using Image-Pro Plus (v 7.1), Media Cybernetics, USA. Briefly, LSM files containing optical sections ($z = 0.34$ μm) of the hybridized nuclei were subjected to 3D surface rendering. Three-dimensional reconstructions of each nucleus were performed on individually cropped nuclei. The acquired images were thresholded and surface rendered for each of the red, green, and blue channels. The geometric center of the DAPI-stained nucleus (blue channel) and the CTs (red and green channels) were determined using plugins from the software, and the distance between the geometric center of the nucleus (A) and that of the territory (B) was measured (X). The vector from the geometric center of nucleus (A) to the geometric center of the CT (B) was extended to a third collinear point at the nuclear periphery (C). The distance between the geometric center (A) of the nucleus and (C) was calculated (Y). The relative distance of a CT from the center of the nucleus was calculated as a percentage of the total distance from the center of the nucleus to the nuclear periphery (Y), $\%\text{radial distance (RD)} = (X/Y) * 100$ (Tanabe et al. 2002).

Measurements for spatial organization of gene loci

Distance measurement from the nuclear periphery

Distances of gene loci from the nuclear periphery were measured (in μm) in 3D using Lamin A signal at the nuclear periphery to demarcate the edge of the nucleus. Briefly, surface rendering was performed for the gene locus (red channel), Lamin A (green channel), Lamin B2 (far-red channel), and the nucleus (DAPI signal blue channel) using Huygens Professional software. For Lamin B2 knockdown (Kd) cells, the nuclei which showed a depletion of Lamin B2 (far-red channel) were used for analysis. Briefly, surface rendering for Lamin A was used as an anchor for measurements. Center of mass (CM) was determined for the gene locus signal of interest, and the closest distance between the CM and surface of the anchor (Lamin A signal) was measured.

Statistical analysis

Graphs were plotted using Graph Pad Prism 5.0 and Sigma Plot 12.0. Statistical comparisons were performed using Graph Pad Prism 5.0 software. Fisher's exact and χ^2 test was used to compare the distribution of % radial distances (RD) of CTs binned in five nuclear sub-shells. For comparison of volumes of CTs and the nucleus between diploid and aneuploid subpopulations, non-parametric ANOVA Kruskal–Wallis test was used. The distance of gene locus *ZNF570* from the lamina was compared using two-sample Kolmogorov–Smirnov (KS) test between control and Lamin B2-depleted cells; p value <0.05 was considered to be statistically significant.

RNA extraction and quantitative reverse transcription-PCR

RNA extraction was performed using PureLink RNA Mini Kit (12183018A). cDNA was synthesized using ImProm II Reverse Transcriptase system (Promega A3800). Quantitative real-time PCR was performed using SYBR Green (SAF Labs). Sequences of primers are in Table S1. *ACTIN* and *GAPDH* served as internal controls.

Gene expression profiling using microarrays

Briefly, RNA was extracted from three independent biological replicates each from control (untreated), Lamin A/C Kd, and Lamin B2 Kd DLD1 cells, and its quality was ascertained using bioanalyzer (Agilent). Cy3-labeled complementary RNA was prepared using T7 promoter-based linear amplification (Agilent Quick Amp Labeling Kit, Cat No. 5190–0442). Qiagen RNeasy Mini Kit (Cat No. 74104) was used for RNA purification. Hybridization was performed using a human 8× 60K array (Agilent single-color 27114) and labeled using

Agilent's in situ hybridization kit (Cat No. 5188-5242). Array scanning was performed, and data acquired was normalized (50th percentile shift normalization). Analyses of gene expression levels were based on comparison of hybridizations between knockdown and control (untreated DLD1 cells) as reference. Gene expression levels (absolute fold change ≥2.0, $p < 0.05$) were used for further analyses. The microarray data can be accessed using GEO Accession number GSE73269. The % deregulation per chromosome was calculated as (no. of deregulated genes on a chromosome / total no. of coding genes on that chromosome) × 100. Number of coding genes and size of chromosomes were obtained from MapViewer (NCBI). Chromosomes showing >0.7 % deregulation were considered significant since this represents >50 % of the total extent of transcriptional deregulation.

Preparation of metaphase spreads

Cells (control, Lamin Kd) were blocked in metaphase using Colcemid (0.1 μg/mL) for 90 min. Hypotonic treatment (0.075 M KCl) was performed for 30 min at RT, followed by fixation in five to six drops of fixative (methanol/acetic acid 3:1), followed by three washes in fixative. Cells were dropped onto glass slides, and metaphases were stained with DAPI, imaged, and counted.

Fluorescence-activated cell sorting analysis by propidium iodide staining

Cells (control, Lamin Kd) were fixed in 70 % ethanol (in 1× PBS), subjected to RNase treatment along with propidium iodide staining (1 h) on ice. Cell suspensions were subsequently run on FACSCalibur (BD Biosciences).

RNA fluorescence in situ hybridization

Probe preparation The probe for RNA FISH for *ZNF570* was prepared by nick translation of the BAC clone ("Preparation of bacterial artificial chromosome DNA probes" section–3D FISH for gene loci above). Upon precipitation, the DNA was resuspended in 8 μL of deionized FA and stored at −20 °C till further use. For hybridization, the probe was equilibrated at 37 °C for 5 min followed by denaturation at 80 °C for 5 min, mixed with equal volume of 2× hybridization mix containing vanadyl ribonucleoside complex, and incubated on ice for 30 min.

Fixation and hybridization Cells were washed twice in 1× PBS (5 min each), followed by treatment with CSK buffer on ice for 5 min and fixation using 4 % PFA (7 min RT). The cells were washed with 70 % ethanol twice and stored at −20 °C until further use. Prior to hybridization, the cells were subjected to an ethanol series (70–90–100 % ethanol) and air-dried. The probe was added to cells and incubated at 37 °C overnight, followed by washes with 50 % FA/2× SSC and 2× SSC (pH 7.2-7.4) at 42 °C (three washes each of 5 min each). The cells were mounted using DAPI–Antifade. All reagents for RNA FISH were prepared using DEPC-treated water (Chaumeil et al. 2008).

Results

Specific chromosomes are transcriptionally deregulated upon Lamin A/C and Lamin B2 depletion

Lamins are filamentous proteins that localize beneath the inner nuclear membrane and maintain nuclear structure and function (Adam and Goldman 2012). In addition to the nuclear periphery, Lamins exist in the nucleoplasm as a meshwork that extends into the nuclear interior and associate directly or indirectly with LAP2α, BANF1, PCNA, and transcription factors (Dechat et al. 2000; Lee et al. 2001; Shumaker et al. 2008). The role of Lamins is therefore not just confined to the nuclear periphery but significantly extends to the nuclear interior, owing to its interaction with proteins at both these nuclear locations (Gruenbaum and Medalia 2015; Kolb et al. 2011). A- and B-type Lamins are implicated in DNA replication and repair, transcription, and senescence (Moir et al. 1994; Shimi et al. 2011; Shumaker et al. 2008; Tang et al. 2008).

We sought to examine the impact of Lamin depletion on the transcriptome and spatial organization of chromosomes in otherwise diploid colorectal cancer cells (DLD1), which are karyotypically stable across passages, distinguishing the same from other cell lines with severe chromosomal aberrations. We first established the conditions for Lamin depletion in DLD1 cells by performing siRNA-mediated knockdowns (Kd). Lamin Kd showed a viability of ~60–70 % in DLD1cells (Fig. S1a). A knockdown of >80–90 % was ascertained at the transcript level by quantitative reverse transcription (qRT)-PCR (Fig. 1a), protein level by immunoblotting (Figs. 1b and S1b–d), and in single cells by immunofluorescence staining (Fig. 1c–f). Immunoblots revealed that Lamin A/C Kd did not significantly affect the levels of B-type Lamins (Figs. 1b and S1b). Likewise, depletion of Lamin B1 or B2 did not affect Lamin A/C levels (Fig. 1b). The exclusivity of the knockdowns enabled us to interpret the consequences of a single Lamin depletion. This is noteworthy since expression levels and stoichiometry of Lamins are important determinants of Lamin localization and function in a cell-type-dependent manner (Guo et al. 2014; Shimi et al. 2015; Swift et al. 2013). Since the extent of siRNA-mediated Lamin B1 depletion (~50-60 %) was not as much as Lamin A/C and B2 in our hands, we focused on examining the effects of Lamin A/C and Lamin B2 knockdowns (Figs. 1b and S1b). Immunostaining showed ~85–90 % depletion of Lamin A and B2 at the single-cell level (Fig. 1d, f). Counterstaining with Lamin B1 in Lamin A/C-depleted cells and

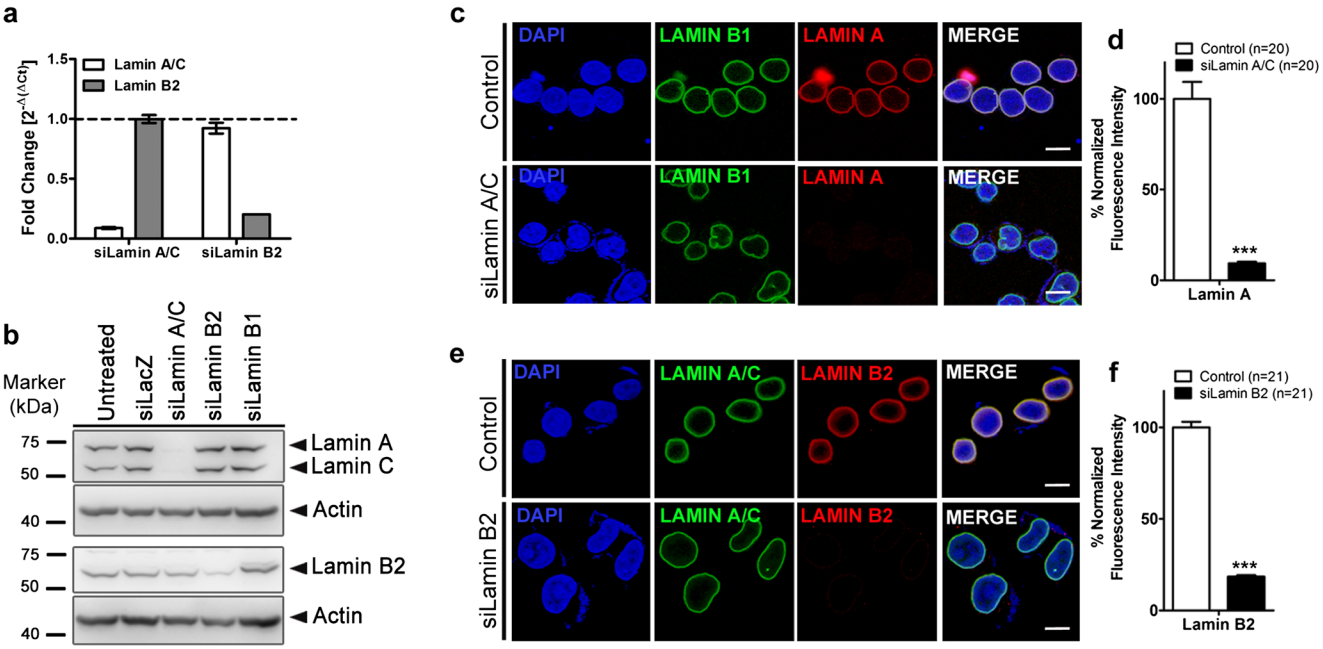

Fig. 1 Depletion of Lamin A/C and B2 in DLD1 cells. **a** qRT-PCR showing siRNA-mediated knockdown of Lamin A/C and Lamin B2 in DLD1 cells, normalized to expression levels of *ACTIN* and compared to non-targeting control (siLacZ). Data shown is a representative out of three independent biological replicates. *Error bars* represent standard error of mean (SEM). **b** Western blots showing knockdowns of Lamin A/C and Lamin B2 in DLD1 cells. Depletion of Lamin A/C does not impact the expression of Lamin B2 and vice versa. Loading control: actin. Data shown is a representative result from five independent experiments. **c** Immunostaining of Lamin B1 (*green*) and Lamin A (*red*) in control (untreated) and Lamin A/C Kd cells. Representative out of four independent experiments. *Scale bar* ~10 μm. **d** Quantification of fluorescence intensity performed by line scans across nuclei from **c. e** Immunostaining of Lamin A/C (*green*) and Lamin B2 (*red*) in control (untreated) and Lamin B2 Kd cells. *Scale bar* ~10 μm. **f** Quantification of fluorescence intensities performed by line scans across nuclei from **e**. *Error bars* in **d**, **f** represent SEM, *n* number of nuclei Knockdown of Lamin A and Lamin B2 was ~85–90 % at the single-cell level ($p < 0.001$, unpaired Student's *t* test)

Lamin A/C upon Lamin B2 Kd revealed distorted nuclear shapes, nuclear invaginations, blebbing, and nuclear furrows (Fig. S2) as found in Lamin A/C- and B1-depleted HeLa cells and in cells derived from laminopathies (Shimi et al. 2008; Taimen et al. 2009). Independently, Lamin A/C and B2 Kd were performed in DLD1 cells, followed by whole-genome expression profiling using gene expression arrays in three independent biological replicates. The data analyses revealed ~300 genes that were significantly deregulated (inclusive of upregulation and downregulation) in either Lamin A/C- or Lamin B2-depleted cells (absolute fold change ≥2.0-fold) (Fig. 2a). Remarkably, in Lamin A/C Kd, 276 out of 298 genes were uniquely deregulated, while in Lamin B2 Kd, 279 out of 301 genes were uniquely deregulated (Fig. 2b). In both Lamin A/C- and B2-depleted cells, 22 genes (~7 %) were commonly deregulated (Fig. 2b). Gene expression levels from expression arrays were independently validated using qRT-PCR for the top deregulated genes (absolute fold change ~2–6-fold). This showed a fold change in the same direction as that obtained from the microarray data set (Fig. S3a, b). We next performed a recovery assay where DLD1 cells were allowed to recover from the Lamin knockdowns by growing cells up to day 8, well beyond the 48-h duration of the knockdown. At the end of day 8, there was ~60–70 % recovery in the transcript and protein levels of Lamin A/C and B2, respectively (Fig. 2c–f). We detected a significant recovery in the transcript levels of candidate genes *ABLIM2* and *SMTNL2* upregulated in Lamin A/C Kd and *TMEM14B* and *CDC42* downregulated in Lamin A/C Kd (Fig. 2g, h). Recovery was also detected for *REG4* and *PTGS2* upregulated in Lamin B2 Kd and *MESDC2* and *KRCC1* downregulated upon Lamin B2 Kd (Fig. 2i, j).

Whole-genome expression profiling using microarrays from Lamin A mutant (E161K) human cardiomyocytes showed deregulated gene expression levels predominantly from gene-poor chromosome 13 (Mewborn et al. 2010). Likewise, mouse fibroblasts lacking functional Lamin B1 revealed transcriptionally deregulated clusters on the peripherally positioned mouse chromosome 18 (Malhas et al. 2007). These evidences prompted us to investigate if specific chromosomes were transcriptionally deregulated upon Lamin A/C or B2 depletion. From our expression array data sets independently derived from Lamin A/C and Lamin B2 knockdowns, we calculated the extent of transcriptional deregulation for each chromosome by expressing the total number of deregulated genes on a chromosome as a fraction of the total number of coding genes from that chromosome (Fig. 2k). Chromosomes showing >0.7 % deregulation in transcript levels were shortlisted. Chromosomes showing significant deregulation upon Lamin A/C Kd were Chr.16, 22, 20, 12, 1, 3, 17, and 19 (descending order of expression deregulation). While upon Lamin B2 Kd, major deregulated chromosomes

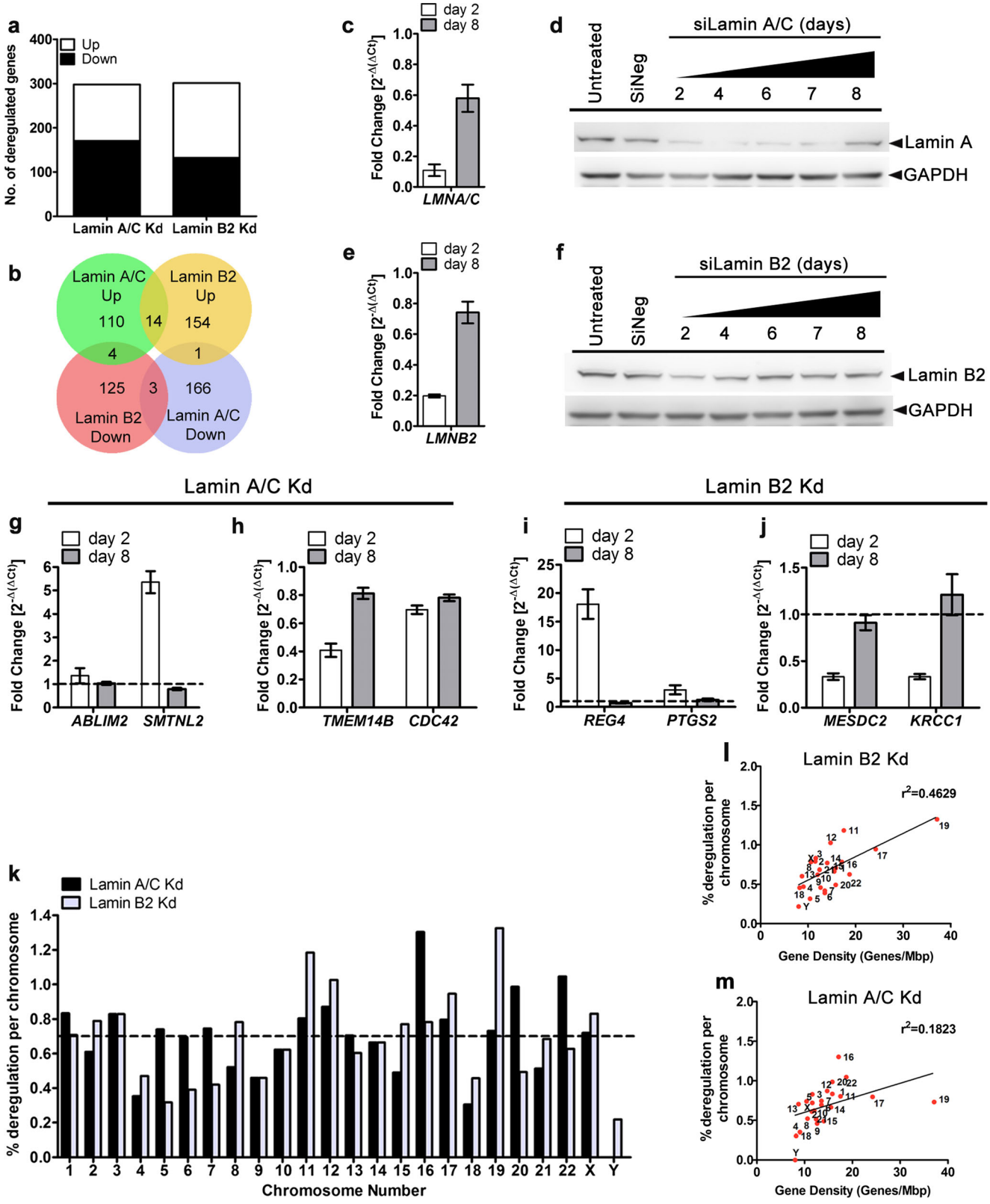

were Chr.19, 11, 12, 17, X, 8, 3, and 2 (descending order of expression deregulation) (Fig. 2k). Comparatively neither Lamin A/C Kd nor Lamin B2 Kd showed a significant transcriptional deregulation from gene-poor chromosomes 13, 18 or 7 (whole chromosomes), although these chromosomes are proximal to the nuclear lamina (Fig. 2k). A plot of

◀ **Fig. 2** Impact of Lamin A/C and B2 depletion on the transcriptome. **a** Number of deregulated genes (up and down) upon Lamin A/C and Lamin B2 depletion (cutoff ≥2.0-fold on absolute scale) from genome-wide expression analyses. **b** Common and uniquely deregulated genes upon Lamin A/C and Lamin B2 depletion. Lamin A/C or B2 Kd reveals ~300 genes that were deregulated (Lamin A/C Kd-128 genes up, 170 genes down and Lamin B2 Kd-169 genes up, 132 genes down). **c** qRT-PCR showing recovery of Lamin A/C transcript at the end of 8 days, normalized to expression of *ACTIN*. **d** Western blot showing levels of Lamin A when DLD1 cells treated with siLamin A/C were grown for 2–8 days to assess recovery from siRNA-mediated knockdown. Loading control: GAPDH. **e** qRT-PCR showing recovery of Lamin B2 transcript at the end of 8 days, normalized to expression of *ACTIN*. **f** Western blot showing levels of Lamin B2 when DLD1 cells treated with siLamin B2 were grown for 2–8 days to assess recovery from siRNA-mediated knockdown. Loading control: GAPDH. Data shown in **d**, **f** are representative results from two independent experiments. **g** Expression levels of genes upregulated upon Lamin A/C Kd (*ABLIM2*, *SMTNL2*) at the end of day 2 were restored at day 8. **h** Genes downregulated upon Lamin A/C Kd (*TMEM14B*, *CDC42*) at the end of day 2 recovered at day 8. **i** Expression levels of genes upregulated upon Lamin B2 Kd (*REG4*, *PTGS2*) at the end of day 2 were restored at day 8. **j** Genes downregulated upon Lamin B2 Kd (*MESDC2*, *KRCC1*) at the end of day 2 recovered at day 8. Data for all qRT-PCRs (**c**, **e**, **g**–**j**) is a compilation of two biological replicates and normalized to expression levels of *ACTIN*. *Error bars* represent SEM. **k** Genes deregulated per chromosome upon depletion of Lamin A/C and Lamin B2 in DLD1 cells. The % deregulation = (no. of deregulated genes on a chromosome / total no. of coding genes on that chromosome) × 100. Details of number of coding genes and size of chromosomes were obtained from MapViewer (NCBI). **l**, **m** Lamin B2 Kd ($r^2 = 0.4629$) shows greater correlation between transcriptional deregulation and gene density as compared to Lamin A/C Kd ($r^2 = 0.1823$)

% transcriptional deregulation against gene density showed a higher correlation with gene density upon Lamin B2 Kd ($r^2 = 0.4629$) as compared to Lamin A/C Kd ($r^2 = 0.1823$) (Fig. 2l, m). This reveals an enhanced transcriptional deregulation from gene-rich chromosomes upon Lamin B2 Kd. Taken together, gene expression profiling of Lamin A/C- or B2-depleted cells uncovered specific chromosomes that were significantly deregulated in their gene expression levels (Fig. 2k).

Lamin depletion induces chromosomal aneuploidies

We next performed three-dimensional fluorescence in situ hybridization (3D-FISH) of specifically those chromosomes that showed greater transcriptional deregulation over others independently in Lamin A/C and B2 depletion. Chromosome territories (CTs) 1 and 16 were examined upon Lamin A/C Kd, and CTs 11 and 17 were examined upon Lamin B2 Kd (Fig. 3a, b). In addition, the most gene-rich chromosome 19 that was deregulated independently in Lamin A/C and B2 Kd was also examined along with gene-poor chromosome 18 of comparable DNA content (Fig. 3c). Furthermore, chromosome 18 showed a relatively lower (~0.5–0.6 %) transcriptional deregulation in either Lamin A/C or B2 Kd (Fig. 2k). Three-dimensional FISH showed that Chr.1, 11, 16, 17, 18, and 19 were diploid in ~95 % control cells (untreated cells and cells treated with non-targeting siRNA (siLacZ)) (Figs. 3d, e and S4a–i). However, while imaging Lamin Kd nuclei, we consistently detected sub-populations (~20–30 % of cells) with more than two CTs (Fig. 3d, e). Chromosomes 18 and 19 were gained (three to four copies) in Lamin A/C Kd cells (~20–30 %) (Figs. 3d and S4c, d), while chromosomes 11, 17, 18, and 19 were gained (three to four copies) in Lamin B2 knockdown cells (Figs. 3e and S4e–h). We also tested for the extent of aneuploidies of chromosomes that were not transcriptionally deregulated and therefore not shortlisted in each of Lamin A/C (CT11, 17) or B2 Kd (CT1, 16) cells. Chromosome 17 was gained (three copies) in Lamin A/C Kd in ~20 % cells, while chromosomes 1 and 16 were not gained upon Lamin B2 Kd (Fig. S4i). Immuno-FISH assays showed a comparable depletion of ~75–80 % of Lamin levels in both the diploid and aneuploid sub-populations of cells (Fig. S5). A scrambled (non-targeting) siRNA oligonucleotide control of Lamin B2 did not show aneuploidy for CT18 and 19, underscoring the specificity of the siRNA against Lamin B2 in DLD1 cells (Fig. S4j, k). In addition, an shRNA sequence against Lamin B2 showed a comparable extent of aneuploidy (>30 %) (data not shown), suggesting that Lamin-depletion-induced aneuploidies were simply not a manifestation of transient siRNA-mediated knockdowns.

We performed fluorescence-activated cell sorting (FACS) profiling to ascertain the ploidy of Lamin-depleted DLD1 cells (Fig. S6a–d). This profile showed a comparable proportion of cycling cells in the control and Lamin Kd populations. In addition, we did not detect polyploid sub-populations in control or Lamin Kd cells (Fig. S6a–d). Further, the levels of the major cell cycle checkpoint proteins Chk1 and Chk2 remained unaffected (Fig. S6e, f). To assess the effect of Lamin depletion on chromosomal instability (CIN), we examined metaphase spreads derived from Lamin knockdown cells (Fig. S7a–c). Control DLD1 cells showed a predominantly pseudo-diploid population (~80 %) (45–46 chromosomes) and another sub-population of ~20 % cells showing chromosomal losses and gains (Fig. S7d). An increase in the number of cells showing chromosomal losses (43–45 chromosomes) ($p = 0.0345$) and gains (47–48 chromosomes) was detected upon Lamin A/C Kd (Fig. S7a, b, d). Remarkably, Lamin B2 Kd showed a significant increase in chromosomal gains (47–49 chromosomes) ($p = 0.018$) (Fig. S7a, c, d). This is consistent with chromosomal aneuploidies induced in DLD1 cells upon Lamin B2 depletion (Kuga et al. 2014). Karyotype analyses from metaphase spreads derived from control, Lamin A/C, or B2 Kd cells did not reveal any consistent chromosomal translocations (Fig. S7a–c). Notably, a comparable level of

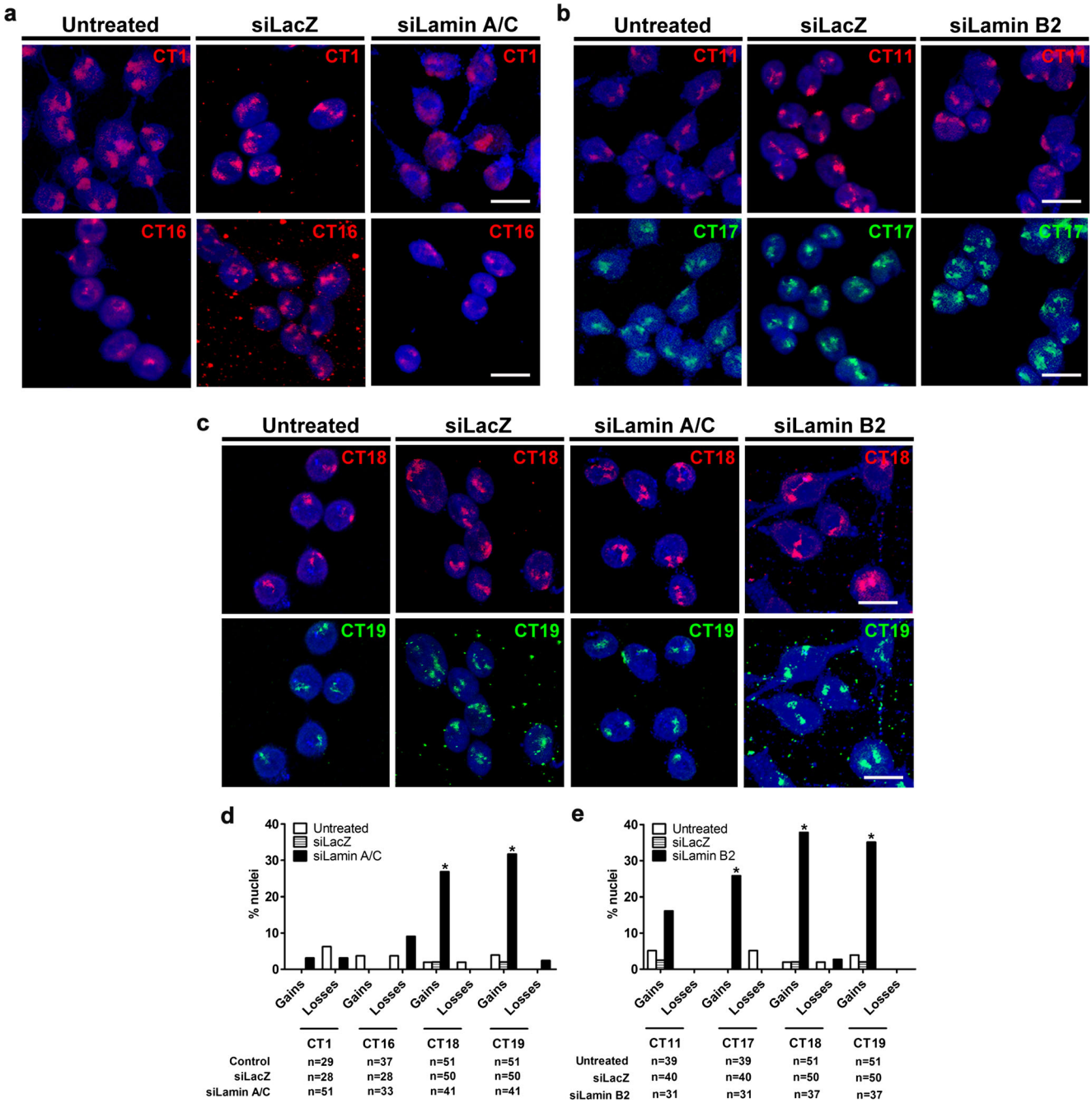

Fig. 3 Lamin depletion induces chromosomal aneuploidies. **a** Merged maximum intensity projection of confocal image stacks of chromosome territories (CT)—CT1 and CT16 for control (untreated and siLacZ treated) and siLamin A/C-treated DLD1 cells. **b** Merged maximum intensity projection of confocal image stacks of chromosome territories (CT)—CT11 and CT17 for control (untreated and siLacZ treated) and siLamin B2-treated DLD1 cells. **c** Merged maximum intensity projection of confocal image stacks of chromosome territories (CT)—CT18 and CT19 for control (untreated and siLacZ treated), siLamin A/C-, and siLamin B2-treated DLD1 cells. Nuclei are stained with DAPI, hybridizations for CT1 and CT16 were single-color hybridizations, while CT11–CT17 and CT18–CT19 were dual color hybridizations. *Scale bar* ~10 μm. **d** Quantification of number of chromosome territories in interphase nuclei of control and Lamin A/C-depleted cells. Number of nuclei scored in each treatment (*n*) ~28–51. Quantification is a representative result out of two biological replicates. Chromosomes 18 and 19 are aneuploid (in ~20–25 % cells) upon Lamin A/C depletion. **e** Quantification of number of chromosome territories in interphase nuclei of control and Lamin B2-depleted cells. Chromosomes 11 and 17 (aneuploid in ~15–25 % cells) and chromosomes 18–19 (aneuploid in ~30–40 % cells) upon Lamin B2 depletion. Number of nuclei scored in each treatment (*n*) ~28–51. Quantification is a representative result out of two biological replicates

CIN (~30 %) is associated with colorectal cancer initiation and progression (Bardi et al. 1995; Ried et al. 1996).

Taken together, these studies show a specific induction of chromosomal aneuploidies upon Lamin A/C and Lamin

B2 depletion in DLD1 cells. We next examined the spatial organization of both the diploid and the aneuploid CTs in Lamin-depleted cells.

Lamin A/C depletion does not perturb conserved positions of diploid and aneuploid chromosome territories

The spatial organization of chromosomes in the interphase nucleus largely correlates with gene density and, therefore, its expression levels, with gene-rich chromosomes in the nuclear interior being more transcriptionally active as against gene-poor chromosomes toward the nuclear periphery (Goetze et al. 2007). We performed 3D-FISH followed by confocal imaging and 3D radial distance measurements of diploid and aneuploid CTs in Lamin-depleted cells. The radial distance measurements have been represented both as a (i) dot scatter plots of raw data (Fig. S8) and (ii) binned into five shells of ~20 % of the nuclear sub-volume (0 %—nuclear center, 100 %—nuclear periphery) (Figs. 4 and 5). It is pertinent to reiterate that the innermost nuclear shell enriched in euchromatin is relatively more transcriptionally active as compared to the peripheral shell (~80–100 %) enriched in heterochromatin (Goetze et al. 2007). Three-dimensional FISH analyses of CT1 (gene density 15.83 genes/Mbp) and 16 (gene density 17.05 genes/Mbp) in Lamin A/C-depleted cells did not show a change in its radial distance distribution

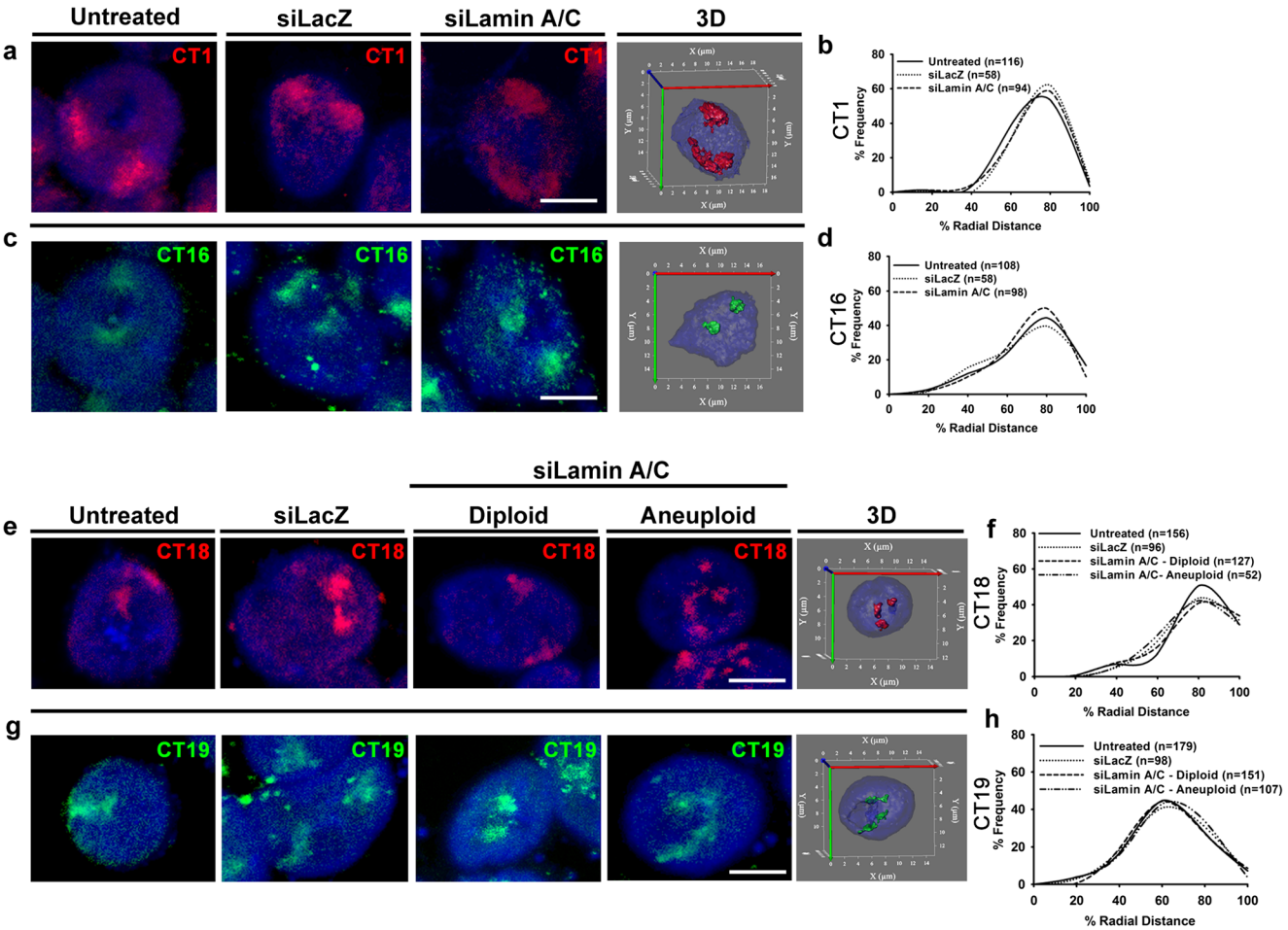

Fig. 4 Diploid and aneuploid chromosome territories assume conserved positions upon Lamin A/C depletion. **a**–**d** Representative images and radial distance distribution profiles for 3D-FISH performed on untreated, siLacZ-treated, and siLamin A/C-treated DLD1 cells for CT1 (**a**, **b**) and CT16 (**c**, **d**). Each *panel* shows merged maximum intensity projections of a representative nucleus from control (untreated, siLacZ) and siLamin A/C cells with its corresponding 3D reconstruction (3D). **b**, **d** Representative radial distance distribution profiles (pooled across experiments) of CT1 ($N=1$) and CT16 ($N=2$) binned into five sub-shells of ~20 % radial distance each. In each replicate, radial distances were measured for ~50–100 CTs. No significant change was detected in the radial distance distribution profiles of either diploid CT1 or CT16 upon Lamin A/C Kd ($p>0.05$). **e**–**h** Merged maximum intensity projections for 3D-FISH images and radial distance distribution profiles for CT18 (**e**, **f**) and CT19 (**g**, **h**) which show aneuploidy upon Lamin A/C Kd. Representative 3D reconstructions show aneuploidy upon Lamin A/C Kd. **f**, **h** Radial distance distribution profiles (pooled across experiments) of CT18 ($N=2$) and CT19 ($N=3$) binned into five sub-shells of ~20 % radial distance each. In each replicate, radial distances were measured for ~50–100 CTs. No significant changes were detected in the distribution profiles for CT18 and CT19 in Lamin A/C Kd diploid or aneuploid cells ($p>0.05$). *Scale bar* ~5 μm. Fisher's exact test and χ^2 test was used to test statistical significance of distribution in different sub-shells of the nucleus. *N* number of independent experiments (biological replicates) contributing to the data, *n* number of chromosome territories

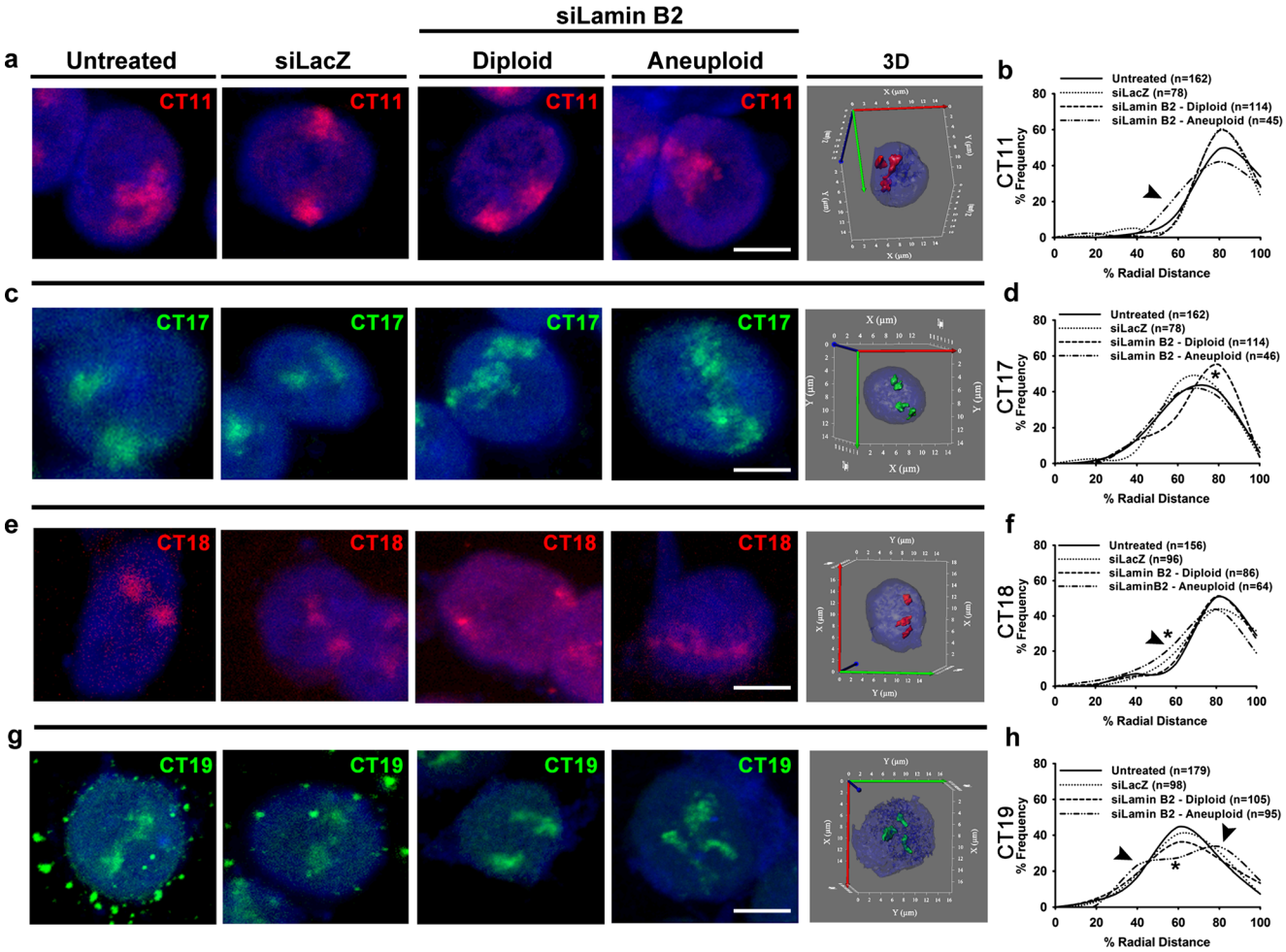

Fig. 5 Aneuploid chromosome territories are mislocalized upon Lamin B2 depletion. Images from merged maximum intensity projection of 3D-FISH and radial distance distribution profiles for CT11 (**a**, **b**), CT17 (**c**, **d**), CT18 (**e**, **f**), and CT19 (**g**, **h**) which show aneuploidy upon Lamin B2 Kd. Representative 3D reconstructions show aneuploidy in the interphase nucleus upon Lamin B2 Kd. **b**, **d**, **f**, **h** Radial distance distribution profiles (pooled across experiments) of CT11 ($N=2$), CT17 ($N=2$), CT18 ($N=2$), and CT19 ($N=3$) binned into five sub-shells of ~20 % radial distance each. In each replicate, radial distances were measured for ~50–100 CTs. **b** Aneuploid CT11 shows an increase in the sub-population in shell III (RD ~60 %) over the control. **d** Diploid CT17 shows an increase in the sub-population in shell IV (RD ~80 %) over the control ($p=0.0145$). **f** Aneuploid CT18 shows an increase in the sub-population in shell III (RD ~60 %) over the control ($p=0.0431$). **h** Aneuploid CT19 showed a significantly different distribution of CT positions as compared to untreated cells ($p=0.0157$). Specifically, it shows a decrease in the sub-population in shell III (RD ~60 %) over the control ($p=0.0061$) and an increase in the subpopulations in shell II (RD ~40 %) and shell IV (RD ~80 %), respectively. *Scale bar* ~5 μm. Fisher's exact and χ^2 test was used to test statistical significance of distribution in sub-shells of the nucleus. *N* number of independent experiments (biological replicates) contributing to the data, *n* number of chromosome territories. *Arrowheads*: mislocalized sub-populations of aneuploid chromosome territories upon Lamin B2 Kd

($p>0.05$) (Figs. 4a–d and S8a, b, Table 1). Furthermore, their relative positions in the nuclear sub-shells remained unchanged and conserved when compared to control cells (Fig. 4a–d). Radial distance measurements of CT18 (shell

Table 1 Median % radial distance (RD) and interquartile range (IQR) of chromosome territories upon Lamin A/C Kd in DLD1 cells

Chromosome no.	Gene density (genes/Mbp)	Untreated		siLacZ		siLamin A/C			
						Diploid		Aneuploid	
		Median	IQR	Median	IQR	Median	IQR	Median	IQR
CT1	15.83	62.27	14.11	65.49	14.98	66.07	19.17	–	–
CT16	17.05	67.42	25.91	64.3	25.31	62.85	22.88	–	–
CT18	8.21	73.63	18.20	72.5	23.61	73.73	22.24	71.14	26.08
CT19	37.08	52.08	27.02	51.73	23.44	54.86	23.8	51.45	23.64

IV, RD ~80 %) and CT19 (shell III, RD ~60 %) in diploid or aneuploid cells remained conserved toward the nuclear periphery and nuclear interior, respectively (Figs. 4e–h and S8c, d). Radial distance measurements of CT1, 16, 18, and 19 in the siLacZ-treated DLD1 cells remained conserved as compared to untreated control cells (Fig. 4b, d, f, h). In summary, despite the specific depletion of Lamin A/C, the diploid or aneuploid gene-rich or gene-poor CTs showed a remarkable conservation in their spatial localization consistent with their gene densities.

Lamin B2 depletion mislocalizes aneuploid chromosome territories

The increase in aneuploid cells upon Lamin B2 Kd is consistent with the known impact of Lamin B2 depletion in colorectal cancer cells (Kuga et al. 2014). We next analyzed the radial distance distributions of chromosomes that were transcriptionally deregulated upon Lamin B2 Kd in DLD1 cells. Although CT11 is gene rich (~17.5 genes/Mbp), it shows a peripheral (shell IV: RD ~80 %) nuclear localization in control cells (Fig. 5a, b). Analyses of radial distance distribution of CT11 in Lamin B2 Kd cells showed a conserved radial distance distribution in diploid cells (shell IV: RD ~80 %) (Fig. 5b). Aneuploid CT11 shows a mislocalized sub-population toward the nuclear interior to shell III: RD ~60 % (Fig. 5b). Interestingly, diploid CT17 (gene rich) showed a significant shift toward the nuclear periphery (shell IV: RD ~80 %) as compared to control cells (shell III: RD ~60 %) (Fig. 5c, d). However, the aneuploid CT17 does not show a mislocalization as compared to control cells and remains clustered in shell III (RD ~60 %) (Fig. 5d). It is plausible that the extra copy of CT17 may cluster into a single shell in Lamin B2 Kd cells, while one of the homologs in the diploid CT17 is mislocalized, suggesting differential effects that are exerted on CT17 in diploid and aneuploid Lamin B2 Kd cells—the functional relevance of which remains to be tested. The gene-poor and diploid CT18 in Lamin B2 Kd cells showed a predominantly peripheral nuclear localization (shell IV, RD ~80 %). In addition, aneuploid CT18 shows an increase in a subpopulation of cells toward the nuclear interior (shell III, RD ~60 %) (Fig. 5e, f). In contrast, the gene-rich CT19 predominantly localized toward the nuclear interior (shell III, RD ~60 %) in control and diploid cells depleted in Lamin B2. However, aneuploid CT19 showed a striking mislocalization in its distribution into nuclear sub-shells, repositioning further toward the nuclear interior (shell II: RD ~40 %) and nuclear periphery (shell IV: RD ~80 %) (Fig. 5g, h). Radial distance measurements of CT11, 17, 18, and 19 in the siLacZ-treated DLD1 cells remained conserved as compared to untreated control cells (Fig. 4b, d, f, h). Taken together, aneuploid CTs show mislocalized sub-populations upon Lamin B2 depletion. We examined the interquartile range (IQR) of the radial distance distributions of the CTs, which consistently showed a greater IQR (22.73–31.19) for the aneuploid cells than for the diploid cells (11.21–29.97) (Table 2).

Spatial organization of gene loci is altered upon Lamin B2 depletion

We show that Lamin B2 depletion mislocalizes aneuploid CTs. We therefore examined if the mislocalization of aneuploid CTs also impinges on the spatial organization and function of a target gene (Fig. 6). We examined the role of Lamin B2 in regulating gene expression of a candidate gene on chromosome 19. The spatial organization of gene loci in the interphase nucleus is non-random and correlates with its expression levels. Gene loci that are overexpressed typically loop-out of their respective CTs (Chambeyron and Bickmore 2004; Volpi et al. 2000). Furthermore, gene loci associate with nuclear landmarks such as the nuclear lamina, Polycomb bodies, which further impact its transcription status (Bracken et al. 2006; Guelen et al. 2008). The nuclear lamina is predominantly a transcriptionally repressive zone, and inactive genes typically associate with nuclear Lamins at the nuclear periphery in contrast to active genes (Guelen et al. 2008; Harr et al. 2015; Peric-Hupkes et al. 2010; Reddy et al. 2008).

We adopted the nuclear lamina as a reference for examining the spatial organization of the gene locus in 3D (Reddy et al. 2008; Zullo et al. 2012) (Fig. 6a). Since we

Table 2 Median % radial distance (RD) and interquartile range (IQR) of chromosome territories upon Lamin B2 Kd in DLD1 cells

Chromosome no.	Gene density (genes/Mbp)	Untreated		siLacZ		siLamin B2			
						Diploid		Aneuploid	
		Median	IQR	Median	IQR	Median	IQR	Median	IQR
CT11	17.5	76.19	17.25	73.55	16.81	75.06	11.21	73.11	22.73
CT17	24.21	57.94	24.53	57.79	18.84	62.22	14.69	57.6	27.87
CT18	8.21	73.63	18.20	72.5	23.61	70.45	19	69.25	23.3
CT19	37.08	52.08	27.02	51.73	23.44	53.88	29.97	57.23	31.19

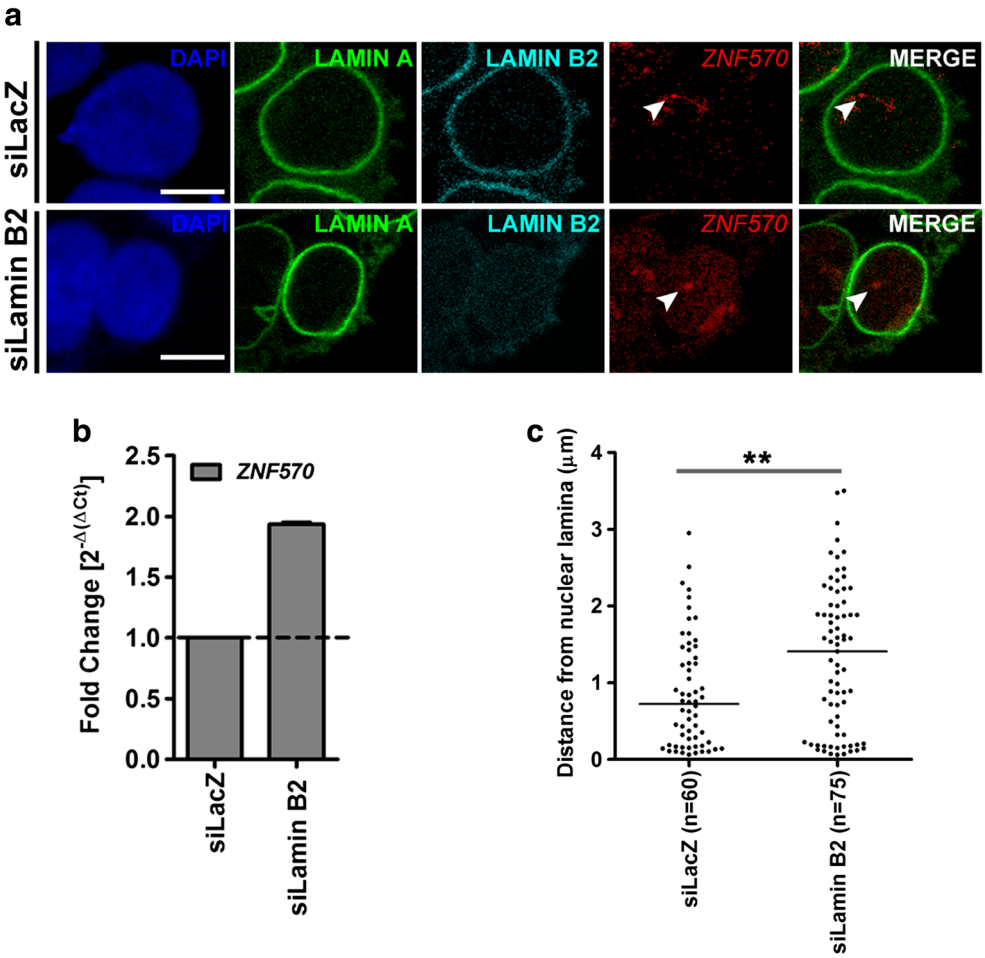

Fig. 6 Enhanced expression level and altered spatial organization of gene loci upon Lamin B2 depletion. **a** Representative images (from a single optical section of a confocal image stack) of 3D Immuno-FISH for Lamin A (*green*), Lamin B2 (*cyan*), *ZNF570* (*red*), and DAPI (*blue*) performed on siLacZ- and siLamin B2-treated DLD1 cells. *Scale bar* ~5 μm. **b** qRT-PCR showing upregulation of *ZNF570* upon Lamin B2 Kd in DLD1 cells. Data shown is a representation out of two independent experiments *Error bars* represent SEM. **c** Dot scatter plot showing least distance between *ZNF570* locus and Lamin A signal in siLacZ- and siLamin B2-treated DLD1 cells, horizontal bar represents median. In each of siLacZ and siLamin B2 cells, ~60–70 gene loci signals were quantified. The distance of *ZNF570* locus with respect to the lamina was significantly greater in the siLamin B2 cells ($p = 0.004$, K-S test). *Arrowheads*: *ZNF570* gene locus

consistently detected chromosome 19 aneuploidies upon Lamin B2 knockdown, we examined the spatial organization of a candidate gene locus *ZNF570* (Chr.19q13.12) (Fig. 6a). The *ZNF570* gene locus was also found to be aneuploid in ~25 % Lamin B2-depleted cells. Gene expression profiling using microarrays showed a ~2.96-fold upregulation of *ZNF570*, which was corroborated by qRT-PCR (~2-fold) (Fig. 6b). We measured the distance of the fluorescently labeled *ZNF570* gene locus with respect to the nuclear lamina (Lamin A) that we considered as the origin, i.e., 0 μm (Fig. 6c). The *ZNF570* gene locus showed a predominant position proximal to the nuclear lamina (median = 0.72 μm) in control cells (siLacZ) and showed a significant shift away from the nuclear lamina upon Lamin B2 depletion (median = 1.40 μm) (Fig. 6c). The spatial organization of *ZNF570* showed a similar repositioning away from the nuclear lamina in diploid and aneuploid Lamin B2 Kd cells (Fig. S9a, b). Furthermore, we detected a significant increase in the number of RNA transcript signals for *ZNF570* in Lamin B2-depleted cells (Fig. S9c, d). Thus, a loss of Lamin B2 repositions *ZNF570* gene locus (diploid and aneuploid) away from the nuclear lamina, which further manifests as an increase in transcript levels detected in single cells (RNA-FISH) as well as at the population level (qRT-PCR).

Chromosome territory volumes are altered in Lamin-depleted cells

Lamin A mutation (E161K) showed a decrease in the volume of chromosome 13 territory in human fibroblasts (Mewborn et al. 2010). Volumes of chromosome 18 and 19 territories showed an increase in Lamin B1-depleted DLD1 cells (Camps et al. 2014). We next examined if Lamin A/C or B2 depletion affects the volumes of CTs in either diploid or aneuploid cells (Fig. 7, Tables 3 and 4). The nuclear volume showed a significant increase (~1.1-fold) upon Lamin A/C Kd (Fig. 7a). Diploid chromosome 1, 18, and 19 territories showed a significant increase in their volumes (~1.2-fold) upon Lamin A/C depletion (Fig. 7b, d, e). Chromosome 16 did not show a change in its volume (Fig. 7c). Aneuploid CT18 and CT19 did not show a significant change in volume upon Lamin A/C Kd (Fig. 7d, e). This suggests a role for Lamin A/C in either directly or indirectly regulating CT volumes, primarily of diploid CTs.

Lamin B2 depletion shows an ~1.2-fold increase in nuclear volume (Fig. 7f). CT11 and CT17 did not show a change in volume in either diploid or aneuploid state (Fig. 7g, h). CT18 showed an increase in volumes (~1.7-fold) in the aneuploid state, and CT19 showed an increase in volume in the diploid (~1.4-fold) as well as aneuploid state (~1.5-fold) (Fig. 7i, j). In summary, Lamin A/C and B2 depletion impacts nuclear volumes. While Lamin A/C Kd primarily affects volumes of diploid CTs, Lamin B2 Kd impacts volumes of mainly aneuploid CTs.

To further probe if mislocalized aneuploid CTs show an altered volume upon Lamin B2 Kd, we examined the volumes of aneuploid CTs across concentric nuclear sub-shells (Fig. 7g'–j'). We did not detect a significant difference in the volumes of aneuploid CTs whether they were localized toward the nuclear interior or toward the nuclear periphery, further suggesting that the altered volume of aneuploid CTs tested here (CT18, CT19) may not correlate with its mislocalization into a different nuclear sub-shell.

Lamin depletion destabilizes spatial constraints that confine chromosome territories into distinct nuclear sub-volumes

We examined the spatial organization of both diploid and aneuploid CTs in Lamin-depleted cells. Lamin depletion showed an increase in nuclear volume of ~1.1-fold in Lamin A/C Kd cells and ~1.2-fold in Lamin B2 Kd cells. A spherical nucleus can be grossly subdivided into five concentric sub-shells, with the gene-rich CTs predominantly toward the nuclear interior (shell II–III), while gene-poor CTs are toward the nuclear periphery (shell IV–V) (Fig. 8a). Chromosomal aneuploidies generated upon Lamin A/C and B2 depletion generate diploid and aneuploid chromosomal sub-populations. Diploid CTs in either Lamin A/C- or B2-depleted cells show conserved positions in a gene-density-dependent manner. However, Lamin A/C knockdown cells showed an increase in CT volume in the diploid sub-population of cells (Fig. 8b). In contrast, aneuploid CTs in Lamin B2-depleted cells are strikingly mislocalized and show altered volumes in the interphase nucleus (Fig. 8c). Our results strongly implicate the presence of additional underlying Lamin B2-dependent mechanisms that facilitate gene-density-based chromosome positioning in the interphase nucleus. This potentially includes (i) direct associations of Lamin B2 with chromatin and (ii) protein–protein interactomes of Lamin B2 or a combination of both these factors. Taken together, our studies highlight a unique role for Lamin B2 in regulating the spatial localization of aneuploid CTs in the interphase nucleus.

Discussion

Lamins are required for the maintenance of nuclear structure and function. Furthermore, Lamins are necessary for the appropriate localization of CTs in the interphase nucleus (Malhas et al. 2007; Mewborn et al. 2010; Shimi et al. 2008). Our results suggest a requirement for Lamin B2 since its absence results in mislocalization of aneuploid CTs. The specific role of Lamin B2 in regulating chromosomal ploidy and chromosome positioning is difficult to uncouple. While both A- and B-type Lamins are involved in regulating spindle assembly during mitosis (Goodman et al. 2010; Kuga et al. 2014; Qi et al. 2015; Tsai et al. 2006), Lamins are primarily structural proteins that maintain the spatial organization of the genome (Peric-Hupkes and van Steensel 2010). While both Lamin A/C and Lamin B2 depletion induced CIN, primarily Lamin B2 depletion resulted in a mislocalization of aneuploid CTs. There are conflicting reports on the expression levels of Lamin A/C in colorectal cancers (Belt et al. 2011; Foster et al. 2011; Moss et al. 1999; Willis et al. 2008; Wu et al. 2009). In contrast, Lamin B2 was shown to be a differentially expressed protein between colorectal cancers with and without CIN—with increase in Lamin B2 expression conferring protection against CIN (Kuga et al. 2014). It is noteworthy from our results that Chr.17, 18, and 19 (from the specific subset of chromosomes that we examined) were consistently gained independently upon Lamin A/C or Lamin B2 depletion (Fig. S4i). This is suggestive of a pattern of chromosomal acquisitions potentially relevant for colorectal cancer progression (Tagawa et al. 1996). It remains to be examined if the extent of Lamin stoichiometry correlates with the extent of these chromosomal gains during colorectal cancer progression (Belt et al. 2011; Roth et al. 2010).

Our study highlights an interesting divergence of roles for Lamin A/C and Lamin B2. The role of Lamin B2 in maintenance of genome organization is rather underappreciated. Diploid DLD1 cells robustly express Lamins A/C, B1, and B2 that potentially compensate for one another in single Lamin knockdowns in order to maintain conserved chromosome positions. This is further reiterated in Lamin B1-depleted DLD1 cells that show a conserved localization of CT18 at the nuclear periphery (Camps et al. 2014). However, in aneuploid cells, an optimum level of Lamin B2 is a likely prerequisite for the correct spatial positioning of CTs. It is plausible that regulation of ploidy and positioning of aneuploid chromosomes are co-regulated by Lamin B2 through its commonly regulated interactors that function during both mitosis and interphase. One such candidate is the inner nuclear membrane protein SUN1 identified in a screen by Kuga et al. (2014) which associates with Lamin B2 during mitosis. However, the precise roles of Lamin B2-associated interactors in the context of maintaining the spatial organization of the genome is unclear.

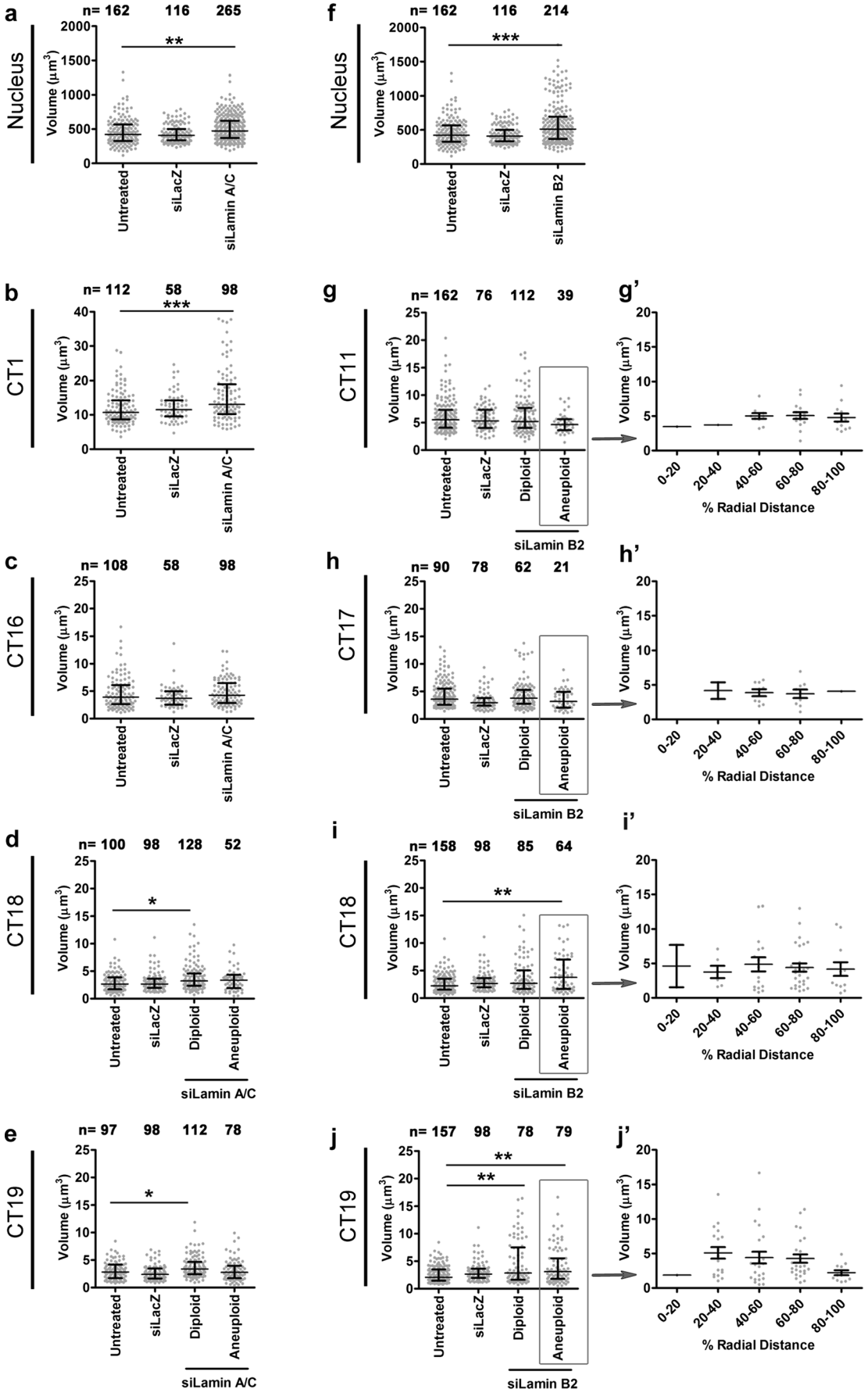
a
Nucleus
n= 162 116 265
**
Volume (µm³)
Untreated
siLacZ
siLamin A/C
f
Nucleus
n= 162 116 214
***
Volume (µm³)
Untreated
siLacZ
siLamin B2
b
CT1
n= 112 58 98
***
Volume (µm³)
Untreated
siLacZ
siLamin A/C
g
CT11
n= 162 76 112 39
Volume (µm³)
Untreated
siLacZ
Diploid
Aneuploid
siLamin B2
g'
Volume (µm³)
0-20
20-40
40-60
60-80
80-100
% Radial Distance
c
CT16
n= 108 58 98
Volume (µm³)
Untreated
siLacZ
siLamin A/C
h
CT17
n= 90 78 62 21
Volume (µm³)
Untreated
siLacZ
Diploid
Aneuploid
siLamin B2
h'
Volume (µm³)
0-20
20-40
40-60
60-80
80-100
% Radial Distance
d
CT18
n= 100 98 128 52
*
Volume (µm³)
Untreated
siLacZ
Diploid
Aneuploid
siLamin A/C
i
CT18
n= 158 98 85 64
**
Volume (µm³)
Untreated
siLacZ
Diploid
Aneuploid
siLamin B2
i'
Volume (µm³)
0-20
20-40
40-60
60-80
80-100
% Radial Distance
e
CT19
n= 97 98 112 78
*
Volume (µm³)
Untreated
siLacZ
Diploid
Aneuploid
siLamin A/C
j
CT19
n= 157 98 78 79
**
**
Volume (µm³)
Untreated
siLacZ
Diploid
Aneuploid
siLamin B2
j'
Volume (µm³)
0-20
20-40
40-60
60-80
80-100
% Radial Distance

◀ **Fig. 7** Chromosome territories show volume changes upon Lamin depletion. **a**–**j** Dot scatter plots for volumes of nuclei and chromosome territories upon Lamin A/C and Lamin B2 depletion in DLD1 cells. *Horizontal bars* indicate median with the interquartile range. **a** A significant increase was detected for the nuclear volume (~1.1-fold) upon Lamin A/C Kd ($p = 0.0001$), $N = 5$. **b** A significant increase was detected for volumes of CT1 ($p = 0.0009$), $N = 1$ upon Lamin A/C Kd. **c** No significant difference in volume was detected for CT16, $N = 2$. **d**, **e** A significant increase in the volume of diploid CT18 ($p = 0.0149$), $N = 2$, and CT19 ($p < 0.0001$), $N = 2$, while aneuploid CT18 and CT19 do not show a significant difference in volume upon Lamin A/C Kd. **f** Nuclear volume shows a significant increase upon Lamin B2 Kd (~1.2-fold, $p < 0.0001$), $N = 5$. **g**, **h** No significant difference in volume for either diploid or aneuploid CT11 ($N = 2$) or CT17 ($N = 1$) upon Lamin B2 Kd. **i** A significant increase in the volume of aneuploid CT18 ($p = 0.0019$), $N = 2$. **j** Significant increase in the volume of diploid and aneuploid CT19 upon Lamin B2 Kd ($p = 0.0004$), $N = 2$. **g'**–**j'** Distribution of the volumes of aneuploid chromosome territories (CT11, CT17, CT18, and CT19) across nuclear sub-shells upon Lamin B2 depletion. No significant difference was detected in the volumes of aneuploid CT across nuclear sub-shells. Kruskal–Wallis test was used to test for statistical significance. *N* number of independent experiments (biological replicates) contributing to the data, *n* number of nuclei (**a**, **f**) or chromosome territories (**b**–**e**, **g**–**j**) scored

Previous studies suggest a remarkable conservation in gene-density-based chromosome positioning patterns of even aneuploid chromosomes in the interphase nucleus in cancer cells (Cremer et al. 2003). A recent study on primary amniocyte cells shows that naturally aneuploid human Chr.18 and 21 territories assume conserved nuclear locations (Hervé et al. 2016). Further, artificially introduced gene-poor human Chr.7 or 18 and gene-rich Chr.19 into otherwise diploid DLD1 cells showed a gene-density-based conservation in their positioning patterns toward the nuclear periphery and nuclear interior, respectively (Sengupta et al. 2007). It is therefore likely that Lamins play a crucial role in the conservation of spatial organization of aneuploid (trisomies) CTs. It is conceivable that Lamin depletion destabilizes different subsets of Lamin interaction networks at the (i) nuclear periphery (linker of nucleoskeleton and cytoskeleton (LINC) complex), (ii) heterochromatin, (iii) nuclear interior, and (iv) perinucleolar heterochromatin (Dechat et al. 2010; Gruenbaum and Medalia 2015). At the nuclear periphery, Lamins interact with LEM-D proteins, LBR, and HP1 involved in heterochromatin organization (Clements et al. 2000; Foisner and Gerace 1993; Smith and Blobel 1994; Solovei et al. 2013). We surmise that Lamin B2 depletion results in a general weakening of the nuclear periphery due to a loss of its association with Lamin A/C and other factors such as LINC complex, LBR (Moir et al. 2000; Shimi et al. 2015; Ye et al. 1997). This not only maintains the integrity of the nuclear periphery but also tethers gene-poor CTs since aneuploid CT18 (in Lamin B2-depleted cells) disengages from the nuclear lamina and moves further into the nuclear interior. In the nucleoplasm, Lamins associate with chromatin organizers—CTCF, BANF1, and Lamina-associated polypeptide (LAP2α/β) that assist chromatin organization (Dechat et al. 2000; Gesson et al. 2016; Yusufzai et al. 2004). This is likely to impinge on the spatial organization of gene-rich CTs such as CT19 toward the nuclear interior. The role of phosphorylated Lamin A (in the nuclear interior as demonstrated in HeLa cells) (Kochin et al. 2014) in genome organization is unclear. Lamin A/C and LBR are required for tethering heterochromatin, while its absence results in a mislocalization of heterochromatin to the nuclear interior and, therefore, an inversion in nuclear architecture in murine rod cells (Solovei et al. 2009, 2013). Our studies suggest a similar alteration in genome organization as evidenced by the mislocalization of the gene-rich CT19 toward the nuclear periphery and gene-poor CT18 toward the nuclear interior specifically in Lamin B2-depleted aneuploid cells (Fig. 5f, h). This suggests a requirement specifically for Lamin B2 and its interactome in maintaining conserved CT positions. A careful biochemical analysis of these nuclear sub-fractions may provide further insights on these potential interactions with Lamin B2 required for the correct maintenance of CTs in a manner consistent with gene density. Alternatively, the decision to place chromosomes in unique nuclear locations is likely to be initiated during mitosis, where Lamins regulate chromosome segregation (Martin et al. 2010).

It is pertinent to note that Lamin-depletion-induced volume changes of CTs may further impinge on the spatial constraints that position CTs and their transcription potential (Fig. 7).

Table 3 Median volume of chromosome territories upon Lamin A/C Kd in DLD1 cells

Chromosome no.	Untreated (μm^3)	siLacZ (μm^3)	siLamin A/C (μm^3)	
			Diploid	Aneuploid
CT1	10.73	11.51	13.05*	–
CT16	3.89	3.69	4.26	–
CT18	2.65	2.65	3.21*	3.36
CT19	2.83	2.39	3.37*	2.75

*Significant ($p < 0.05$)

Table 4 Median volume of chromosome territories upon Lamin B2 Kd in DLD1 cells

Chromosome no.	Untreated (μm^3)	siLacZ (μm^3)	siLamin B2 (μm^3)	
			Diploid	Aneuploid
CT11	5.53	5.32	5.22	4.64
CT17	2.99	2.94	3.32	4.07
CT18	2.23	2.65	2.66	3.76*
CT19	2.06	2.65	2.84*	3.08*

*Significant ($p < 0.05$)

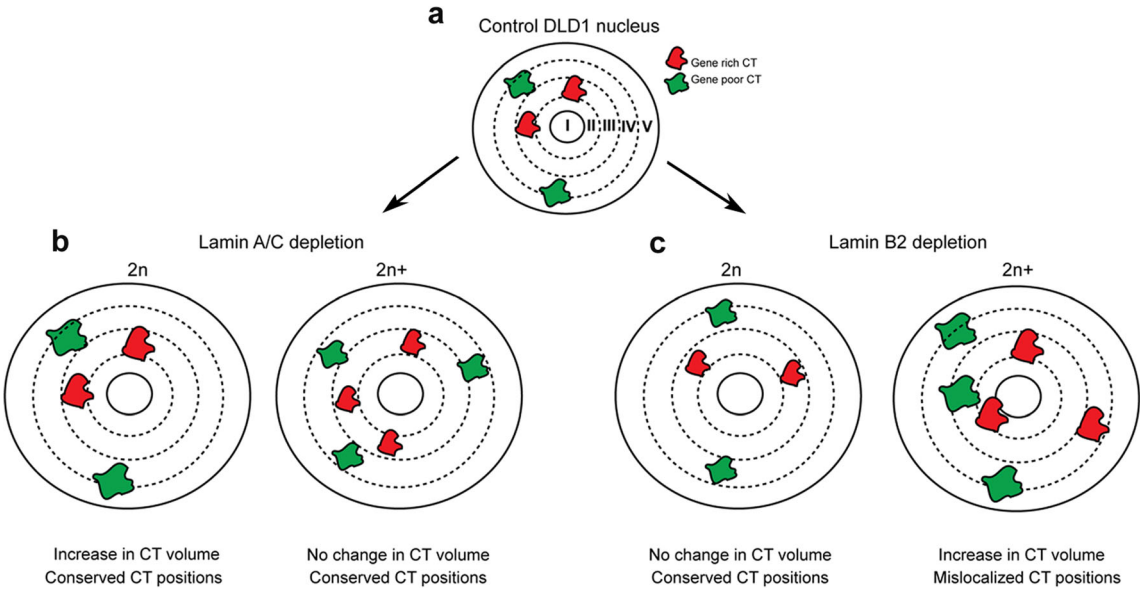

Fig. 8 Lamin B2 depletion perturbs positioning constraints of aneuploid chromosome territories in the interphase nucleus. **a** Schematic representation of the nucleus divided into five concentric sub-shells (I–V) of ~20 % radial distance. Gene-rich CT occupies the nuclear interior (sub-shell: III), while gene-poor CT occupies the nuclear periphery (sub-shell: IV). Nuclear volume shows an increase in both Lamin A/C and Lamin B2 Kd. **b** Representation of the diploid (2n) and the aneuploid (2n+) nucleus upon Lamin A/C Kd. Both diploid and aneuploid CTs show conserved positions, while diploid CTs show a significant increase in volume upon Lamin A/C Kd. **c** Representation of the diploid (2n) and the aneuploid (2n+) nucleus upon Lamin B2 Kd. Diploid CTs show conserved chromosome positions and no change in volume, while aneuploid CTs show mislocalization of CTs and significant change in volume upon Lamin B2 Kd

However, our studies reveal that the volumes of aneuploid CTs are comparable irrespective of the nuclear space (sub-shells) that they occupy (Fig. 7). Notably, diploid CTs showed an increase in volume upon Lamin A/C Kd (Fig. 7). Gene expression profiling showed a downregulation of *SMC1A* (~2-fold) upon Lamin A/C but not in Lamin B2 knockdown. SMC1A regulates chromatin architecture and could potentially impinge on volumes of CTs upon Lamin A/C depletion (Phillips-Cremins et al. 2013). Essentially, our data suggests that maintenance of CT position and function is not just dependent on gene density but additionally requires Lamins and its interactors to function as the "zip code" for the correct placement and regulation of transcriptional activity of either diploid or aneuploid CTs in the interphase nucleus.

The altered position of the aneuploid chromosomes could potentially have a bearing on their interaction with the nuclear lamina and with neighboring CTs (Branco and Pombo 2006). Haploid and diploid KBM7 cells show variability in their LAD profiles, suggesting that LAD profiles are modulated by the ploidy of cells (Kind et al. 2015). It would be useful to compare LAD profiles in diploid versus aneuploid Lamin-depleted cells, although a potential technical limitation is to specifically enrich number of cells with chromosomal aneuploidies. In addition, the identification of chromatin contacts in single cells by Hi-C studies and RNA-Seq analyses would enable assessing the impact of chromosomal aneuploidies on chromatin contact frequencies and transcription (Hashimshony et al. 2012; Islam et al. 2012; Nagano et al. 2013).

Whole chromosomal gains in colorectal cancer cell lines and patient samples positively correlate with gene expression levels (Grade et al. 2007). Gene expression profiling of human Chr.5 and Chr.7 in colorectal cancer cells (HCT116 and DLD1 cells, respectively), Chr.13 trisomy (Edward's syndrome), and Chr.21 trisomy in Down's syndrome showed an upregulation of transcripts from the aneuploid chromosomes by ~1.1–1.5-fold (FitzPatrick et al. 2002; Mao et al. 2003; Stingele et al. 2012; Upender et al. 2004). Lamin depletion followed by gene expression profiling of Lamin A/C and B2 Kd DLD1 cells showed an ~1 % deregulation of the transcriptome in a non-overlapping manner (Fig. 2a). It remains to be examined if aneuploid chromosomes are transcriptionally active even when they are mislocalized in the interphase nucleus in Lamin-depleted cells.

Relatively fewer studies have previously examined the correlation between the spatial organization and expression status of gene loci in aneuploid cells. Amplified *C-MYC* (Chr.8q24) gene loci are localized external to chromosome 8 territory in colon cancer cell line HT-29 (Harnicarova et al. 2006). Interestingly, these loci were found to be transcriptionally active. The lamina is a transcriptionally repressive zone, and repositioning of gene loci away from the nuclear lamina is associated with an increase in its gene expression levels (Peric-Hupkes et al. 2010; Shachar et al. 2015), as shown for artificially targeted reporter genes (LacO gene visualized

using LacI-GFP) in single cells (Finlan et al. 2008; Reddy et al. 2008) as well as an endogenous gene *TCRB*, in contact with the nuclear Lamina (Schlimgen et al. 2008; Shachar et al. 2015). Our studies reveal altered spatial organization of gene loci consistent with an increase in its expression levels in Lamin B2-depleted cells. The candidate gene locus *ZNF570* was not only repositioned away from the nuclear lamina in both diploid and aneuploid cells but also showed a significant increase in transcript signals in Lamin B2-depleted cells (Figs. 6 and S9).

Taken together, our studies suggest that chromosomal aneuploidies induced in Lamin-deficient cells may achieve enhanced transcriptional deregulation by sampling diverse subnuclear microenvironments in the interphase nucleus. Conversely, the presence of Lamins serves to not only prevent chromosomal aneuploidies but also dampen their spatial excursions in the nucleus. A thorough understanding of transcriptional outputs of aneuploid chromosomes in the context of their spatial organization would undoubtedly have far-reaching consequences on the mechanisms of cancer initiation and diseases associated with chromosomal aneuploidies.

Acknowledgments We gratefully acknowledge facilities provided by IISER, Pune. We acknowledge members of the chromosome biology lab for their critical comments on the manuscript. Authors thank Genotypic, Bangalore, for gene expression profiling using microarrays and Bionivid, Bangalore, for microarray data analyses. We thank Wellcome Trust–DBT India Alliance for all their support. We sincerely thank all the referees for their critical inputs and suggestions on the manuscript.

Compliance with ethical standards

Funding This work was supported by funding from the Wellcome Trust–DBT India Alliance intermediate fellowship (Grant No. 30711044) awarded to K.S. and intramural funding from IISER Pune. D.R. acknowledges a fellowship from Council of Scientific and Industrial Research (CSIR, New Delhi).

Conflict of interest The authors declare that they have no conflict of interest.

Ethical approval This article does not contain any studies with human participants or animals performed by any of the authors.

References

Adam SA, Goldman RD (2012) Insights into the differences between the A- and B-type nuclear lamins. Adv Biol Regul 52:108–113. doi:10.1016/j.advenzreg.2011.11.001

Bardi G, Sukhikh T, Pandis N, Fenger C, Kronborg O, Heim S (1995) Karyotypic characterization of colorectal adenocarcinomas. Genes Chromosomes Cancer 12:97–109

Belmont AS, Zhai Y, Thilenius A (1993) Lamin B distribution and association with peripheral chromatin revealed by optical sectioning and electron microscopy tomography. J Cell Biol 123:1671–1685

Belt EJ et al (2011) Loss of lamin A/C expression in stage II and III colon cancer is associated with disease recurrence. Eur J Cancer 47:1837–1845. doi:10.1016/j.ejca.2011.04.025

Bracken AP, Dietrich N, Pasini D, Hansen KH, Helin K (2006) Genome-wide mapping of Polycomb target genes unravels their roles in cell fate transitions. Genes Dev 20:1123–1136. doi:10.1101/gad.381706

Branco MR, Pombo A (2006) Intermingling of chromosome territories in interphase suggests role in translocations and transcription-dependent associations. PLoS Biol 4:e138. doi:10.1371/journal.pbio.0040138

Burke B, Stewart CL (2002) Life at the edge: the nuclear envelope and human disease. Nat Rev Mol Cell Biol 3:575–585. doi:10.1038/nrm879

Butin-Israeli V et al (2015) Role of lamin b1 in chromatin instability. Mol Cell Biol 35:884–898. doi:10.1128/MCB.01145-14

Camps J, Wangsa D, Falke M, Brown M, Case CM, Erdos MR, Ried T (2014) Loss of lamin B1 results in prolongation of S phase and decondensation of chromosome territories. FASEB J 28:3423–3434. doi:10.1096/fj.14-250456

Chambeyron S, Bickmore WA (2004) Chromatin decondensation and nuclear reorganization of the HoxB locus upon induction of transcription. Genes Dev 18:1119–1130. doi:10.1101/gad.292104

Chaumeil J, Augui S, Chow JC, Heard E (2008) Combined immunofluorescence, RNA fluorescent in situ hybridization, and DNA fluorescent in situ hybridization to study chromatin changes, transcriptional activity, nuclear organization, and X-chromosome inactivation. Methods Mol Biol 463:297–308. doi:10.1007/978-1-59745-406-3_18

Cimini D, Degrassi F (2005) Aneuploidy: a matter of bad connections. Trends Cell Biol 15:442–451. doi:10.1016/j.tcb.2005.06.008

Clements L, Manilal S, Love DR, Morris GE (2000) Direct interaction between emerin and lamin A. Biochem Biophys Res Commun 267:709–714. doi:10.1006/bbrc.1999.2023

Constantinescu D, Gray HL, Sammak PJ, Schatten GP, Csoka AB (2006) Lamin A/C expression is a marker of mouse and human embryonic stem cell differentiation. Stem Cells 24:177–185. doi:10.1634/stemcells.2004-0159

Cremer M et al (2001) Non-random radial higher-order chromatin arrangements in nuclei of diploid human cells. Chromosome Res 9:541–567

Cremer M et al (2003) Inheritance of gene density-related higher order chromatin arrangements in normal and tumor cell nuclei. J Cell Biol 162:809–820. doi:10.1083/jcb.200304096

Croft JA, Bridger JM, Boyle S, Perry P, Teague P, Bickmore WA (1999) Differences in the localization and morphology of chromosomes in the human nucleus. J Cell Biol 145:1119–1131

de Las Heras JI, Meinke P, Batrakou DG, Srsen V, Zuleger N, Kerr AR, Schirmer EC (2013) Tissue specificity in the nuclear envelope supports its functional complexity. Nucleus 4:460–477. doi:10.4161/nucl.26872

Dechat T, Korbei B, Vaughan OA, Vlcek S, Hutchison CJ, Foisner R (2000) Lamina-associated polypeptide 2alpha binds intranuclear A-type lamins. J Cell Sci 113(Pt 19):3473–3484

Dechat T, Gesson K, Foisner R (2010) Lamina-independent lamins in the nuclear interior serve important functions. Cold Spring Harb Symp Quant Biol 75:533–543. doi:10.1101/sqb.2010.75.018

Dixon JR et al (2012) Topological domains in mammalian genomes identified by analysis of chromatin interactions. Nature 485:376–380. doi:10.1038/nature11082

Finlan LE et al (2008) Recruitment to the nuclear periphery can alter expression of genes in human cells. PLoS Genet 4:e1000039. doi:10.1371/journal.pgen.1000039

FitzPatrick DR, Ramsay J, McGill NI, Shade M, Carothers AD, Hastie ND (2002) Transcriptome analysis of human autosomal trisomy. Hum Mol Genet 11:3249–3256

Foisner R, Gerace L (1993) Integral membrane proteins of the nuclear envelope interact with lamins and chromosomes, and binding is modulated by mitotic phosphorylation. Cell 73:1267–1279

Foster HA, Abeydeera LR, Griffin DK, Bridger JM (2005) Non-random chromosome positioning in mammalian sperm nuclei, with migration of the sex chromosomes during late spermatogenesis. J Cell Sci 118:1811–1820. doi:10.1242/jcs.02301

Foster CR, Robson JL, Simon WJ, Twigg J, Cruikshank D, Wilson RG, Hutchison CJ (2011) The role of Lamin A in cytoskeleton organization in colorectal cancer cells: a proteomic investigation. Nucleus 2:434–443. doi:10.4161/nucl.2.5.17775, **http://dx.doi.org/10.4161/nucl.2.5.17775**

Galiova G, Bartova E, Kozubek S (2004) Nuclear topography of beta-like globin gene cluster in IL-3-stimulated human leukemic K-562 cells. Blood Cells Mol Dis 33:4–14. doi:10.1016/j.bcmd.2004.03.006

Gesson K, Rescheneder P, Skoruppa MP, von Haeseler A, Dechat T, Foisner R (2016) A-type lamins bind both hetero- and euchromatin, the latter being regulated by lamina-associated polypeptide 2alpha. Genome Res. doi:10.1101/gr.196220.115

Goetze S et al (2007) The three-dimensional structure of human interphase chromosomes is related to the transcriptome map. Mol Cell Biol 27:4475–4487. doi:10.1128/MCB.00208-07

Goldman AE, Maul G, Steinert PM, Yang HY, Goldman RD (1986) Keratin-like proteins that coisolate with intermediate filaments of BHK-21 cells are nuclear lamins. Proc Natl Acad Sci U S A 83:3839–3843

Goodman B, Channels W, Qiu M, Iglesias P, Yang G, Zheng Y (2010) Lamin B counteracts the kinesin Eg5 to restrain spindle pole separation during spindle assembly. J Biol Chem 285:35238–35244. doi:10.1074/jbc.M110.140749

Grade M et al (2007) Gene expression profiling reveals a massive, aneuploidy-dependent transcriptional deregulation and distinct differences between lymph node-negative and lymph node-positive colon carcinomas. Cancer Res 67:41–56. doi:10.1158/0008-5472.CAN-06-1514

Gruenbaum Y, Medalia O (2015) Lamins: the structure and protein complexes. Curr Opin Cell Biol 32:7–12. doi:10.1016/j.ceb.2014.09.009

Guelen L et al (2008) Domain organization of human chromosomes revealed by mapping of nuclear lamina interactions. Nature 453:948–951. doi:10.1038/nature06947

Guo Y, Kim Y, Shimi T, Goldman RD, Zheng Y (2014) Concentration-dependent lamin assembly and its roles in the localization of other nuclear proteins. Mol Biol Cell 25:1287–1297. doi:10.1091/mbc.E13-11-0644

Harnicarova A, Kozubek S, Pachernik J, Krejci J, Bartova E (2006) Distinct nuclear arrangement of active and inactive c-myc genes in control and differentiated colon carcinoma cells. Exp Cell Res 312:4019–4035. doi:10.1016/j.yexcr.2006.09.007

Harr JC, Luperchio TR, Wong X, Cohen E, Wheelan SJ, Reddy KL (2015) Directed targeting of chromatin to the nuclear lamina is mediated by chromatin state and A-type lamins. J Cell Biol 208:33–52. doi:10.1083/jcb.201405110

Hashimshony T, Wagner F, Sher N, Yanai I (2012) CEL-Seq: single-cell RNA-Seq by multiplexed linear amplification. Cell Rep 2:666–673. doi:10.1016/j.celrep.2012.08.003

Hervé B et al (2016) Aneuploidy: the impact of chromosome imbalance on nuclear organization and overall genome expression. Clin Genet. doi:10.1111/cge.12731

Hoger TH, Zatloukal K, Waizenegger I, Krohne G (1990) Characterization of a second highly conserved B-type lamin present in cells previously thought to contain only a single B-type lamin. Chromosoma 100:67–69

Islam S, Kjallquist U, Moliner A, Zajac P, Fan JB, Lonnerberg P, Linnarsson S (2012) Highly multiplexed and strand-specific single-cell RNA 5′ end sequencing. Nat Protoc 7:813–828. doi:10.1038/nprot.2012.022

Kalhor R, Tjong H, Jayathilaka N, Alber F, Chen L (2012) Genome architectures revealed by tethered chromosome conformation capture and population-based modeling. Nat Biotechnol 30:90–98. doi:10.1038/nbt.2057

Kind J et al (2013) Single-cell dynamics of genome-nuclear lamina interactions. Cell 153:178–192. doi:10.1016/j.cell.2013.02.028

Kind J et al (2015) Genome-wide maps of nuclear lamina interactions in single human cells. Cell 163:134–47. doi:10.1016/j.cell.2015.08.040

Kochin V et al (2014) Interphase phosphorylation of lamin A. J Cell Sci 127:2683–2696. doi:10.1242/jcs.141820

Kolb T, Maass K, Hergt M, Aebi U, Herrmann H (2011) Lamin A and lamin C form homodimers and coexist in higher complex forms both in the nucleoplasmic fraction and in the lamina of cultured human cells. Nucleus 2:425–433. doi:10.4161/nucl.2.5.17765

Kuga T et al (2014) Lamin B2 prevents chromosome instability by ensuring proper mitotic chromosome segregation. Oncog 3:e94. doi:10.1038/oncsis.2014.6

Lee KK, Haraguchi T, Lee RS, Koujin T, Hiraoka Y, Wilson KL (2001) Distinct functional domains in emerin bind lamin A and DNA-bridging protein BAF. J Cell Sci 114:4567–4573

Lieberman-Aiden E et al (2009) Comprehensive mapping of long-range interactions reveals folding principles of the human genome. Science 326:289–293. doi:10.1126/science.1181369

Malhas A, Lee CF, Sanders R, Saunders NJ, Vaux DJ (2007) Defects in lamin B1 expression or processing affect interphase chromosome position and gene expression. J Cell Biol 176:593–603. doi:10.1083/jcb.200607054

Mao R, Zielke CL, Zielke HR, Pevsner J (2003) Global up-regulation of chromosome 21 gene expression in the developing Down syndrome brain. Genomics 81:457–467

Martin C, Chen S, Jackson DA (2010) Inheriting nuclear organization: can nuclear lamins impart spatial memory during post-mitotic nuclear assembly? Chromosome Res 18:525–541. doi:10.1007/s10577-010-9137-8

Meaburn KJ et al (2007) Primary laminopathy fibroblasts display altered genome organization and apoptosis. Aging Cell 6:139–153. doi:10.1111/j.1474-9726.2007.00270.x

Mehta IS, Figgitt M, Clements CS, Kill IR, Bridger JM (2007) Alterations to nuclear architecture and genome behavior in senescent cells. Ann NY Acad Sci 1100:250–263. doi:10.1196/annals.1395.027

Mehta IS, Kulashreshtha M, Chakraborty S, Kolthur-Seetharam U, Rao BJ (2013) Chromosome territories reposition during DNA damage-repair response. Genome Biol 14:R135. doi:10.1186/gb-2013-14-12-r135

Meuleman W et al (2013) Constitutive nuclear lamina-genome interactions are highly conserved and associated with A/T-rich sequence. Genome Res 23:270–280. doi:10.1101/gr.141028.112

Mewborn SK et al (2010) Altered chromosomal positioning, compaction, and gene expression with a lamin A/C gene mutation. PLoS One 5:e14342. doi:10.1371/journal.pone.0014342

Moir RD, Montag-Lowy M, Goldman RD (1994) Dynamic properties of nuclear lamins: lamin B is associated with sites of DNA replication. J Cell Biol 125:1201–1212

Moir RD, Yoon M, Khuon S, Goldman RD (2000) Nuclear lamins A and B1: different pathways of assembly during nuclear envelope formation in living cells. J Cell Biol 151:1155–1168

Moss SF et al (1999) Decreased and aberrant nuclear lamin expression in gastrointestinal tract neoplasms. Gut 45:723–729

Nagano T et al (2013) Single-cell Hi-C reveals cell-to-cell variability in chromosome structure. Nature 502:59–64. doi:10.1038/nature12593

Neusser M, Schubel V, Koch A, Cremer T, Muller S (2007) Evolutionarily conserved, cell type and species-specific higher order chromatin arrangements in interphase nuclei of primates. Chromosoma 116:307–320. doi:10.1007/s00412-007-0099-3

Nora EP et al (2012) Spatial partitioning of the regulatory landscape of the X-inactivation centre. Nature 485:381–385. doi:10.1038/nature11049

Ondrej V, Lukasova E, Krejci J, Matula P, Kozubek S (2008) Lamin A/C and polymeric actin in genome organization. Mol Cells 26:356–361

Paz N, Zabala A, Royo F, Garcia-Orad A, Zugaza JL, Parada LA (2013) Combined fluorescent-chromogenic in situ hybridization for identification and laser microdissection of interphase chromosomes. PLoS One 8:e60238. doi:10.1371/journal.pone.0060238

Peric-Hupkes D, van Steensel B (2010) Role of the nuclear lamina in genome organization and gene expression. Cold Spring Harb Symp Quant Biol 75:517–524. doi:10.1101/sqb.2010.75.014

Peric-Hupkes D et al (2010) Molecular maps of the reorganization of genome-nuclear lamina interactions during differentiation. Mol Cell 38:603–613. doi:10.1016/j.molcel.2010.03.016

Petrova NV, Yakutenko II, Alexeevski AV, Verbovoy VA, Razin SV, Iarovaia OV (2007) Changes in chromosome positioning may contribute to the development of diseases related to X-chromosome aneuploidy. J Cell Physiol 213:278–283. doi:10.1002/jcp.21118

Phillips-Cremins JE et al (2013) Architectural protein subclasses shape 3D organization of genomes during lineage commitment. Cell 153:1281–1295. doi:10.1016/j.cell.2013.04.053

Qi R et al (2015) The lamin-A/C-LAP2alpha-BAF1 protein complex regulates mitotic spindle assembly and positioning. J Cell Sci 128:2830–2841. doi:10.1242/jcs.164566

Reddy KL, Zullo JM, Bertolino E, Singh H (2008) Transcriptional repression mediated by repositioning of genes to the nuclear lamina. Nature 452:243–247. doi:10.1038/nature06727

Ried T et al (1996) Comparative genomic hybridization reveals a specific pattern of chromosomal gains and losses during the genesis of colorectal tumors. Genes Chromosomes Cancer 15:234–245. doi:10.1002/(SICI)1098-2264(199604)15:4<234::AID-GCC5>3.0.CO;2-2

Rober RA, Weber K, Osborn M (1989) Differential timing of nuclear lamin A/C expression in the various organs of the mouse embryo and the young animal: a developmental study. Development 105:365–378

Roth U et al (2010) Differential expression proteomics of human colorectal cancer based on a syngeneic cellular model for the progression of adenoma to carcinoma. Proteomics 10:194–202. doi:10.1002/pmic.200900614

Schlimgen RJ, Reddy KL, Singh H, Krangel MS (2008) Initiation of allelic exclusion by stochastic interaction of Tcrb alleles with repressive nuclear compartments. Nat Immunol 9:802–809. doi:10.1038/ni.1624

Sengupta K et al (2007) Artificially introduced aneuploid chromosomes assume a conserved position in colon cancer cells. PLoS One 2:e199. doi:10.1371/journal.pone.0000199

Shachar S, Voss TC, Pegoraro G, Sciascia N, Misteli T (2015) Identification of gene positioning factors using high-throughput imaging mapping. Cell 162:911–923. doi:10.1016/j.cell.2015.07.035

Shete A, Rao P, Pati D, Merchant F (2014) Spatial quantitation of FISH signals in diploid versus aneuploid nuclei. Cytometry A 85:339–352. doi:10.1002/cyto.a.22426

Shimi T et al (2008) The A- and B-type nuclear lamin networks: microdomains involved in chromatin organization and transcription. Genes Dev 22:3409–3421. doi:10.1101/gad.1735208

Shimi T et al (2011) The role of nuclear lamin B1 in cell proliferation and senescence. Genes Dev 25:2579–2593. doi:10.1101/gad.179515.111

Shimi T et al (2015) Structural organization of nuclear Lamins A, C, B1 and B2 revealed by super-resolution microscopy. Mol Biol Cell. doi:10.1091/mbc.E15-07-0461

Shumaker DK et al (2008) The highly conserved nuclear lamin Ig-fold binds to PCNA: its role in DNA replication. J Cell Biol 181:269–280. doi:10.1083/jcb.200708155

Smith S, Blobel G (1994) Colocalization of vertebrate lamin B and lamin B receptor (LBR) in nuclear envelopes and in LBR-induced membrane stacks of the yeast Saccharomyces cerevisiae. Proc Natl Acad Sci U S A 91:10124–10128

Solovei I et al (2009) Nuclear architecture of rod photoreceptor cells adapts to vision in mammalian evolution. Cell 137:356–368. doi:10.1016/j.cell.2009.01.052

Solovei I et al (2013) LBR and lamin A/C sequentially tether peripheral heterochromatin and inversely regulate differentiation. Cell 152:584–598. doi:10.1016/j.cell.2013.01.009

Spann TP, Goldman AE, Wang C, Huang S, Goldman RD (2002) Alteration of nuclear lamin organization inhibits RNA polymerase II-dependent transcription. J Cell Biol 156:603–608. doi:10.1083/jcb.200112047

Stingele S, Stoehr G, Peplowska K, Cox J, Mann M, Storchova Z (2012) Global analysis of genome, transcriptome and proteome reveals the response to aneuploidy in human cells. Mol Syst Biol 8:608. doi:10.1038/msb.2012.40

Swift J et al (2013) Nuclear lamin-A scales with tissue stiffness and enhances matrix-directed differentiation. Science 341:1240104. doi:10.1126/science.1240104

Szczerbal I, Foster HA, Bridger JM (2009) The spatial repositioning of adipogenesis genes is correlated with their expression status in a porcine mesenchymal stem cell adipogenesis model system. Chromosoma 118:647–663. doi:10.1007/s00412-009-0225-5

Tagawa Y, Sawai T, Nakagoe T, Morinaga M, Yasutake T, Ayabe H, Tomita M (1996) Numerical aberrations of chromosomes 11 and 17 in colorectal adenocarcinomas. Surg Today 26:869–874

Taimen P et al (2009) A progeria mutation reveals functions for lamin A in nuclear assembly, architecture, and chromosome organization. Proc Natl Acad Sci U S A 106:20788–20793. doi:10.1073/pnas.0911895106

Tanabe H et al (2002) Evolutionary conservation of chromosome territory arrangements in cell nuclei from higher primates. Proc Natl Acad Sci U S A 99:4424–4429. doi:10.1073/pnas.072618599

Tang CW et al (2008) The integrity of a lamin-B1-dependent nucleoskeleton is a fundamental determinant of RNA synthesis in human cells. J Cell Sci 121:1014–1024. doi:10.1242/jcs.020982

Towbin BD et al (2012) Step-wise methylation of histone H3K9 positions heterochromatin at the nuclear periphery. Cell 150:934–947. doi:10.1016/j.cell.2012.06.051

Tsai MY, Wang S, Heidinger JM, Shumaker DK, Adam SA, Goldman RD, Zheng Y (2006) A mitotic lamin B matrix induced by RanGTP required for spindle assembly. Science 311:1887–1893. doi:10.1126/science.1122771

Upender MB, Habermann JK, McShane LM, Korn EL, Barrett JC, Difilippantonio MJ, Ried T (2004) Chromosome transfer induced aneuploidy results in complex dysregulation of the cellular transcriptome in immortalized and cancer cells. Cancer Res 64:6941–6949. doi:10.1158/0008-5472.CAN-04-0474

van Berkum NL et al (2010) Hi-C: a method to study the three-dimensional architecture of genomes. J Vis Exp. doi:10.3791/1869

Volpi EV et al (2000) Large-scale chromatin organization of the major histocompatibility complex and other regions of human chromosome 6 and its response to interferon in interphase nuclei. J Cell Sci 113(Pt 9):1565–1576

Williamson I et al (2014) Spatial genome organization: contrasting views from chromosome conformation capture and fluorescence in situ hybridization. Genes Dev 28:2778–2791. doi:10.1101/gad.251694.114

Willis ND et al (2008) Lamin A/C is a risk biomarker in colorectal cancer. PLoS One 3:e2988. doi:10.1371/journal.pone.0002988

Wu Z, Wu L, Weng D, Xu D, Geng J, Zhao F (2009) Reduced expression of lamin A/C correlates with poor histological differentiation and prognosis in primary gastric carcinoma. J Exp Clin Cancer Res 28:8. doi:10.1186/1756-9966-28-8

Yang SH, Jung HJ, Coffinier C, Fong LG, Young SG (2011) Are B-type lamins essential in all mammalian cells? Nucleus 2:562–569. doi:10.4161/nucl.2.6.18085

Ye Q, Callebaut I, Pezhman A, Courvalin JC, Worman HJ (1997) Domain-specific interactions of human HP1-type chromodomain proteins and inner nuclear membrane protein LBR. J Biol Chem 272:14983–14989

Yusufzai TM, Tagami H, Nakatani Y, Felsenfeld G (2004) CTCF tethers an insulator to subnuclear sites, suggesting shared insulator mechanisms across species. Mol Cell 13:291–298

Zewe M, Hoger TH, Fink T, Lichter P, Krohne G, Franke WW (1991) Gene structure and chromosomal localization of the murine lamin B2 gene. Eur J Cell Biol 56:342–350

Zullo JM et al (2012) DNA sequence-dependent compartmentalization and silencing of chromatin at the nuclear lamina. Cell 149:1474–1487. doi:10.1016/j.cell.2012.04.035

Recent Trends in Gene Expression

Subhrangsu S. Mandal
Editor

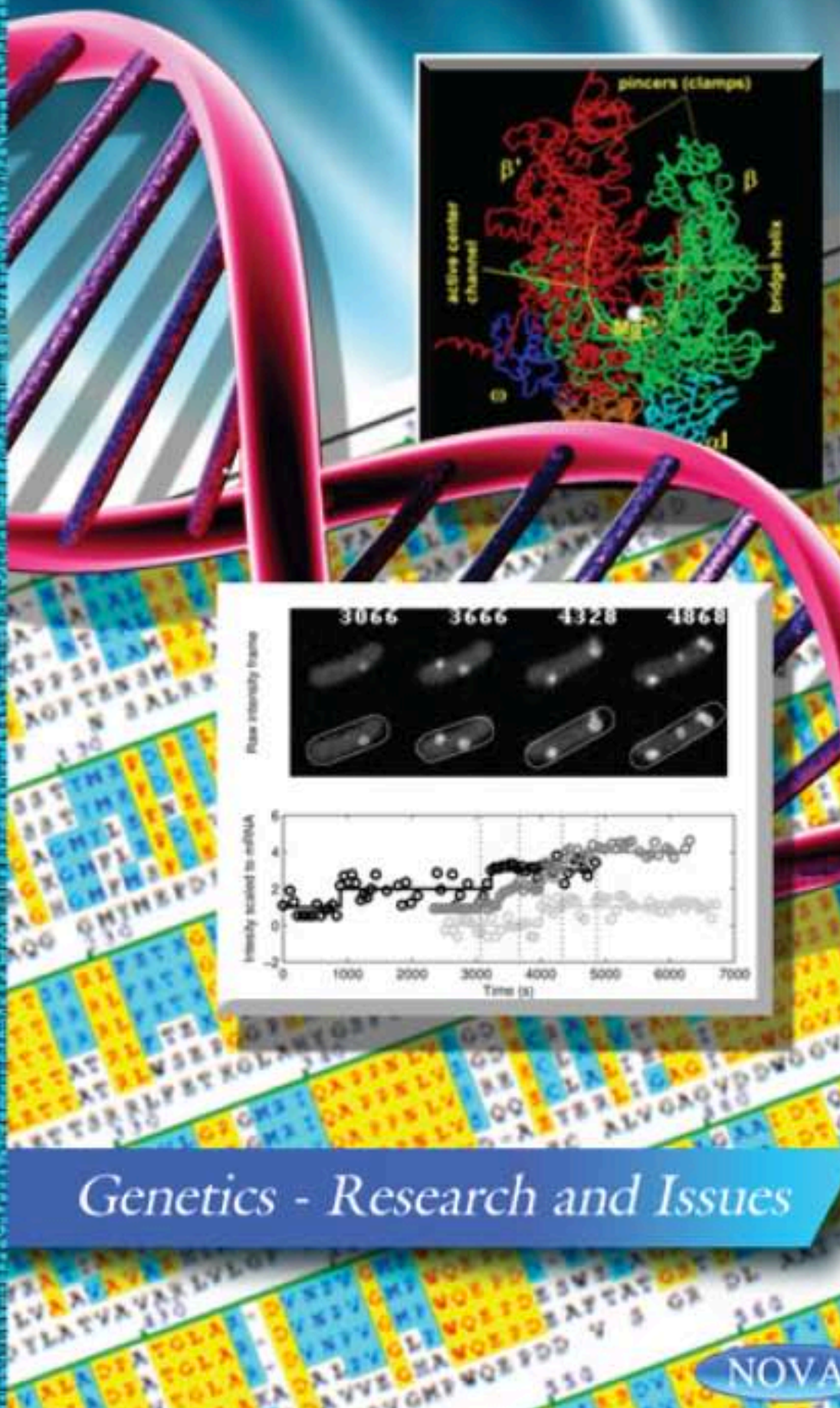

Genetics - Research and Issues

Nova Biomedical

NOVA

Nuclear Organization of Cancer Cells

Devika Ranade and Kundan Sengupta
Chromosome Biology Laboratory,
Indian Institute of Science Education and Research, Pune, India

Abstract

Over a century ago, Carl Rabl (1885) and Theodor Boveri (1909) proposed that chromosomes assume a distinct sub-volume in the nucleus, referred to as the chromosome territory. Chromosomes assume a non-random position in the interphase nucleus with gene rich chromosomes predominantly localized towards the nuclear center while gene poor chromosomes are closer to the nuclear periphery. Such an arrangement is also conserved in higher eukaryotes suggesting a strong functional significance for non-random chromosome positioning. Gene loci on chromosomes also show a non-random position in the nucleus, where in actively transcribing gene loci are "looped-out" of their respective chromosome territories to access transcription factories. The molecular mechanisms that regulate non-random positions of chromosome territories (~10^8 bp) or of individual gene loci (~10^3 bp) in the interphase nucleus are unclear. Diseases of the genome such as cancers are characterized by genome instability and aneuploidy. Studies of chromosome positions in either diploid or aneuploid cancer cells using 3-dimensional fluorescence *in situ* hybridization (3D-FISH) followed by confocal imaging and 3D reconstructions of labeled chromosomes, show that human chromosome 18 (peripheral) and 19 (central) largely assume conserved nuclear locations. However, the extent of aneuploidy could disturb conserved chromosome locations that may in turn affect transcription. In cancer cells, individual gene loci are amplified, which along with whole chromosomal aneuploidies severely destabilizes transcription in cancer cells. However, cancer cells may achieve further transcriptional deregulation by allowing extra chromosomes and amplified genes to assume diverse nuclear locations that additionally imbalance transcription. Taken together, we speculate that cancer cells acquire a hyperdynamic genome organization, where in amplified gene loci and transcription factories populate the entire nucleus that further facilitate a strikingly elevated level of transcriptional deregulation – a hallmark of cancer cells. A careful study of genomic imbalances in cancer in the context of nuclear architecture therefore assumes paramount significance.